School of Applied Chemistry

# Electrochemical Studies on Carbon Dioxide Corrosion and Its Inhibition

by

Yong-jun Tan

(B.Eng., M.Eng.)

This thesis is presented as part of the requirements for the award of the Degree of Doctor of Philosophy of the Curtin University of Technology, Western Australia

August 1996

**I declare that this thesis is my own account of my research and contains as its main content work which has not previously been submitted for a degree at any tertiary educational institution**

**Yong-jun Tan**

# Table of contents

# Acknowledgments

I would firstly express my sincere thanks to Dr. Stuart I. Bailey, Mr. Brian J. Kinsella and Dr. Anthony Parentich (retired 1994) for their supervision, invaluable advice and encouragement throughout this research.

I am very grateful to Miss Jean L. Edward for her technical assistance throughout this work. I also greatly appreciate Mr. Yadran Marinovich for his assistance with computer packages and for proof-reading some parts of this thesis.

I wish to thank the Western Australian Corrosion Research Group for financial support to this research project, the School of Applied Chemistry for various very helpful service, and Professor J. F. Chambers for his efforts in initiating the program.

Sincere thanks are also to Mr. Dave A. Walton for his assistance in the making of electrodes and weight-loss coupons, Mr. Peter G. Chapman for his assistance in FTIR experiments, Professor De-Yu Li for his assistance in XRD experiments, Ms Elaine Miller for her assistance in SEM experiments, Steve Haddon of Applied Chemicals Pty. Ltd. for providing inhibitor samples.

I also wish to thank the Australian Government for awarding me the Overseas Postgraduate Research Scholarship for paying my tuition fees.

Last but not least, I sincerely thank my wife, Bo Chen, for giving me her encouragement, time and support to finish this thesis. I also like to take the opportunity to express my sincere thanks to my father and mother who gave me so much support and encouragement throughout these years.

# Abstract

This thesis mainly concerns the application of electrochemical impedance spectroscopy (EIS) and electrochemical noise analysis (ENA) to the study of $CO_2$ corrosion of mild steel and its inhibition. The primary focus is on the use of EIS and ENA to monitor inhibitor film performance and to evaluate inhibitor film persistency.

EIS was shown to be a suitable technique to study $CO_2$ corrosion product scale, and inhibitor films. The formation and deterioration of protective scales and inhibitor films is found to be accompanied by characteristic spectral changes and a rapid change in electrode impedance. EIS data were used to calculate corrosion related parameters such as the resistances and capacitances of inhibitor layers, and the charge transfer resistance and double layer capacitance. These parameters were used to analyse inhibitor mechanisms, determine corrosion rates and the persistency of inhibitor films.

ENA is also a suitable technique to monitor the formation and deterioration of inhibitor films. It has the advantage of being able to monitor rapid processes which occur within one second. Several technical and theoretical developments were made in this thesis including the development of a new method to remove DC trends in noise recording (moving average removal) and a method of instantaneous corrosion rate measurement to study fast corrosion processes (the 'continuous noise resistance calculation' method). Experimentally, the noise resistance was confirmed to be similar to linear polarisation resistance in the systems studied. The theoretical background and the advantages and disadvantages of the ENA technique are also discussed.

Corrosion product scales formed under different conditions were investigated using EIS and surface analysis techniques. Temperature, pressure and exposure time were

confirmed to be the important factors influencing the degree of protection given by the scale. The morphology of corrosion scales showed an obvious correlation to their protective ability. Electron microscopy revealed two types of crystal structures on corroded steel coupons. The smaller crystals associated with one of these structures was found to contribute most to corrosion protection.

Several typical $CO_2$ corrosion inhibitors, including an imidazoline and a quaternised amine, were studied by EIS. A multi-layer model was employed to explain the EIS characteristics and self-repairing ability of imidazoline films. A quaternised amine film is most probably a physically or electrostatically adsorbed molecular layer which forms rapidly and desorbs easily.

The deterioration of films, formed by commercial batch treatment inhibitors, was found to occur in three stages which were indicated or characterised by Bode phase-angle plots. A method to determine inhibitor film persistency was developed. This method is based on determining the three stages of inhibitor film deterioration, and the continuous measurement of corrosion rate, which is accessible at the second and third stages of film deterioration.

# List of Publications

**(i) Journal papers:**

Y. J. Tan, S. Bailey and B. Kinsella, 'Investigations on the formation and destruction processes of corrosion inhibitor films using electrochemical impedance spectroscopy (EIS)', *Corrosion Science*, vol.38, p1545 - p1561

Y. J. Tan, S. Bailey and B. Kinsella, 'The monitoring of the formation and destruction of corrosion inhibitor films using electrochemical noise analysis (ENA), *Corrosion Science*, vol.38, no.10, p1681 - p1695

S. Bailey, Y.J. Tan and B. Kinsella, 'Use of electrochemical impedance spectroscopy for the study of $CO_2$ corrosion protection by batch-treatment inhibitors', *British Corrosion Journal*, in press (accepted)

Y. J. Tan, B. Kinsella and S. Bailey, 'Monitoring batch treatment inhibitor performance continuously using electrochemical noise analysis', *British Corrosion Journal*, submitted

B. Kinsella, Y. J. Tan, and S. Bailey, 'Studies of $CO_2$ corrosion product scales using electrochemical impedance spectroscopy and surface characterisation techniques', *Corrosion* - NACE, submitted

**(ii) Conference Papers:**

Y. J. Tan, B. Kinsella and S. Bailey, 'Use of electrochemical techniques for monitoring the formation and corrosion protective ability of carbon dioxide corrosion product scales and inhibitor films', 13th International Corrosion Congress, 25-29 November 1996, Melbourne (AMAC Australasian Corrosion Research Award paper)

Y. J. Tan, B. Kinsella and S. Bailey, 'The evaluation of corrosion inhibitor film persistency using electrochemical impedance spectroscopy and electrochemical noise analysis', Corrosion 96, paper 352, NACE, Denver (1996, as an oral report)

Y. J. Tan, B. Kinsella and S. Bailey, 'An experimental comparison of corrosion rate measurement techniques: weight-loss measurement, linear polarisation, electrochemical impedance spectroscopy and electrochemical noise analysis', Proc. ACA Conference Corrosion & Prevention 95, Perth, Australia (1995, as an oral report)

B. Kinsella, Y. J. Tan, and S. Bailey, 'The application of electrochemical techniques and cylinder electrodes in the study of inhibitor film persistency', Proc. ACA Conference Corrosion & Prevention 95, Perth, Australia (1995, as an oral report)

Y. J. Tan, S. Bailey, B. Kinsella, A. Parentich 'An electrochemical and spectroscopic investigation of $CO_2$ corrosion product scales and their effects on further corrosion', Paper 54, Corrosion & Prevention 94, Adelaide (1994, as an oral report)

B. Kinsella, S Bailey, A Parentich and Y. J. Tan, 'Corrosion Inhibitor Film Persistency', Proc. ACA Conference Corrosion & Prevention 94, Adelaide, Australia (1994, as an oral report)

# List of Symbols and Abbreviations

## (i). Roman Symbols and Abbreviations

| Symbol | Meaning |
|---|---|
| $A$ | the preexponential factor in the kinetic equation of $CO_2$ corrosion |
| $A'$ | the preexponential factor in the kinetic equation of $CO_2$ corrosion |
| $a$ | Tafel constant |
| $b$ | Tafel slope |
| $b_a$ | anodic Tafel slope |
| $b_c$ | cathodic Tafel slope |
| $C_1$ | the capacitance of the first inhibitor layer |
| $C_2$ | the capacitance of the second inhibitor layer |
| $C_3$ | the capacitance of the third inhibitor layer |
| $C_4$ | the capacitance of the fourth inhibitor layer |
| $C_{dl}$ | double layer capacitance |
| $C_{film}$ | the capacitance of surface film |
| $C_h$ | an empirically determined constants in the kinetic equation of $CO_2$ corrosion |
| $[CO_2(l)]$ | the concentration of $CO_2$ dissolved in the water phase |
| $C_{pore}$ | the capacitance of a surface film due to the pore areas |
| $C_{scale}$ | the capacitance of corrosion product scale |
| EIS | electrochemical impedance spectroscopy |
| ENA | electrochemical noise analysis |
| $F$ | (a) Faraday's constant<br>(b) Fourier transform |
| FFT | fast Fourier transformation |
| $f$ | frequency |

| | |
|---|---|
| $[H_2CO_3]$ | the concentration of carbonic acid |
| $H(s)$ | transfer function |
| $i$ | (a) current density |
| | (b) the number of a data point |
| $i_a$ | anodic polarisation current density |
| $i_c$ | cathodic polarisation current density |
| $i_{corr}$ | corrosion current density |
| $I_i$ | an individual current value |
| $I_{noise}(t)$ | current noise at time $t$ |
| $\bar{I}(s)$ | the Laplace transforms of the time-dependent current |
| $j$ | $\sqrt{-1}$ |
| $K_a$ | dissociation constant |
| $K^G$ | the proportional factor which is a function of the gas production rate |
| $K^o$ | an empirically determined constant in the kinetic equation of $CO_2$ |
| | corrosion |
| $m$ | the mean |
| MAR | moving average removal |
| MEM | the maximum entropy method |
| $m_i$ | the mean of current noise data |
| $m_v$ | the mean of voltage noise data |
| mm/y | millimetres/year |
| mpy | mils/year |
| $n$ | (a) the order of the reaction in the kinetic equation of $CO_2$ corrosion |
| | (b) the total number of electrons transferred in the anodic reaction |
| | (c) the total number of datum points |
| $n'$ | the number of electrons transferred in the cathodic reaction |
| $P$ | pressure |
| $pCO_2$ | $CO_2$ partial pressure |
| $P_{scale}$ | the permeability of the scale for a corrosion reaction |

| | |
|---|---|
| $PSD$ | noise power spectral density |
| $\overline{PSD}$ | the average power-spectrum density |
| $Q_{H2O}$ | water production rate in barrels per million cubic feet of gas |
| $Q_{gas}$ | gas production rate in million cubic feet per day |
| $R$ | the universal gas constant |
| $R_1$ | the resistance of the first inhibitor layer |
| $R_2$ | the resistance of the second inhibitor layer |
| $R_3$ | the resistance of the third inhibitor layer |
| $R_4$ | the resistance of the fourth inhibitor layer |
| RE | reference electrode |
| $R_{film}$ | coating film resistance |
| $R_n$ | noise resistance |
| $R_{ohm}$ | solution resistance |
| $R_p$ | polarisation resistance |
| $R_{pore}$ | the resistance of a surface film due to the pore areas |
| $R_t$ | charge transfer resistance |
| $s$ | Laplace frequency |
| $T$ | absolute temperature |
| $t$ | (a) temperature in Celsius |
| | (b) time |
| $u_n$ | a series of $n$ data |
| $\widetilde{u}_n$ | a polynomial fitting of the original data value |
| $V$ | potential |
| $V_a(t)$ | the potential of electrode 'a' at time $t$ |
| $V_{a,noise}(t)$ | the potential noise of electrode 'a' at time $t$ |
| $V_b(t)$ | the potential of electrode 'b' at time $t$ |
| $V_{b,noise}(t)$ | the potential noise of electrode 'b' at time $t$ |
| $V_{cor}$ | the charge transfer controlled corrosion reaction rate in the de Waard-Milliams equation |

| | |
|---|---|
| $V_{corr}$ | corrosion potential |
| $V_{DC}$ | DC potential shift in voltage noise recording |
| $V_{DC}(t)$ | DC potential shift in voltage noise recording at time $t$ |
| $V_i$ | an individual voltage value |
| $\overline{V}(s)$ | the Laplace transforms of the time-dependent voltage |
| $V_{system}(t)$ | system potential at time $t$ |
| $V_{noise,\ system}(t)$ | system noise potential at time $t$ |
| $W_1$ | no.1 working electrode of a dual electrode |
| $W_2$ | no.2 working electrode of a dual electrode |
| $Z_f$ | Faraday impedance |
| $Z(j\omega)$ | impedance |
| $Z_{re}$ | real part of impedance |
| $Z_{im}$ | imaginary part of impedance |

**(ii). Greek Symbols**

| **Symbol** | **Meaning** |
|---|---|
| $\alpha$ | (a) transfer coefficient |
| | (b) an exponent describing the depression of the Nyquist semicircle |
| $\beta$ | transfer coefficient (1 - $\alpha$) |
| $\delta$ | corrosion scale thickness |
| $\Delta E$ | the apparent activation energy in the kinetic equation of $CO_2$ corrosion |
| $\Delta t$ | the time window of noise resistance calculation |
| $\sigma_i$ | the standard deviation of current noise |
| $\sigma_v$ | the standard deviation of voltage noise |
| $\eta$ | overpotential |
| $\eta_a$ | anodic overpotential |
| $\eta_c$ | cathodic overpotential |

| | |
|---|---|
| $\tau$ | time constant |
| $\tau_{dl}$ | the time constant for the double layer |
| $\tau_{film}$ | the time constant for coating film |
| $\phi$ | phase angle |
| $\omega_m$ | the resonance frequency at the maximum value of Z'' |

# Chapter I

# INTRODUCTION

$CO_2$ is a naturally occurring component in many oil and gas fields. The concentration of $CO_2$ in the gas phase of certain oil and gas wells can vary from a trace to more than 50% associated with water, oil and gas production. $CO_2$ is sometimes also intentionally added at high pressures to oil fields to enhance oil recovery.

Although dry $CO_2$ is noncorrosive to metals and alloys at moderate temperatures, if liquid water or aqueous solutions are present, $CO_2$ forms carbonic acid and becomes quite corrosive. $CO_2$ corrosion of matels results in severe corrosion damage to a variety of downhole and surface oil and gas producing equipment such as oil and gas wells, pipelines, pumps, condensers, gas scrubbers, storage systems and also equipment for the refining of crude oil and natural gas.

The severity of $CO_2$ corrosion and its economic impact on oil and gas producing operations was first recognised in 1943 (NACE Task Group T-1-3 1984). Since then, $CO_2$ corrosion has become a more and more serious problem due to the changes in oil/gas well corrosion environment and the use of new oil and gas production technologies. In the 1950's, corrosion occurring in acid gas ($H_2S$, $CO_2$ or both) fields increased due to increasing primary water production with field age and due to the implementation of many waterfloods for secondary recovery. Development of sour gas fields starting in the 1950's resulted in more severe corrosion problems associated

with $CO_2$ and $H_2S$. The development of $CO_2$ enhanced oil recovery in the late 1960's again significantly increased $CO_2$ corrosion (NACE Task Group T-1-3 1984).

Since 1944, a lot of research work has been carried out on $CO_2$ corrosion mechanism and its control (NACE Task Group T-1-3 1984). Since then, techniques such as cathodic protection, corrosion inhibitors and coatings were developed to prevent metals against $CO_2$ corrosion. Significant progress has also made on $CO_2$ corrosion mechanism and kinetics since 1944, especially during the 1970s and 1980s when intensive studies were carried out.

Although many questions in $CO_2$ corrosion have already been answered, such as 'why $CO_2$ has a strong corrosivity?', many theoretical and technical questions are still not satisfactorily answered and $CO_2$ corrosion is still a major problem in the oil and gas production industry.

In this Chapter, following a brief review of current knowledge on $CO_2$ corrosion, inhibition and testing techniques, some of the important unanswered questions will be listed and discussed in section 1.4. This thesis sets out to resolve some of these unsolved problems. The general objective of this research work is to investigate the possibility of using electrochemical impedance spectroscopy (EIS) and electrochemical noise analysis (ENA) as new tools to study $CO_2$ corrosion product scale and $CO_2$ corrosion inhibitor films, especially to evaluate inhibitor film persistency.

## 1.1 Fundamental Aspects of Carbon Dioxide Corrosion

### 1.1.1 Carbonic acid and its corrosivity

$CO_2$ corrosion is essentially a carbonic acid corrosion problem. $CO_2$ corrosivity is due to its dissolution in water to form carbonic acid:

$$CO_2 + H_2O \rightleftharpoons H_2CO_3$$

Due to the above reaction, the solubility of $CO_2$ in water is much higher than oxygen, as shown in Table 1.1.

**Table 1.1.** The solubility of $CO_2$ and $O_2$ in water when the partial pressure of the gas is 760 mm Hg (Treseder 1980, p45).

| Temperature (C°) | $CO_2$ (g/L) | $O_2$ (g/L) |
|---|---|---|
| 0 | 3.36 | 0.070 |
| 10 | 2.35 | 0.054 |
| 20 | 1.72 | 0.044 |
| 30 | 1.31 | 0.037 |
| 40 | 1.04 | 0.033 |
| 50 | 0.86 | 0.030 |
| 60 | 0.71 | 0.028 |
| 70 | | 0.026 |
| 80 | | 0.025 |

Carbonic acid is a weak acid: at room temperature only less than 0.1% of the molecules dissociate.

$$H_2CO_3 \rightleftharpoons H^+ + HCO_3^- \qquad K_{a,1} = 4.31 \times 10^{-7}$$
$$HCO_3^- \rightleftharpoons H^+ + CO_3^{2-} \qquad K_{a,2} = 4.70 \times 10^{-11}$$

If carbon dioxide corrosion were similar to normal weak acid corrosion, where steel is corroded due to the reduction of $H^+$ and the oxidation of iron, obviously, according to the above equations the corrosivity of $CO_2$ should be very weak considering the low percentage of dissociated molecules.

However, the real corrosivity of carbonic acid is much stronger than the corrosivity suggested by above equations. A well-known phenomenon that was first found in 1924 (Whitman *et al.* 1924) is that at a given pH, more corrosion of steel is caused by aqueous $CO_2$ solution than by hydrochloric acid. These experimental facts suggest that hydrogen ion is unlikely to be the major corrosive species in $CO_2$ corrosion, i.e. the reduction of $H^+$ is unlikely to be the main cathodic reduction reaction in $CO_2$ corrosion.

The reason for the high corrosivity of carbonic acid was not revealed until the 1970's when systematic investigations of the $CO_2$ corrosion mechanism were carried out. In 1975, a cathodic reduction reaction was first suggested by de Waard and Milliams (de Waard and Milliams 1975a). From their experimental results, de Waard and Milliams concluded that the cathodic hydrogen evolution in $CO_2$ corrosion proceeds in a 'catalytic' way by direct reduction of undissociated adsorbed carbonic acid. A mechanism suggested by de Waard and Milliams (1975a) is,

$$H_2CO_3 + e^- \rightarrow H\cdot + HCO_3^- \quad \text{(rate determining step)}$$

$$HCO_3^- + H^+ \rightleftharpoons H_2CO_3$$

$$2\,H\cdot \rightarrow H_2$$

In addition to this main reaction, other cathodic reduction reactions may also occur simultaneously such as the direct reduction of $H^+$ and the further reduction of hydrogen in the bicarbonate species:

$$H^+ + e^- \rightarrow H\cdot$$

$$HCO_3^- + e^- \rightarrow H\cdot + CO_3^{2-}$$

This mechanism was confirmed by Schmitt and Rothmann (1977) although they give a different opinion about rate-determining step (Schmitt 1984b). This mechanism is now generally accepted as the explanation of the strong corrosivity of carbonic acid. The detailed process of the cathodic reduction reaction of $CO_2$ corrosion was studied by Schmitt and Rothmann (1977) and reviewed by Schmitt (1984b).

### 1.1.2 The overall reactions of $CO_2$ corrosion

Based on their experimental results, de Waard and Milliams found that the active iron dissolution obeys the Bockris pH-dependent mechanism (de Waard and Milliams 1975a):

$$Fe + OH^- \rightarrow FeOH + e^-$$

$$FeOH \rightarrow FeOH^+ + e^- \quad \text{(rate determining step)}$$

$$FeOH^+ \rightarrow Fe^{2+} + OH^-$$

Later Schmitt and Rothmann (1978a) confirmed this anodic reaction mechanism of $CO_2$ corrosion.

The overall reaction mechanism of $CO_2$ corrosion of iron in oxygen-free carbonic acid solutions was formulated by Schmitt and Rothmann (1978a):

(a). Cathodic half-reaction:

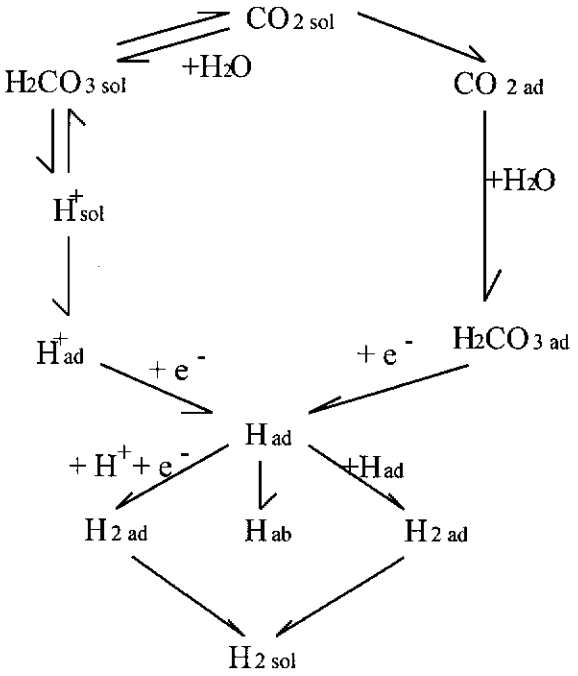


(b). Anodic half-reaction:

$$Fe + H_2O \rightleftharpoons FeOH_{ad} + H^+ + e^-$$

$$FeOH_{ad} \rightarrow FeOH^+ + e^- \qquad \text{(slow step)}$$

$$FeOH^+ + H^+ \rightleftharpoons Fe^{2+} + H_2O$$

The gross anodic reaction:

$$Fe \rightarrow Fe^{2+} + 2e^-$$

The overall reaction of $CO_2$ corrosion therefore is :

$$Fe + 2\ H_2CO_3 \rightarrow Fe^{2+} + H_2 + 2\ HCO_3^-$$

### 1.1.3 Equations of $CO_2$ corrosion kinetics

It is generally agreed that the cathodic hydrogen evolution process is the rate-controlling step of the $CO_2$ corrosion of steel in an oxygen-free environment at ambient temperature (de Waard and Milliams 1975a; 1975b; Schmitt and Rothmann 1977; 1978a) although the anodic process was also found to affect the corrosion rate to a smaller extent (de Waard 1993).

de Waard and Milliams deduced a kinetic equation of $CO_2$ corrosion by assuming the following $CO_2$ corrosion rate determining step (de Waard and Milliams 1975a; 1975b):

$$H_2CO_3 + e^- \rightarrow H\cdot + HCO_3^- \qquad (1.1.3.1)$$

According to this rate determining reaction, the charge transfer controlled corrosion reaction rate, $V_{cor}$, can be generally written as:

$$V_{cor} = A \times [H_2CO_3]^n \, e^{-(\Delta E/RT)} \qquad (1.1.3.2)$$

where A is the preexponential factor; $[H_2CO_3]$ is the concentration of carbonic acid; $n$ is the order of the reaction which was found to be about 0.7; $\Delta E$ is the apparent activation energy which has been found by various authors to be in the order of 50 kJ/mol (de Waard and Milliams 1975a; 1993).

$[H_2CO_3]$ is directly proportional to the concentration of $CO_2$ in water phase, $[CO_2(l)]$, which is determined according to Henry' law. Equation (1.1.3.2) can be re-written as,

$$V_{cor} = A' . pCO_2^n \, e^{-(\Delta E/RT)} \qquad (1.1.3.3)$$

Taking logarithms and fitting to corrosion rate data, the following relation is obtained:

$$log(V_{cor}) = 5.8 - 1710/(273+t) + 0.67log(pCO_2) \quad (1.1.3.4)$$

where $pCO_2$ is $CO_2$ partial pressure in gas phase, $t$ is temperature in Centigrade.

This is the new version of the de Waard-Milliams equation (de Waard 1993). An older version of this formula uses a different temperature dependence of Henry's constant and was deduced by de Waard and Milliams in 1975 (de Waard and Milliams 1975a; 1975b):

$$log(V_{cor}) = 7.96 - 2320/(273+t) - 0.00555t + 0.67log(pCO_2) \quad (1.1.3.5)$$

The de Waard-Milliams equation was generally accepted in various laboratories for quantitative prediction of corrosion rates of bar steel as a function of the $CO_2$ partial pressure and the temperature under the pre-requisite that 'passivation' does not occur (Eriksrud and Sontvedt 1984; Ikeda *et al.* 1984; Schmitt 1984b; Murata *et al.* 1984).

The de Waard-Milliams equation also showed a satisfactory agreement with industrial field data at low temperature and low pressure conditions (Townsend *et al.* 1972).

However, at higher $CO_2$ partial pressures and temperatures, the observed experimental corrosion rates are generally lower than those calculated from the de Waard-Milliams equation, even in short-term experiments, e.g. 24 hours (Schmitt 1984b). Limiting conditions have to be set to for the equation's validity.

The validity limits established by Schmitt were $pCO_2 < 2$ bar and $t < 60$ °C (Schmitt 1984b); by Eriksrud $pCO_2 = 1$ bar and 20 °C (Eriksrud and Sontvedt 1984); by Ikeda $pCO_2 = 2$ bar and 60 °C (Ikeda *et al.* 1984) and by Murata $pCO_2 = 70$ bar and 60 °C (Murata *et al.* 1984).

In general, the valid temperatures and pressures for the de Waard-Milliams equation are far below the temperatures and pressures found in the oil and gas industry. So the practical application of the equation is very limited.

It is generally believed that the loss of validity of the de Waard-Milliams equation at higher temperature and pressure is due to the 'passivation' of the steel surface, i.e. the formation of more or less protective corrosion product scales (de Waard and Milliams 1975a; Eriksrud and Sontvedt 1984; Ikeda *et al.* 1984; Schmitt 1984b; Murata *et al.* 1984).

### 1.1.4 $CO_2$ corrosion product scale and its effect on further corrosion

It has been known for a long time that a protective corrosion product scale can form on a steel surface at certain conditions and results in 'passivation' of the steel.

The importance of this scale on the $CO_2$ corrosion mechanism, kinetics and even the corrosion pattern has already been well recognised. First of all, this scale can result in the invalidity of the de Waard-Milliams equation (de Waard and Milliams 1975a). It was found that the formation of scale can reduce initial corrosion rates by as much as three orders of magnitude (Hausler 1984). Repeated laboratory evidence showed that the formation of corrosion scale can result in a qualitative change in $CO_2$ corrosion kinetics. When protective corrosion product scale is present, mass transfer to and from the metal surface, instead of cathodic hydrogen evolution, can become the corrosion rate controlling factor (Hausler 1984; Eriksrud and Sontvedt 1984; Ikeda *et al.* 1984; Schmitt 1984b; Dunlop *et al.* 1984). The corrosion product scale, its nonuniform formation and localised destruction, is also supposed to be the key factor of localised $CO_2$ corrosion (Schmitt 1984b; Palacios and Shadley 1991; Heusler 1989).

The formation of surface scale is due to the precipitation of corrosion products on the metal surface during $CO_2$ corrosion. However, at low temperature and low $CO_2$ partial pressure, the surface scale is not protective and is often rather amorphous and exhibits only poor adherence to the metal surface. Only at higher temperatures and higher $CO_2$ partial pressures does the surface scale become protective and have a more crystalline structure and good adherence to the metal surface (Schmitt 1984b).

Besides temperature and pressure, the corrosion protective property of the scale was also found to be affected by many other factors such as pH, steel structure and doping, brine composition etc. (Hausler 1984). An important fact regarding the mechanism of scale formation is that scale forms prior to saturation of the solution with $FeCO_3$, which suggests that the micro-environment near the metal surface results in the earlier precipitation of $FeCO_3$. This can be rationalised by assuming that iron carbonate precipitates because of high local pH and ferrous ion concentration near the metal surface (Schmitt 1984b). Two possible mechanisms were suggested by Hausler (1984) regarding scale formation: topochemical scale growth and interphase precipitation.

Although most researchers agree that $FeCO_3$ is the main composition of the protective corrosion product scale, Xia *et al.* (1989), however, believed that $Fe(HCO_3)_2$ is the key corrosion product which constructs a tight, adherent and protective corrosion scale. They thought that $FeCO_3$ only forms a less voluminous, non-adherent, porous and non-protective surface layer.

Iron carbide is also often found in the corrosion scales. It is probably a residue of corroded steel after the corrosion process etches out the metallic iron because under normal experimental conditions, the formation of $Fe_3C$ from iron and $CO_2$ is thermodynamically forbidden (Jasinski 1987). The role of iron carbide in corrosion

scale has been studied only very recently by Crolet *et al.* (1994, 1996) and van Hunnik *et al.* (1996).

Iron oxides and iron hydroxides are also found in the corrosion scales. The presence of iron oxides and iron hydroxides may be the reason that corrosion scales are normally brown or black in colour because the natural colour of $FeCO_3$ and $Fe(HCO_3)_2$ should be white or yellowish (Xia *et al.* 1989). The formation of iron oxides at temperatures above 100 °C is due to the Schikorr reaction (Schmitt 1984b):

$$3Fe + 4H_2O \rightarrow Fe_3O_4 + 4H_2.$$

In individual studies, various workers have reported varying results on the composition of corrosion scales (Hausler 1984; Shah 1993; Xia *et al.* 1989; Vera *et al.*, 1994). No conclusions have been reached about the correlation between the composition of the scale and its corrosion protective ability.

Some laboratory observations and SEM investigations have contributed towards more understanding of the morphology of corrosion scales (Dunlop *et al.* 1983; Jasinski 1987; Palacios and Shadley 1991), however, the correlation between the morphology of corrosion product scale and its corrosion protective ability has not been completely addressed.

### 1.1.5 $CO_2$ corrosion kinetics when corrosion scale is present

As discussed above, when protective corrosion scale is present, the de Waard-Milliams equation is no longer valid. New relationships have to be found for corrosion rate prediction.

Empirical relationships were found by Hausler (1984) for stagnant and flowing systems which have different mass transfer patterns.

(i). Stagnant system

If a system is closed and stagnant such as an autoclave, corrosion rate was assumed to be controlled by scale permeability and scale thickness because under this condition the scale permeability determines mass transfer. Based on this assumption and parabolic rate theory, Hausler (1984) suggested that the instantaneous corrosion rate is inversely proportional to the scale thickness:

$$\text{Corrosion rate} \sim P_{scale} / \delta \qquad (1.1.5.1)$$

where $P_{scale}$ represents the permeability of the scale for corrosion reactions; $\delta$ stands for the scale thickness. Scale permeability is dependent on temperature, alkalinity and brine composition. Specific additives such as mercury, aluminium and silica were found to increase the scale permeability and so increase the corrosion rate (Hausler 1984; Schmitt 1984b; Gatzke and Hausler 1984).

(ii). Flowing system

In a flowing system, corrosion rate was found to be determined by the dissolution of corrosion scale which is mass transfer dependent and the scale permeability becomes a minor factor (Hausler 1984). In this case, the corrosion rate-limiting factor which greatly affects the dissolution of scale was found to be the flow rate of produced fluid and gas, i.e. the water and gas production rates (Gatzke and Hausler 1984; Bradburn 1977). Based on their experience, Gatzke and Hausler suggested a 'corrosion rate - production rate' relationship for corrosion rate estimation in the case of gas production (Gatzke and Hausler 1984):

$$\text{Average corrosion rate (mpy)} = K^G \times Q_{H2O} \qquad (1.1.5.2)$$

where $Q_{H2O}$ = water production rate in barrels per million cubic feet of gas (BPMMCF); $K^G$ is the proportional factor which is a function of the gas production rate:

$$log\, K^G = logC_h + K^o \times logQ_{gas} \qquad (1.1.5.3)$$

where $Q_{gas}$ is the gas production rate in million cubic feet per day (MMCFD), and $C_h$ and $K^o$ are empirically determined constants related to the chemistry of the system.

In another work, Dunlop *et al.*(1984) also found that corrosion rates calculated on the basis of iron carbonate solubility limitations provide reasonable, order-of magnitude estimates which can be extremely useful in assessing possible corrosion losses in sweet gas systems. A transport controlled corrosion rate was also supported by other experimental measurements (Mishra *et al.* 1993).

In this case, obviously, the main factor affecting the corrosion rate is the flow rate of produced fluid and gas. Other factors which influence the iron carbonate solubility could also affect corrosion rate. For example, increasing temperature and alkalinity reduce the iron carbonate solubility in sodium chloride brines and decrease the corrosion rate, whereas increasing $CO_2$ partial pressure and calcium-magnesium ions in the brine increase the iron carbonate solubility and increase the corrosion rate (Hausler 1984).

## 1.2 The Inhibition of Carbon Dioxide Corrosion

### 1.2.1 Techniques for $CO_2$ corrosion prevention

Many $CO_2$ corrosion control technologies have been developed and used in the oil and gas production industry, including inhibition, corrosion resistant metals and alloys, surface coatings, cathodic protection, nonmetallic materials, corrosion environment control and corrosion protection design etc..

Inhibition plays a key role in $CO_2$ corrosion control in the oil and gas production industry. Since the introduction of inhibitors in the mid-1940's, the industry acceptable corrosion rate has already been reduced from 15 - 20 mpy to 1 - 5 mpy mainly due to the use of inhibitors (Fisher 1993).

Although corrosion resistant metals and alloys such as titanium and stainless steel are very effective in $CO_2$ corrosion control, they are normally only used in severe corrosion environments because they are expensive and are difficult to weld. Some of them, such as chromium-nickel stainless steels, are often sensitive to pitting and crevice corrosion. The history of the development and application of corrosion resistant metals has been reviewed recently by Rice (1993) and Schofield and Kane (1993).

Internal protective organic coatings such as epoxy phenolic coating and coal tar epoxy have also been used for protecting tubing, downhole equipment and vessels etc.. Successful use of organic coatings is usually accompanied by inhibition and cathodic protection because internal coatings are subject to damage and are difficult to repair.

Cathodic protection is commonly used to supplement the internal coating and inhibitors because there will always be imperfections in coatings and inhibitor films where corrosion can occur (NACE 1979). The principle and design of cathodic protection in the oil and gas industry are similar to other industries.

Nonmetallic materials such as plastics and rubber have found increasing use in recent years because they do not corrode. However, nonmetallic materials have limited working temperatures and pressures and have low strength and low resistance to vibration, mechanical damage, freezing etc. (NACE 1979).

Corrosion environment control is also a method for preventing $CO_2$ corrosion. For example, the use of anti-hydrate treatments and associated pH control appears to be a safe method to control $CO_2$ corrosion in long crude gas multiphase pipelines (Crolet and Samaran 1993). Techniques such as temperature and velocity control are also found to be useful in some cases (Byars and Galbraith 1984).

Correct design is also important for controlling $CO_2$ corrosion especially for avoiding localised corrosion. For example, electrical insulation is obviously necessary if dissimilar metals are connected.

Although the selection and application of exact corrosion control technologies at any location depends on the specific corrosive environment and economic considerations, inhibition still represents the most cost effective and flexible means of $CO_2$ corrosion control (Webster *et al.* 1993). Inhibitor, combined with mild steel, is the most economical $CO_2$ corrosion control method under many circumstances (Noegroho 1990) and so inhibition is one of the most important issues in $CO_2$ corrosion control in the oil and gas production industry. The evaluation and monitoring of inhibitor performance will be the main subject of this thesis.

### 1.2.2 $CO_2$ corrosion inhibitors

A corrosion inhibitor is a substance which, when added to a liquid in relatively small quantity, diminishes corrosion (Evans 1981). For diminishing $CO_2$ corrosion of carbon steel in the oil and gas industry, many commercial inhibitor products have been developed. They can be generally classified into several common types or mechanistic classes: passivating, cathodic, anodic, film forming, neutralising. They can also be classified into two major types according to the methods by which they are applied: continuous treatment inhibitors and batch treatment inhibitors. Most of the inhibitors are organic molecules with a long dipolar chain. Some inorganic inhibitors are also used.

The first generation of oil well corrosion inhibitors are inorganic molecules such as arsenic compounds (Cizek 1993). Inorganic inhibitors are usually passivators which combat against corrosion by improving the protective ability of corrosion scales. Inorganic compounds such as sodium arsenite ($Na_2HAsO_3$), ferrocyanide and sodium metavanadate ($NaVO_3$), have long been used to inhibit carbon dioxide corrosion in oil wells and gas treatment plants (Williams and Leckie 1968). Inorganic inhibitors have also been used in oil and gas production pipelines satisfactorily in the 1950s (Fisher 1993). However certain shortcomings were found to be associated with applying inorganic inhibitors (Fisher 1993) and they have been overtaken by organic inhibitors.

In the mid-1940s, the earliest organic $CO_2$ corrosion inhibitor, a film-forming amine, was developed (Blair and Gross 1949; Gross and Andrews 1948). This discovery led to the development of many organic chemical inhibitor formulations based on the use of a film-forming amine and its salts. Although industry was slow to accept these materials at first, their use has greatly expanded and organic inhibitors are now the most widely used agents for corrosion control (Fisher 1993). This development has

greatly improved corrosion protection in oil and gas well and has dramatically decreased the high cost of corrosion.

During about 20 years' development from the late 1940's to the late 1960's, many new inhibitors or their derivatives were developed. They are normally nitrogenous in nature and can be classified as: (i) amides/imidazolines; (ii). salts of nitrogenous molecules with carboxylic acids; (iii). nitrogen quaternaries; (iv). polyoxyalkylated amines, amides, imidazolines; (v). nitrogen heterocyclics. There are other non-nitrogenous inhibitors that contain phosphorus, sulfur, or oxygen atoms but they are used less frequently. Among these inhibitor bases, amides and imidazolines are the most important and frequently used. Many of the commercial oil and water soluble inhibitors contain amides and/or imidazolines.

Commercial inhibitors are normally unique mixtures. These inhibitors usually contain three elements: (i). inhibitor bases, the active inhibitor components; (ii). a solvent base; (iii). certain additives, such as surfactants, film enhancers, demulsifiers, defoamers and oxygen scavengers.

During the past decades, the primary improvements in inhibitor technology have been in the refinement of formulations and the development of improved methods of applying inhibitor to solve problems associated with inhibitor transport and reduction of inhibitor-caused operating problems and inhibitor thermal stability.

In recent years, inhibitors were also found to be useful in controlling localised $CO_2$ corrosion (Schmitt *et al.* 1993; Alkire *et al.*; Kolts 1993).

### 1.2.3 Methods of inhibitor application

Whilst development of effective inhibitors is important, it is equally important to develop and select the proper treatment method because a good inhibitor will not successfully control corrosion if it does not reach the troublesome area.

Initially, inhibitors were used only by continuous injection. Continuous treatment of producing wells and pipeline systems is accomplished by a chemical-proportioning pump that operates constantly. Inhibitor is continuously injected in order to maintain an inhibitor concentration of a few parts per million to thousands of parts per million (most commonly 25 to 100 ppm) in the produced fluid.

Later, it was found that organic inhibitors offer lasting protection. Some operators take advantage of this finding through the use of intermittent injections, i.e. batch treatment (Fisher 1993). With batch treatment of flowlines, a concentrated solution of inhibitors is drawn through the tubing between two "*pigs*". For downhole application the well is shut-in and the inhibitor allowed to drop through the column of gas or oil and water. Alternatively, in gas wells the inhibitor may be applied by a brush. These processes allow the inhibitor to form a protective coating or film on the steel surface. The process needs to be repeated periodically because the inhibitor film is gradually removed by dissolution in the produced fluids flowing through the tubing. Batch treatment has already become the most widely used gas well treatment technique [Linda Garverick Essential Research 1994].

Under some situations a combination of batch and continuous treatment, squeeze treatment, is also used. Squeeze treatment is a method in which the inhibitor solution is placed into the oil well formation. The inhibitor and diluent are displaced down the tubing and into the formation by a large amount of displacing fluid (e.g. 25 to 75 drums), which is usually clean crude, diesel fuel or nitrogen (Hilliard 1978). When the well is returned to production after a squeeze, the initial concentration of

chemicals in the returned fluid is high and forms an inhibitor film. The inhibitor continuously returns from the formation to repair any breaks in the inhibitor film. This method is used on gas-lift wells having a high-pressure, a high gas-oil ratio, and a high rate of water production.

The common requirements for all these inhibitor treatment methods are: (i). to convey inhibitor to every troublesome area and (ii). to maintain effective corrosion prevention, i.e. keep sufficient inhibitor concentration for continuous treatment and keep a protective inhibitor film for batch treatment.

### 1.2.4 Mechanism of $CO_2$ corrosion inhibitors

Generally speaking, inhibitors work by interfering with the anodic or cathodic corrosion electrochemical reaction, by forming a protective barrier layer against corrosive agents on the metal surface, or by a combination of these actions.

For organic $CO_2$ corrosion inhibitors in the oil and gas production industry, it is generally believed that their inhibition is the result of physical adsorption and chemisorption (Fisher 1993). In many cases, the principles and mechanism of inhibitor protection seems to be similar to that of inhibition in other corrosion environments. However, little work has been published in this area addressing the details of the mechanism of $CO_2$ corrosion inhibitors.

An interesting conclusion on the inhibition mechanism is that inhibitors work by retarding the mass transfer dependent dissolution rate of the corrosion product layer (Gatzke and Hausler 1984). It was concluded that inhibitors adsorb on the iron carbonate scale, or are built into it, thereby retarding the mass transfer dependent dissolution rate of the iron carbonate scale.

When a protective corrosion scale is present, mass transfer to or from the corroding surface is corrosion rate determining. A detailed analysis led to the conclusion that the dissolution of a protective (passivating) iron carbonate layer is the rate determining step and is mass transfer dependent. Inhibitors retard the mass transfer dependent dissolution rate of the corrosion product layer and so inhibit corrosion (Gatzke and Hausler 1984).

Dunlop *et al.* (1984) suggested an inhibition mechanism based on the synergistic effect between inhibitor film and corrosion product scales. They found that the substantial protectiveness of an iron carbonate scale can be greatly enhanced through addition of an effective inhibitor. The protectiveness was due to the combined effect of the inhibitor and the iron carbonate scale, rather than to the inhibitor alone.

In some cases, several corrosion processes may operate at the same time in an oil-well or oil-line system and an effective inhibitor may affect these processes by different mechanisms.

## 1.3 Techniques for Studying and Evaluating $CO_2$ Corrosion and Its Inhibitors

Although $CO_2$ corrosion may be predicted using the de Waard-Milliams equation as shown in equation (1.1.3.4) or other empirical equations such as equation (1.1.5.2), generally speaking these equations are only applicable in very simple conditions. In practice, *in-situ* corrosion monitoring and laboratory tests are very important requirements for $CO_2$ corrosion study and management.

### 1.3.1 *In-situ* $CO_2$ corrosion monitoring techniques

The main objectives of *in-situ* corrosion monitoring are to optimise corrosion management by measuring corrosion rate, predicting probable corrosion penetration or failure and detecting unexpected changes in the corrosion environment.

Although there are similar requirements in other industrial areas, *in-situ* $CO_2$ corrosion monitoring is more important in the oil and gas industry because the corrosion environment in the oil and gas production industry is more complicated and variable. For example, the depth of oil wells can vary from about 2000 metres to more than 6000 metres and $CO_2$ partial pressures can reach 20.7 Mpa (3000 psi) and temperature can approach 230 °C (Hilliard 1978; Linda Garverick Essential Research 1994, p259). This complexity in corrosion environment makes the $CO_2$ corrosion mechanism, process and pattern very complicated and variable. So *in-situ* corrosion monitoring is critical for $CO_2$ corrosion management in the oil and gas production industry.

The weight-loss coupon method of exposing metal coupons to the corrosive environment is the traditional and the most widely used method for *in-situ* corrosion monitoring. In the oil and gas industry, the coupons are usually exposed to oil/water or gas streams flowing through piping. A coupon is normally of the same metal as the piping or oil/gas well. The exposure period for metal coupons may range from a few days to several years. Ordinarily, coupons are examined at intervals. Total corrosion can be measured by weight-loss; corrosion type can be seen by visual examination; and the rate of penetration can be determined by examining pit depths or the thickness of the remaining metal. As a classical corrosion test method, the weight-loss coupon method has produced a great deal of useful information. However, the weight-loss coupon method has many limitations: (i). The weight-loss coupon method is cumbersome, slow and cannot be carried out automatically. In many cases, *in-situ* weight-loss measurements are not applicable due to the difficulties in putting weight-loss coupons into and withdrawing them from corrosion sites. A meaningful weight-loss test often takes several months to complete. On the other hand, the weight-loss coupon method can only provide limited information regarding the corrosion process and mechanism. Weight-loss measurements, in some cases, may interrupt the production process. (ii). In the oil and gas production industry, the weight-loss coupon can give misinformation in some cases. An example is the paraffin problem, where paraffin can build up on the coupon surfaces (so the coupon becomes fouled) over time and that causes erroneous corrosion rates to be calculated (Chamberlain 1985). (iii). The weight-loss coupon method can only give an average corrosion rate over the test period and can not give the instantaneous corrosion rate. Thus the weight-loss method is not suitable for detecting unexpected changes in the corrosion environment or to determine inhibitor film persistency.

Iron counts, the chemical analysis and determination of iron compounds in the product fluid, is also an *in-situ* technique for detecting the occurrence and the extent of $CO_2$ corrosion. However, the accuracy of iron counts can be affected by many

factors. For example, errors may occur due to the formation of corrosion product scales. $CO_2$ corrosion product is often not soluble and can attach to the metal surface, so the iron content in product fluid may not reflect the real corrosion situation especially when corrosion starts to occur. Another important source of error is the content of iron in produced water. Some of the deep, hot Tuscaloosa Trend wells produce water with over 100 ppm of iron (Linda Garverick Essential Research 1994, p277). This iron can not be separated from corrosion iron and so sometimes large errors in the deduction of corrosion rates can occur. Other disadvantages of the iron counts method include that it can not be used to detect localised corrosion such as pitting corrosion and it gives little information about the corrosion mechanism.

The electrical resistance probe is an oil-field corrosion monitoring method utilising an automated electrical resistance probe. As the cross-sectional areas of thin strips or wires of the testing metal are reduced due to corrosion, increases in electrical resistance can be measured and converted into weight-loss. A concern when using the electrical resistance probe is that probes may become fouled, or covered by deposits which will result in incorrect results without notice (Kirkley 1982). Another concern is that probes need to be changed or replaced at fairly short intervals because probes are usually thin with small cross-sectional areas for increased sensitivity. So the electrical resistance probe is usually not suitable for tests over long periods.

Linear polarisation measurements can be used to detect instantaneous corrosion rates. Instruments using such techniques may be used in conjunction with computerised systems to monitor, analyse and control corrective treatments. However, the linear polarisation technique has limitations when used in the oil and gas industry because the large solution resistance and surface film resistance, which are common in oil and gas wells and flowlines, can cause large measurement errors without notice. Long-term corrosion measurements in the field with linear polarisation probes were found not to be possible because of oil fouling of the electrodes (Cameron and Coker 1986).

Radiographic examination, using X-rays or radioactive isotopes, can also be used to monitor corrosion (NACE 1979). The main advantage of radiography is that it provides metal corrosion information in a picture record that can be understood by nontechnical personnel. Some other techniques are also used, less frequently, in the *in-situ* monitoring of oil and gas well corrosion such as hydrogen measurement; ultrasonic devices etc..

### 1.3.2 Laboratory $CO_2$ corrosion monitoring techniques

The main objectives of laboratory simulated $CO_2$ corrosion tests are to investigate the $CO_2$ corrosion mechanism and kinetics, to assess the corrosivity of the environment, to select corrosion prevention technologies and to evaluate the efficiency of corrosion preventive materials such as inhibitors and organic coatings.

Although *in-situ* corrosion monitoring is a traditional method for the selection and evaluation of corrosion prevention techniques and materials, it is obviously not a completely effective method. Laboratory tests, however, can accelerate corrosion processes and so can be finished in a shorter time. Furthermore, laboratory tests are more easily repeated and so laboratory tests are often used for studying corrosion mechanisms.

Techniques which can be used in *in-situ* corrosion monitoring such as the weight-loss coupon method; iron counts; the electrical resistance probe; linear polarisation measurements and radiographic examination can also be used in laboratory tests. The key issues in laboratory tests are the simulation of the corrosion environment and the acceleration of corrosion.

Laboratory tests should attempt to simulate the actual corrosion environment. However, the simulation of the corrosion environment in the oil and gas production industry is very difficult because the $CO_2$ corrosion environment in the oil and gas industry is very complicated and variable. In fact, it is difficult to set up a standard all-purpose laboratory test for fully simulating the corrosion conditions in oil and gas wells. A reasonable laboratory simulation of $CO_2$ corrosion in the oil and gas industry requires a detailed understanding of the particular corrosion environmental conditions and their effects on the corrosion mechanism, process and pattern.

There are several test methods which are usually used to simulate the corrosion environment in the oil and gas industry:

(i). The wheel test (NACE Task Group T-1D-8 1982) is a dynamic corrosion test which is normally used for corrosion inhibitor evaluation. There are basically two versions of the test, both of which rely on determining the weight loss of a steel coupon to calculate the corrosion rate. The first version (constant contact) of the test simulates continuous inhibitor treatment. The second version (film persistency) of the test corresponds to the conditions experienced during inhibitor batch treatment. The procedure involves placing pre-weighed coupons into test vessels with hydrocarbon and synthetic brine (or actual produced fluids) that have been saturated with carbon dioxide. The inhibitor is introduced into the test vessels at the concentration actually used in the field (e.g. 50 ppm for the constant contact version; 2000 ppm for the film persistency version). Then the test vessels are loaded on a wheel that rotates inside a heated cabinet. In the film persistency version the coupons are removed after a short period of time (e.g. 1 hour) and then are placed in fresh uninhibited fluid for the corrosion test. At the end of the total test period (usually 24 to 72 hours), the coupons are removed, cleaned and reweighed for weight-loss and corrosion rate calculation. The wheel test, including the normal low pressure wheel test and a high pressure version, is often used for laboratory evaluation of inhibitors (Goodson and Jackson

1986; Garber *et al.* 1994; Wu 1994). However, its application for assessing inhibitor film persistency is still not completely satisfactory and there is a lack of a consensus understanding (NACE Task Group T-1D-8 1982). Inconsistent values are obtained at times by the film persistency wheel test due to unrealistic simulation of the downhole environment (NACE T-D-2 1966; Choi and Cepulis 1989).

(ii). The $CO_2$ sparged beaker test is probably the simplest test simulating $CO_2$ corrosion in the oil and gas industry. About 800 mL of a laboratory brine or a brine/hydrocarbon mixture in a 1000 mL beaker is pre-sparged with $CO_2$ to saturate the brine with $CO_2$ and remove oxygen. The test uses linear polarisation measurement. Test electrodes are allowed to pre-corrode for two hours while $CO_2$ is continuously sparged into the solution. Neat inhibitor is injected under the brine surface and the corrosion rate is continuously monitored. The test is allowed to run for 24 hours after which the final inhibited and uninhibited corrosion rates are measured and the corrosion protection can be calculated. The $CO_2$ sparged beaker test is used in many laboratories (Goodson and Jackson 1986; Webster *et al.* 1993; Wu 1994; Chesnut and Choi 1994; Garber *et al.* 1994) and will be used in this thesis to simulate the $CO_2$ corrosion environment.

(iii). The flow loop is a test apparatus which can simulate various corrosion environments especially flowing environment under conditions such as turbulent flow. The most commonly used flow loops are ambient-pressure circulating loops; high-pressure/high-temperature flow loops and jet impingement loops. The ambient-pressure circulating loop, which consists of a reservoir, a centrifugal pump and a specimen chamber, is probably the simplest flow loop and is used to simulate ambient-pressure corrosion at various temperatures and flow conditions (Goodson and Jackson 1986; Choi and Cepulis 1987). The high-pressure/high-temperature flow loop, which consists of an autoclave, a centrifugal pump and a specimen chamber, can simulate high pressure corrosion under various temperature and flow conditions (Choi

and Cepulis 1987; 1989; Webster *et al.* 1993; Chesnut and Choi 1994). The jet impingement loop, using a high speed jet of liquid impacting onto a test specimen, is used to simulate very high shear stresses which will occur at locations such as bends of oil pipelines (Webster *et al.* 1993). Some other types of flow loops such as high speed autoclaves and disposal flow loops were also used in laboratory tests (Webster *et al.* 1993). The main disadvantage of the flow loop technique is that it is cumbersome and uses expensive equipment.

Generally speaking, $CO_2$ corrosion testing techniques consist of combinations of the basic corrosion testing techniques such as weight-loss coupons, linear polarisation, electrical resistance probes and the simulation of the corrosion environment. The applications of common techniques were compared and reviewed by Cole (1979) and Garber *et al.* (1994).

The techniques using *in-situ* corrosion monitoring such as the weight-loss coupon method; iron counts; electrical resistance probes; linear polarisation measurements and radiographic examination can also be used in the laboratory. In addition to these traditional techniques, corrosion potential measurement (Choi and Cepulis 1987; Martin 1993) and potentiodynamic polarisation curves (Chamberlain 1985) were used to evaluate inhibitor film persistency. The potentiodynamic technique was also used to detect the occurrence of localised corrosion in various oilfield systems (Goodson and Jackson 1986). High performance liquid chromatography measurement was used for monitoring corrosion inhibitor residuals (Cossar and Carlile 1993). Raman and infrared spectroscopy were used to detect the presence of a corrosion inhibitor on a metal surface (Lynch *et al.* 1982). An impinging jet electrode has been used to evaluate inhibitor film persistency in high-speed fluid flow (Esteban *et al.* 1990). Electrochemical impedance spectroscopy has also been used in the studies of $CO_2$ corrosion and its inhibitors (Dawson *et al.* 1990; Lotz *et al.* 1990). However, a detailed investigation is lacking on these applications.

## 1.4 Problems and Difficulties in $CO_2$ Corrosion and the Objectives of This Research Work

Although significant progress has been made in $CO_2$ corrosion inhibition and testing techniques, many questions are still left unanswered. Some of these questioned will be the target of this thesis.

### 1.4.1 Unsolved problems

Unsolved problems remain in every aspect of $CO_2$ corrosion, inhibition and testing techniques and some of them are listed below:

(i). The prediction of $CO_2$ corrosion rate and the corrosivity of the environment.
An answer to this problem is important not only in $CO_2$ corrosion science but also in $CO_2$ corrosion engineering. Although the de Waard-Milliams equation (de Waard and Milliams 1975a; 1975b) was generally accepted for quantitative prediction of corrosion rates of bare steel as a function of the $CO_2$ partial pressure and the temperature, it is only applicable in simple laboratory conditions under the pre-requisite that 'passivation' does not occur. Although the modified forms of the de Waard-Milliams equation (de Waard *et al.* 1991; de Waard and Lotz 1993) introduced 'correction factors' to quantify the influence of environmental parameters and corrosion product scale formed under various conditions, a new question then arose as how to accurately determine these 'correction factors'.

As discussed in section 1.1.3, the key to this problem is the corrosion product scale.

(ii). How to quantify the protection of $CO_2$ corrosion product scale and its effects on further $CO_2$ corrosion?

This question was posed by de Waard and Lotz (1993) as the most difficult topic in $CO_2$ corrosion engineering. This question is also obviously related to the determination of 'correction factors' in the modified de Waard-Milliams equation because it is well-known that corrosion product scale is a major factor affecting $CO_2$ corrosion mechanism and controlling the corrosion rate (Hausler 1983; Schmitt 1984a; Burke 1984). $CO_2$ corrosion product scale may also be the key to understanding localised $CO_2$ corrosion (Schmitt 1984b; Palacios and Shadley 1991) and the effects of environmental factors such as temperature; pressure; velocity of fluid; pH etc., on $CO_2$ corrosion rate and mechanism. New developments in techniques for testing and studying the scale may be the key for answering this question.

(iii). The corrosion kinetics when corrosion scale is present.

Although Hausler (1984) developed equations such as equation (1.1.5.2) to predict the $CO_2$ corrosion rate when corrosion scale is present, generally speaking these equations are empirical and only applicable under very simple conditions. A detailed understanding about under-scale corrosion kinetics is still lacking. A prerequisite to solve this problem may rest on a better understanding of the corrosion product scale and its effects on the corrosion process and kinetics. However, The kinetic effects of corrosion product scales have not been detailed to any extent (Hausler 1984)

(iv). Questions about factors affecting $CO_2$ corrosion.

Although the most important factors affecting $CO_2$ corrosion were found to be temperature, $CO_2$ partial pressure, pH, water chemistry, gas and oil composition, fluid flow speed and flow regime, solid particles content, metal surface condition, and the microstructure of steel, their effects and the mechanism of these effects have not been fully addressed.

For bare steel corrosion, higher temperatures accelerate the electrochemical and chemical corrosion reactions and give a higher corrosion rate according to the de Waard-Milliams equation. Higher $CO_2$ partial pressure reduces the pH and increases the rate of the carbonic acid reduction reaction, and so gives a higher corrosion rate according to the de Waard-Milliams equation (Nesic *et al.* 1993). But what is the relationship between the temperature and pressure and the formation of protective corrosion product scale?

It was also found that the combined effect of scale formation and pH can lead to a 20 times reduction of the corrosion rate when the pH was raised from 3.8 to 6.2 (Videm 1993). What is the mechanism of the pH effect? According to the cathodic reduction reactions suggested by de Waard and Milliams (1975a) and the discussion in section 1.1.1, pH should not greatly affect the corrosion process. Nesic (1993) suggested that higher pH means lower solubility of iron carbonate giving a higher probability of protective film formation.

Schmitt (1984a) thought that below 60 °C, the corrosion rate is generally independent of flow. Nesic *et al.* (1993) thought that higher flow rate usually gives higher corrosion rates by increasing the transport rates of reacting species to the metal surface and by preventing the formation of, or destroying, protective scales. On the other hand, Nesic *et al.* (1993) found that under some conditions higher flow rates mean lower corrosion rates when iron carbide films, which may cause galvanic corrosion, are removed. Overall, the effects of flow on corrosion have not been completely addressed.

The microstructure of steel has also been found to affect the corrosion rate because of its impact on the corrosion scale characteristics (Mishra *et al.* 1993). The mechanism is not clear.

Generally speaking, it seems that many factors affect $CO_2$ corrosion through affecting the formation and structure of corrosion product scale. The study of corrosion product scale may provide very important information on the mechanism of factors affecting $CO_2$ corrosion.

(v). How to predict localised $CO_2$ corrosion, i.e. what are the main factors governing the $CO_2$ corrosion pattern? Pitting corrosion, stress corrosion cracking and mesa-type corrosion are very common in the oil and gas production industry (Schmitt 1984b; Schmitt and Rothmann 1978b; Dunlop *et al.* 1984). Only limited research work has been done in this area. Although the localised destruction or nonuniform growth of corrosion product scale was suggested to be the most important factor (Schmitt, G. 1984b), no quantitative conclusion was reached.

(vi). Why is $CO_2$ corrosion product scale protective? No conclusion has been reached about the correlation between the corrosion protective ability and the composition and morphology of corrosion scale. Although it is generally agreed that iron carbonate is the main corrosion product (Hausler 1983; Dunlop *et al.* 1983; Shah 1993; Vera *et al.* 1994), there are different opinions about the chemical composition of the scale (Xia *et al.* 1989). Some laboratory observations and SEM investigations have contributed towards more understanding of the morphology of corrosion scales (Dunlop *et al.* 1983; Jasinski 1987; Palacios and Shadley 1991), however, no clear conclusion was made about the effect on scale corrosion protective ability.

(vii). Is it possible to prevent $CO_2$ corrosion by improving corrosion product scale? Passivation may be the simplest approach to $CO_2$ corrosion control. A small amount of foreign ions could have a doping effect on the corrosion scale, forming a denser scale (Hausler 1984). However, little work has been done regarding how to improve the protective properties of the corrosion scale through optimising scaling conditions. The reliability of a complete protection afforded by scale cannot be sufficiently

quantified at present (de Waard and Lotz 1993). There is a possibility to improve scale protection by using improved inorganic inhibitors as discussed in section 1.2.2.

(viii). How to continuously monitor and evaluate $CO_2$ corrosion inhibitor performance and inhibitor film persistency? Inhibitors are most commonly used in the oil and gas production industry. However, there is not a good technique which can be used to continuously monitor and evaluate $CO_2$ corrosion inhibitor performance and persistency. The current technology for assessing inhibitor film persistency is a subject of much discussion and, in many cases, disagreement (NACE Task Group T-1D-8 1982).

(ix). The mechanism of $CO_2$ corrosion inhibitor film formation and destruction. The understanding of $CO_2$ corrosion inhibitors is limited, especially since very little is known about the inhibitor film formation and destruction mechanisms. Obviously a better understanding of the inhibitor film formation and destruction processes is important for the development of new $CO_2$ corrosion inhibitors which have better film persistency, and the safe application of inhibitors.

### 1.4.2 Objectives of this research work

This thesis sets out to resolve some of the above problems. The general objective of this research work is to develop and use electrochemical impedance spectroscopy (EIS) and electrochemical noise analysis (ENA) as new tools to study $CO_2$ corrosion product scale and inhibitor films. Additionally, surface characterisation techniques such as X-ray diffraction (XRD), Fourier transform infrared spectrometry (FTIR) and scanning electron microscope (SEM) will be used to study $CO_2$ corrosion product scales. In particular:

(a). EIS will be used to quantify the protection of $CO_2$ corrosion product scale and its effects on further $CO_2$ corrosion, i.e. addressing question (ii) above. This work may also be relevant to questions (i); (iii); (iv) and (v) because corrosion product scale supposedly plays a key role in answering these questions.

(b). EIS and ENA will be used to study $CO_2$ corrosion inhibitor films, including continuous and batch treatment inhibitor films, focusing on the study of their mechanism and persistency, i.e. addressing questions (viii) and (ix). This work may also be relevant to question (vii).

(c). SEM, XRD and FTIR will be used to investigate the correlation between the composition, the morphology of corrosion product scale and its corrosion protective ability, i.e. addressing question (vi).

# Chapter II

# CORROSION STUDIES USING ELECTROCHEMICAL IMPEDANCE SPECTROSCOPY (EIS) AND ELECTROCHEMICAL NOISE ANALYSIS (ENA)

## 2.1 Introduction

Metallic corrosion is essentially an electrochemical process and so can be studied by electrochemical techniques. Many electrochemical techniques have been developed during the past several decades for investigating the causes and mechanisms of corrosion processes, for detecting the corrosivity of the environment and for evaluating the efficiency of corrosion resistant materials etc.. Compared with traditional techniques, electrochemical techniques have great advantages of the relatively short measuring time, a high accuracy and the possibility of continuous corrosion monitoring (Lorenz and Mansfeld 1981).

Although electrochemical techniques are supposed to be versatile tools in corrosion science and engineering, the most common application of them is to determine the metal corrosion rate because the metal corrosion rate is the most obvious and often the most important parameter in detecting the corrosivity of the environment, in selecting corrosion prevention technologies and in evaluating corrosion resisting materials etc.. Electrochemical techniques offer the possibility of fast, continuous and automatic corrosion rate determination.

The measurement of corrosion rate is actually equivalent to determination of the kinetics of the corrosion electrochemical process. The fundamental formula for describing the kinetics of an electrochemical reaction is the Butler-Volmer equation.

### 2.1.1 The Butler-Volmer equation

According to mixed-potential theory, for corrosion in the absence of externally applied potentials, the oxidation and the reduction processes occur simultaneously at the metal/electrolyte interface and there can be no net electrical charge accumulation. Under these circumstances the net measurable current is zero, i.e. the corrosion current can not be measured directly.

For determining electrochemical corrosion kinetics, a perturbation of the corroding electrode by an externally imposed polarisation potential, $V$, is needed to shift the corrosion system from the corrosion potential $V_{corr}$. If the anodic and cathodic reactions on the working electrode are totally activation-controlled and the corrosion potential is far away from the equilibrium potentials of the individual anodic and cathodic reactions, then the Butler and Volmer equation can be applied:

$$i = i_{corr}[\exp(\frac{\alpha nF}{RT}\eta) - \exp(\frac{-\beta n' F}{RT}\eta)] \qquad (2.1.1)$$

Where $\eta$ is the overpotential (= $V$ - $V_{corr}$), $i$ is the measured current density, $i_{corr}$ is the corrosion current density, $F$ is Faraday's constant, $R$ is the universal gas constant, $T$ is the absolute temperature, $n$ and $n'$ are the number of electrons transferred in the anodic and cathodic reactions, and $\alpha$ and $\beta$ are coefficients related to the potential drop through the electrochemical double layer.

The equation (2.1.1), developed by Butler (1924) and Volmer (1930), is the fundamental formula for electrochemical reaction kinetics determination. However,

in its practical application to calculate the electrochemical corrosion current, the equation has to be simplified.

Although there are other ways of simplifying the Butler-Volmer equation such as the three point method (Barnartt 1970), the two most commonly used simplified forms of the equation are the Tafel equation and the Stern-Geary equation.

### 2.1.2 The Tafel equation

The Tafel equation was first found empirically by Tafel (1905). It can be deduced from equation (2.1.1) for sufficiently high values of the applied potential:

For anodic polarisation, when $\eta >> RT/\beta n'F$, the following equations are obtained

$$i = i_{corr}[\exp(\frac{\alpha nF}{RT}\eta)] \tag{2.1.2}$$

i.e. $$\eta = -\frac{2.3RT}{\alpha F}\log i_{corr} + \frac{2.3RT}{\alpha F}\log i \tag{2.1.3}$$

or, for cathodic polarisation, when $-\eta >> RT/\alpha nF$

$$i = i_{corr}[\exp(\frac{-\beta n'F}{RT}\eta)] \tag{2.1.4}$$

i.e. $$-\eta = -\frac{2.3RT}{\beta F}\log i_{corr} + \frac{2.3RT}{\beta F}\log i \tag{2.1.5}$$

The equations (2.1.3) and (2.1.5) have the form of the Tafel equation:

$$|\eta| = a + b\log i \tag{2.1.6}$$

where $a$ and $b$ are Tafel constants: $a = -\frac{2.3RT}{\alpha F}\log i_{corr}$ and $b = \frac{2.3RT}{\alpha F}$ for anodic polarisation or, $a = -\frac{2.3RT}{\beta F}\log i_{corr}$ and $b = \frac{2.3RT}{\beta F}$ for cathodic polarisation.

However, the Tafel method (also referred as the Tafel line extrapolation method) has a major disadvantage that it is destructive to test samples due to the use of high polarisation potentials. So the Tafel method is therefore of only limited value for continuous corrosion rate monitoring.

### 2.1.3 The Stern-Geary equation

In 1957, Stern and Geary simplified the Butler-Volmer formula for low polarisation (≤ 10 mV) and developed a famous equation which can be used with linear polarisation measurements to determine corrosion rate without significantly damaging the test sample (Stern and Geary 1957):

$$i_{corr} = \frac{b_a b_c}{2.3(b_a + b_c)} \times \frac{1}{R_p} \tag{2.1.7}$$

Where $i_{corr}$ is the corrosion current density, $b_a$, $b_c$ are anodic and cathodic Tafel slopes, $R_p$ is the polarisation resistance, which is defined as the tangent of a polarisation curve at the corrosion potential:

$$R_p = \left(\frac{d\eta_c}{di_c}\right)_{\eta_c \to 0} = \left(\frac{d\eta_a}{di_a}\right)_{\eta_a \to 0} \tag{2.1.8}$$

Where $\eta_a$ and $\eta_c$ are anodic and cathodic overpotentials, $i_a$ and $i_c$ are anodic and cathodic polarisation current densities.

The Stern-Geary method as shown in equation (2.1.7) has become a most popular electrochemical technique since the work of Stern and Geary. When measuring

corrosion rate using the Stern-Geary equation, only a small polarisation voltage (normally ± 10 mV) is applied to the corroding electrode. Compared to techniques using very large anodic or cathodic overpotentials such as the Tafel method, the Stern-Geary method obviously has advantages because it is basically a non-destructive technique.

The basic requirement when using equation (2.1.7) is the knowledge of $R_p$ and $b_a$, $b_c$.

The $b_a$ and $b_c$ are normally determined by Tafel curve or weight-loss measurements. They can also be estimated by linear polarisation measurement by performing a non-linear least-squares fit of the DC linear polarisation data to the Stern-Geary equation (Mansfeld 1976a; EG&G Princeton Applied Research 1993). For a more rapid corrosion rate estimation, values of the Tafel constants may be assumed to be approximately 100 mV/decade. Pourbaix (1973) has found that if $b_a$ and $b_c$ are assumed to be 100 mV/decade, the calculated corrosion rate will be correct within a factor of 2.2.

In this thesis, $b_a$ and $b_c$ were determined using the method described by Mansfeld (1976a) using software developed by EG&G Princeton Applied Research (1993).

The determination of polarisation resistance $R_p$ is the key to corrosion rate measurement using the Stern-Geary equation. Techniques such as DC linear polarisation (Stern and Geary 1957), EIS (Epelboin *et al.* 1972) and ENA (Eden *et al.* 1986) were found to be useful for determining $R_p$.

Although the DC linear polarisation is a traditional method for the experimental measurement of the $R_p$ value, under some circumstances it was found to be unreliable. Researchers in many laboratories have found that large errors can occur in measuring corrosion rates by DC linear polarisation and the corrosion rate was under-estimated

(Mansfeld 1976b; Bandy and Jones 1976; Lorenz and Mansfeld 1981; Mansfeld 1988; Tan *et al.* 1995).

The main reason for this error is that the experimental $R_p$ value contains contributions from ohmic resistances, such as the electrolyte layer resistance between the Luggin capillary and test electrode, surface scale resistance and inhibitor film resistance etc.. Although methods such as the positive feedback technique and the interrupter technique were developed to remove the effects of ohmic resistances, a detailed study of these techniques has shown that they have limitations and are very difficult to apply (Mansfeld 1988).

In some other cases, it was also reported that the DC linear polarisation technique can actually over-estimate the actual rate of corrosion (Beavers *et al.* 1993).

For these reasons, the DC linear polarisation technique is generally not applicable for systems where there is large electrolyte resistance, surface scale resistance or inhibitor film resistance etc..

Compared with the DC linear polarisation technique, EIS is a more reliable technique because EIS is supposed to be able to separate different corrosion electrochemical processes and thus be able to eliminate measurement errors due to solution resistance and surface film resistance. The application of EIS in corrosion studies will be briefly reviewed in section 2.2.

ENA showed many advantages over DC linear polarisation and EIS techniques. Electrochemical noise measurements do not apply a perturbation to the test system by an externally imposed polarisation, which would lead to inevitable changes of the system-specific properties such as the surface structure and roughness, sorption processes of inhibitors, etc.. Thus ENA might be applicable to the study of various

corrosion processes which can not be investigated by other techniques. Furthermore, electrochemical noise recording requires only simple instruments and thus offers greater convenience for on-site application (Rothwell and Eden 1992; Tan *et al.* 1996b; 1996c). Since Iverson (1967) first noted the random potential noise, the application of ENA in corrosion studies has attracted great interest around the world (Murphy 1991; Mills 1994). ENA and its application in corrosion studies will be briefly reviewed in section 2.3.

## 2.2 A Review on Corrosion Studies Using Electrochemical Impedance Spectroscopy

Since Epelboin and coworkers introduced AC impedance techniques in electrochemistry in the 1960s (Epelboin *et al.* 1972; Epelboin *et al.* 1984), EIS has been developed into a powerful and practical tool for studying corrosion electrochemical problems in various systems during the last several decades especially during the 1980's. Although there are pitfalls (Macdonald 1990) and critical issues (Orazem *et al.* 1994) associated with its application, EIS has become a very important technique which has broadened the range of corrosion phenomena which can be studied using electrochemical techniques (Mansfeld 1988). EIS has been used to study electrochemical and corrosion phenomena in areas such as semiconductors, batteries, electrodeposition, electro-organic synthesis and organic coating evaluation. In these areas EIS offers some distinct advantages over DC techniques. First, EIS uses very small excitation potential amplitudes, generally in the range of 5 to 10 mV peak-to-peak, which cause only minimal perturbation of the electrochemical test system. Second, EIS offers valuable mechanistic information because EIS can provide data on both electrode capacitance and charge transfer kinetics. Third, EIS can be used for electrodes in low conductivity solutions and with organic coatings (Mansfeld 1981).

However, only limited attention has been paid to the application of EIS in the study of $CO_2$ corrosion and its inhibitors. Only little published information can be found on the application of EIS to study $CO_2$ corrosion product scale. Although EIS was used to study and to evaluate the corrosivity of gas condensate and some continuous treatment $CO_2$ corrosion inhibitors (Lotz *et al.* 1990; Dawson *et al.* 1990; 1993; Chen 1994), only limited interpretation on experimental spectra has been carried out. Very

little attention has been paid to the potential possibility of EIS applications in the monitoring of inhibitor film persistency and in the study of inhibitor mechanisms.

In this work, attempts will be made to use EIS as a new tool for studying $CO_2$ corrosion product scales, for monitoring inhibitor film persistency and for studying inhibitor mechanisms.

This section will briefly and critically review the fundamental aspects of EIS and its application in corrosion studies, focusing on its application in corrosion rate determination in the presence of an adsorbed surface film or a dielectric organic coating.

### 2.2.1 Fundamental aspects of EIS

A number of reviews have discussed the theory of EIS and the application of EIS in corrosion studies (Gabrielli 1980; Mansfeld and Lorenz 1981; Silverman and Carrico 1988; Macdonald 1990; 1991; Mansfeld and Lorenz 1991). These reviews suggest that two main areas of application are rapid estimates of a wide range of corrosion rate and practical insights into corrosion mechanisms, especially in the presence of an adsorbed film or an applied organic coating.

The power of EIS lies in the fact that it is essentially a steady-state technique that is capable of accessing relaxation phenomena with relaxation times varying over many orders in magnitude (Macdonald 1991). The steady-state character permits the use of signal averaging methods within a single experiment to gain the desired level of precision, and the wide frequency bandwidth (e.g. $10^6$ - $10^{-4}$ Hz) permits a wide range of interfacial processes to be investigated. So EIS can be one of the principal methods for investigating electrode interfacial reaction mechanisms (Macdonald 1991).

A theoretical definition of impedance was given by Macdonald (1990) which is important for understanding the power and limitations of the technique and will be reviewed as follows:

The response of any linear system to a perturbation of arbitrary form may be described by a transfer function *H(s)*:

$H(s) = \frac{\overline{V}(s)}{\overline{I}(s)}$, where $s$ is the Laplace frequency, $\overline{V}(s)$ and $\overline{I}(s)$ are the Laplace transforms of the time-dependent voltage and current.

In terms of the steady-state sinusoidal frequency domain, the transfer function becomes

$H(j\omega) = \frac{F\{V(t)\}}{F\{I(t)\}} = \frac{V(j\omega)}{I(j\omega)}$, where $F$ signifies the Fourier transform, and $V(j\omega)$ and $I(j\omega)$ are the sinusoidal voltage and current. Provided that the system is linear, causality is obeyed, and the interface is stable over the time of sampling, the transfer function may be identified as an impedance, $Z(j\omega)$.

From a theoretical viewpoint, the impedance is one of the most important quantities that can be measured in electrochemistry and corrosion science. This is because, if it is sampled over an infinite bandwidth, it contains all the information that can be obtained from the system by purely electrical means (Macdonald 1991). In practice, although EIS measurements only sample over a limited bandwidth, EIS still provides important information about the system.

According to the discussion above, obviously, the prerequisite conditions of EIS application are: the system studied is linear, causality, and the interface is stable over the time of sampling. The amount of information depends on the sampling bandwidth. In most cases, electrochemical systems can be considered linear if the

applied perturbation amplitudes are sufficiently low. The causality can be checked using the Kramers-Kronig analysis (Mansfeld and Lorenz 1991).

In corrosion studies using EIS, normally the corroding system under test is perturbed from an initial steady state (normally the corrosion potential) by a broad band, small amplitude signal (in most cases sinusoidal). In this thesis, all EIS measurements employ a small sinusoidal signal (amplitude 5 mV). The $CO_2$ corrosion system was found to be reasonably stable and so EIS should be applicable.

Impedance is commonly written in the form $Z(j\omega) = Z_{re} - jZ_{im}$, where $j = \sqrt{-1}$, and $Z_{re}$ *and* $Z_{im}$ are frequency-dependent real and imaginary numbers, often referred to as the real and imaginary components of the impedance respectively, which are related to the magnitude of the impedance and the phase by

$$|Z(j\omega)| = \sqrt{Z_{re}^2 + Z_{im}^2}$$

$\tan\phi = -\frac{Z_{im}}{Z_{re}}$, where $\phi$ is the phase angle.

Another mathematical expression of impedance is

$$Z(j\omega) = |Z|e^{j\phi}$$

These two mathematical forms lead directly to the two common methods for displaying impedance data: the Nyquist plot ($Z_{re}$ versus $Z_{im}$) and Bode plots ($log|Z|$ vs. $log\omega$ - the Bode modulus plot, and $log\phi$ *vs.* $log\omega$ - the Bode phase plot). In this thesis both the Nyquist and Bode plots will be used because each of them offers specific advantages in certain situations. The Nyquist plot is clearer for mechanistic analysis because the number of relaxations and their mechanistic implications are

often more apparent. The Bode plots employ frequency directly as the independent variable, so that more precise comparison between experimental and calculated impedance spectra can be made.

### 2.2.2 The interpretation of EIS

The interpretation of EIS data allows one to determine the electrochemical parameters of the electrode surface and to acquire information about the corrosion process and mechanism. The corrosion rate can be calculated by determining the polarisation resistance or charge transfer resistance. Characterisation of the adsorption and desorption and film formation on the electrode surface may be studied by determining its surface capacitance.

However, the interpretation of experimental EIS data is far from easy. In fact, the power of the EIS technique is often not fully used due to the difficulties in developing suitable models for simulating the impedance behaviour and in developing fitting programs for analysing EIS data.

In this section, a brief review will be made on the interpretation of EIS data from common corrosion systems.

#### 2.2.2.1 Ideal corrosion system

In the simplest case, when corrosion is uniform and corrosion reactions are strictly charge transfer-controlled, the electrode impedance Nyquist plot will be as in Figure 2.1 (a).

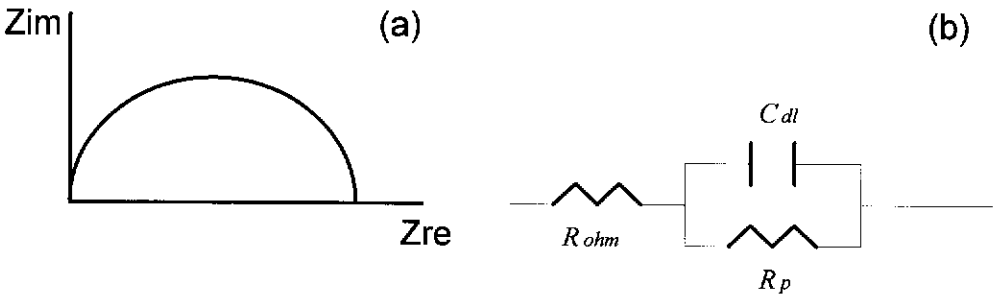


**Figure 2.1.** (a). The impedance Nyquist plot of an electrode undergoing a simple corrosion reaction. (b). Equivalent circuit simulating the simple electrode impedance. $R_{ohm}$ is the solution resistance. $R_p$ is the polarisation resistance. $C_{dl}$ is the double layer capacitance.

A simple equivalent circuit as shown in Figure 2.1 (b) can be employed to describe the impedance characteristics. The impedance for this simple equivalent circuit is given by

$$Z(j\omega) = R_{ohm} + \frac{R_p}{1 + j\omega C_{dl} R_p} \tag{2.2.1}$$

or, $$Z(j\omega) = Z_{re} - jZ_{im} \tag{2.2.2}$$

where, $$Z_{re} = R_{ohm} + \frac{R_p}{1 + (\omega C_{dl} R_p)^2}, \quad Z_{im} = -\frac{\omega C_{dl} R_p^{\,2}}{1 + (\omega C_{dl} R_p)^2} \tag{2.2.3}$$

Eliminating the frequency $\omega$ in the equations leads to

$$(Z_{re} - R_{ohm} - \frac{R_p}{2})^2 + (Z_{im})^2 = (\frac{R_p}{2})^2 \tag{2.2.4}$$

which is the equation of a semicircle in the Nyquist plot, as shown in Figure 2.1 (a), with $R_p$ as its diameter; an intercept of $R_{ohm}$ for $\omega \rightarrow \infty$; an intercept of $R_{ohm} + R_p$ for

$\omega \rightarrow 0$. The capacitance $C_{dl}$ can be determined from the resonance frequency $\omega_m$ at the maximum value of $Z_{im}$:

$$C_{dl} = \frac{1}{\omega_m R_p} \tag{2.2.5}$$

In this way, electrochemical parameters of the corrosion system, $R_{ohm}$, $R_p$ and $C_{dl}$ can be determined and the impedance characteristic of a simple corrosion system can be interpreted. $R_{ohm}$ may give information about solution conductivity; $R_p$ can be related to corrosion rate by the Stern-Geary equation: $i_{corr} = \frac{b_a b_c}{2.3(b_a + b_c)} \times \frac{1}{R_p}$, and $C_{dl}$ can provide information on adsorption and desorption phenomena, film formation processes at the electrode, and the integrity of surface films (Mansfeld 1982).

### 2.2.2.2 Practical corrosion system

However, in practice, the impedance spectra observed in simple corrosion systems experimentally often deviate from ideal behaviour and this deviation often causes confusion as to its correct interpretation.

Usually there are three forms of deviation: (i) the centre of the Nyquist semicircle depresses below the $Z_{re}$ axis; (ii) the semicircle is in a flattened form and (iii) there are one or more low frequency inductive loops. Typical impedance data which show these deviations from ideal behaviour are shown in Figure 2.2.

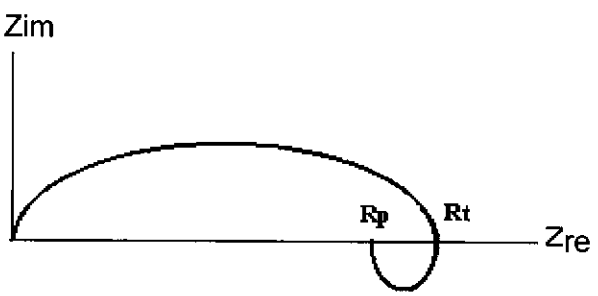


**Figure 2.2.** A typical Nyquist plot

The depressed and flattened semicircle arcs are commonly observed but are not easily explained (Williams and Asher 1984). A common interpretation for them is based on the assumption of frequency or time constant dispersion according to Cole and Cole (1941). Epelboin *et al.* (1970; 1972) have used this type of analysis of experimental impedance data. However, Lorenz and Mansfeld (1981) thought that this analysis has limitations and suggested another analysis method which was based on two severely interacting time constants. On the other hand, Roberge *et al.* (1992) attributed the depressed semicircle to localised corrosion. Orazem *et al.* (1994), however, found that several other models can actually also fit the depressed and flattened semicircles. This controversy may suggest that a careful analysis is critical for correctly interpreting impedance data in every individual corrosion system.

Mansfeld and Kendig (1985) have accounted for the depression of the semicircle arc by introducing an exponent $\alpha$ into Equation (2.2.1):

$$Z(j\omega) = R_{ohm} + \frac{R_p}{1 + (j\omega C_{dl} R_p)^{\alpha}} \tag{2.2.6}$$

However, the use of the exponent $\alpha$ in Equation (2.2.6) is only a formal description of experimental data and the physical meaning of $\alpha$ is not entirely clear (Mansfeld and Lorenz 1991).

The occurrence of low frequency loops in many experimental spectra was explained as a pseudo-inductance effect which was suggested to be due to an adsorption-desorption phenomenon in the vicinity of the corrosion potential (Epelboin *et al.* 1972).

For corrosion rate calculation from experimental impedance data, it is necessary to determine the polarisation resistance ($R_p$) or charge transfer resistance ($R_t$). Although

$R_p$ can be determined as shown in Figure 2.2, there is controversy and confusion in the determination and use of $R_t$.

According to Epelboin and co-workers (Epelboin *et al.* 1972; Epelboin *et al.* 1980), $R_t$ can be advantageously used instead of $R_p$ in a Stern-type equation. They reached this conclusion by comparing the corrosion rate deduced from $R_t$ with the weight-loss for uninhibited, inhibited and painted iron. They determined $R_t$ by the intercept of the experimental impedance data with the real axis, as shown in Figure 2.2.

However, Lorenz and Mansfeld (1981) thought that the method used by Epelboin *et al.* could lead to erroneous results. They suggested another method to determine the charge transfer resistance ($R_t$), as shown in Figure 2.3 (Lorenz and Mansfeld 1981). The $R_t$ from this method is smaller than the polarisation resistance.

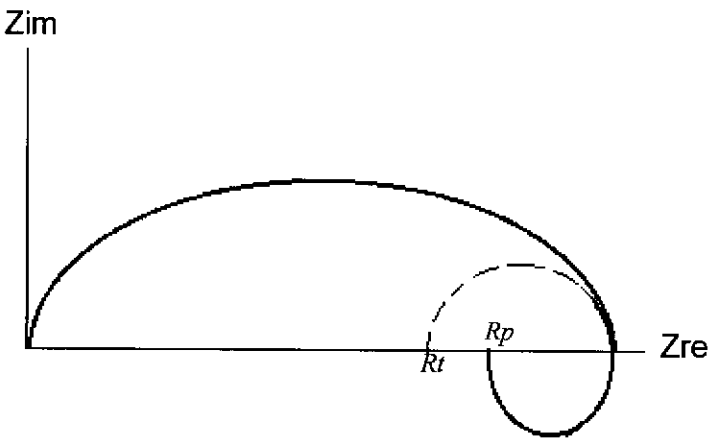


**Figure 2.3.** A method of $R_t$ and $R_p$ determination

Although there is controversy, the charge transfer resistance ($R_t$) is often used in practice to estimate corrosion currents using the Stern-Geary equation (Silverman and Carrico 1988):

$$I_{corr} = \frac{b_a b_c}{2.303(b_a + b_c)} \times \frac{1}{R_p} \approx \frac{b_a b_c}{2.303(b_a + b_c)} \times \frac{1}{R_t}$$

In the Stern-Geary equation, the non-steady state parameter $R_t$ was used instead of the steady state parameter $R_p$. From the point of view of industrial application, the error due to this is negligible. The corrosion currents can then be converted into corrosion rates, and finally used to estimate the average corrosion rate over the given exposure periods.

### 2.2.2.3. Corrosion under a non-conductive surface film

EIS was found to be especially useful in corrosion systems where an adsorbed film or an applied organic coating is present (Silverman and Carrico 1987). The $CO_2$ corrosion/inhibitor system that will be studied in this thesis is also this type of corrosion system.

The common Nyquist plot of electrode impedance of this system is shown in Figure 2.4 (a). This impedance characteristic is very common in the organic coating/metal electrode and inhibitor film/metal electrode corrosion systems and will be met frequently in this research work. The two semi-circles suggest that this is a multiple time-constant system. The semicircle at lower frequency is usually due to the corrosion electrochemical process (Silverman and Carrico 1988; Silverman 1990). The semicircle into high frequency range would be due to the inhibitor film because a surface dielectric film normally has a small time constant (Feliu *et al.* 1990; Tsai and Mansfeld 1993; Thompson and Campbell 1994). The impedance characteristics of this electrode surface can be simulated by an electrical circuit used by a number of workers for coated metal electrodes (Beaunier *et al.*; Mansfeld and Tsai), as shown in Figure 2.4 (b).

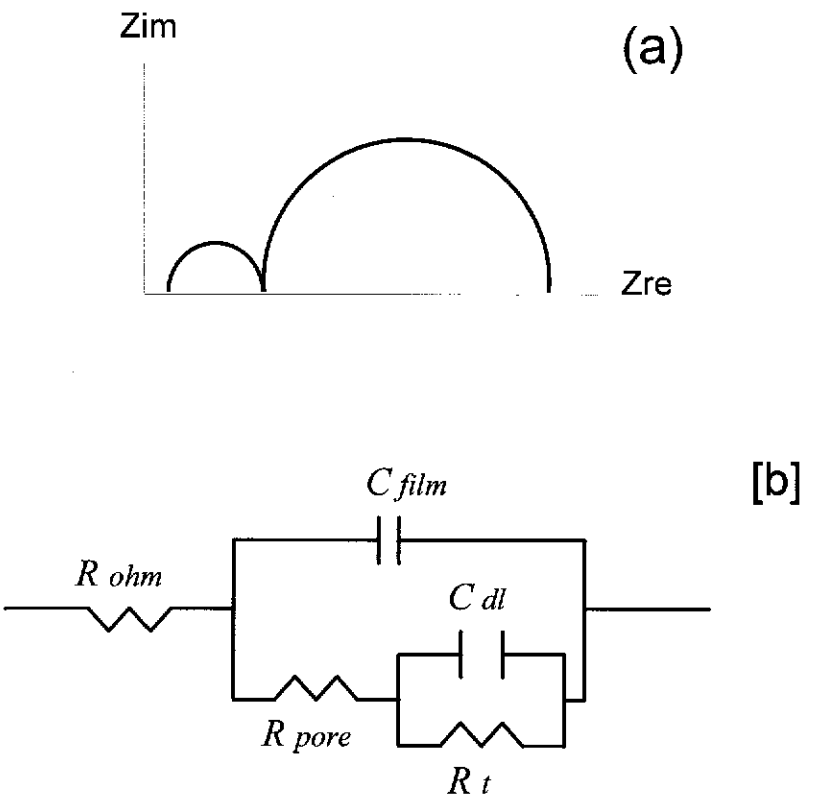


**Figure 2.4.** (a). The impedance Nyquist plot of an electrode filmed with a non-conducting surface film. (b). Equivalent circuit for the electrode. $R_{ohm}$ is the solution resistance. $R_{pore}$ is the resistance of the surface film in pore area. $C_{film}$ is the capacitance of the surface film. $R_t$ is the charge transfer resistance. $C_{dl}$ is the double layer capacitance.

However, in practical systems, there are also some difficulties in the analysis of spectra of this type. The deviations shown in the previous section (2.2.2.2) can also occur here. The shape of the Nyquist plot will appear as two distinct semicircles only if both the following criteria are met (Walter 1986): $0.2 \leq (R_t/R_{film}) \leq 5$; $\tau_{dl}/\tau_{film} \geq 20$, where $R_t$ is charge transfer resistance; $R_{film}$ coating film resistance; $\tau_{dl}$ is the time constant for the double layer; $\tau_{film}$ is the time constant for the coating film. If these relationships are not met, then the two semicircles will interact with each other or maybe even only one semicircle will be recognisable, causing difficulties in separating the components of the equivalent electrical circuit, or incorrect data analysis. In these cases, the Bode phase plot is normally used to identify the presence

of plot shape irregularities. If clear separation into two time constants does not occur, then the spectra may require more complicated data analysis to extract all component values. A computer program (Boukamp 1989), which uses a non-linear least square fit (NLLS-fit) and simulation methods to fit experimental EIS data, may help to give a correct analysis on complicated EIS data.

#### 2.2.2.4. The ambiguity in EIS interpretation

Although EIS showed its advantages in the studies of many corrosion and electrochemical problems, its limitations and pitfalls are also generally recognised (Macdonald 1990; Orazem *et al.* 1994). One of these pitfalls is the ambiguity in EIS interpretation, which was analysed in detail by Orazem *et al.* (1994).

A number of investigators have discussed the ambiguity inherent in selecting an appropriate model for interpreting impedance spectra (Macdonald 1987; Silverman 1991; Orazem *et al.* 1994). It was pointed that a number of plausible models can be found to fit a given EIS result. The true situation of the system may be different from the simplest suggested model which would normally be used to simulate the practical system. Therefore, model identification requires additional information and the improvement of model identification capabilities is especially important (Orazem *et al.* 1994). EIS, like any other electrochemical technique, can not be regarded as being a 'stand-alone' technique.

The development of proper models requires a knowledge of the chemistry and physics sufficient to suggest reasonable models, prior or new information sufficient to allow the researcher to reject inadequate models, and an understanding of the characteristics of the measured values to be used for comparison to the model (Orazem *et al.* 1994).

For these reasons, as with all other electrochemical measurement methods, EIS has to be applied only very cautiously, with a prior knowledge of the system-specific corrosion behaviour. Moreover, experimental as well as theoretical results, established in one corroding system, cannot be generalised and applied to other corroding systems without great care (Lorenz and Mansfeld 1981).

### 2.2.3 The application of EIS in corrosion and prevention

EIS has been used in almost every aspect of metal corrosion and prevention to acquire mechanism related information and to evaluate the corrosivity of the environment and the efficiency of corrosion control methods.

#### 2.2.3.1 The investigation of anodic film and corrosion product scales using EIS

The formation of an anodic film and the precipitation of corrosion product scale are common phenomena and may greatly affect further corrosion processes and mechanisms. EIS has been used to provide new and more detailed information concerning these surface layers and their effect on further corrosion. Several typical examples are given as follows:

As early as 1962, Hoar and Wood studied the sealing of porous anodic oxide films on aluminium with AC bridge measurements and proposed relevant equivalent circuits (Hoar and Wood 1964). Bodu *et al.* (1977) used EIS to evaluate the corrosion resistance of anodised Al and concluded that the impedance test could be equivalent to the salt spray test. Mansfeld and Kendig (1985) have attempted to develop a quality control and corrosion test for anodised Al alloys based on EIS.

Park and Macdonald (1983) studied the growth of oxide films on carbon steel in high temperature aqueous systems using EIS. It was concluded that EIS is well suited for studying the growth of porous surface films in high-temperature systems.

Lotz *et al.* (1990) successfully recorded the $CO_2$ corrosion scale formation process using EIS. They found that with the exposure of the electrode in a $CO_2$ saturated brine, a protective corrosion scale was built up which resulted in changes in spectral characteristics. Unfortunately, however, that study was not detailed and the results were not analysed in detail because it was not the main purpose of that work. A more detailed investigation of $CO_2$ corrosion scale using EIS will be carried out in the work of this thesis.

Agarwal *et al.* (1993) studied the formation of oxide film on a copper surface using EIS. They recorded spectra, with obviously different behaviour, from copper electrodes in solutions of different pH values. The oxide film formed at pH 11.5 was found to be very protective which was indicated by the large electrode impedance. The oxide formation at pH 7 was found to be much slower and that process was monitored by EIS. In acid solutions, however, EIS showed a decrease in polarisation resistance which was attributed to the dissolution of the oxide film.

Phosphate conversion layer, which has similar characterisations to normal corrosion product scales, was also studied using EIS (Bretherton *et al.* 1993). It was found that the subsequent film growth, after the end of coating formation, has a significant role in improving the protective properties of the phosphate conversion layer.

### 2.2.3.2 The evaluation of organic coatings using EIS

One of the most successful applications of EIS has been in the study and evaluation of organic coatings, which cannot be readily investigated with traditional DC techniques.

With the recent introduction of convenient electrochemical impedance measurement instrumentation, the EIS technique is rapidly gaining popularity in this area. EIS is also used to produce both quantitative kinetic and mechanistic information for the development of improved coating systems.

The large amount of literature published in this area makes it clear that EIS is suitable for the study of polymer coated metals. These applications of EIS include the evaluation of water uptake by a coating film; degradation of coatings with exposure time; the investigation of the disbonding of coatings; determination of the active area at which corrosion occurs and the estimation of corrosion rates at the metal/coating interface. Several review papers have been published in this area (Walter 1986; Mansfeld 1994) describing the power and limitations of the EIS technique.

The most interesting application of EIS to industry is the possibility of using impedance parameters, which were measured at early exposure times, to predict significant long-term coating deterioration. Kendig *et al.* (1983) discussed the possibility of predicting the long-term corrosion behaviour of a coated metal based on the measurement of $R_p$. Scully (1989) compared impedance data developed at short times to the coating system's performance after 550 days exposure and found that coating resistance, changes in the frequency for a 45 degree phase angle, and low frequency impedance data detected at exposure times ranging from 2 to 200 days can be used to predict long-term coating performance.

### 2.2.3.3 The study of corrosion inhibitors using EIS

EIS has also been successfully used to study metal/inhibitor systems. EIS has provided useful information concerning the interaction of inhibitors with metal surfaces during exposure to corrosive media, and on inhibition efficiency (Mansfeld and Lorenz 1991).

One of the first systems to be investigated by EIS was iron in sulfuric acid containing propargylic alcohol (Epelboin *et al.* 1972). Later, Lorenz and Mansfeld (1981) reinvestigated this system and also investigated systems such as iron and steel in aerated and deaerated 0.5 M sulfuric acid and 1 M hydrochloric acid in the absence and presence of triphenylbenzylphosphonium chloride, 2-butyne-1,4-diol and hexynol. Although experimental spectra are often complicated, much mechanism and inhibition efficiency related information was deduced from these data. A concept of interface and interphase inhibition was discussed by Mansfeld *et al.* (1985) based on EIS analysis.

The inhibition in neutral, aerated media was also studied by EIS. Mansfeld and co-workers (Mansfeld *et al.* 1982b; Mansfeld and Lorenz 1991) investigated inhibition by $NaNO_2$, a fatty amine containing inhibitor, and $Na_2Cr_2O_7$ in neutral, aerated environments. In inhibitor-free $Na_2SO_4$ solutions, very similar impedance spectra were observed in the presence and absence of $NaNO_2$. However, in deionised water containing 10 mM $NaNO_2$, two time constants can be resolved in the impedance spectra. For the fatty amine containing inhibitor, an additional time constant can also be observed at high frequencies in the spectra which were similar to those for polymer coatings on steel. From the high-frequency portion of the impedance spectrum, the pore resistance of the inhibitor film and its changes with time can be determined. Two time constants in the impedance spectrum have also been observed after short exposure times in NaCl containing $Na_2Cr_2O_7$. The impedance at high frequencies, which corresponds to the porous corrosion product layer containing the inhibitor, becomes larger with increasing exposure time as the surface layer becomes denser.

EIS was also found to be very helpful in studying corrosion inhibition in low-conductivity media (Mansfeld *et al.* 1982b; Duprat *et al.* 1985). In deionised water, a large solution resistance, which was much larger than the polarisation resistance, was recorded (Mansfeld and Lorenz 1991). EIS shows the ability to separate solution

resistance from polarisation resistance and so errors due to 'ohmic drop' can be avoided.

Synergism is a very important phenomenon in inhibition technology. EIS was shown to be useful to elucidate the mechanism of synergism. For example, Kalman *et al.* (1994) studied the possible cooperation between the surface oxide layer and carbon steel inhibitor 1-hydroxy-ethane-1,1-diphosphonic acid. Azim and co-workers (Azim *et al.* 1995) studied the influence of iodide ions on the synergistic inhibition of mild steel in an acidic solution.

Although the application of EIS for the evaluation of oilfield corrosion inhibitors in brine/$CO_2$ systems is rarely reported in the literature, reports in recent publications have shown the possibility of this application. Dawson and co-workers (1990; 1993) used EIS to evaluate the effect of shear stress on inhibitors tetraethyl ammonium chloride and benzyl dimethyl n-hexadecylammonium chloride. Chen (1994) used EIS to evaluate several continuous treatment inhibitors. However, these studies have not been carried out in a detailed way. Very little attention was paid to the potential possibility of EIS applications in the monitoring of inhibitor film persistency and in the study of inhibitor mechanisms.

## 2.3 A Review on Corrosion Studies Using Electrochemical Noise Analysis

Since Iverson (1968) first noted random potential noise in electrochemical corrosion systems, the possibility of applying electrochemical noise analysis (ENA) in corrosion studies has attracted great interest all around the world. After being developed for more than two decades, ENA has already been shown to be a useful tool in corrosion rate measurement (Eden *et al.* 1986; Searson and Dawson 1988), and also in localised corrosion studies (Hladky and Dawson 1981), even though these applications are still controversial subjects (Mansfeld and Xiao 1993; Gusmano *et al.* 1993).

ENA offers many advantages over other electrochemical techniques. Firstly, electrochemical noise measurement supposes to be working in a free corrosion condition and does not need to apply a perturbation on the test system by an externally imposed polarisation, which would lead to inevitable changes of the system-specific properties such as the surface structure and roughness, sorption processes of inhibitors, etc.. Thus ENA might be applicable to the study of various corrosion processes which can not be investigated by other techniques. Secondly, electrochemical noise recording requires only simple instruments and is experimentally simple, thus offering greater convenience for on-site application. Furthermore, ENA is supposed to be able to continuously monitor both general corrosion and localised corrosion, thus offering great potential to overcome the problems in the continuous monitoring of uniform corrosion rate and in localised corrosion monitoring.

However, ENA is still a developing technique. Most of its applications are still very

controversial and are based on empirical correlations. In the work of this thesis, attempts will be made to further develop this technique and to use it as a new tool for studying and monitoring inhibitor film persistency in $CO_2$ corrosion environment.

This section will briefly review the fundamental aspects of ENA, its applications in corrosion studies, controversies and problems associated with these applications.

### 2.3.1 Fundamental findings on electrochemical noise

Although spontaneous fluctuations of electrode potential are a well known and an easily observable phenomenon, any possible links to electrochemical corrosion processes were not documented until 1968. In a series of experiments, Iverson (1968) measured potential fluctuations between a platinum electrode and various working electrodes, including aluminium, magnesium, iron, mild steel, zinc and another platinum electrode. It was found that aluminium and magnesium electrodes exhibited rapid voltage fluctuations with frequency 1-2 Hz and with amplitude greater than 100 μV. Iron, steel and zinc electrodes exhibited a different type of voltage fluctuations with frequency 0.2-0.6 Hz and with amplitude between 50-60 μV. However, it was also observed that the voltage fluctuations between two platinum electrodes, which are supposed to be corrosion-resistant, are negligible. When an inhibitor (sodium nitrite) was introduced into the solution with mild steel and aluminium electrodes, it was found that the voltage fluctuations disappeared. Based on these experimental results, Iverson concluded that voltage fluctuations were directly related to the corrosion reactions and corrosion rates. He further hypothesised that electrode voltage fluctuations may relate quantitatively to the electrode corrosion rate. He suggested the possibility of studying the corrosion process and quantitatively measuring the corrosion rate by analysing electrode voltage fluctuations.

This type of spontaneous voltage (or current) fluctuations is defined as electrochemical noise (Barker 1969).

To explain the nature, production mechanism and meaning of electrode voltage and current noise, Iverson (1968) postulated that the electrode voltage fluctuations are a result of minute transient changes in the electrical charge on the electrode produced during the corrosion process. These minute transient changes in the electrical charge may be due to a difference in charge between the anodic and cathodic reactions present at any small interval in time, or due to the transient changes in cathodic and anodic areas. Barker (1969) concluded that the production of electrochemical noise is expected if electrode charge transfer is catalysed by a minor component of the interface or if an electrochemical system is remote from its equilibrium. Gabrielli *et al.* (1978) connected the electrochemical noise of an electrocrystallization process to the structural organisation of electrodeposits. Epelboin *et al.* (1979) concluded that electrochemical noise could be linked to gaseous hydrogen evolution. Bertocci (1980; 1981) linked electrochemical noise to localised corrosion processes. Hladky and Dawson (1982) thought that the corrosion potential fluctuation reflects changes in the state of dynamic equilibrium of a real corroding electrode. However, these explanations are generally qualitative and lack detailed experimental evidence. Generally, until now, the nature, production mechanism, and meaning of electrode voltage and current noise are not clearly understood.

Although there are difficulties in explaining electrochemical noise, several important findings have already shown the possibility of applying electrochemical noise in corrosion studies.

### 2.3.1.1 Findings regarding corrosion rate determination by ENA

Although Hladky and Dawson (1982) observed and supposed a qualitative correlation between the rate of corrosion and the standard deviation of voltage noise, the first quantitative relationship between electrochemical noise and corrosion rate was found by Eden *et al.* (1986). Eden *et al.* found that a noise resistance ($R_n$), which can be deduced from voltage and current noise data by $R_n = \sigma_V / \sigma_i$, is comparable to polarisation resistance ($R_p$), i.e. $R_n \approx R_p$. This relationship can thus be used to calculate the corrosion rate from electrochemical noise analysis. However, Mansfeld and Xiao (1993) maintained that the similarity between noise resistance and polarisation resistance does not hold for every system. Studies on the theoretical background of this empirical relationship are obviously necessary and important for understanding its potential and limitations.

In a recent paper, a theoretical analysis on the physical meaning of noise resistance was made by Chen and Bogaerts (1995), where it was shown that the noise resistance is equivalent to the polarisation resistance under certain conditions. Tan *et al.* (1996a; 1996b; 1996c) confirmed the similarity between noise resistance ($R_n$) and polarisation resistance ($Rp$) experimentally and explained the noise resistance as a 'Statistical Linear Polarisation' resistance. The limitations and advantages of noise resistance are also discussed as a part of this thesis.

Another quantitative relationship between electrochemical noise and corrosion rate was found by Searson and Dawson (1988). After analysing the correlations between weight-loss and standard deviation of voltage noise, Searson and Dawson suggested an empirical linear relationship between standard deviation of voltage noise ($\sigma_V$) and corrosion rate: $\sigma_V \times 10^{-5}$ = corrosion rate (mpy). Although this linear relationship was not confirmed by Gusmano *et al.* (1993), it was agreed by Gusmano *et al.* that there is a 'reliable' correlation between the standard deviation of voltage noise and corrosion attack. Instead of a linear relationship, Gusmano *et al.* suggested a

logarithmic relation between $R_p$ and the standard deviation of voltage noise. However, Legat and Zevnik (1993) did not confirm these relationships and found that the correlation between voltage noise and corrosion rate was very poor. Tan *et al.* (1996b; 1996c) did not confirm these relationships either. In fact, upon examining the experimental data points which were used to deduce these relationships (Searson and Dawson 1988; Gusmano *et al.* 1993), large scatter can be found. More careful and detailed investigations are obviously necessary to confirm or refute these empirical relationships.

The third relationship between electrochemical noise and corrosion rate was suggested by Legat and Zevnik (1993). They calculated the average power-spectrum density ($\overline{PSD}$) for current noise at various frequency intervals (from 1 mHz to 1 Hz) and found that the current noise power-spectrum density calculated in the frequency interval from 10 to 100 mHz can be an exact measure of general corrosion.

#### 2.3.1.2 Findings regarding localised corrosion monitoring by ENA

Electrochemical noise was also found to be linked with localised corrosion. Bertocci and co-workers (Bertocci 1980; 1981; Bertocci and Kruger 1980; Bertocci *et al.* 1983) studied passive film breakdown, pit initiation, and transpassivity by computing noise spectra from current fluctuations under potentiostatic conditions. It was found that below the pitting potential, the amplitude of the noise spectra was indistinguishable from instrumentation noise. However, spectra recorded close to the pitting potential yielded larger noise amplitudes, particularly at lower frequencies. When the potentials were more noble than the pitting potential, the amplitudes of the current noise increased by over two orders of magnitude. Significant increases in low frequency current noise were also detected in advance of pit propagation.

Hladky and Dawson (1981) also observed characteristic potential fluctuations on electrodes undergoing either pitting or crevice corrosion. It was found that pitting of Al in NaCl exhibited bursts of noise every 10 - 15 minutes with an amplitude of about 0.1 mV. Hladky and Dawson (1982) investigated the low frequency spectra of the corrosion potential fluctuations, using a spectrum analyser, and observed a constant amplitude over a range of very low frequencies (below 10 mHz) which decreases in amplitude at higher frequencies (roll-off). It was found that the noise power spectrum was unique for the type of corrosion. Based on these findings, Hladky and Dawson (1981; 1982) suggested that the form of the noise power spectra could give information on the nature of attack and differentiate between uniform and localised corrosion and that electrochemical noise analysis could be used as an indicator of localised corrosion. In particular, Searson and Dawson (1988) observed a roll-off of -20 dB/decade for pitting attack and -40 dB/decade for general-type corrosion.

However, these findings by Hladky and Dawson were not completely corroborated by researchers in other laboratories. Mansfeld and Xiao (1993) found that a roll-off of -20 dB/decade in noise power spectrum is not necessarily the characteristic of localised corrosion. Legat and Zevnik (1993) concluded that it is the difference between voltage and current noise power-spectrum densities, not the 'roll-off' in the noise power spectrum, that is related to the type of corrosion. Gusmano *et al.* (1993) did not completely confirm the findings of Hladky and Dawson. In general, they did not find any clear correlation between noise power spectrum slopes, test parameters and corrosion behaviour.

The link between electrochemical noise and localised corrosion may be explained by the stochastic nature of corrosion processes (Gabrielli *et al.* 1991). However, more investigation is obviously necessary in this area.

### 2.3.2 The analysis of electrochemical noise

Although raw electrochemical noise data contains information about corrosion potential trends (DC shift) and some general information about the noise pattern such as noise amplitude, it does not provide answers about the corrosion rate and corrosion pattern. Further analysis is needed for the application and interpretation of electrochemical noise.

At present, voltage and current noise are assumed to represent a stochastic process and are therefore classified as nondeterministic and are described in terms of probability and statistics (Searson and Dawson 1988). Three main types of statistical function can be used to describe the basic properties of stationary random processes: mean square values, probability density functions, and spectral density functions (Bendat and Piersol 1986). Although noise analysis can be conducted in several ways, normally electrochemical noise data can be analysed by two methods: (i). to analyse the noise-time records statistically; (ii). to transform noise-time data into the frequency domain and analyse noise power spectral density plots. The former approach is used to estimate the corrosion rate and the later is normally used to differentiate corrosion pattern, based on the findings described in the previous sections (2.3.1.1 and 2.3.1.2).

Before all of these analyses, a preprocess has to be applied to raw noise data. This consists of removing the DC trend from noise recordings (Uruchurtu and Dawson 1987; Searson and Dawson 1988; Lumsden *et al.* 1992).

#### 2.3.2.1 Removing DC trends from raw noise data

Corrosion potential shift (DC trend), a very low-frequency component of the raw noise record, is very common in electrochemical corrosion systems. If such low-frequency

trends are not removed from the data, large distortions can occur in the later processing of noise analysis (Bendat and Piersol 1986; Searson and Dawson 1988).

The standard technique for trend removal is to fit a low-order polynomial to the data using the least squares procedures (Bendat and Piersol 1986; Uruchurtu and Dawson 1987). Specifically, let the original data value $u_n$ be fit with a polynomial of degree $K$ defined by

$$\tilde{u}_n = \sum_{k=0}^{K} b_k (n\Delta t)^k \qquad n = 1, 2, .....N$$

A 'least square' fit is obtained by minimising the squared discrepancies between the data values and the polynomial given by

$$Q = \sum_{n=1}^{N} (u_n - \tilde{u}_n)^2 = \sum_{n=1}^{N} [u_n - \sum_{k=0}^{K} b_k (n\Delta t)^k]^2$$

To minimise the Q value, the partial derivatives of Q with respect to $b_k$ are taken and set equal to zero:

$$\frac{\partial Q}{\partial b_k} = 0$$

A detailed mathematical procedure for the least squares fit was given by Bendat and Piersol (1986). In nature, this procedure is equivalent to applying a high pass filter to the data and, as this type of frequency component can not be removed by digital filtering, a mathematical algorithm for correction is used (Searson and Dawson 1988).

The least-squares method is traditionally used to remove DC trend from the electrochemical current and potential noise and was used by many researchers (Searson and Dawson 1988; Lumsden *et al.* 1992). However, a serious problem exists in this method. In practice, DC trend may follow any pattern and is normally not

linear, nor in fact can it be fitted by a simple polynomial. So in most cases the least-squares method is not practical, and an improved method has to be developed.

### 2.3.2.2 The statistical analysis of noise data

The statistical analysis of electrochemical noise data is based on the findings described in the previous section (2.3.1.1). The standard deviation of voltage or current noise is often used to estimate the corrosion rate from noise data.

Standard deviation is defined as the root mean square deviation from the mean. For voltage noise,

$$\sigma_V = \sqrt{\frac{\sum_{i=1}^{n}(V_i - m_v)^2}{n}}$$

where $V_i$ is an individual voltage value; $n$ is the number of total datum points; $m_v$ is the mean of all of the voltage noise datum points:

$$m_v = \frac{\sum_{i=1}^{n} V_i}{n}$$

Similarly, for current noise,

$$\sigma_i = \sqrt{\frac{\sum_{i=1}^{n}(I_i - m_i)^2}{n}}$$

$$m_i = \frac{\sum_{i=1}^{n} I_i}{n}$$

Thus,

$$\sigma_i = \sqrt{\frac{\sum_{i=1}^{n}\left(I_i - \frac{\sum_{i=1}^{n} I_i}{n}\right)^2}{n}}$$

The noise resistance, defined by Eden *et al.* (1986) is written as,

$$R_n = \frac{\sigma_V}{\sigma_i}$$

Where $\sigma_V$ and $\sigma_i$ are the standard deviations of voltage and current noise in an experimental 'run', e.g. 1000 seconds.

The statistical analysis of noise data is widely used and thought to have advantages over other analysis techniques (Mansfeld and Xia 1993).

### 2.3.2.3 Noise power spectral density plots

Another method of electrochemical noise analysis is by noise power spectral density (*PSD*) plots, which is the standard procedure of presenting noise data in the frequency domain. This method is commonly used to differentiate between uniform and localised corrosion. The findings on which this method is based were described in the previous section (2.3.1.2).

*PSD* is one of the frequency domain representations of a time domain signal and is defined as the power of a signal at a given frequency. The *PSD* tells what frequencies are present in a noise signal and what are their magnitudes because the *PSD* value at a particular frequency is proportional to the square of the signal amplitude at that frequency, thus *PSD* is often used to characterise the source of signals (Harris and Ledwidge 1974). A typical *PSD* plot contains three basic parameters: the slope of the high frequency linear region, the roll-off frequency, and the DC limit at the lowest frequencies. These parameters are used to differentiate between uniform and localised corrosion

The *PSD* functions can be produced by transforming the voltage and current records from the time domain into the frequency domain by Fast Fourier Transformation (FFT) or the maximum entropy method (MEM). FFT is one of usual mathematical tools for signal analysis. A detailed mathematical procedure of FFT is given by Bendat and Piersol (1986). MEM can also be used to transfer noise data from the time domain into the frequency domain. MEM produces smoother plots than those obtained with the FFT and does not make any assumptions about the variables outside the sampling times (Simoes and Ferreira 1987; Searson and Dawson 1988), so MEM is used more frequently in electrochemical noise analysis.

PSD has units of $V^2$/Hz for voltage noise and $A^2$/Hz for current noise, which is used by several research groups (Bertocci 1981; Gabrielli and Keddam 1992; Monticelli, *et al.* 1992). However, another group preferred to use spectral density, which is represented as noise amplitude rather than noise power and has the traditional unit decibel (db) (Hladky and Dawson 1982; Uruchurtu and Dawson 1987). The noise amplitude is the square root of noise power and is given by db = 20 log (voltage ratio). An amplitude of 1 V is arbitrarily defined as 0 db, and so spectral density can be calculated by db = 20 log (voltage or current value). Uruchurtu and Dawson (1987) argued that this procedure offers greater convenience.

## 2.4 Some New Developments in ENA Technique and Theory

As reviewed in the previous section (2.3), ENA is still a developing technique and there are controversies and problems associated with almost all of its applications. Several basic questions associated with ENA application may be expressed as follows:

(i). What are the theoretical backgrounds of electrochemical noise analysis techniques? It is a fact that almost all applications of ENA are based on empirical correlations. The origin of electrochemical noise is not clearly known.

(ii). Why are published ENA data often strongly fluctuating? In fact, in the study for this thesis, large fluctuations were also experienced when raw noise records were analysed.

(iii). Regarding the noise resistance ($R_n$) method, what is the theoretical meaning of $R_n$ and what are its limitations? Although a theoretical analysis on the physical meaning of $R_n$ was recently made by Chen and Bogaerts (1995), the exact theoretical meaning of $R_n$ and its limitations are still not clear. Mansfeld *et al.* (1993) believed that the similarity between $R_n$ and polarisation resistance ($Rp$) does not hold for every system. Dawson *et al.* (1993) thought that ENA can be used to determine corrosion rates but only in systems which are accessible to LP and EIS, and also in systems which have a lower conductivity. However, no evidence was given to support these statements. It is very important to know in which systems the $R_n$ technique can be correctly used.

As contributions to the ENA technique, two new methods and a theoretical analysis are developed and will be described in the following sections to address some of the

above questions. These new methods will be used and tested experimentally in this thesis.

### 2.4.1 Moving Average Removal

This is a new method for removing the DC trend from electrochemical noise data.

The collected noise-time record may be a combination of a random noise component and a DC trend component. A pre-processing treatment of removing DC trend from noise data should be essential for further noise data analysis because the DC trend may cause large distortions in the later processing of noise data. In this work, a new method of electrochemical noise analysis, moving average removal (MAR), was used for DC trend removal. The idea of this method is to remove the average values from the noise record because the average values (changing with time) should be a good estimation of the DC trend. Although a similar method has been in use for some time for high pass filtering of signals, MAR has not been used for electrochemical noise analysis. This method is briefly explained as follows:

A series of voltage-time records ($k$ data points), $\{V_n\}_{n=1,2,3,...i,\ i+1,\ i+2,...k}$, is experimentally recorded. Any individual data point in the group $\{V_n\}$, $V_i$, is a combination of the random noise component and the DC trend component which are functions of time, $t$.

$$V_i(t) = V_{i,noise}(t) + V_{i,DC}(t)$$

$V_{i,noise}(t)$ is the real noise and is required for future noise analysis. $V_{i,DC}(t)$ is the DC trend component which has to be removed.

The central assumption is that an average value of adjacent data points of $V_i$, $\bar{V}_i$, can be taken as an estimation of $V_{i,DC}$ *(t)*.

$\bar{V}_i(p) = \{ \sum_{i-p}^{i+p+1} V_i \} / (2p+2)$ , where $p$ can be 1, 2, 3 or more. For example, if we take $p$ = 3, this means taking three data points on the left and four data points on the right of $V_i$ for the average calculation,

$$\bar{V}_i(3) = [V(i-3) + V(i-2) + V(i-1) + \mathbf{V(i)} + V(i+1) + V(i+2) + V(i+3) + V(i+4)]/8$$

The DC trend in the voltage-time record can therefore be removed and the random fluctuation $V_{i,noise}$ can be deduced as,

$$V_{i,noise} = V_i - \bar{V}_i$$

Obviously, for each voltage-time record point, an individual average voltage can be calculated and so the average voltage is 'moving'. These average values actually form a 'base' line along which the noise signals fluctuate. Figure 2.5 schematically shows the moving average removal of a hypothetical noise signal.

The trend removal using the moving average removal method was carried out in Microsoft Excel, and with a value of $p$ = 3. The same method can also apply for current noise.

This method will be used and tested in the experimental work of this thesis.

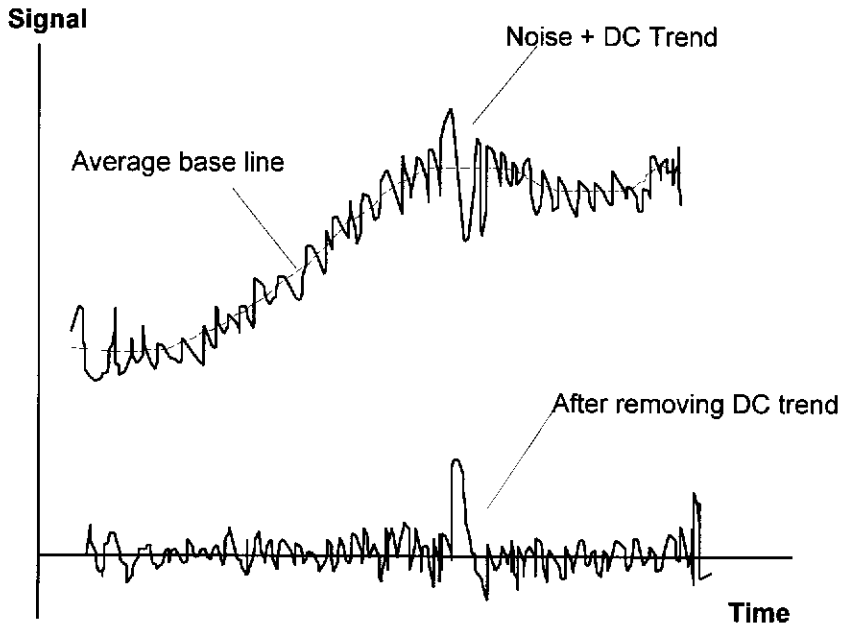


**Figure 2.5.** A schematic diagram showing the moving average removal (DC trend removal).

### 2.4.2 A New Method of Instantaneous Corrosion Monitoring

The noise resistance ($R_n$) is given by the ratio of the standard deviation of voltage noise and the standard deviation of current noise:

$$R_n = \frac{\sigma_V}{\sigma_i}$$

In previous applications, the time window used for $R_n$ calculation was quite large, normally an experimental 'run', e.g. 1024 seconds (Eden and Rothwell 1992) or 500 seconds (Lumsden *et al.* 1992; Mansfeld and Xiao 1993). In these applications, only an average $R_n$ can be obtained over the large time window.

A new method may be used for instantaneous corrosion monitoring. Instead of using a large time window, small continuous time windows may be used.

If a series of voltage-time records ($k$ data points), $\{V_1; V_2; V_3;....V_{i-1}; V_i; V_{i+1};....V_k\}$, and corresponding current-time records, $\{I_1; I_2; I_3;....I_{i-1}; I_i; I_{i+1};....I_k\}$, are experimentally recorded. For a datum point of voltage and current noise, $V_i$ and $I_i$, a small data series of $2m+1$ neighbour points (in time window $\Delta t$), can be used to calculate noise resistance $V_{n,i}$.

$$R_{n,i} = \frac{\sigma V\{V_{i-m}; V_{i-m+1}....V_i; V_{i+1};.....V_{i+m}\}}{\sigma I\{V_{i-m}; V_{i-m+1}....V_i; V_{i+1};.....V_{i+m}\}}$$, Where $\sigma_V\{V_{i-m}; V_{i-m+1}; V_i;....V_{i+m}\}$ and $\sigma_I\{I_{i-m}; I_{i-m+1}; I_i;....I_{i+m}\}$ are the standard deviations of voltage and current noise data ($2m+1$ neighbour points of $i$).

In this way, a $R_n$ value can be calculated for each data point of voltage and current noise, forming a series of $R_n$ values: $\{R_{n,m}.....R_{n,i-1};R_{n,i}; R_{n,i+1};.... R_{n,k-m}\}$. Thus, a corrosion process can be continuously monitored by plotting the $R_n$ value series.

This technique has special advantages when analysing corrosion systems where parameters such as potential are subject to rapid change, e.g. immediately after inhibitor addition. In this study, a small time window $\Delta t$ = 9.5 seconds was used, which means $m$ = 9 because the sampling rate was 2 points/second.

### 2.4.3 A Theoretical Analysis of Noise Resistance

The noise resistance may be explained using a concept of statistical linear polarisation.

Electrodes a and b, as shown in Figure 2.6, are assumed to be identical and exist in the same environment. Voltage and current are recorded using high input impedance voltage- and zero resistance current-meters.

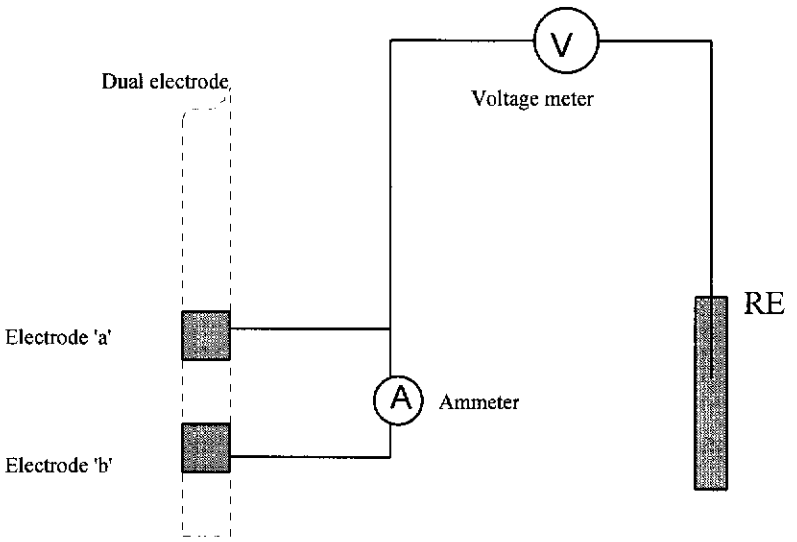


**Figure 2.6.** A schematic diagram showing the dual electrode and noise measurement system

It can be assumed that all electrochemical properties of the two identical electrodes are the same. For example, the electrodes have the same surface area, corrosion potential ($V_{corr}$), corrosion current density ($i_{corr}$), DC potential shift ($V_{DC}$), Tafel slopes ($b_a, b_c$) and polarisation resistance ($R_p$) etc..

However, the electrochemical potentials of the two electrodes, at a certain time $t$, are not necessary identical due to random signals of electrochemical noise.

For electrode 'a', potential at time '$t$' can be written,

$$V_a(t) = V_{DC}(t) + V_{a,noise}(t) \qquad (2.4.3.1)$$

where $V_{DC}(t)$ is the DC component of the potential and $V_{a,noise}(t)$ is the potential noise of electrode 'a' at time '$t$'.

For electrode 'b', similarly

$$V_b(t) = V_{DC}(t) + V_{b,noise}(t) \quad (2.4.3.2)$$

By substituting (2.4.3.2) into (2.4.3.1), the potential difference between electrodes 'a' and 'b' can be deduced:

$$V_a(t) - V_b(t) = V_{a,noise}(t) - V_{b,noise}(t) \quad (2.4.3.3)$$

Obviously, the difference between $V_a(t)$ and $V_b(t)$ is due to the difference in random potential noise, which could produce current noise between electrodes 'a' and 'b', $I_{noise}(t)$ .

If the combined potential of the coupled electrode system at time $t$ is $V_{system}(t)$, which is determined using a high input impedance voltage meter simultaneously with current noise recording, and $V_a(t) < V_{system}(t) < V_b(t)$, i.e. at time $t$ electrode a is anodically polarised and electrode b is cathodically polarised, the overpotential for electrode 'a', $\Delta V_a(t)$, is

$$\Delta V_a(t) = V_{system}(t) - V_a(t) \quad (2.4.3.4)$$

Similarly, the absolute value of the overpotential for electrode 'b', $\Delta V_b(t)$, is

$$|\Delta V_b(t)| = V_b(t) - V_{system}(t) \quad (2.4.3.5)$$

The amplitude of electrochemical noise is very small, so $\Delta V_a(t)$ and $\Delta V_b(t)$ are much smaller than 10 mV. If the corrosion reactions are totally activation-controlled and corrosion is uniform, then polarisation is linear and the Stern-Geary equation can be used to calculate the corrosion current for each of the two electrodes (Stern and Geary 1957).

From electrode a, the corrosion current can be calculated by the equation,

$$i_{corr}(t) = \frac{b_a b_c}{2.3(b_a + b_c)} \left(\frac{i_{noise}(t)}{\Delta V_a(t)}\right) \quad (2.4.3.6)$$

where $i_{noise}(t)$ is the noise current at time $t$.

Similarly for electrode b, the corrosion current can be calculated by the equation,

$$i_{corr}(t) = \frac{b_a b_c}{2.3(b_a + b_c)} \left(\frac{i_{noise}(t)}{|\Delta V_b(t)|}\right) \qquad (2.4.3.7)$$

Re-writing and combining equations (2.4.3.7) and (2.4.3.6),

$$\Delta V_a(t) + |\Delta V_b(t)| = 2 \times \frac{b_a b_c}{2.3(b_a + b_c)} \left(\frac{i_{noise}(t)}{i_{corr}(t)}\right) \qquad (2.4.3.8)$$

The Stern-Geary equation can also be written as

$$i_{corr}(t) = \frac{b_a b_c}{2.3(b_a + b_c)} \times \frac{1}{R_p} \qquad (2.4.3.9)$$

Substituting (2.4.3.9) into (2.4.3.8) gives

$$[\Delta V_a(t) + |\Delta V_b(t)|]/2 = i_{noise}(t) \times R_p \qquad (2.4.3.10)$$

Substituting (2.4.3.3), (2.4.3.4) and (2.4.3.5) into (2.4.3.10) gives,

$$[V_{b,noise}(t) - V_{a,noise}(t)]/2 = i_{noise}(t) \times R_p \qquad (2.4.3.11)$$

The standard deviations of both sides of the equation 2.4.3.11 during the testing period should be equal:

$$\sigma\{[V_{b,noise} - V_{a,noise}]/2\} = \sigma\{i_{noise} \times R_p\} \qquad (2.4.3.12)$$

At time $t$, the potential measured by the voltage meter in Figure 2.6 is the combined potential of the coupled electrode system, $V_{system}(t)$. After removing DC trend in the system potential, the noise component, $V_{noise,\ system}(t)$ can be deduced :

$$V_{noise,\ system}(t) = V_{system}(t) - V_{DC,\ system}(t) \qquad (2.4.3.13)$$

Because the system is under linear polarisation and the anodic and cathodic polarisation have the same slope ($1/R_p$), the combined system noise potential should be the mean of the two individual electrodes. $V_{noise,\ system}(t)$ can be written as,

$$V_{noise,\ system}(t) = [V_{b,noise}(t) + V_{a,noise}(t)]/2 \qquad (2.4.3.14)$$

The standard deviations of both sides of the equation 2.4.3.14 during the testing period should be equal:

$$\sigma V_{noise,\ system} = \sigma\{(V_{b,noise} + V_{a,noise})/2\} \qquad (2.4.3.15)$$

$V_{b,noise}(t)$ and $V_{a,noise}(t)$ are independent identical random signals. Statistically, it is expected that,

$$\sigma\{(V_{b,noise} - V_{a,noise})/2\} = \sigma\{(V_{b,noise} + V_{a,noise})/2\} \qquad (2.4.3.16)$$

Substituting equations 2.4.3.12 and 2.4.3.14 into 2.4.3.16 gives,

$$\sigma V_{noise,\ system} = \sigma\{i_{noise} \times R_p\} \qquad (2.4.3.17)$$

The standard deviation of system noise voltage noise is

$$\sigma V_{noise,\ system} = \sqrt{\frac{\sum_{j=1}^{n}(V_{j,\ noise,\ system} - m)^2}{n}} \qquad (2.4.3.18)$$

where $n$ is the number of data points recorded during the testing period. $m$ is the mean $(\frac{\sum V_j}{n})$ of potential in the time period, which should be zero in value because the potential noise is a random signal.

Similarly,

$$\sigma\{i_{noise} \times R_p\} = R_p \times \sqrt{\frac{\sum_{j=1}^{n}(i_{j,\,noise} - 0)^2}{n}} = R_p \times \sigma i_{noise} \qquad (2.4.3.19)$$

Substituting equations 2.4.3.19 into 2.4.3.17 gives,

$$\sigma V_{noise,\,system} / \sigma i_{noise} = R_p \qquad (2.4.3.20)$$

i.e. $$\sigma V / \sigma i = R_p \qquad (2.4.3.21)$$

Equation 2.4.3.21 indicates that the ratio of the standard deviation of the potential noise and the standard deviation of current noise is indeed equal to the polarisation resistance.

# Chapter III

# STUDIES OF $CO_2$ CORROSION PRODUCT SCALES USING ELECTROCHEMICAL AND SURFACE CHARACTERISATION TECHNIQUES

## 3.1. Introduction

As discussed in sections 1.1.4 and 1.1.5, the $CO_2$ corrosion product scale plays an important role in the mechanism of, and protection against $CO_2$ corrosion. In fact, the formation of corrosion product scale is linked to almost all of the most important issues in $CO_2$ corrosion science and engineering. For example, the scale is the key factor resulting in the invalidity of the de Waard-Milliams equation, significant changes in $CO_2$ corrosion mechanism and kinetics, and localised $CO_2$ corrosion.

Although the importance of the $CO_2$ corrosion product scale has led to intensive investigation during the last two decades, as discussed in section 1.4.1, the question of how to quantify the protection of $CO_2$ corrosion product scale and its effects on further $CO_2$ corrosion is still one of the most difficult topics in $CO_2$ corrosion engineering.

In this chapter, EIS is used to study the formation of the corrosion product scales using pre-scaled electrodes, as an attempt to quantify the protection of $CO_2$ corrosion product scale and to achieve a better understanding of the electrochemical properties of the scales.

For a better understanding of the protection mechanism of corrosion product scales, in addition to the EIS experiments, X-ray diffraction (XRD), Fourier transform infrared spectrometry (FTIR) and the scanning electron microscope (SEM) are used to examine the chemical composition, crystal structure and surface morphology of corrosion product scales.

## 3.2. Experimental

### 3.2.1. Materials and Solutions

(i). Electrodes

Mild steel K1035 (AS 1441-1983) was used for all working electrodes (cylinder electrodes, 1.2 cm in diameter and 0.8 cm in length, surface area 3.02 $cm^2$) and weight-loss coupons (2 cm in length and 1 cm in width, surface area 4.0 $cm^2$). The electrodes were made from rod steel whereas coupons were made from thin sheet steel. Spectrographic analysis gave the chemical composition of the steel as,

| C | Mn | Si | S | P | Ni | Cr | Mo | Cu | Al |
|---|---|---|---|---|---|---|---|---|---|
| 0.35 | 0.75 | 0.21 | 0.009 | 0.015 | 0.03 | 0.03 | 0.01 | 0.01 | 0.024 |

An Ag/AgCl electrode was used as a reference electrode. A platinum plate electrode with large surface area (about 20 $cm^2$) was used as the counter electrode.

(ii). Testing Solution

A 3% NaCl solution, pre-sparged with $CO_2$ for 2 hours, was used as the test solution for $CO_2$ corrosion scale formation and as the electrochemical test fluid. NaCl was of AR quality. Water was purified by a Millipore Milli-Q system. The $CO_2$ used was of food grade and was pre-treated with a catalysed copper system to remove the traces of oxygen. The oxygen removal system contains 30% copper highly dispersed on a carrier with activating substances in the form of 5 × 5 mm pellets and was made by Wyandotte Corp. USA.

### 3.2.2. The pre-scaling of electrodes and coupons

Ideally, the formation of corrosion product scales should be studied *in-situ*. However, due to the limitations in experimental instruments, in this work, pre-scaled electrodes were used for electrochemical measurements and pre-scaled weight-loss coupons were used for FTIR, XRD, SEM analysis.

Electrodes and coupons, polished with 400 and 800 grit Silicon Carbide paper and cleaned with ethanol and isopropanol, were pre-scaled under several typical temperature, pressure and brine volume conditions. At low pressure (1 atm), electrodes and coupons were pre-scaled in a beaker containing 640 mL of brine. At high pressure, electrodes and coupons were pre-scaled in a high pressure reactor (PARR Instrument Company, USA) containing 640 mL of brine and also a high pressure autoclave (Autoclave Engineers, Pennsylvania USA) containing 64 mL of brine.

After a certain period of scaling time, EIS measurements were carried out using the pre-scaled electrode. Although the atmospheric pressure EIS measurements were simply carried out in the scaling solution, the electrochemical measurements studying high pressure scales could not be carried out in high pressure due to instrumental limitations. In these tests, pre-scaled electrodes were taken out from the high pressure reactor or autoclave and rapidly transferred into an electrochemical testing cell operating under normal pressure of 1 atmosphere. EIS measurements were carried out immediately after this transference. $CO_2$ sparging was continued during electrode transfer for minimising air contact of the pre-scaled electrodes. In this way, the electrochemical measurements for studying high pressure scales were greatly simplified because these measurements did not need to be carried out at high pressure. Direct electrochemical measurement using a high pressure electrochemical system would be very complicated and expensive. The procedure used here, although not

ideal, indeed greatly simplified the experimental procedure and effectively decreased the requirements for expensive apparatus.

For further examination, the pre-scaled coupons were not washed but only dried in a vacuum at room temperature. Then, a $N_2$ sparged desiccator was used to store dried coupons to protect against further corrosion before using for FTIR and XRD, and SEM examinations and finally weight-loss measurement.

$CO_2$ sparging was continued during all the experimental procedures except in the high pressure reactor and autoclaves where $CO_2$ was pre-sparged and then sealed under $CO_2$ pressure to maintain an $O_2$-free environment.

### 3.2.3. Electrochemical measurements

The electrochemical cell for EIS measurements is schematically shown in Figure 3.1.

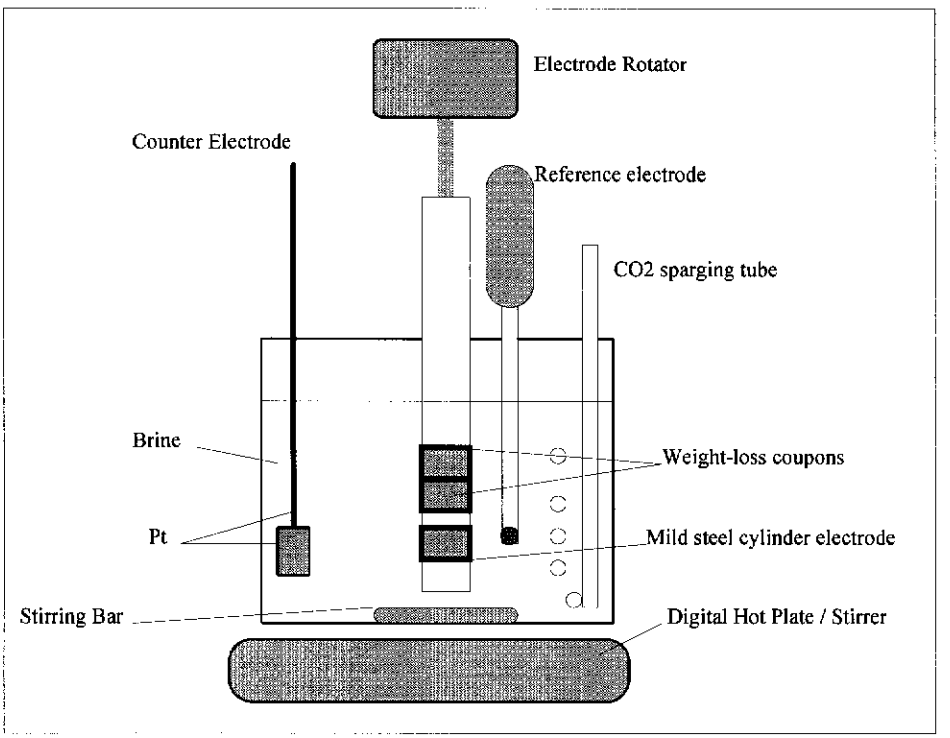


**Figure 3.1.** A schematic diagram of the electrochemical cell setup

A computer controlled system (software model 398, EG&G Princeton Applied Research) with a model 5210 Lock-in Amplifier and a model 273A Potentiostat/Galvanostat was used for EIS measurements. EIS measurements were carried out at the open circuit potential with an amplitude of 5 mV in the frequency range from about 1 mHz to 100 kHz. The basic testing solution was 640 mL of 3% NaCl brine. The working electrode was fitted to an electrode rotator which was controlled by a speed controller (Model MSRX, Pine Instrument Company). A three electrode system with Ag/AgCl as the reference electrode and platinum as the auxiliary electrode was used for electrochemical measurements. EIS measurements were carried out at one atmosphere and different temperatures with continuous $CO_2$ sparging.

### 3.2.4. Surface Characterisation

(a). X-ray diffraction (XRD)

An XRD instrument model DACO-MP (Siemens) was used for direct XRD measurement of scale on coupon surfaces. The determination of chemical composition was carried out by comparison of experimental lines with standard data as listed in Table 3.1.

**Table 3.1.** Standard higher intensity peaks of substances (JCPDS-ICDD 1991)

| Name | Standard Higher Intensity Peaks 1 | | | Standard Higher Intensity Peaks 2 | | | Standard Higher Intensity Peaks 3 | | | Standard Higher Intensity Peaks 4 | | |
|---|---|---|---|---|---|---|---|---|---|---|---|---|
| | d (Å) | $I/I_1$ | 2θ | d (Å) | $I/I_1$ | 2θ | d (Å) | $I/I_1$ | 2θ | d (Å) | $I/I_1$ | 2θ |
| Fe | 2.03 | 100 | 44.6 | 1.17 | 30 | 82.3 | 1.43 | 20 | 65.0 | | | |
| $Fe_3C$ | 2.07 | 100 | 43.7 | 2.10 | 80 | 42.9 | 1.98 | 65 | 45.9 | 1.85 | 45 | 49.1 |
| $FeCO_3$ | 2.79 | 100 | 32.0 | 1.73 | 35 | 52.8 | 1.96 | 20 | 46.2 | 2.13 | 20 | 42.4 |
| $Fe_2O_3$ | 2.70 | 100 | 33.2 | 2.52 | 70 | 35.6 | 1.69 | 45 | 54.1 | 1.84 | 40 | 49.5 |
| $Fe_3O_4$ | 2.53 | 100 | 35.5 | 1.61 | 85 | 57.0 | 1.48 | 85 | 62.6 | 2.10 | 70 | 43.1 |
| FeO | 1.52 | 100 | 60.7 | 1.51 | 100 | 61.2 | 0.96 | 100 | 106.1 | 0.96 | 100 | 107 |
| Cr | 2.04 | 100 | 44.4 | 1.18 | 30 | 81.7 | 0.91 | 20 | 115.3 | | | |
| Mn | 2.14 | 100 | 42.2 | 1.89 | 35 | 48.1 | 1.13 | 25 | 85.7 | 0.84 | 25 | 132.7 |
| *$Fe(HCO_3)_2$ | 6.38 | | ~13.9 | | | | | | | | | |

* From Xia *et al.* (1989)

(b). Fourier transform infrared spectrometry (FTIR)

A Perkin-Elmer model 1720 instrument was used for FTIR measurements on detached scale (using a KBr disc). The determination of chemical composition was made by comparing experimental vibrational bands with standard data as listed in Table 3.2.

**Table 3.2.** Standard vibrational bands of substances (Nakamoto 1986)

| Name | vibrational bands ( $\upsilon_1$ ) $cm^{-1}$ | vibrational bands ( $\upsilon_2$ ) $cm^{-1}$ | vibrational bands ( $\upsilon_3$ ) $cm^{-1}$ | vibrational bands ( $\upsilon_4$ ) $cm^{-1}$ |
|---|---|---|---|---|
| $H_2O$ | 3219 | 1627 | 3445 | |
| $CaCO_3$ (Calcite) | | 879 | 1429 - 1492 | 706 |
| $CaCO_3$ (Aragonite) | 1080 | 866 | 1492, 1504 | 706, 711 |
| $FeCO_3$ (Siderite) ♣ | | 866 | 1418 - 1441 | 737 |
| $\alpha$-$Fe_2O_3$ # | 650 - 630 | 580 - 525 | 480 - 440 | 380 - 300 |
| $Fe_3O_4$ # | | 570 | 450 | 390 |

♣ Standard sample test result (CSIRO, Australia)
# From Bewick *et al.* (1991)

(c). Optical microscopy and scanning electron microscopy

A Nikon LABOPHOT-2 microscope was used to visually investigate corroded coupon surfaces and to take microscopic photographs on typical areas of the surface of corroded coupons. A JEOL JSM-35C scanning electron microscope was used for SEM analysis.

## 3.3. Results and Discussion

### 3.3.1 The formation of $CO_2$ corrosion product scales

Electrodes pre-corroded under several typical conditions were studied using EIS for monitoring the formation of corrosion product scales and for investigating the electrochemical properties of the scales.

#### 3.3.1.1. Corrosion scale formation under high pressure conditions

The formation of corrosion product scales under four typical high pressure scaling conditions was investigated in this work:

(i). 100 psi (689.5 kPa) pure $CO_2$; 30 °C; 640 mL brine in a high pressure reactor

(ii). 100 psi pure $CO_2$; 30 °C; 64 mL of brine in a high pressure autoclave

(iii). 100 psi pure $CO_2$; 70 °C; 640 mL brine in a high pressure reactor

(iv). 100 psi pure $CO_2$; 70 °C; 64 mL brine in a high pressure autoclave

The volume of $CO_2$ in high pressure reactor was 360 mL and in the high pressure autoclave was 36 mL.

Test (i) was carried out in a relatively large volume pressure reactor. A mild steel cylindrical electrode was exposed in the pressure reactor, which contained 640 mL of $CO_2$-saturated 3% NaCl brine at 30 °C. The pressure reactor was carefully pre-sparged with $CO_2$ before being pressured to 100 psi pressure. The non-working areas of the electrodes were sealed with Silicone sealant (made by Dow Corning Australia Pty Ltd.) before scaling tests. The electrodes were kept stationary during the scaling test periods. After being scaled, each electrode was rapidly transferred from the pressure reactor into an electrochemical cell which contained 640 mL of $CO_2$-saturated 3% NaCl brine (30 °C, 1 atmospheric pressure) for EIS measurements.

Test (ii) was carried out in a small volume autoclave. Four mild steel cylindrical electrodes were individually pre-scaled for different durations at 30 °C, under 100 psi pure $CO_2$ pressure in the autoclave which contained only 64 mL of $CO_2$-saturated 3% NaCl brine. The electrode preparation, exposure, transference and EIS measurement procedures were the same as test (i).

Test (iii) was carried out in a large volume pressure reactor in a similar way to test (i) except that the scaling temperature was 70 °C. After being scaled, each electrode was rapidly transferred from the pressure reactor into an electrochemical cell which contained 640 mL of $CO_2$-saturated 3% NaCl brine (70 °C, atmospheric pressure) for EIS measurements.

Test (iv) was carried out in a small volume autoclave. The experimental procedures were similar to the high pressure reactor test (iii) except that the brine in the autoclave was only 64 mL in volume.

3.3.1.1.1 Small volume autoclave tests

Rapid corrosion product scale formation, indicated by characteristic changes in EIS plots, occurred in the small volume autoclave tests. Figures 3.2 and 3.3 show EIS Nyquist and Bode plots recorded from electrodes exposed to high $CO_2$ pressure in small volume autoclaves at 70 °C for various periods of time (test iv) and at 30 °C for various periods of time (test ii) individually. These plots were recorded immediately after the pre-scaled electrodes were transferred into electrochemical testing cells.

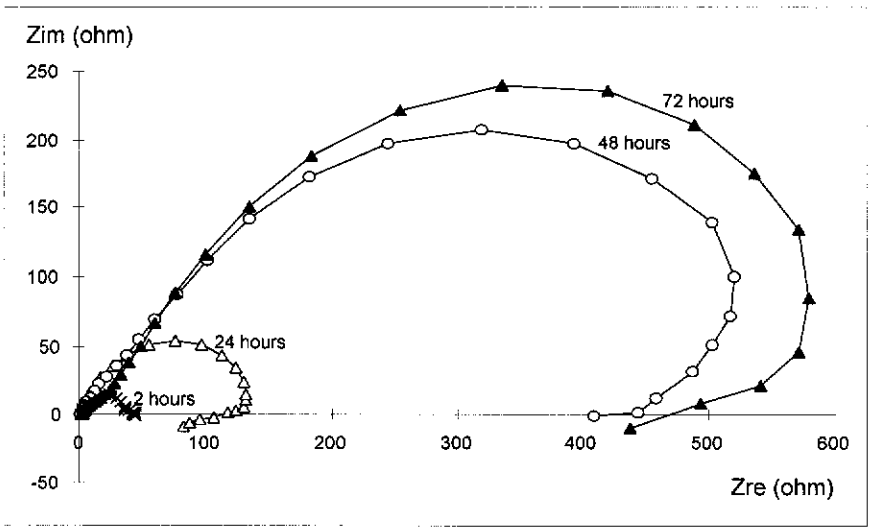


Figure 3.2 (a)

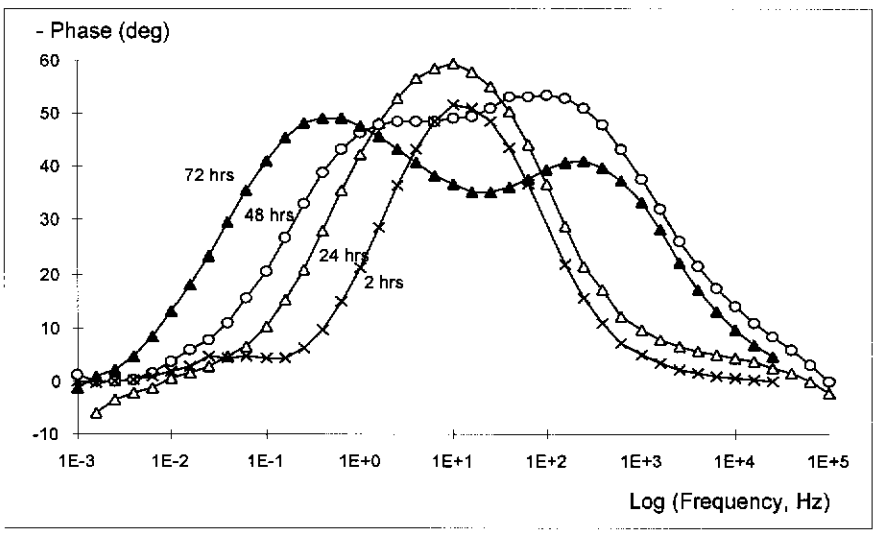


Figure 3.2 (b)

**Figure 3.2.** (a) Nyquist plots and (b) Bode phase plots recorded from pre-scaled electrodes which were exposed individually to 64 mL of $CO_2$-saturated 3% NaCl brine for 2; 24; 48 and 72 hours at 70 °C, 100 psi pure $CO_2$.

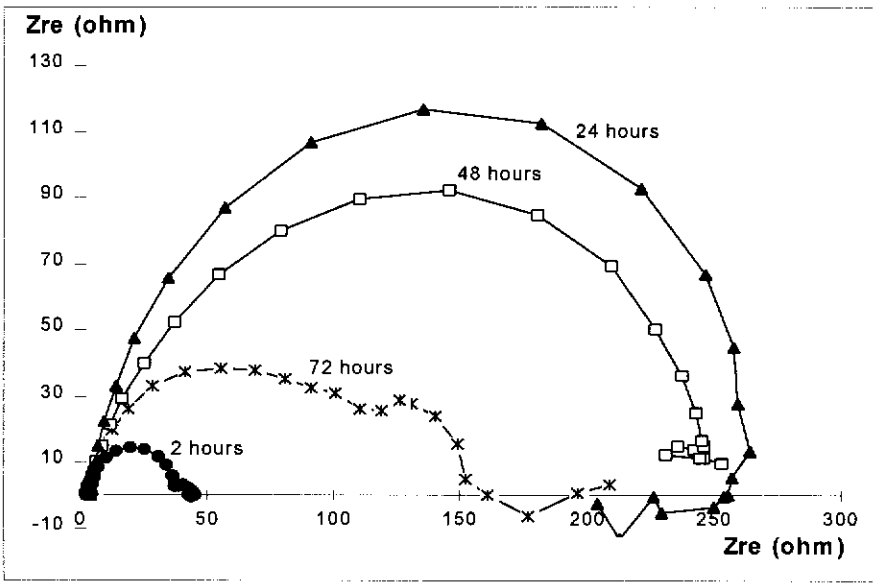


Figure 3.3 (a)

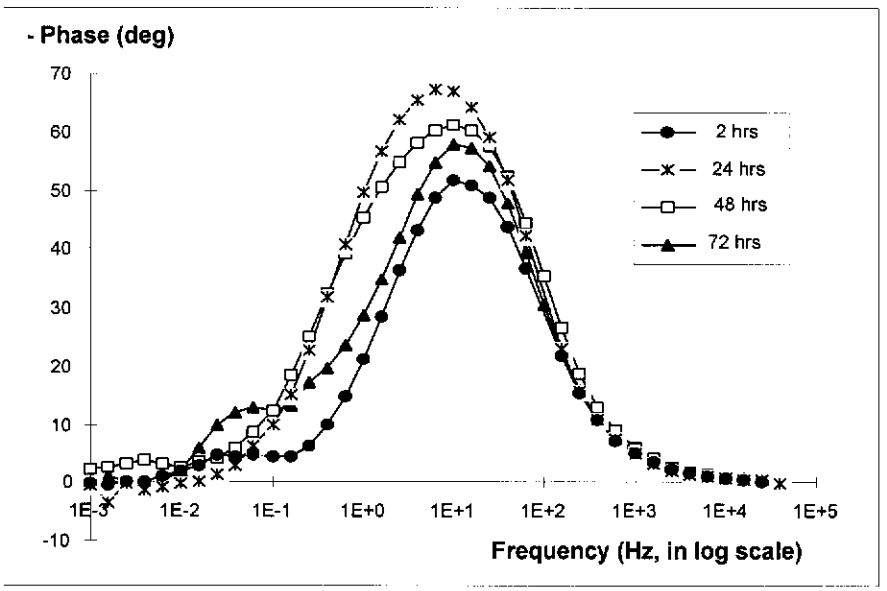


Figure 3.3 (b)

**Figure 3.3.** (a) Nyquist plots and (b) Bode phase plots recorded from pre-scaled electrodes which were exposed individually to 64 mL of $CO_2$-saturated 3% NaCl brine for 2; 24; 48 and 72 hours at 30 °C, 100 psi pure $CO_2$ pressure.

A significant increase in electrode impedance, indicated by the diameters of Nyquist plots, has already occurred after the electrodes were exposed to the corrosion environment for 24 hours, as shown in Figures 3.2 (a) and 3.3 (a). This suggests that the electrochemical corrosion kinetics of the electrode surface have been greatly changed by the exposure. These changes can be attributed to the formation of corrosion product scales.

In the case of scale formation at 70 °C, the diameter of Nyquist semi-circles in Figure 3.2 (a) shows a continuous increase with exposure time, which suggests the formation of a protective corrosion product scale and a continuous improvement in the corrosion scale protective ability. Its corresponding Bode phase angle plots in Figure 3.2 (b), which were plotted using the same experimental data used for the Nyquist format plots, show that the single phase angle peak showing in the 2 and 24 hours plots was overtaken by two phase angle peaks showing in the 48 and 72 hours plots, which suggests the occurrence of significant changes in the electrode interfacial structure. The new phase angle shift in the higher frequency range is most likely due to the formation of corrosion product scale because its appearance correlates with the corrosion scale formation and also because a surface dielectric film normally has a small time constant and so has a phase angle shift in the high frequency range (Feliu *et al.* 1990; Tsai and Mansfeld 1993; Thompson and Campbell 1994). The phase angle shift at lower frequency can be attributed to the corrosion electrochemical process (Silverman and Carrico 1988; Silverman 1990).

Different EIS plots were recorded from electrodes which were pre-scaled at 30 °C, as shown in Figure 3.3, the diameter of Nyquist semi-circles did not show a continuous increase with exposure time. As shown in Figure 3.3 (a), electrode impedance decreased after 24 hours. This suggests that the corrosion product scale, formed during the first 24 hours, was destroyed in some way, e.g. due to changes in scale structure and adherence loss with extended exposure. The Bode phase angle plots in

Figure 3.3 (b), which were plotted using the same experimental data used for the Nyquist format plots, do not show an extra high frequency peak as was observed in Figure 3.2 (b). This suggests that the surface scales formed at 30 °C were not intact and there must be weak areas in the scale. These weak areas, according to the experiments by Thompson and Campbell (1994), can result in a very small pore resistance and thus a very small scale time constant which is too small to respond in the frequency range applied.

These results confirmed that corrosion product scale formed at higher temperature is more protective. However, the experimental results question the validity limits of the de Waard-Milliams equation, 60 °C, established by most of researchers (de Waard and Milliams 1975a; Schmitt 1984b; Ikeda *et al.* 1984; Murata *et al.* 1984) because corrosion product scale with a certain protective ability can actually form at 30 °C under high $CO_2$ pressure. Only the validity limit set by Eriksrud and Sontvedt (1984), 20 °C, is consistent with this experimental result.

Figures 3.2 and 3.3 clearly show that the formation of a corrosion product scale on the electrode surface can result in characteristic changes in the EIS plots. This demonstrates that EIS can be an indicator of corrosion scale formation. It also proves that the simplified test procedure used in this work, although being not ideal, indeed can provide useful information about the corrosion product scale.

By further analysing EIS data, in principle, it is possible to derive all of the electrochemical parameters of the electrode through semicircle fitting of Nyquist plots and more information about corrosion scale formation can be deduced. As an example, as shown in Figure 3.4 (a) and (b), the 72 hours Nyquist plot in Figure 3.2 (a) is fitted by semicircles using the equivalent circuit model in Figure 3.5. This equivalent electric circuit model, as discussed in section 2.2.2.3, is commonly used to simulate the electrode surface with a non-conductive surface film present. Methods

discussed in section 2.2.2 were employed in calculating electrode electrochemical parameters: solution resistance ($R_{ohm}$); the resistance of the corrosion product scale in pore areas ($R_{pore}$); the capacitance of the corrosion product scale ($C_{scale}$); the electrochemical charge transfer resistance ($R_t$) and the double layer capacitance ($C_{dl}$).

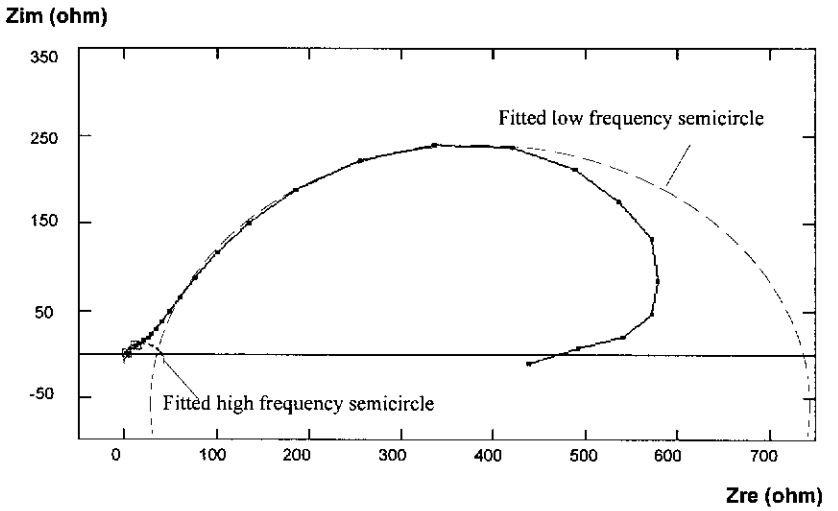


Figure 3.4 (a)

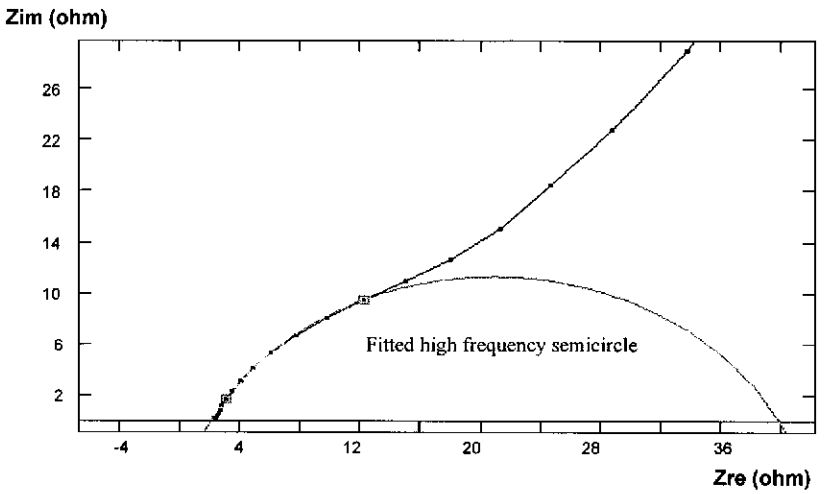


Figure 3.4 (b)

**Figure 3.4.** (a), semicircle fittings of the 72 hours Nyquist plot from Figure 3.2. (b), enlargement of semicircle fitting of high frequency data points.

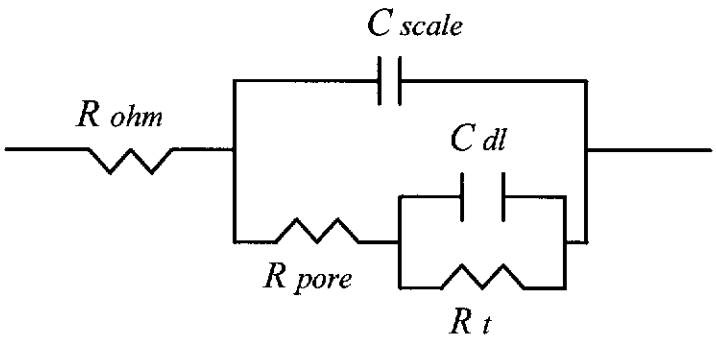


**Figure 3.5.** Equivalent circuit for an electrode filmed with a non-conducting corrosion product scale.

As shown in Figure 3.4 (a), two semicircles can be fitted to the Nyquist plot, although one is much smaller than the other and is not very clearly resolved. The higher frequency semicircle fitting is enlarged in Figure 3.4 (b). The lower frequency semicircle fitting, however, is not good for the very low frequency data points because they deviate from ideal behaviour. There are several possible causes for this deviation. The most obvious possibility is that the surface scale deteriorated during the measurement period, resulting in lower impedance values, affecting the low frequency impedance measurements which took a much longer time to acquire than high frequency impedance measurements. As a consequence, the semicircle fitting in this work was based mainly on the higher frequency data points. Despite being not ideal, this analysis gives a reasonable estimation of the electrochemical parameters of the pre-scaled electrodes. The ideal experimental procedure which would solve this problem, of course, is the expensive and technically challenging high pressure *in-situ* electrochemical tests. Cole and Cole (1941) frequency dispersion, as discussed in section 2.2.2.2, may be another reason for this large low frequency deviation. The cause for the dispersion may be local scale thickness variation, surface heterogeneity, surface roughness etc..

3.3.1.1.2 Large volume pressure reactor tests

Figures 3.6 and 3.7 show EIS plots recorded from electrodes exposed to 640 mL of $CO_2$-saturated brine at 70 °C in a pressure reactor (test iii) and from other electrodes exposed to 640 mL of $CO_2$-saturated brine at 30 °C in a pressure reactor (test i). These plots were recorded immediately after the pre-scaled electrodes were transferred into electrochemical testing cells at atmospheric pressure.

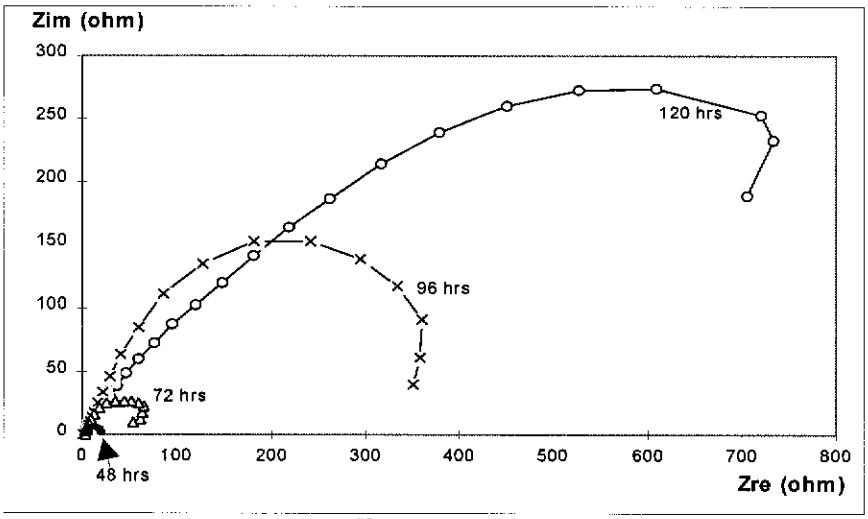


Figure 3.6 (a)

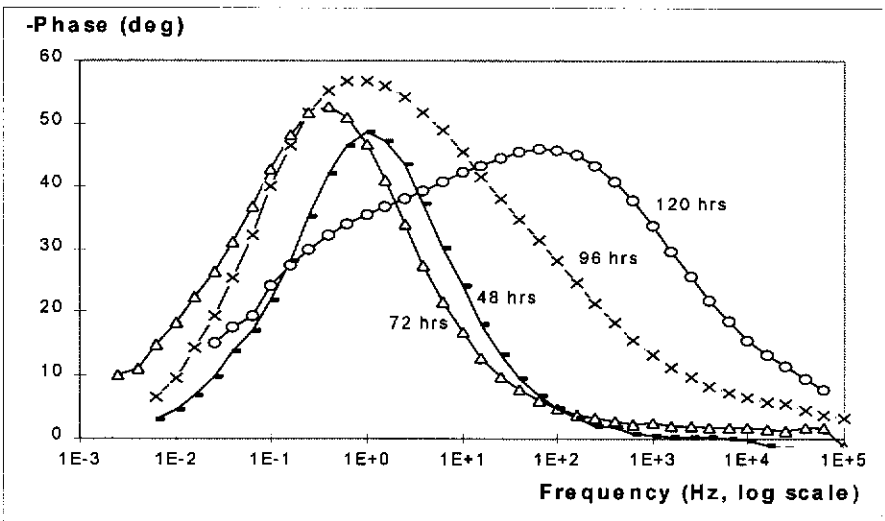


Figure 3.6 (b)

**Figure 3.6.** (a) Nyquist plots and (b) Bode phase plots recorded from pre-scaled electrodes which were exposed individually to 640 mL of $CO_2$-saturated 3% NaCl brine for 48; 72; 96 and 120 hours at 70 °C, 100 psi pure $CO_2$.

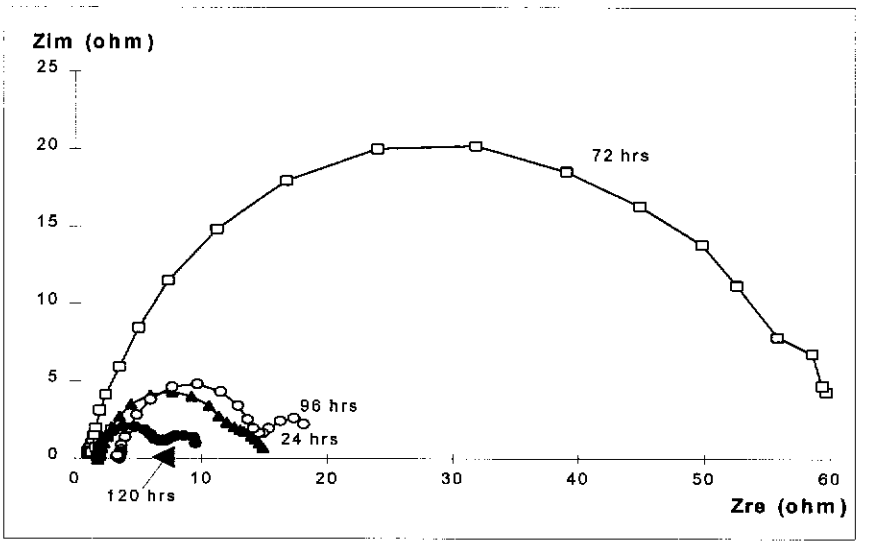


Figure 3.7 (a)

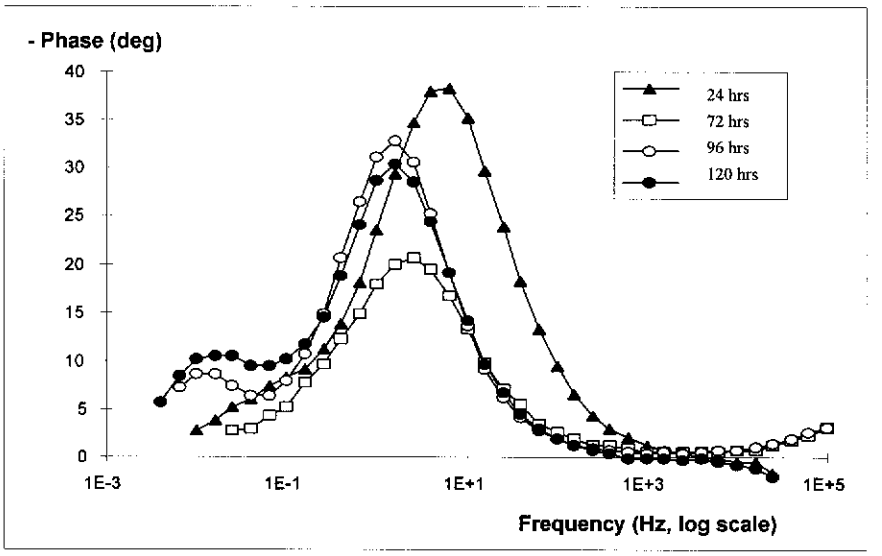


Figure 3.7 (b)

**Figure 3.7.** (a) Nyquist plots and (b) Bode phase plots recorded from pre-scaled electrodes which were exposed individually to 640 mL of $CO_2$-saturated 3% NaCl brine for 24; 72; 96 and 120 hours at 30 °C, 100 psi pure $CO_2$.

Similar to Figure 3.2, a new high frequency time constant appeared in the 120 hours curve of Figure 3.6 which suggests that an intact protective scale can also form in the large volume pressure reactor at 70 °C. However, comparing Figure 3.2 with Figure

3.6, obviously the formation of corrosion product scale in the large volume pressure reactor was much slower than in the small volume autoclave. In the large volume reactor, a large increase in electrode impedance did not occur until 96 hours, whereas it has already occurred in the small autoclave in 48 hours. This indicates that brine volume significantly affects the formation of corrosion product scale.

In the case of corrosion scale formation at 30 °C, Figure 3.7 shows similar trends to Figure 3.3. The diameter of Nyquist semi-circles did not show a continuous increase with exposure time, but rather, as shown in Figure 3.7 (a), electrode impedance decreased after the increase in the initial 72 hours. This suggests that the corrosion product scale, formed in the first 72 hours, was destroyed or disrupted in some way. The fact that Bode phase angle plots in Figure 3.7 (b) do not show an extra high frequency peak as was observed in Figure 3.6 (b) suggests that the surface scales formed at 30 °C were not intact. This result again suggests that the protective corrosion product scale formed at 30 °C is not persistent.

### 3.3.1.2. Corrosion scale formation under low pressure conditions

The formation of corrosion product scales under low pressure conditions (1 atmosphere pressure or 101.3 kPa) was also investigated in this work. During these atmospheric pressure experiments, the testing electrodes were consistently kept in a $CO_2$ sparged electrochemical cell vessel, which contained 640 mL of $CO_2$-saturated 3% NaCl brine, at 70 °C or 30 °C, for corrosion scale formation and also for regular EIS measurements.

Figures 3.8 and 3.9 show EIS plots recorded during the 70 °C and 30 °C experiments.

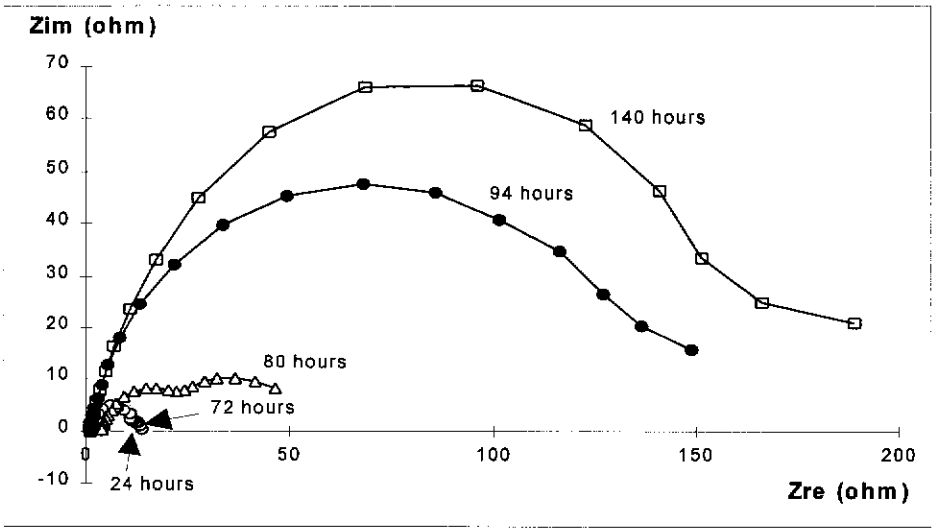


Figure 3.8 (a)

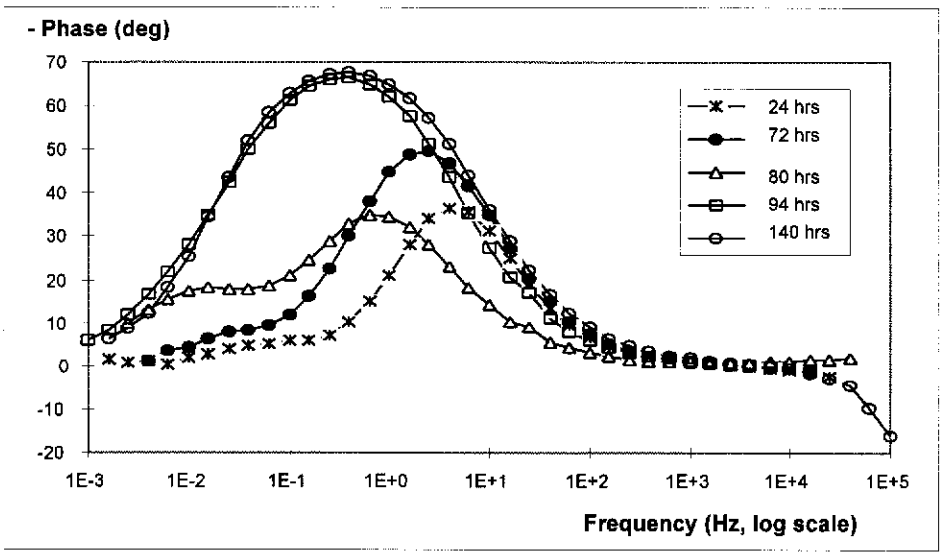


Figure 3.8 (b)

**Figure 3.8.** (a) Nyquist plots and (b) Bode phase plots recorded from an electrode exposed to 640 mL of $CO_2$-saturated 3% NaCl brine for different periods at 70 °C, atmospheric pressure pure $CO_2$.

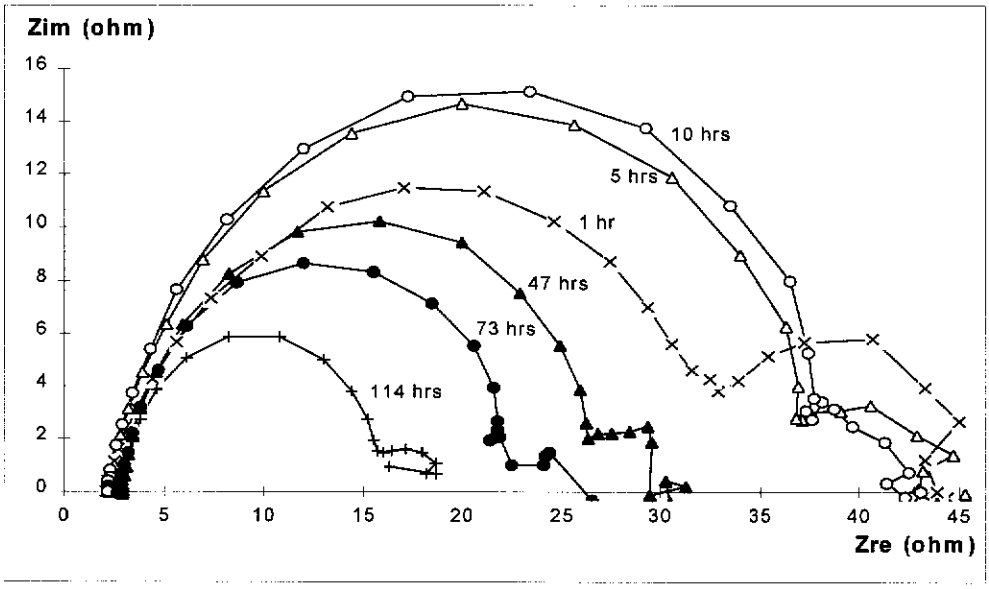


Figure 3.9 (a)

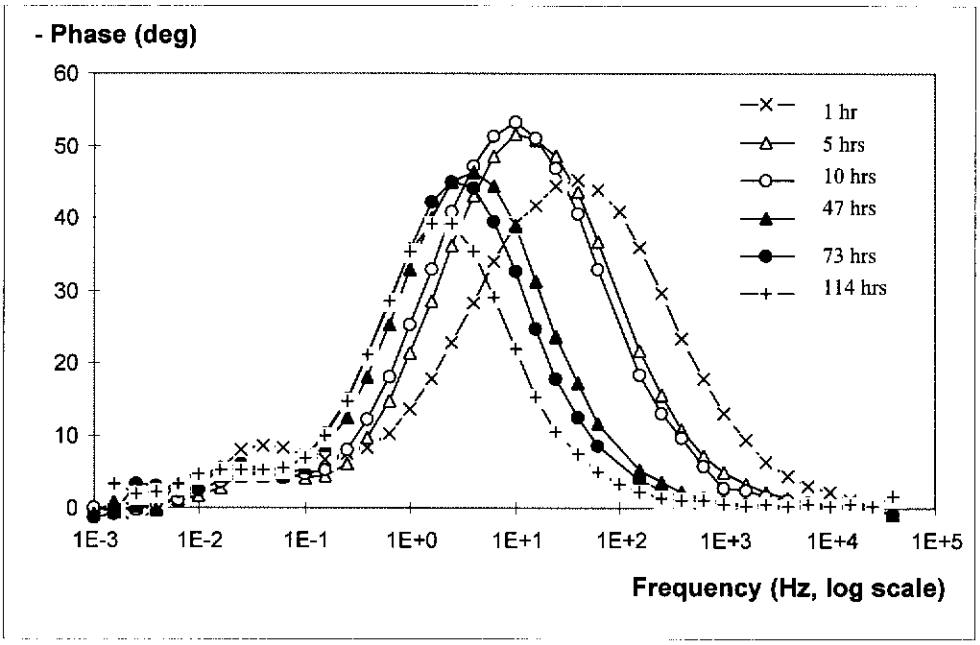


Figure 3.9 (b)

**Figure 3.9.** (a) Nyquist plots and (b) Bode phase plots recorded from an electrode which was exposed to 640 mL of $CO_2$-saturated 3% NaCl brine for different periods at 30 °C, atmospheric pressure pure $CO_2$.

Under 1 atmosphere pressure, as indicated by the increase in the diameter of Nyquist semicircles in Figure 3.8, protective corrosion scale can also form at 70 °C. However, the protective ability of this scale was far worse than that of high pressure scales as shown in Figure 3.6. Here pressure showed strong effects on the protective ability of corrosion product scales.

The 30 °C EIS plots, as shown in Figure 3.9, again show the behaviour observed in higher pressure tests shown in Figures 3.3 and 3.7. The electrode impedance decreased after the slight increase in the initial 10 hours. The initial increase in electrode impedance may be attributed to the effect of corrosion product precipitation. This result again confirms that the surface scales formed at 30 °C were not intact and not persistent.

### 3.3.1.3. Analysis of corrosion scale formation processes

Comparisons of EIS experimental data were made to acquire more information about corrosion scale formation processes.

#### 3.3.1.3.1 Scale formation under fixed $CO_2$ pressures

As discussed above, under fixed pressures of $CO_2$, corrosion product scales have a better chance to form in a smaller volume of brine than in larger volumes of brine, and the scales formed at higher temperatures have better protective ability than those formed at lower temperatures. These results are summarised in Figures 3.10 (a) and (b), using the charge transfer resistance ($R_t$) as an indicator because the $R_t$ is related to the corrosion rate (section 2.2.2.2).

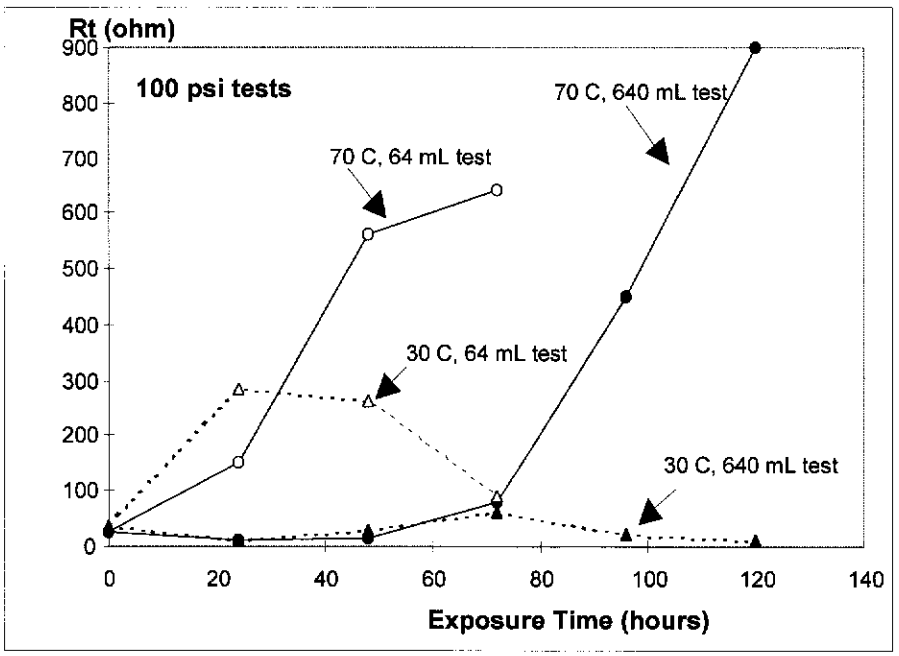


Figure 3.10 (a)

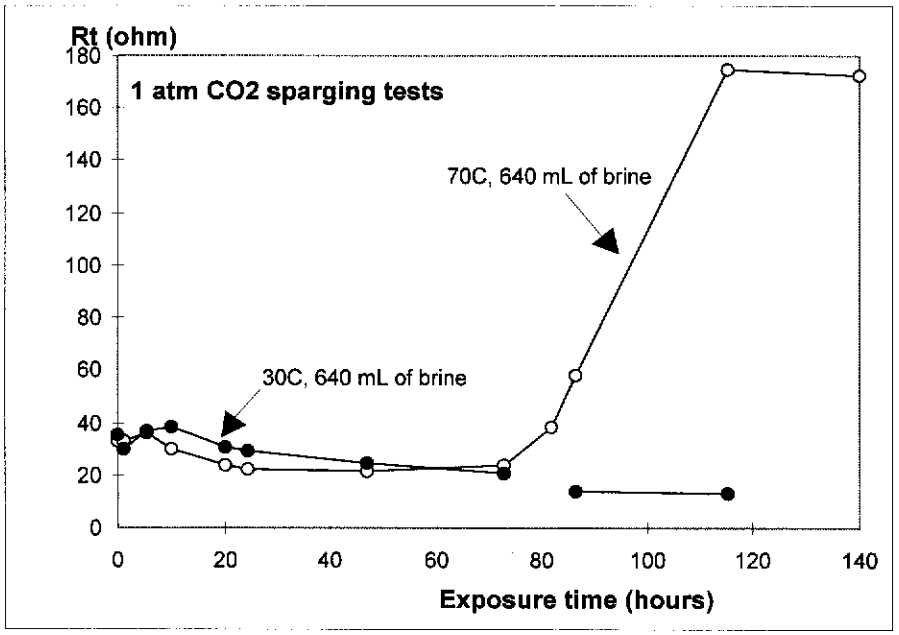


Figure 3.10 (b)

**Figure 3.10.** Comparisons of corrosion product scale formation under 100 psi $CO_2$ (a), and 1 atm $CO_2$ sparging (b), at different temperature and brine volume conditions. The charge transfer resistances were calculated from experimental data shown in previous sections (3.3.1.1 and 3.3.1.2).

Figure 3.10 confirms the conclusion made in the previous sections that under certain pressure conditions the corrosion product scales formed at higher temperatures have better corrosion protective ability. It can also be seen that the volume of brine has a strong link with the protective corrosion scale initiation time, i.e. the period taken to start filming with protective corrosion scale. As shown in Figure 3.10 (a), faster scale formation always occurred in the smaller volume autoclave. This is not surprising because smaller brine volume means a larger metal surface/brine volume ratio and a faster increase in $Fe^{++}$ concentration. Obviously, in the small volume autoclave it will therefore take a shorter time to exceed the solubility limit of $Fe^{++}$ and result in the precipitation of a corrosion product scale. This is in agreement with the results of Videm and Dugstad (1987) and the conclusion made by Burke (1984) that corrosion scale is strongly dependent upon experimental conditions such as surface-to-volume ratios, test duration, etc.. These experimental findings may also be useful for explaining why corrosion scale is easier to form in autoclaves than in flow loops (Burke 1984; Ikeda *et al.*).

3.3.1.3.2 Scale formation under fixed temperatures

At a fixed temperature, the corrosion scale formation processes can be compared as shown in Figure 3.11.

Figure 3.11 confirms the conclusion made in previous sections that at certain temperatures corrosion product scales formed under higher pressures of $CO_2$ have better corrosion protective ability. An interesting phenomenon can be found in Figure 3.11 that although the scales formed at 100 psi $CO_2$ and 1 atm sparging tests have very different protective ability, the initiation times of the corrosion scales are quite similar. This suggests again that the volume of brine is the major factor determining

how fast a protective corrosion scale initiates but seems not to be a factor determining how protective the scale is.

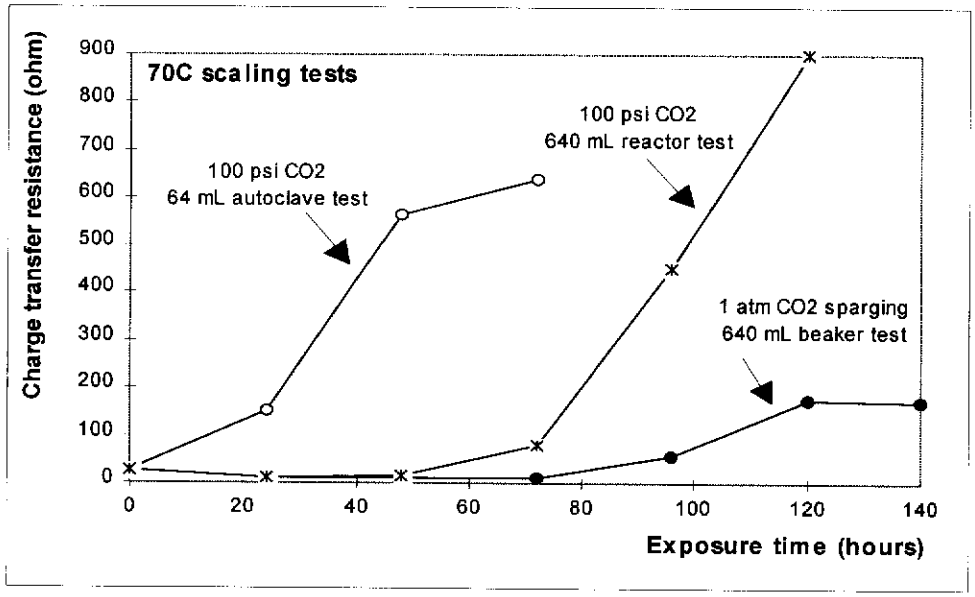


**Figure 3.11.** A comparison of corrosion product scale formation at 70 °C under different pressures and brine volume conditions. The charge transfer resistances were calculated from experimental data shown in previous sections (3.3.1.1 and 3.3.1.2).

3.3.1.3.3 Weight-loss measurements

Weight-loss measurements using mild steel coupons were carried out to compare with the expected weight-loss values calculated using EIS data. The test weight-loss coupons were pre-corroded in the relevant corrosion environments (see section 3.2.2) for a period of time and then were withdrawn from the corrosion environments and were cleaned with Clarke's solution (An acid solution containing inhibitor which was made by adding 20 g of $Sb_2O_3$ and 59 g of $SnCl_2.2H_2O$ into 1 litre of concentrated HCl). Then the coupons were re-weighed and the weight-losses were recorded.

Although weight-loss measurement results showed some scatter, the general trends from the weight-loss coupon method were in agreement with the EIS analysis using $R_t$ (see section 2.2.2.2), as shown in Figure 3.12.

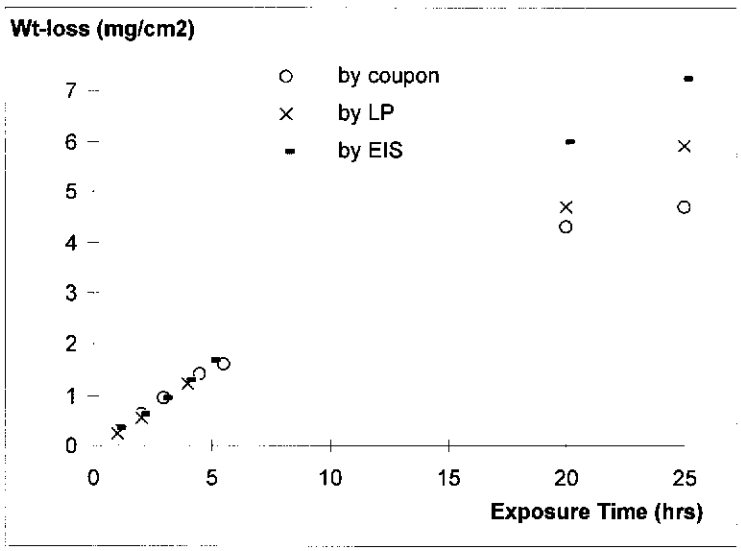


**Figure 3.12.** A comparison of weight-loss measured using weight-loss coupons, EIS and linear polarisation (LP) of bare electrodes and coupons in a 640 mL of 3% NaCl brine with $CO_2$ sparging at 50 °C.

Although the weight-loss measurement method is not able to detect the instantaneous corrosion rate, it can be used to measure the average corrosion rates over a given time interval. In this work, weight-loss coupons were withdrawn from the corrosion environments after being exposed in the corrosion environments for different periods, in order to calculate the average corrosion rate over the time intervals. For example, if the weight-loss of a coupon after 24 hours exposure is $L_{24}$ and the weight-loss of an identical coupon after 48 hours exposure is $L_{48}$, then the weight-loss from 24 hours to 48 hours should be $L_{48}$ - $L_{24}$. This weight-loss can therefore be used to estimate the average corrosion rate from 24 hours to 48 hours.

Figure 3.13 shows a comparison of average corrosion rates during relatively long term experiments. The changes in average corrosion rates estimated from EIS and weight-loss measurements vs. exposure time show similar trends although the long-term weight-loss data often showed some degree of scatter.

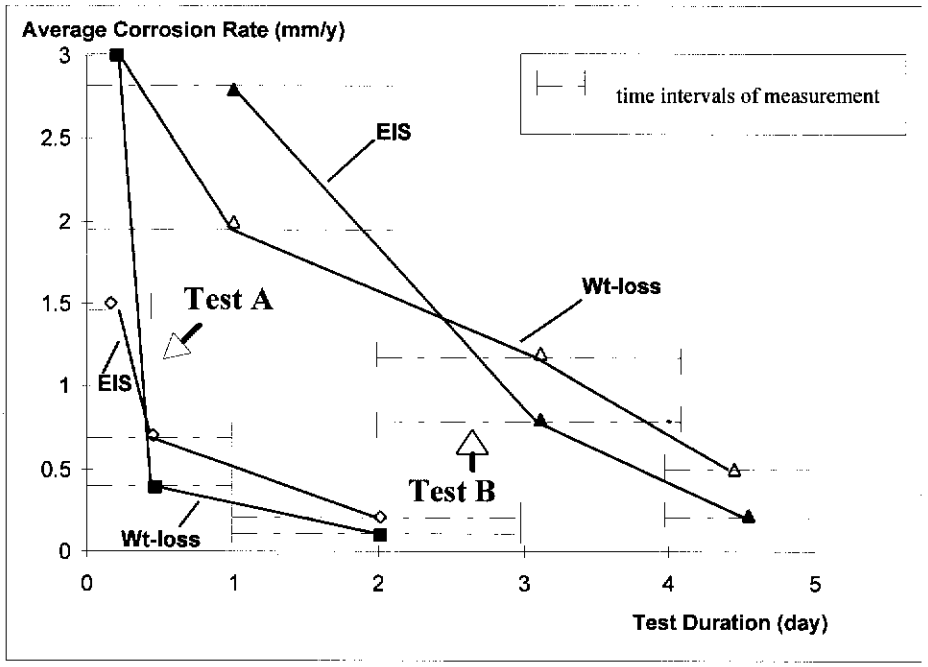


**Figure 3.13.** A comparison between EIS and weight-loss measurements. Test A: autoclave tests (64 mL of brine at 70 °C, 100 psi $CO_2$ pressure, referring to Figure 3.2). Test B: pressure reactor tests (640 mL of brine at 70 °C, 100 psi $CO_2$, referring to Figure 3.6). The dotted lines indicate the time intervals for which the values were obtained.

In this work, as shown in Table 3.3, the correlation between weight-loss measurement results and the calculations using the de Waard-Milliams equation was poor (the de Waard-Milliams equation was discussed in section 1.1.3). The only similar result was from the 30 °C, 1 atm pressure beaker test which may meet the validity limits of the de Waard-Milliams equation as discussed in sections 1.1.3 and 1.1.4. This is

understandable because all of the tests were run under steady state conditions and corrosion product scales formed on electrode and coupon surfaces.

**Table 3.3.** A comparison of corrosion rate estimated from weight-loss measurements and from the de Waard-Milliams equation.

| Test Conditions | Corrosion Rate (24 hours' average) | Corrosion Rate (120 hours' average) | de Waard-Milliams equation |
|---|---|---|---|
| **Beaker test, 30 °C** (1 atm $CO_2$; 640 mL brine) | 1.6 mm/y | 1.0 mm/y | 1.45 mm/y |
| **Beaker test, 70 °C** (1 atm $CO_2$; 640 mL brine) | 1.5 mm/y | 0.6 mm/y | 6.60 mm/y |
| **Reactor test, 30 °C** (100 psi $CO_2$; 640 mL brine) | 1.6 mm/y | 1.5 mm/y | 5.18 mm/y |
| **Reactor test, 70 °C** (100 psi $CO_2$; 640 mL brine) | 2.0 mm/y | 1.3 mm/y | 23.59 mm/y |
| **Autoclave test, 30 °C** (100 psi $CO_2$; 64 mL brine) | 0.3 mm/y | 0.1 mm/y | 5.18 mm/y |
| **Autoclave test, 70 °C** (100 psi $CO_2$; 64 mL brine) | 0.4 mm/y | 0.1 mm/y | 23.59 mm/y |

### 3.3.2. The Composition and Morphology of $CO_2$ Corrosion Scales

What are the factors affecting the protective ability of $CO_2$ corrosion product scale? The morphology and composition of $CO_2$ corrosion product scale are thought to play a major role in the corrosion protective ability of scales (Burke 1984). However, as discussed in section 1.1.5, no conclusion has been reached about the correlation between the corrosion protective ability and the composition and morphology of corrosion scale. In fact, although it is generally agreed that iron carbonate is the main corrosion product (Hausler 1983; Dunlop *et al.* 1983; Shah 1993; Vera *et al.* 1994), there are still different opinions about the chemical composition of the scale (Xia *et al.* 1989). Some laboratory observations and SEM investigations have contributed towards a better understanding of the morphology of corrosion scales (Dunlop *et al.* 1983; Jasinski 1987; Palacios and Shadley 1991), however, no clear conclusion was made about their effect on the corrosion protective ability of the scale.

This work sets out to resolve some of the above problems and to get a better understanding about the protective ability of $CO_2$ corrosion product scales.

#### 3.3.2.1 The composition of $CO_2$ corrosion product scales

X-ray diffraction (XRD) and Fourier transform infrared spectrometry (FTIR) measurements were made on corrosion scales formed under different scaling conditions. XRD measurements were performed directly on well kept weight-loss coupon specimens. FTIR measurements were made on KBr discs prepared from scale material. Typical XRD patterns are shown in figure 3.14 and typical FTIR spectra are shown in Figure 3.15.

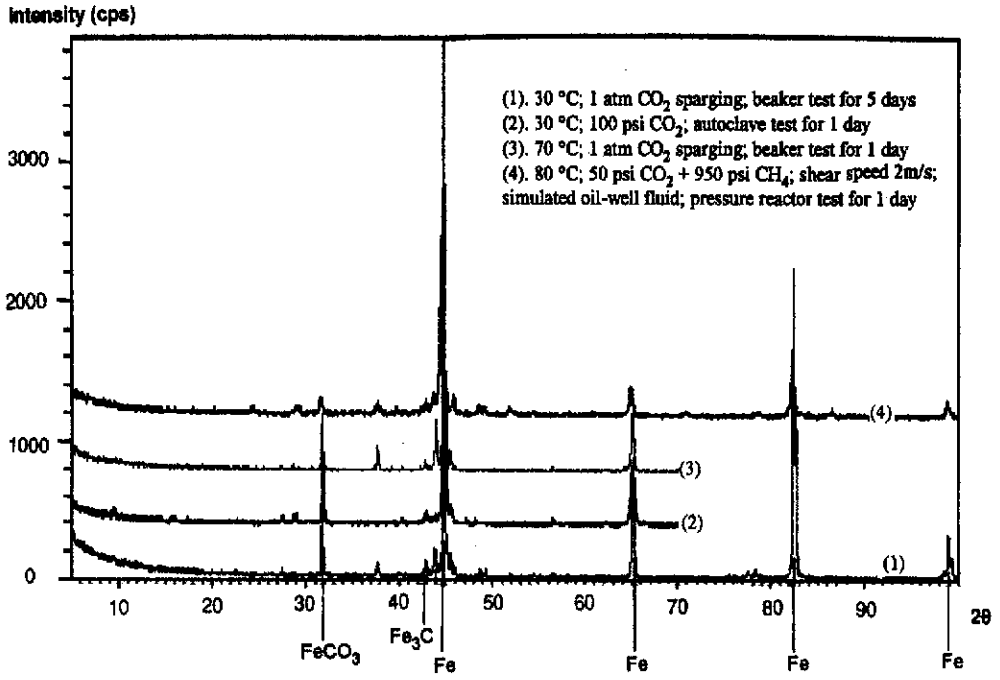


**Figure 3.14.** Typical XRD patterns of corrosion product scales

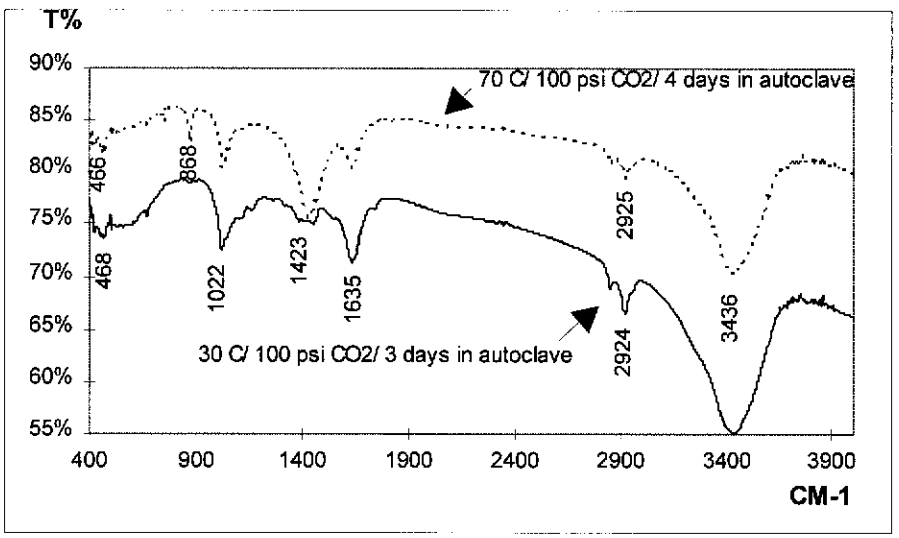


**Figure 3.15.** Typical FTIR spectra of corrosion product scales

In Figure 3.14, the characteristic high intensity XRD peaks for Fe (2θ = 44.6°; 82.4° and 65.2°), $FeCO_3$ (2θ = ~32°) and $Fe_3C$ (2θ = 42.8° and 43.7°) can be found for all samples tested. In Figure 3.15, the FTIR vibrational bands around 866 and 1429 $cm^{-1}$ correspond well to the Siderite ($FeCO_3$) spectrum (KBr) and the band around 1022 $cm^{-1}$ is most likely due to iron oxide (Shah 1993).

Tables 3.4 and 3.5 show FTIR and XRD detected composition of corrosion product scales formed under different scaling conditions.

**Table 3.4.** XRD and FTIR results of corrosion product scales formed in 3% NaCl brine under different scaling conditions.

| Sample No: | Scaling condition | Composition of scale (by XRD) | Composition of scale (by FTIR) | Corr. rate (by wt-loss) |
|---|---|---|---|---|
| 1 | 30 °C, 1atm, 640 mL brine, 1 day | $FeCO_3$ (major); $Fe_3C$ (significant); $Fe_3O_4$ (possible) | iron oxide; $FeCO_3$ (minor) | 1.52 mm/y |
| 2 | 30 °C, 1atm, 640 mL brine, 5days | $FeCO_3$ (major); $Fe_3C$ (significant) | iron oxide; $FeCO_3$ (minor) | 0.96 mm/y |
| 3 | 30 °C, 100 psi pure $CO_2$, 64 mL brine, 1day | $FeCO_3$ (major); $Fe_3C$ (minor); $Fe_3O_4$ (minor) | | 0.24 mm/y |
| 4 | 30 °C, 100 psi pure $CO_2$, 64 mL brine, 3days | $FeCO_3$ (major); $Fe_3C$ (significant) | iron oxide; $FeCO_3$ | 0.10 mm/y |
| 5 | 30 °C, 100psi $CO_2$ (1500 psi total pressure), 64 mL brine, 1day | $FeCO_3$ (major); $Fe_3C$ (minor) | iron oxide; $FeCO_3$ (minor) | 0.37 mm/y |
| 6 | 70 °C, 1atm, 640 mL brine, 1day | $Fe_3C$ (significant); $FeCO_3$ (significant); | iron oxide (minor); $FeCO_3$ | 1.53 mm/y |
| 7 | 70 °C, 1atm, 640 mL brine, 5days | $FeCO_3$ (major); $Fe_3C$ (significant) | iron oxide (minor); $FeCO_3$ | 0.53 mm/y |
| 8 | 70 °C, 100psi pure $CO_2$, 64 mL brine, 4days | $FeCO_3$ (major); $Fe_3C$ (minor) | $FeCO_3$ (significant); iron oxide (significant) | 0.04 mm/y |
| 9 | 70 °C, 100 psi $CO_2$ (1500 psi total pressure), 64 mL brine, 1day | $FeCO_3$ (major); $Fe_3C$ (minor) | iron oxide; $FeCO_3$ | 0.94 mm/y |

The 'major', 'significant', 'minor' and 'possible' descriptions in table 3.4 are qualitative comparisons of the relative intensity of XRD peaks and relative intensity of FTIR absorption bands.

**Table 3.5.** XRD and FTIR results for the composition of corrosion product scales formed under high temperature, high pressure and high shear speed conditions.

| Steel sample | Scaling duration | Detected composition of scale (by XRD) | Detected composition of scale (by FTIR) | Corr. rate (mm/y, by weight-loss) |
|---|---|---|---|---|
| **L80** | 24 hours | $Fe_3C$ | $FeCO_3$ and iron oxide | 11.64 |
| **L80** | 96 hours | $Fe_3C$ | $FeCO_3$ and iron oxide | 12.31 |
| **N80** | 24 hours | $Fe_3C$ | $FeCO_3$ | 14.44 |
| **N80** | 96 hours | $FeCO_3$ (major) $Fe_3C$ | $FeCO_3$ and iron oxide | 11.72 |
| **T95** | 24 hours | $Fe_3C$ | $FeCO_3$ and iron oxide | 11.0 |
| **T95** | 96 hours | $Fe_3C$ (major) $FeCO_3$ | $FeCO_3$ and iron oxide | 8.51 |
| **C90** | 24 hours | $Fe_3C$ | $FeCO_3$ and iron oxide | 8.97 |
| **C90** | 96 hours | $Fe_3C$ | $FeCO_3$ and iron oxide | 9.30 |

Corrosion product scales described in Table 3.5 were formed at 80 °C; 1500 psi total pressure ($CO_2$ partial pressure 50 psi, Methane 1450 psi) and a tangential velocity of 2 m/s in a simulated oil well fluid mixture (140 mL Diesel and 560 mL synthetic typical oil-well water which contains $Na^+$, $Ca^{2+}$, $Mg^{2+}$, $SO_4^{2-}$, $Cl^-$ and $HCO^{3-}$). C90, L80, N80 and T95 are steels with certain mechanical properties which are frequently used in the oil and gas industry. Their corrosion resistance performance depends on their chemical composition and microstructure.

Tables 3.4 and 3.5 show that iron carbonate, iron carbide and iron oxide are three major compounds in the scales examined even though sometimes XRD can not detect iron carbonate and FTIR can not detect iron carbide. The percentage of each varies according to the scale growth conditions. Iron carbonate would be present as the major $CO_2$ corrosion product, while iron carbide would be a residue of the steel itself because the formation of $Fe_3C$ from iron and carbon dioxide is thermodynamically forbidden. It is likely that the corrosion process etches out the metallic iron, leaving iron carbide behind. Some iron oxides were also detected by FTIR. Since the interfacial pH under the experimental conditions is expected to be relatively high, dissolved iron ions can precipitate as the corresponding hydroxides and oxides (Shah 1993).

The results of this work agree very well with those of Vera *et al.* (1994) but show differences to other results (Hausler 1983; Shah 1993; Xia, *et al.* 1989; Dunlop *et al.* 1983). The XRD line for $Fe(HCO_3)_2$ ($2\theta$ = ~14° and ~17°) detected by Xia *et al.* (1989) was not found in any of the above tests, and so this study does not support the hypothesis that the initial corrosion product is $Fe(HCO_3)_2$ which is tight, adherent and very protective, and that longer exposure results in the transformation of $Fe(HCO_3)_2$ into a less voluminous, non-adherent and porous layer of $FeCO_3$ which is not protective (Xia *et al.* 1989). $Fe(HCO_3)_2$ may only form under certain conditions such as those studied by Xia *et al.* (1989).

No clear correlation is apparent between scale composition and the corrosion rates listed in Tables 3.4 and 3.5.

### 3.3.2.2 The morphology of $CO_2$ corrosion product scales

Optical microscopy and SEM were used to investigate the morphology of the scales. Photographs were taken of scales formed under a wide range of conditions. Table 3.6 compares observations of scale morphology and corrosion rates.

The results in Table 3.6 suggest that the bigger the crystal size and the larger the non-filmed area, the poorer the corrosion protective ability of the scale. This result corresponds well to laboratory experience that protective scales are often very smooth and the poorly protective scales are porous and rough. The surface morphology is obviously dependent upon scaling conditions and correlated with the corrosion protective ability of scales. For example, the scales formed under 1 atm $CO_2$ are generally rough and porous and are not protective.

**Table 3.6.** Results of optical microscopic and SEM observation of corrosion product scales formed in 3% NaCl brine, and weight-loss measurements.

| Sample No: | Scaling condition | Optical microscopic or SEM observation | Corr. rate (mm/y) |
|---|---|---|---|
| 1 | 30 °C, 640 mL brine, 1atm $CO_2$ sparging, 1 day | Microscopic observation: (× 100 and ×400): Average particle size: ~ $1 \times 10^{-3}$ cm. Percentage of non-filmed area: 3 %. | 1.47 |
| 2 | 50 °C, 640 mL brine, 1atm $CO_2$ sparging, 1 day | Microscopic observation: (× 100 and ×400): Average particle size: ~ $3 \times 10^{-3}$ cm. Percentage of non-filmed area: 8 %. | 1.89 |
| 3 | 70 °C, 640 mL brine, 1atm $CO_2$ sparging, 1day | Microscopic observation: (× 100 and ×400): Average particle size: ~ $2.5 \times 10^{-3}$ cm. Percentage of non-filmed area: 5 %. | 1.53 |
| 4 | 70 °C, 640 mL brine, 1atm $CO_2$ sparging, 4day | Microscopic observation: (× 100 and ×400): Average particle size: ~ $1 \times 10^{-3}$ cm. Percentage of non-filmed area: 0 %. | 0.57 |
| 5 | 30 °C, 100 psi $CO_2$ (1500 psi total pressure), 1day, 64 mL brine | Microscopic observation: (× 400): Two kinds of particles were found. The average particle size of the finer one was < $1 \times 10^{-4}$ cm, of the bigger one was ~ $4 \times 10^{-3}$ cm. Percentage of non-filmed area: 0%. | 0.43 |
| 6 | 50 °C, 100 psi $CO_2$ (1500 psi total pressure), 1day, 64 mL brine. | Microscopic observation: (× 400): Two kinds of particles were found. The average particle size of the finer one was ~ $2 \times 10^{-4}$ cm, of the bigger one was ~ $4 \times 10^{-3}$ cm. Percentage of non-filmed area: 0%. | 1.08 |
| 7 | 70 °C, 100 psi $CO_2$ (1500 psi total pressure), 1day, 64 mL brine. | Microscopic observation: (× 400): Two kinds of particles were found. The average particle size of the finer one was ~ $2 \times 10^{-4}$ cm, of the bigger one was ~ $3 \times 10^{-3}$ cm. Percentage of non-filmed area: 0%. | 1.00 |
| 8 | 30 °C, 640 mL brine, 1atm $CO_2$ sparging, 1 day | SEM observation: (× 1000): Two kinds of particles were found. The average particle size of the finer one was ~ $3 \times 10^{-4}$ cm, of the bigger one was ~ $2 \times 10^{-3}$ cm. | 1.51 |
| 9 | 30 °C, 100 psi $CO_2$, 1day, 64 mL brine, in a autoclave. | SEM observation: (× 1000): Two kinds of particles were found as shown in Figure 3.16 (a). The average particle size of the finer one was too small to estimate, of the bigger one was ~ $1.6 \times 10^{-3}$ cm. Percentage of non-filmed area: 0%. | 0.24 |
| 10 | As above | SEM observation (× 30000) of the fine particle area: Very fine crystals were found as shown in Figure 3.16 (b). The biggest particle size of them was about $4 \times 10^{-5}$ cm. | As above |

Two kinds of crystals were found on corroded coupon surfaces: one is larger in size (~ $1.5 - 4 \times 10^{-3}$ cm), as shown in Figure 3.16 (a), and the other is about 100 times smaller in size ($\leq 4 \times 10^{-5}$ cm), as shown in Figure 3.16 (b). It was also found that the

size of the larger crystals is similar for all samples no matter if the scales are protective or not: an example is shown in Figure 3.17 (a). However, the size and crystalline structure of the fine structures (crystalline or amorphous) is strongly dependent on the scaling conditions and obviously related to the corrosion protective ability of the scale. For example, the size of the fine crystals for sample 10 as shown in Figure 3.16 (b) is less than $4 \times 10^{-5}$ cm (corrosion rate: 0.24 mm/y), whereas the size of the fine amorphous structure for sample 8 as shown in Figure 3.17 (b) is about $3 \times 10^{-4}$ cm (corrosion rate: 1.51 mm/y). These results correspond very well with laboratory experience that $CO_2$ corrosion scales consist of two layers: the top layer is very easily removed manually and readily dissolved in Clarke's solution (an inhibited acid); the bottom layer is difficult to clean manually or to dissolve in Clarke's solution. The larger crystals were also observed by other researchers (Dunlop *et al.*; Palacios and Shadley 1991; Jasinski 1987) using a scanning electron micrograph at relatively low amplification (×1000 or ×2000).

These tests above revealed that the morphology of scale is strongly correlated with its corrosion protective ability. This gives rise to the possibility of improving the corrosion protective ability of scales by optimising the crystallisation process.


Figure 3.16 (a) (×1000)

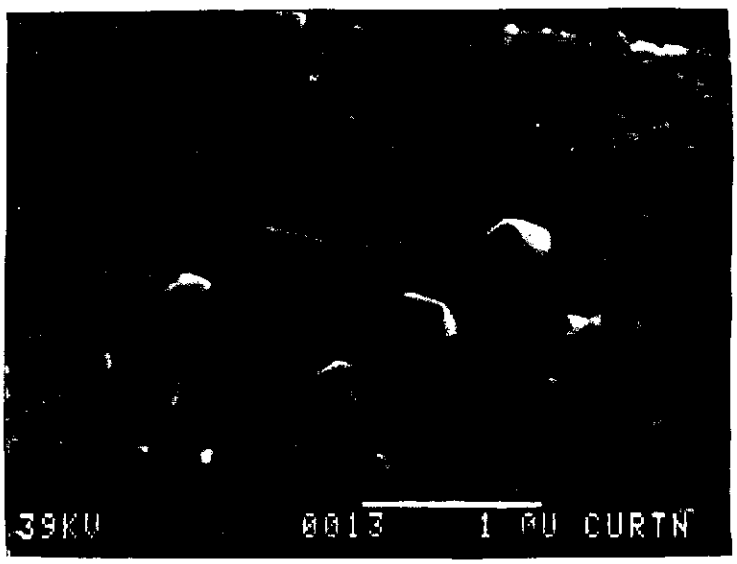


Figure 3.16 (b) (×30000)

**Figure 3.16.** SEM photographs (×1000 and ×30000) of a corrosion product scale, sample no. 10, formed at 30 °C, 100 psi $CO_2$, 24 hours in a high-pressure autoclave with 64 mL of 3% NaCl brine present. Corrosion rate (by wt-loss measurement) was 0.24 mm/y for the sample.

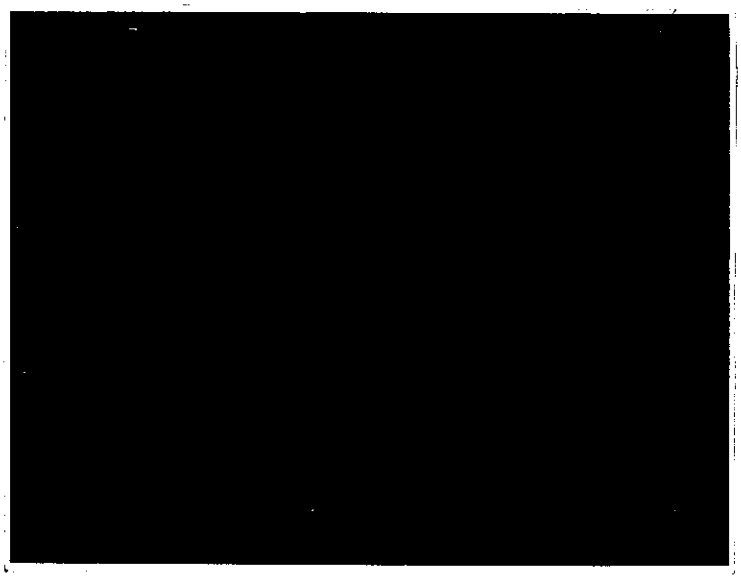

Figure 3.17 (c) (×1000)

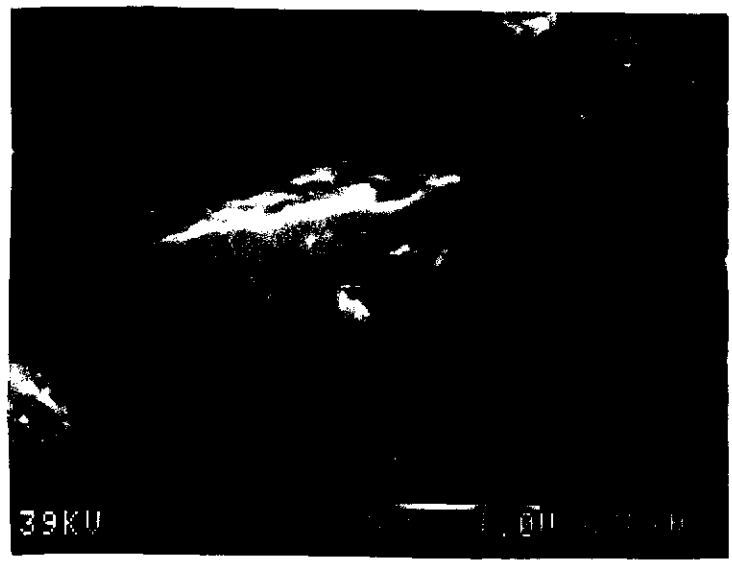


Figure 3.17 (d) (×30000)

**Figure 3.17.** SEM photographs (×1000 and ×30000) of a corrosion product scale, sample no. 8, formed at 30 °C, 640 mL of 3% NaCl brine sparged with 1 atm $CO_2$ for 24 hours. Corrosion rate (by wt-loss measurement) was 1.51 mm/y for the sample.

## 3.4. Conclusions

(i). Electrochemical impedance spectroscopy was used to monitor the formation of corrosion product scales and their corrosion protective ability. A simplified experimental method was employed to study high pressure corrosion product scales. The results of these measurements showed that EIS is a suitable technique for studying corrosion product scales.

(ii). EIS results suggested that the volume of brine is a factor determining how fast scale initiates. It was confirmed that corrosion scales formed at higher temperatures and high pressures have better protective ability. It was also confirmed that the protectiveness of $CO_2$ corrosion product scales is a function of exposure time. So the duration of $CO_2$ corrosion tests should be long enough to stabilise the corrosion scale. Short time corrosion experiments, which are frequently reported in the literature, should be treated with care (Schmitt 1984).

(iii). Under certain conditions, it was found that corrosion scale can form at 30 °C which questions the validity limits often given for the de Waard-Milliams equation. The correlation between weight-loss measurement results and the calculations using the de Waard-Milliams equation was poor.

(iv). The surface morphology showed obvious correlation to the protective ability of scales. Two kinds of corrosion product crystals were found on the surface of corroded coupons by SEM. One is large in size and one is very fine in size, which suggests the contribution of different crystallisation processes. The large crystals obviously do not contribute to the protective ability of the scale and seem to result from re-crystallisation from solution. The fine crystals contribute to the corrosion protection and seem to result from the initial fast corrosion rate and crystallisation processes.

These observations are consistent with known properties of $CO_2$ corrosion product scales, e.g. obvious different solubility of layers of scale in acid and different adhesion of the layers. It is suggested that the conditions which produce fine adhesive crystals will produce better corrosion protective scale.

(v). The chemical compositions were found to be quite similar for all scales formed under different conditions and did not show correlation to its corrosion protective ability. $FeCO_3$, $Fe_3C$, and iron oxides were found to be the main corrosion products. No $FeHCO_3$ was found in any sample tested in this study.

# Chapter IV

# STUDIES OF CONTINUOUS TREATMENT INHIBITOR FILMS USING ELECTROCHEMICAL IMPEDANCE SPECTROSCOPY AND ELECTROCHEMICAL NOISE ANALYSIS

## 4.1 Introduction

As reviewed in section 1.2, inhibition is the most cost effective and flexible means of corrosion control in the oil and gas production industry and so hundreds of commercial inhibitor products are used in oil and gas fields. Continuous treatment and batch treatment are the two main methods of inhibitor application.

Continuous treatment, which will be dealt with in this Chapter, is the most common technique which involves simply injecting inhibitor into the oil or gas well fluid by a chemical proportional pump, and maintaining a certain inhibitor concentration in the fluid for protecting against $CO_2$ corrosion. Inhibitors suitable for continuous treatment are called continuous treatment inhibitors. These are water soluble, water dispersible or oil soluble fluids.

In practice, however, inhibitors can actually cause problems if they are not properly applied. As discussed in sections 1.2 and 1.4, the selection and application of inhibitors are complicated problems because the corrosion environments in oil and gas fields are very variable. An inhibitor that works in one oil or gas well may not

work in another well due to the differences in corrosion environment. Inhibitor may chemically react with other oil-field chemical additives such as bactericide and lose efficiency. Serious corrosion such as localised corrosion may occur if the inhibitor film loses persistency. Thus the monitoring of inhibitor performance and the evaluation of the inhibitor film persistency are very important requirements for the proper application of inhibitors.

Indeed, the persistency of the inhibitor film is an important aspect of inhibitor assessment. When applying an inhibitor in oil and gas wells and flowlines, a most important concern is to make sure that an inhibitor film is formed with the anticipated film persistency (Hilliard 1978). Even when the inhibitor treatment is continuous, inhibitor may not really be continuously applied on some parts of the pipeline, e.g. valves in the pipeline may plug and the well may need to be shut-in for service. When an inhibitor is applied at a low concentration (e.g. 10 ppm), it is actually difficult to maintain an adequate inhibitor concentration everywhere over a long pipeline. So, good film persistency remains an important requirement even for continuous treatment inhibitors.

However, as mentioned in section 1.4.1, there is not a good technique available which can quickly evaluate and monitor inhibitor efficiency and inhibitor film persistency. The current technology for assessing inhibitor film persistency using the wheel test is a subject of much discussion and, in many cases, disagreement (NACE Task Group T-1D-8 1982).

On the other hand, as mentioned in section 1.2.4, the understanding about $CO_2$ corrosion inhibitors is limited, especially since very little is known about the inhibitor film formation and destruction mechanisms. Obviously a better understanding about the inhibitor film formation and destruction processes is important for the development of new $CO_2$ corrosion inhibitors which have better film persistency.

In this work, electrochemical impedance spectroscopy (EIS) and electrochemical noise analysis (ENA) will be used as new tools for studying the mechanism and persistency of continuous treatment inhibitors.

As reviewed in section 2.2, EIS has already been successfully used in various corrosion and protection fields such as organic coatings studies, passive layer analysis and water treatment corrosion inhibitor evaluation. In Chapter 3, EIS was shown to be a very useful tool in the studies of corrosion product scales. However, very little attention has been paid to the potential possibility of EIS application in the monitoring of inhibitor film persistency and in the study of oilfield inhibitor mechanisms. In this work, EIS has been used to study the inhibitor film and the electrochemical corrosion kinetics under the inhibitor film. The possibilities of using EIS as a method for evaluating inhibitor film persistency and for studying inhibitor mechanisms will be explored in this chapter.

As reviewed in section 2.3, ENA has already been shown to be a useful tool in corrosion rate measurements, and also in localised corrosion studies, even though these applications are still controversial subjects. Electrochemical noise measurement takes data points continuously and can have very fast sampling rates (e.g. two or more data points per second), so ENA may be able to monitor inhibitor film performance continuously and to study the rapid inhibitor film formation and breakdown processes. Electrochemical noise measurement supposes to be working in a free corrosion condition and does not need to apply a perturbation on the test system by an externally imposed polarisation which will lead to inevitable changes of the system-specific properties such as the surface structure and roughness, sorption processes of inhibitors, etc.. Furthermore, electrochemical noise recording requires only simple instruments and is experimentally easy. Thus ENA may offer greater convenience for on-site application. In this work, experiments were carried out to test the reliability of

the noise resistance method for corrosion rate estimation and for inhibitor performance monitoring. The possibility of using ENA to continuously monitor the film formation and destruction processes of the carbon dioxide ($CO_2$) corrosion inhibitor film will be examined.

## 4.2 Experimental

### 4.2.1 Materials and Solutions

(i). Electrodes

A cylinder electrode with a surface area of 3.02 $cm^2$ (diameter 1.2 cm; length 0.8 cm) was used for EIS and linear polarisation (LP) measurements. A dual cylinder electrode, which has two identical mild steel cylindrical electrodes (with surface area of 3.02 $cm^2$ each), was used for ENA experiments. Weight-loss rings (with working area of 3.02 $cm^2$ each), which can be attached to the shaft of the electrodes, were used as a reference method. All of the electrodes and weight-loss rings were made from mild steel K1035 (AS 1441-1983). The chemical composition of the steel was given earlier in section 3.2.1. The working surfaces of the electrodes and rings were polished with 400 and 800 grit Silicon Carbide paper and cleaned with ethanol and isopropanol. The non-working areas of the electrodes were sealed with Silicone sealant (made by Dow Corning Australia Pty Ltd.) before use.

An Ag/AgCl electrode was used as a reference electrode. A platinum plate with large surface area (about 20 $cm^2$) was used as counter electrode.

(ii). Solutions and inhibitors

The base testing solution was a 3% NaCl solution, which was prepared in the same way as the testing solution described in section 3.2.1.

A commercial formulated $CO_2$ corrosion inhibitor and three commercial inhibitor bases, an imidazoline; a quaternised amine; and a polymerised vegetable fatty acid were chosen to be studied in this work. However, work was focused on the imidazoline because it is a most important inhibitor base and is used extensively in

water and oil soluble inhibitor formulations. The molecular structure of the imidazoline is shown in Figure 4.1. Quaternised amine is also commonly used in commercial inhibitor products. Some products rely on it to inhibit corrosion but more commonly it is blended with other components, acting similarly to the surfactants. Its molecular structure is also shown in Figure 4.1. Polymerised vegetable fatty acid, derived from castor oil and containing a mixture of monomer, dimer, trimer and some higher analogues, is used extensively in inhibitor formulations to enhance the film persistency of inhibitors.

All the inhibitors used were commercial grade and were provided by Applied Chemicals Pty. Ltd., Australia.

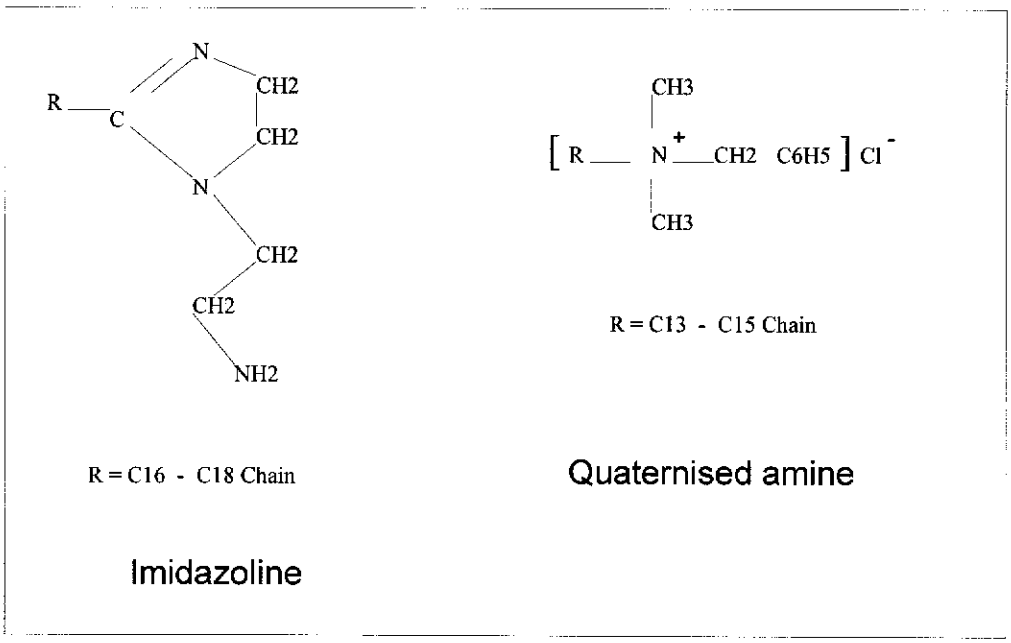


**Figure 4.1.** The molecular structure of imidazoline and quaternised amine

### 4.2.2. Electrochemical measurements

(i). EIS and LP measurements

EIS and LP measurements used an electrochemical cell and instruments which are the same as those described in section 3.2.3.

(ii). ENA measurements

The electrochemical cell and the experimental arrangement for electrochemical noise recording is schematically shown in Figure 4.2.

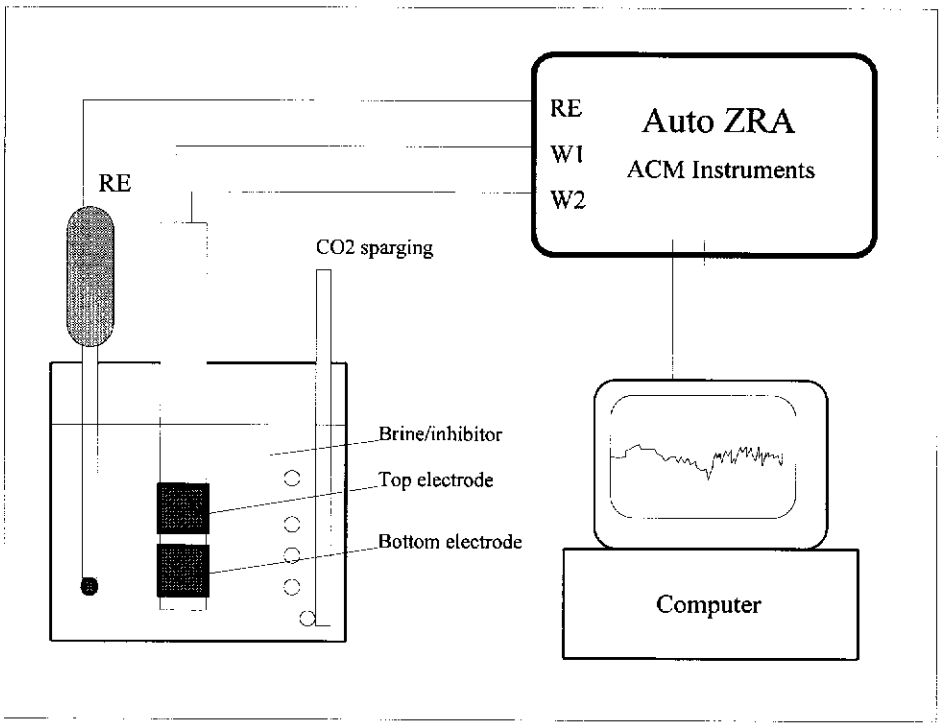


**Figure 4.2.** The experimental arrangement for electrochemical noise recording

An Automatic Zero Resistance Ammeter (AutoZRA, ACM Instruments, England) was used for electrochemical noise recording. The AutoZRA enables accurate current (325 mA to 10 pA) and voltage measurements to be taken and displayed automatically. Its data logging and extensive analysis software run in the Microsoft Windows environment complete with a real time Excel link. Thus the noise data can

be analysed using the AutoZRA analysis software (FFT, point to point) and additional analysis can be performed with Microsoft Excel.

Voltage noise was recorded by measuring the free corrosion potential of the two identical electrodes (connected) against an Ag/AgCl reference electrode. The potential measurements and recording were performed using an AutoZRA connected to a personal computer. The readings were taken with 0.5 second sampling intervals. The current flow between the two identical electrodes was monitored simultaneously with potential measurements to obtain current noise using the same sampling interval of 0.5 second. A period of 1000 seconds was set for each noise recording 'run'. There is only a one second interval between neighbouring 'runs'.

### 4.2.3. Experimental Procedures

(i). EIS studies of inhibitor films

The working electrode was filmed in a filming fluid (made by adding 50 ppm or 25 ppm inhibitor fluid into the base 3% NaCl brine). EIS measurements were carried out regularly in the filming fluid to monitor the film formation process over a period of time. The filming fluid was then diluted to 5 ppm and the inhibitor filmed electrode was tested to investigate the inhibitor film deterioration behaviour when the inhibitor concentration is very low. Then the electrode was quickly transferred into an inhibitor-free fresh brine to investigate inhibitor film destruction. The electrode was stationary during all of the above processes. Finally the electrode was rotated at 1000 rpm to investigate the effects of fluid shear stress on the inhibitor film.

(ii). ENA monitoring of inhibitor films

The dual working electrode was first placed in an inhibited fluid (made by adding 50 or 25 ppm imidazoline inhibitor into the base 3% NaCl brine) to investigate the inhibitor film formation process over a period of time. Then the electrode was

quickly transferred into an inhibitor-free fresh brine with stirring at 1000 rpm to investigate the destruction of the inhibitor film. EIS and LP measurements, as reference techniques, were carried out alternately or in parallel with electrochemical noise recording.

## 4.3 Results and discussion I: EIS studies of continuous treatment inhibitor films and their persistency

Mild steel electrodes were placed in brine solutions containing 50 ppm or 25 ppm of inhibitors for filming. EIS measurements were carried out regularly for monitoring the inhibitor film formation process. Then the filmed electrodes were transferred into a corrosive environment to study the inhibitor film deterioration process. Studies were focused on imidazoline although several other inhibitors were also briefly studied for comparison, and discussed.

### 4.3.1 Imidazoline

Imidazoline is obviously a most important inhibitor base and is used extensively in water and oil soluble inhibitor formulations. However, its corrosion protection mechanism and film properties have not been fully understood.

#### 4.3.1.1. The formation of imidazoline film

Figure 4.3 shows EIS Nyquist and Bode plots which were recorded during the 42 hours of the filming process of imidazoline at 50 ppm.

The continuous increase in the diameter of Nyquist semi-circles, as shown in Figure 4.3 (a), suggests that the presence of inhibitor greatly but gradually changed the corrosion kinetics on the electrode surface. The Bode $\theta$ *vs.* $\log f$ plots which were plotted using the same experimental data as those used in the Nyquist plots, are shown in Figure 4.3 (b). These plots show a new phase angle shift in the higher frequency range and a continuous increase in the phase angle shift with filming time. This new phase shift means that the formation of inhibitor film changes the electrode interfacial

structure and results in an extra time constant. The continuous increase in the phase angle shift obviously correlates with the inhibitor film growth.

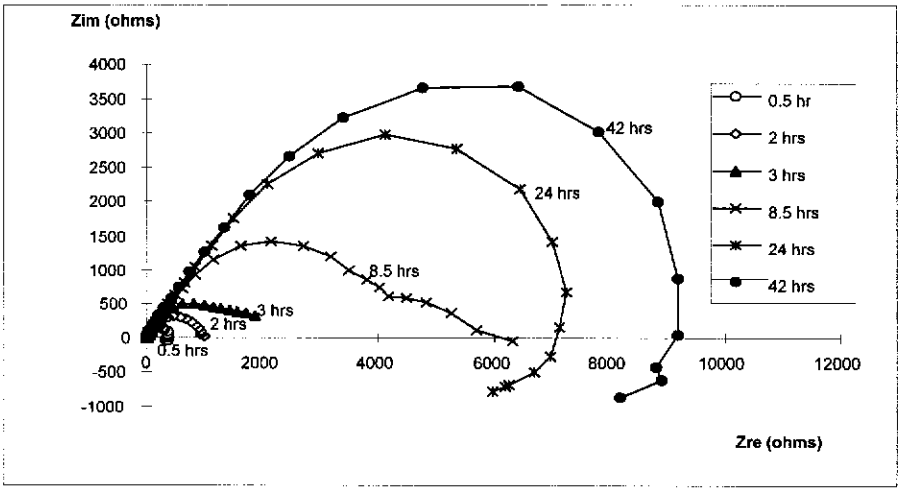


Figure 4.3 (a). EIS Nyquist plots

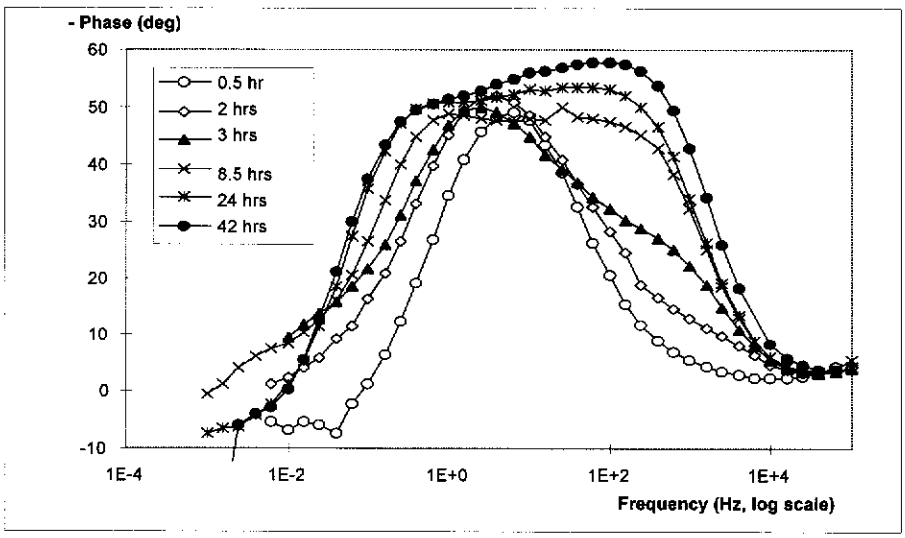


Figure 4.3 (b). EIS Bode plots

**Figure 4.3.** EIS plots (in Nyquist format and in Bode θ *vs.* log *f* format) recorded on the electrode after filming with the inhibitor imidazoline for different periods. The test solution was 3% NaCl brine, with continuous $CO_2$ sparging. Inhibitor concentration was 50 ppm and the temperature was 30 °C. The electrode was kept stationary.

Two peaks in the θ *vs.* log *f* plots mean that there are two major electrochemical kinetic processes on the electrode surface. In the Nyquist plots, as shown in Figure 4.3 (a), two semicircles appear, one of which is much smaller than the other one and can not be clearly recognised. The semicircle at lower frequency, which shows peaks around 1 Hz in Figure 4.3 (b), is due to the corrosion electrochemical process, which is suggested by other researchers (Silverman and Carrico 1988; Silverman 1990), and has been confirmed using weight-loss data by the author and co-authors (Tan *et al.* 1995). The semicircle in the high frequency range would be due to the inhibitor film because a surface dielectric film normally has a small time constant and so has a phase angle shift in the high frequency range (Feliu *et al.* 1990; Mansfeld and Lorenz 1991; Tsai and Mansfeld 1993; Thompson and Campbell 1994). The impedance characteristics of this electrode surface could be simulated by an electrical circuit that is normally used for coated metal electrodes (Beaunier *et al.* 1976; Mansfeld and Tsai 1991), as shown in Figure 4.4.

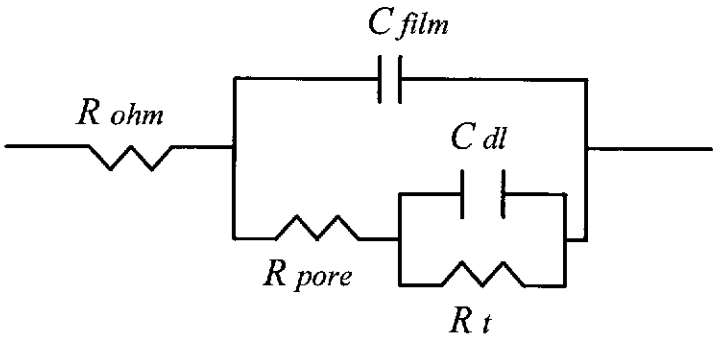


**Figure 4.4.** Equivalent circuit for an electrode filmed with a non-conducting inhibitor film. $R_{ohm}$ is the solution resistance. $R_{pore}$ is the resistance of the inhibitor film in pore areas. $C_{film}$ is the capacitance of the inhibitor film. $R_t$ is the charge transfer resistance. $C_{dl}$ is the double layer capacitance.

However, as shown in Figures 4.5 (a) and 4.5 (b), the semicircle fitting according to the model in Figure 4.4 obviously does not fit the data points between the high and low frequency semicircles although the poor fitting of very low frequency data points

can be explained as a pseudo-inductance effect which was suggested to be due to an adsorption-desorption phenomena of the inhibitor in the vicinity of the corrosion potential (Epelboin *et al.* 1972; Lorenz and Mansfeld 1981; Silverman 1989). The poor fitting of the data points at intermediate frequencies suggests that there are some other interfacial structures on the electrode surface which have intermediate time constants. The large phase angle shift in the higher frequency range in Figure 4.3 (b) also suggests a complicated interfacial structure. A likely explanation is that the inhibitor film is a multi-layered film and so shows more than one time constant. An equivalent circuit is suggested in Figure 4.6 for an electrode with a four-layer inhibitor film (the choice of 4 layers is fairly arbitrary).

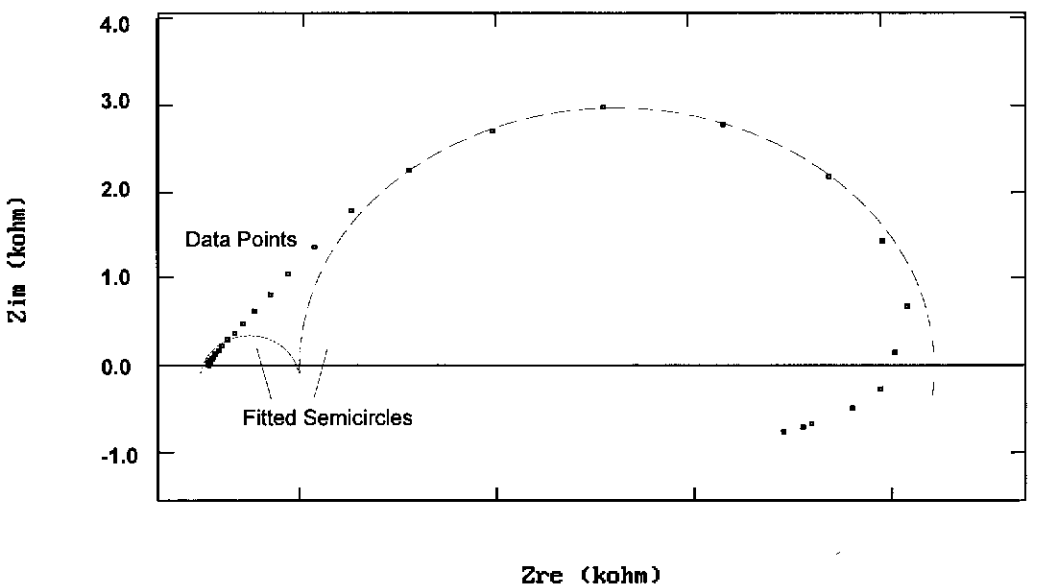


Figure 4.5 (a)

**Figure 4.5.** (a). Semicircle fitting of a typical Nyquist plot using the equivalent circuit in Figure 4.4.

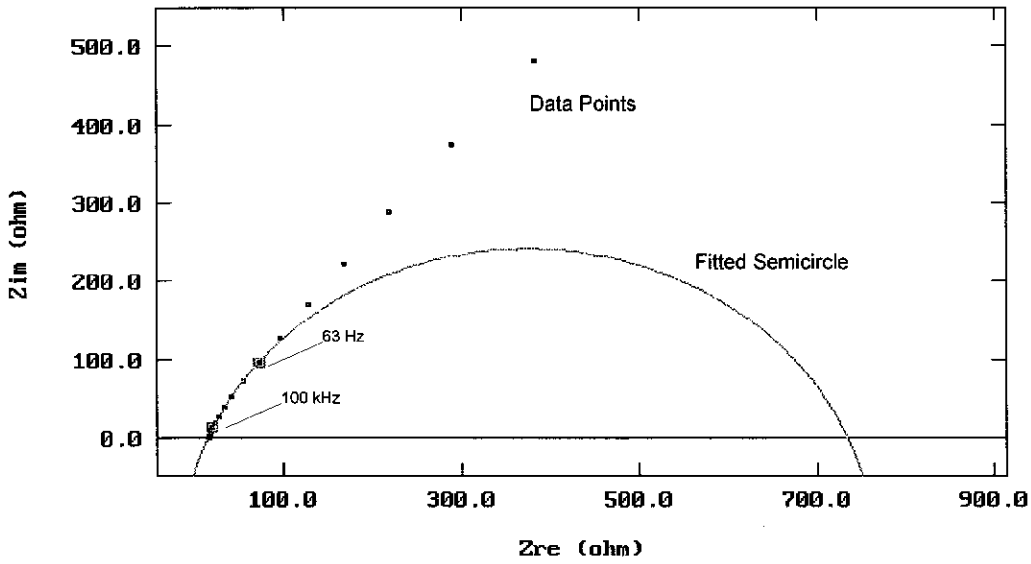


Figure 4.5 (b)

**Figure 4.5.** (b). Enlargement of semicircle fitting of high frequency data points.

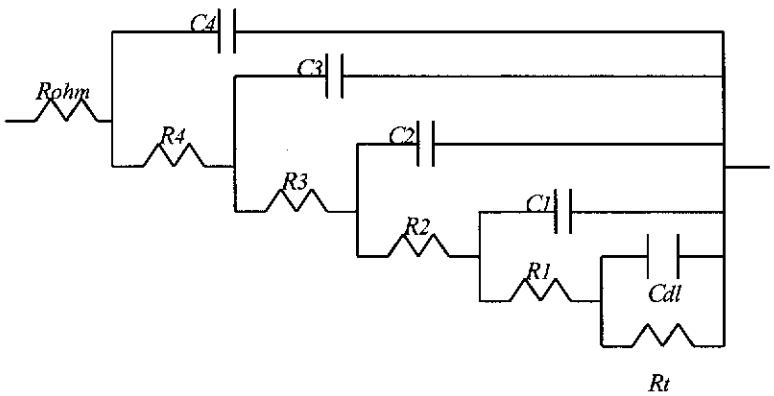


**Figure 4.6.** Equivalent circuit for an electrode filmed with a multi-layer, non-conducting inhibitor film (shows 4 layers only). $R_{ohm}$ is the solution resistance. $R_1$ - $R_4$ are the resistances of inhibitor layers. $C_1$ - $C_4$ are the capacitance of inhibitor layers. $R_t$ is the charge transfer resistance. $C_{dl}$ is the double layer capacitance.

The spectra were fitted satisfactorily using the four-layer model by a non-linear least square fit (NLLS-fit) and simulation computer program (Boukamp 1989). Figure 4.7 shows the fitting of the typical Nyquist plot in Figure 4.5.

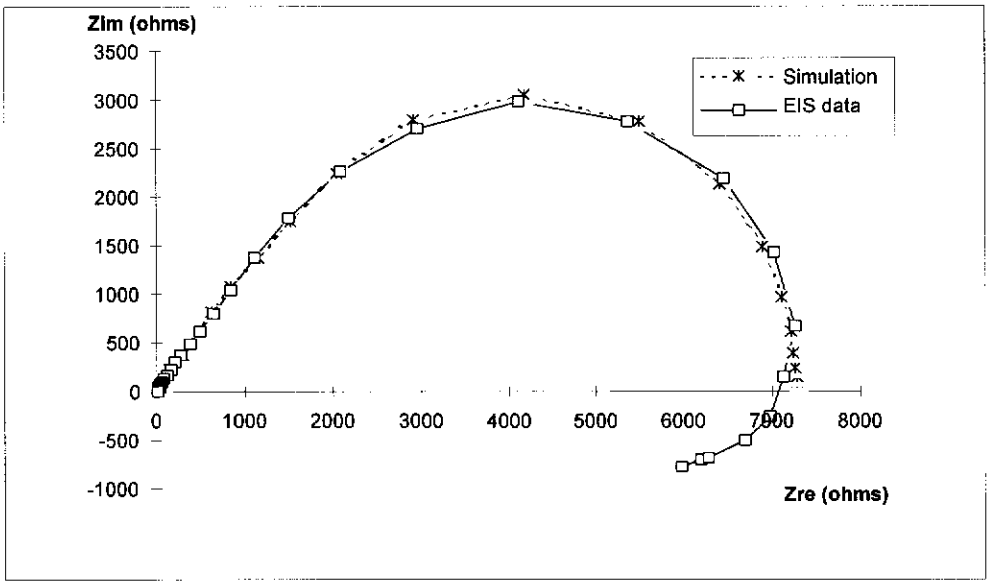


**Figure 4.7.** Computer simulation of a typical Nyquist plot using a four-layer model.

The electrochemical kinetics parameters of the electrode surface, including the resistances and capacitances of inhibitor layers ($R_1$ - $R_4$ and $C_1$ - $C_4$), electrochemical charge transfer resistance ($R_t$) and double layer capacitance ($C_{dl}$) can be deduced using the NLLS-fit and simulation program, and then the properties of the inhibitor film and electrochemical double layer can be defined. Table 4.1 shows the electrode surface electrochemical kinetics parameters during the formation of the inhibitor film.

**Table 4.1.** The continuous changes of the resistances and capacitances of inhibitor layers ($R_1$ - $R_4$ and $C_1$ - $C_4$), charge transfer resistance ($R_t$), and capacitance ($C_{dl}$) during inhibitor film formation. All measurements were carried out at 30 °C and with $CO_2$ sparging.

| Filming Hours | $R_t$ (ohms) | $C_{dl}$ ($\mu F$) | $R_1$ (ohms) | $C_1$ ($\mu F$) | $R_2$ (ohms) | $C_2$ ($\mu F$) | $R_3$ (ohms) | $C_3$ ($\mu F$) | $R_4$ (ohms) | $C_4$ ($\mu F$) |
|---|---|---|---|---|---|---|---|---|---|---|
| Before filming | 15 | 1690 | | | | | | | | |
| 0.5 | 122 | 951 | 159 | 193 | 63 | 119 | 10 | 83 | 2 | 22 |
| 2 | 207 | 7461 | 398 | 407 | 257 | 160 | 57 | 96 | 9 | 15 |
| 3 | 460 | 1678 | 649 | 211 | 205 | 103 | 49 | 39 | 20 | 12 |
| 4 | 483 | 4003 | 845 | 244 | 321 | 111 | 77 | 36 | 31 | 12 |
| 8.5 | 1119 | 1717 | 2082 | 169 | 600 | 63 | 200 | 22 | 62 | 11 |
| 13 | 2458 | 283 | 1736 | 98 | 565 | 34 | 178 | 13 | 61 | 11 |
| 18 | 3506 | 241 | 2110 | 91 | 653 | 34 | 198 | 13 | 63 | 10 |
| 24 | 3933 | 237 | 2312 | 89 | 719 | 33 | 221 | 13 | 69 | 11 |
| 28 | 4751 | 186 | 1619 | 57 | 424 | 19 | 102 | 10 | | |
| 33 | 4741 | 223 | 2538 | 77 | 827 | 28 | 235 | 11 | 69 | 10 |
| 37 | 5020 | 220 | 2690 | 74 | 875 | 27 | 250 | 11 | 72 | 10 |
| 42 | 5246 | 213 | 2732 | 72 | 880 | 27 | 249 | 11 | 72 | 10 |

The satisfactory simulation of the impedance characteristics of the inhibitor filmed electrode surface by a four-layer model, as shown in Figure 4.7 and Table 4.1, confirmed that the inhibitor film has a multi-layered structure. The resistance values of the four inhibitor layers are different from each other, which suggests that each inhibitor layer has a different inhibitor molecular density because the inhibitor layer resistance value is a reflection of the penetration of the inhibitor layer by electrolyte and so is related to the inhibitor molecular density in the layer. The first layer has the largest resistance and the fourth layer has the lowest resistance, i.e. the first inhibitor layer should have the densest inhibitor molecular structure and the fourth layer has the lowest inhibitor molecular density. Figure 4.8 shows linear relationships between the resistance of the 1st layer ($R_1$) and the resistances of other layers ($R_2$, $R_3$, $R_4$) during the inhibitor filming process. These linear relationships suggest that the molecular structure in each layer is closely related.

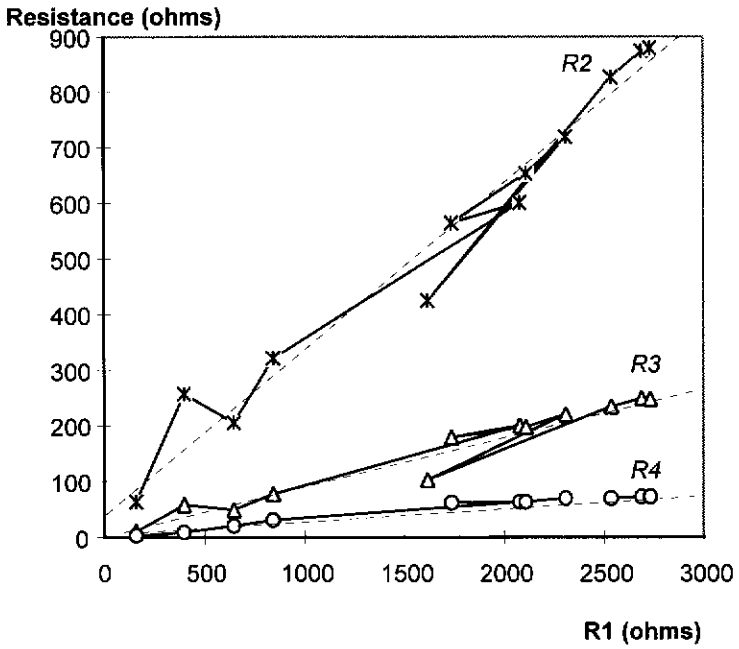


**Figure 4.8.** The relationships between the resistance of the first layer ($R_1$) and the resistances of the other layers ($R_2$, $R_3$, $R_4$) with the passage of time during the inhibitor filming process (time is a hidden variable).

During the first 8.5 hours inhibitor filming, as shown in Table 4.1, the resistances of the inhibitor layers quickly increased (10 times increase). After 8.5 hours, the resistances of inhibitor layers only increased slightly. The capacitances of inhibitor layers also quickly changed in the first 8.5 hours and kept relatively stable after 8.5 hours. These results suggest that the main structure of the inhibitor film was built-up in the first 8.5 hours.

However, after the rapid increase in the first 8.5 hours, the charge transfer resistance ($R_t$) maintained a continuous increase (from 1119 ohms to 5246 ohms) during the 42 hours of inhibitor film formation. Figure 4.9 shows the relationship between $R_t$ and the 1st layer resistance ($R_1$), which shows a linear relationship over the first 8.5 hours and after which $R_t$ showed a much faster increase than $R_1$. These results suggest a continuous change in the electrochemical double layer. An explanation is that a slow chemical reaction occurs at the electrode surface and forms a chemically bonded thin

surface film which results in a continuous increase in the charge transfer resistance. Actually the fact that the electrochemical equilibrium is achieved only very slowly may suggest that a slow surface chemical or chemisorptive reaction rather than an adsorption equilibrium process occurs because an adsorption equilibrium would likely be achieved much faster.

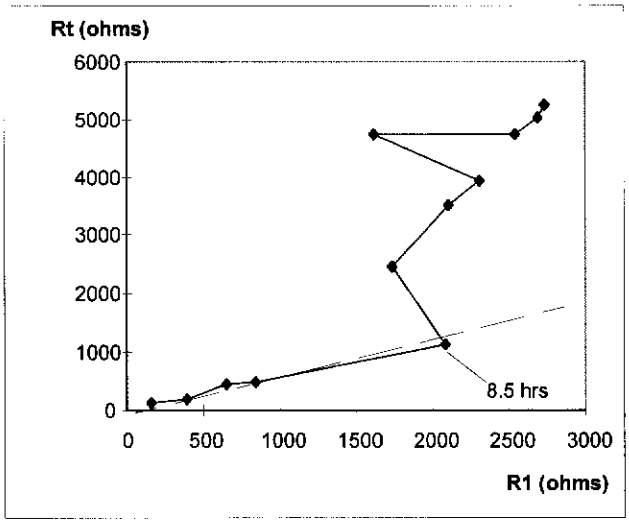


**Figure 4.9.** The relationship between charge transfer resistance and the resistance of the 1st layer ($R_1$) during the inhibitor filming process.

The $C_{dl}$ value is larger than the $C_{dl}$ of iron in oxygen corrosion system (typically 40 - 100 $\mu F/cm^2$). This may be due to the formation of surface scale which changes the electrode surface area and results in a larger capacitance due to the corrosion product layer impregnated with inhibitor.

According to the discussion above, a physical model can be suggested as shown in Figure 4.10. The inhibitor film is supposed to be a combination of an inner-layer (the 1st layer) which would basically be an inhibitor-metal complex and several outer-layers (the 2nd, the 3rd and the 4th layers) which would be inhibitor layers of different molecular density with possible inhibitor molecular cross-linking.

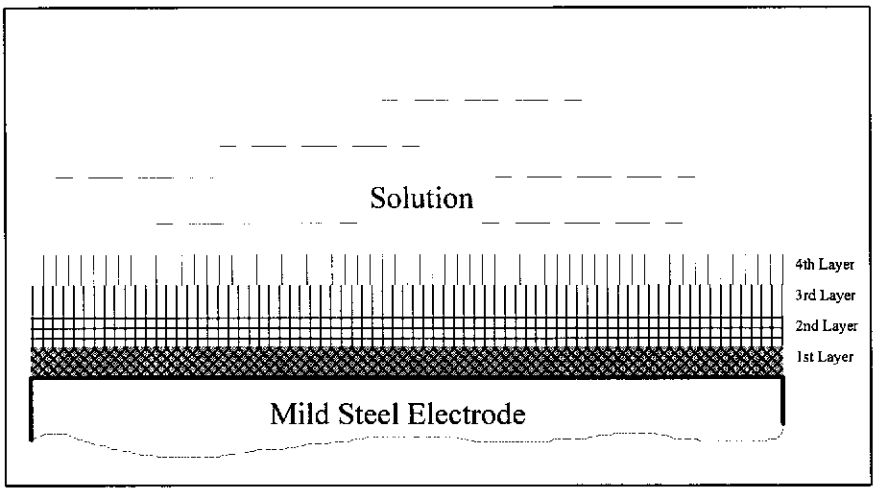


**Figure 4.10.** A physical model of an electrode surface filmed with a multi-layer, non-conducting inhibitor film (shows 4 layers only).

The changes in double layer capacitance and inhibitor layer capacitances also give information about the inhibitor film formation. The capacitance of a parallel-plate capacitor is related to the dielectric constant of the insulator, the area of the plates and the distance of separation between plates. Because the area of the electrode surface and the thickness of layers can be assumed to be unchanged, the changes in capacitance should be due to the changes in the dielectric constant of the layers, which is related to the formation of a chemically bonded film and the molecular density in the inhibitor layers. For example, the decrease in the capacitances of the inhibitor layers suggests a denser inhibitor molecular structure in the layers.

When the concentration of imidazoline inhibitor in brine decreases, significant changes can be observed in the EIS plots. Figure 4.11 shows EIS Nyquist and Bode phase plots which were recorded in 25 ppm imidazoline in brine during the inhibitor filming process. Compared with the EIS Nyquist plots which were recorded in 50 ppm imidazoline in brine, as shown in Figure 4.3 (a), the diameters of the Nyquist plots in Figure 4.11 (a) are much smaller, indicating less protection against corrosion. The Bode phase plots in Figure 4.11 (b) are quite different from those in Figure 4.3

(b). The higher frequency and lower frequency peaks in Figure 4.11 (b) are quite well resolved, which suggests that a simple equivalent circuit such as that shown in Figure 4.4 could be used to simulate the electrode surface. This result may suggest that an intact multi-layer inhibitor film can only form when inhibitor (imidazoline) concentration is high.

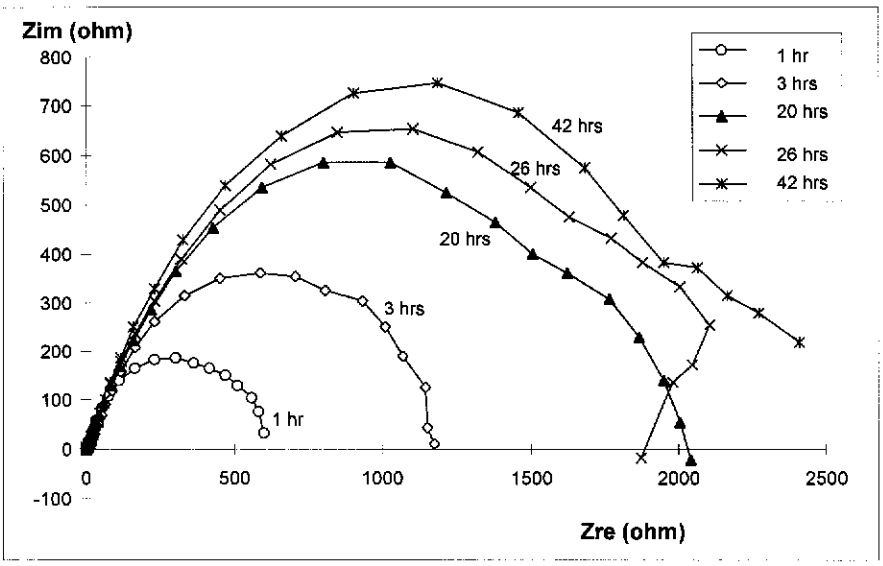


Figure 4.11 (a)

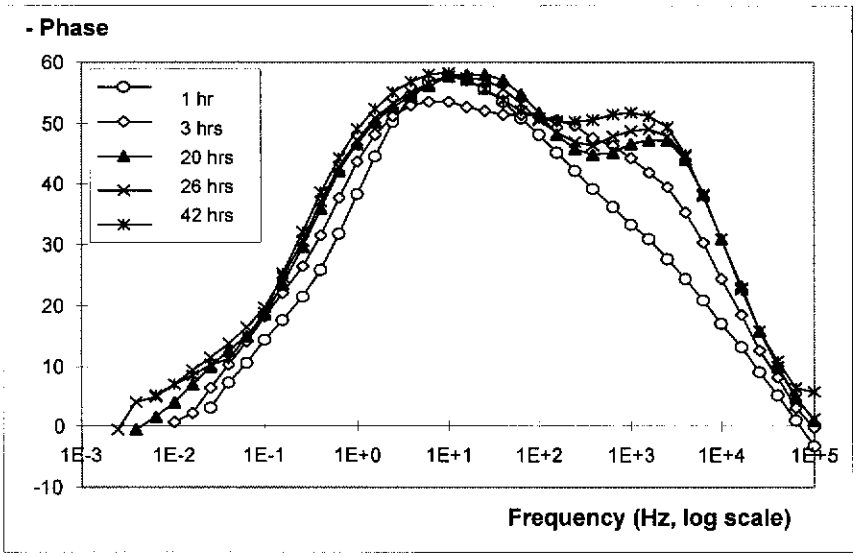


Figure 4.11 (b)

**Figure 4.11.** EIS plots recorded on a mild steel electrode after filming with imidazoline inhibitor (25 ppm) for different periods. Test solution was 3% NaCl brine with continuous $CO_2$ sparging at 30 °C. The electrode was kept stationary.

### 4.3.1.2. The deterioration of imidazoline film

After about 48 hours filming, the electrodes (in 50 ppm imidazoline) were transferred into environments where the inhibitor film may deteriorate. EIS measurements were carried out to monitor and study the inhibitor film deterioration process.

4.3.1.2.1 Inhibitor film in a diluted inhibitor brine and in an inhibitor-free fluid.

After being used in the inhibitor filming experiment, the inhibitor fluid was diluted from 50 to 5 ppm inhibitor concentration for studying the behaviour of the inhibitor film at low inhibitor concentration (The electrode was always kept in the solution phase). This test simulates the situation where inhibitor concentration drops for some reason such as blockage of the inhibitor supply valve. Figure 4.12 (a, b) shows EIS plots recorded on the electrode after different immersion times. Table 4.2 shows electrochemical parameters calculated from the EIS data.

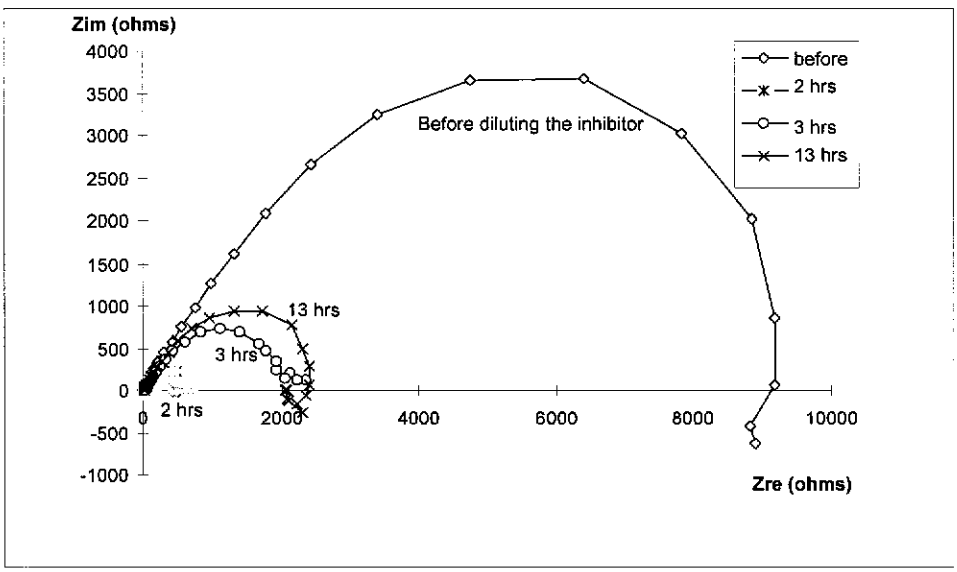


Figure 4.12 (a), EIS Nyquist plots

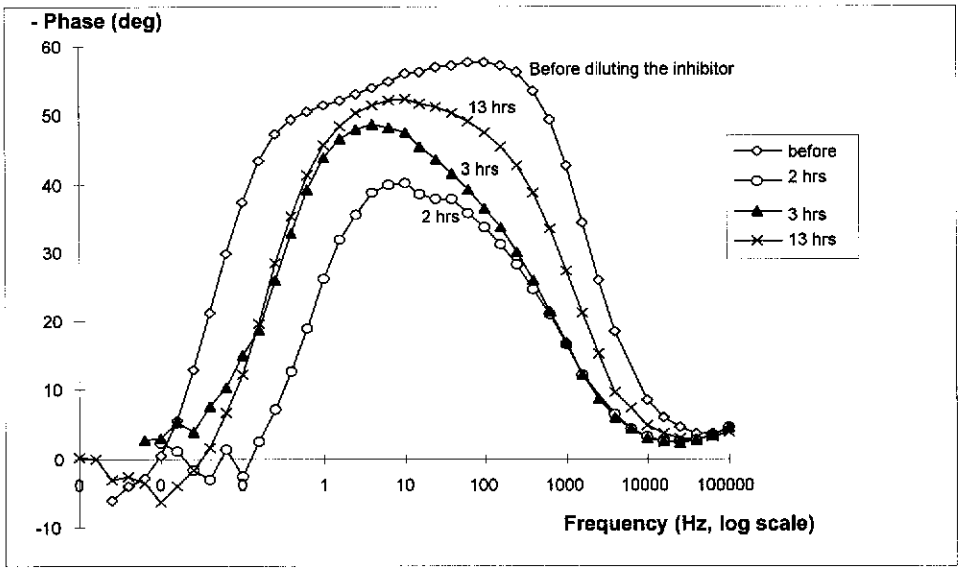


Figure 4.12 (b), EIS Bode phase plots

**Figure 4.12.** (a) EIS Nyquist plots and (b) EIS Bode phase plots after exposing the inhibitor filmed electrode to 5 ppm inhibitor in 3% NaCl brine.

**Table 4.2.** The continuous changes of the resistances and capacitances of inhibitor layers ($R_1$ - $R_4$ and $C_1$ - $C_4$), charge transfer resistance ($R_t$), and capacitance ($C_{dl}$) after diluting the inhibited brine from 50 ppm to 5 ppm inhibitor concentration. All measurements were carried out at 30 °C and with $CO_2$ sparging.

| Testing Hours | $R_t$ (ohms) | $C_{dl}$ ($\mu F$) | $R_1$ (ohms) | $C_1$ ($\mu F$) | $R_2$ (ohms) | $C_2$ ($\mu F$) | $R_3$ (ohms) | $C_3$ ($\mu F$) | $R_4$ (ohms) | $C_4$ ($\mu F$) |
|---|---|---|---|---|---|---|---|---|---|---|
| Before diluting | 5246 | 213 | 2732 | 72 | 880 | 27 | 249 | 11 | 72 | 10 |
| 2 | 225 | 419 | 266 | 97 | 102 | 31 | 38 | 14 | 4 | |
| 3 | 504 | 861 | 889 | 134 | 396 | 56 | 115 | 24 | 39 | 14 |
| 4 | 1383 | 246 | 907 | 77 | 274 | 35 | 76 | 13 | 28 | 12 |
| 8 | 1104 | 250 | 793 | 70 | 276 | 31 | 83 | 12 | 29 | 12 |
| 13 | 1150 | 247 | 847 | 71 | 309 | 31 | 92 | 13 | 33 | 12 |
| 18 | 1160 | 251 | 868 | 71 | 321 | 30 | 94 | 13 | 32 | 12 |
| 22 | 966 | 293 | 835 | 76 | 329 | 31 | 99 | 14 | 34 | 12 |

As expected, the inhibitor layer resistances ($R_1$- $R_4$) and electrochemical charge transfer resistance ($R_t$) immediately dropped after diluting the inhibited brine, as shown in Table 4.2. However, it was not expected that the electrode impedance would increase again, as shown in Figure 4.12 (a) and Table 4.2, which may mean the inhibitor film is recovered by some means. A similar result was also observed after

moving the testing electrode into an inhibitor-free 3% NaCl solution, as shown in Figure 4.13 and Table 4.3.

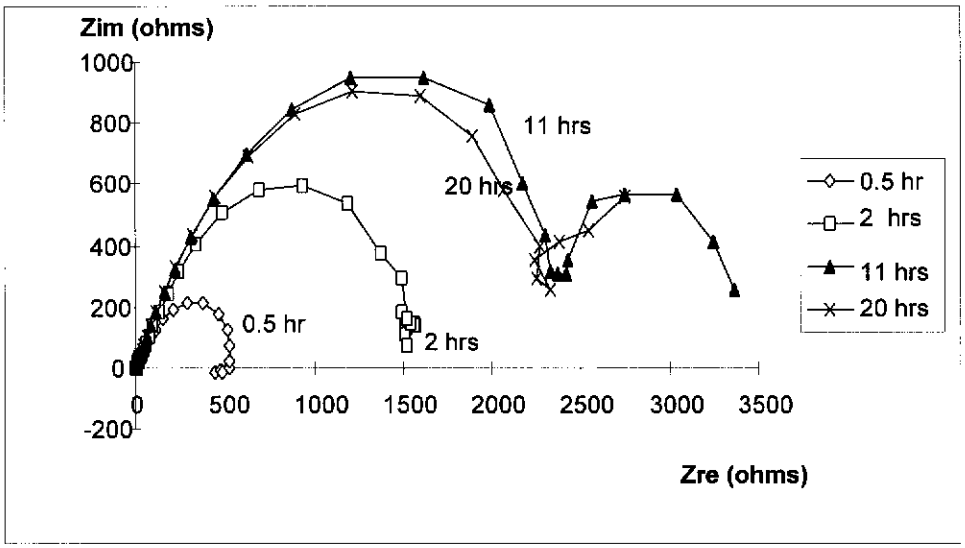


**Figure 4.13.** EIS Nyquist plots after transferring the inhibitor filmed electrode into an inhibitor-free 3% NaCl brine.

**Table 4.3.** The continuous changes of the resistances and capacitances of inhibitor layers ($R_1$ - $R_4$ and $C_1$ - $C_4$), charge transfer resistance ($R_t$), and capacitance ($C_{dl}$) after transferring the inhibitor filmed electrode into an inhibitor-free fresh brine. All measurements were carried out at 30 °C and with $CO_2$ sparging.

| Testing Hours | $R_t$ (ohms) | $C_{dl}$ ($\mu F$) | $R_1$ (ohms) | $C_1$ ($\mu F$) | $R_2$ (ohms) | $C_2$ ($\mu F$) | $R_3$ (ohms) | $C_3$ ($\mu F$) | $R_4$ (ohms) | $C_4$ ($\mu F$) |
|---|---|---|---|---|---|---|---|---|---|---|
| Before diluting | 966 | 293 | 835 | 76 | 329 | 31 | 99 | 14 | 34 | 12 |
| 0.5 | 225 | 340 | 208 | 103 | 77 | 40 | 27 | 13 | 11 | 13 |
| 2 | 739 | 299 | 557 | 93 | 159 | 39 | 45 | 14 | 14 | 14 |
| 7 | 1138 | 284 | 833 | 77 | 251 | 35 | 59 | 13 | 18 | 13 |
| 11 | 1177 | 282 | 867 | 74 | 268 | 34 | 62 | 13 | 20 | 12 |
| 16 | 1141 | 300 | 888 | 73 | 280 | 34 | 62 | 13 | 21 | 12 |
| 20 | 1106 | 268 | 814 | 67 | 258 | 34 | 57 | 12 | 20 | 12 |

Although the inhibitor layer resistances and double layer resistance experienced large changes, as shown in Tables 4.2 and 4.3, the inhibitor layer capacitances and electrochemical double layer capacitance only had relatively small changes after the electrode was transferred to 5 ppm and 0 ppm inhibitor brine. This suggests that the

main structures of the inhibitor film and the electrochemical double layer have not been changed. A possible explanation for the sudden decrease of film resistance and electrochemical charge transfer resistance may be localised breakdown of the inhibitor film by an unknown mechanism. In that case, the resistances in 'pore' areas of the inhibitor film, which is much smaller than the inhibitor film resistance, will be measured, resulting in a very small resistance value.

The inhibitor film recovery, which is indicated by the increase of inhibitor film and charge transfer resistances in both 5 ppm and 0 ppm inhibitor in brine solutions, may be due to a self-repairing (self-sealing) effect of the inhibitor film. The multi-layer characteristic of the inhibitor film, as discussed above, makes the self-repairing possible. The self-repairing characteristic in fact provides further evidence of the multi-layer structure of the inhibitor film.

$CO_2$ corrosion product may also contribute to the sealing of the inhibitor film. As the inhibitor film is broken down locally, the corrosion rate increases greatly in these small areas and a protective corrosion product may thus form in these local 'pore' areas.

The fact that the charge transfer resistance and inhibitor layer resistances in 5 ppm inhibitor brine after about 22 hours, as shown in Table 4.2, is similar as that in inhibitor-free brine after about 20 hours, as shown in Table 4.3, suggests that the electrochemical kinetics and inhibitor surface coverage of the electrode surface are independent of inhibitor concentration. Thus, it can be concluded that the inhibitor does not obey adsorption laws and the inhibitor film is not an adsorptive film, but rather that a chemisorbed layer is formed. These characteristics of the inhibitor imidazoline seem to match the characterisation of interphase inhibition suggested by Mansfeld *et al.* (1985).

4.3.1.2.2 Inhibitor film destruction by surface shear stress

Finally, the electrode was rotated at 1000 rpm to investigate inhibitor film destruction by surface shear stress. Figure 4.14 (a ,b) shows EIS plots recorded on the electrode at different times. Table 4.4 shows electrochemical parameters calculated from EIS data.

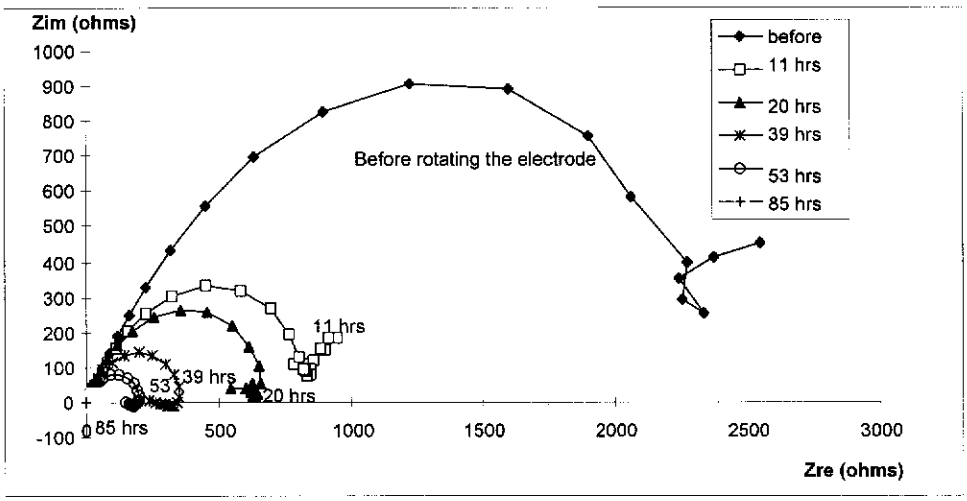


Figure 4.14 (a). EIS Nyquist plots

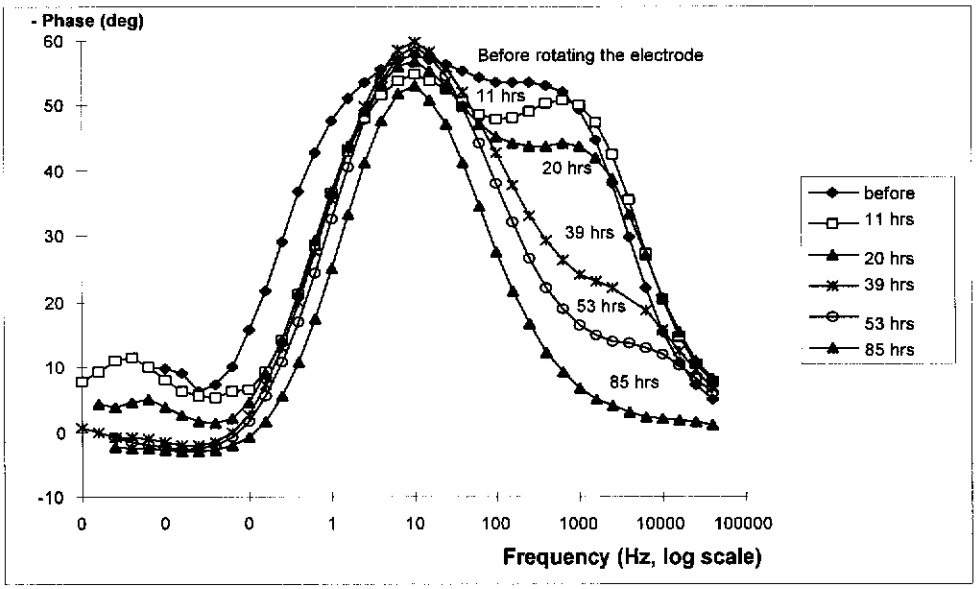


Figure 4.14 (b). EIS Bode phase plots

**Figure 4.14.** EIS plots before and after rotating the inhibitor filmed electrode (1000 rpm) in an inhibitor-free 3% NaCl brine.

**Table 4.4.** The continuous changes of the resistances and capacitances of inhibitor layers ($R_1$ - $R_4$ and $C_1$ - $C_4$), charge transfer resistance ($R_t$), and capacitance ($C_{dl}$) after rotating the electrode at 1000 rpm in the fresh brine. All measurements were carried out at 30 °C and with $CO_2$ sparging.

| Testing Hours | $R_t$ (ohms) | $C_{dl}$ ($\mu F$) | $R_1$ (ohms) | $C_1$ ($\mu F$) | $R_2$ (ohms) | $C_2$ ($\mu F$) | $R_3$ (ohms) | $C_3$ ($\mu F$) | $R_4$ (ohms) | $C_4$ ($\mu F$) | Corr. Rate (mm/y) |
|---|---|---|---|---|---|---|---|---|---|---|---|
| **before Stirring** | 1106 | 268 | 814 | 67 | 258 | 34 | 57 | 12 | 20 | 12 | **0.02** |
| 2 | 428 | 424 | 459 | 82 | 181 | 36 | 46 | 13 | 19 | 12 | **0.04** |
| 6 | 353 | 396 | 373 | 86 | 130 | 45 | 35 | 14 | 15 | 13 | **0.05** |
| 11 | 356 | 347 | 341 | 81 | 92 | 47 | 27 | 12 | 9 | 12 | **0.05** |
| 15 | 322 | 386 | 312 | 87 | 73 | 53 | 22 | 15 | 9 | 12 | **0.06** |
| 20 | 283 | 447 | 291 | 97 | 62 | 59 | 17 | 17 | 7 | 12 | **0.06** |
| 29 | 219 | 526 | 226 | 120 | 42 | 69 | 10 | 30 | 5 | 12 | **0.08** |
| 34 | 173 | 712 | 198 | 142 | 42 | 90 | 7 | 42 | 4 | 12 | **0.10** |
| 39 | 128 | 941 | 168 | 162 | 43 | 114 | 7 | 59 | 3 | 13 | **0.29** |
| 43 | 105 | 1122 | 142 | 186 | 34 | 139 | 5 | 65 | 2 | 13 | **0.35** |
| 53 | 68 | 1497 | 99 | 231 | 25 | 185 | 4 | 99 | 2 | 14 | **0.54** |
| 70 | 56 | 1609 | 82 | 261 | 23 | 213 | 3 | 111 | 1 | 14 | **0.66** |
| 75 | 38 | 2136 | 59 | 340 | 17 | 280 | 2 | 143 | 1 | 19 | **0.97** |
| 80 | 24 | 2894 | 41 | 445 | 13 | 336 | 2 | 230 | 0.5 | 33 | **1.54** |

The corrosion rates in Table 4.4 were estimated using $R_t$ data and the Stern-Geary equation:

$$I_{corr} = \frac{b_a b_c}{2.303(b_a + b_c)} \times \frac{1}{R_p} \approx \frac{b_a b_c}{2.303(b_a + b_c)} \times \frac{1}{R_t}$$

The continuous decrease in the diameter of Nyquist plots and the gradual disappearance of the high frequency phase angle shift, as shown in Figure 4.14(a) and (b), means that the inhibitor film is gradually removed by surface shear stress. The film destruction process was very slow, suggesting a strong interaction between the electrode and the inhibitor. On comparison of Figure 4.14 (b) with Figure 4.3 (b), very similar trends are seen, but in the opposite time series. This suggests that the film destruction and film formation probably follow a 'reversible' process.

4.3.1.2.3 Evaluation of inhibitor film persistency

The inhibitor failure process is clearly shown in Figure 4.14 (a), (b) and in Table 4.4. This means that the inhibitor film persistency (the time before inhibitor failure) can be assessed using EIS to give data such as those shown in Figure 4.15.

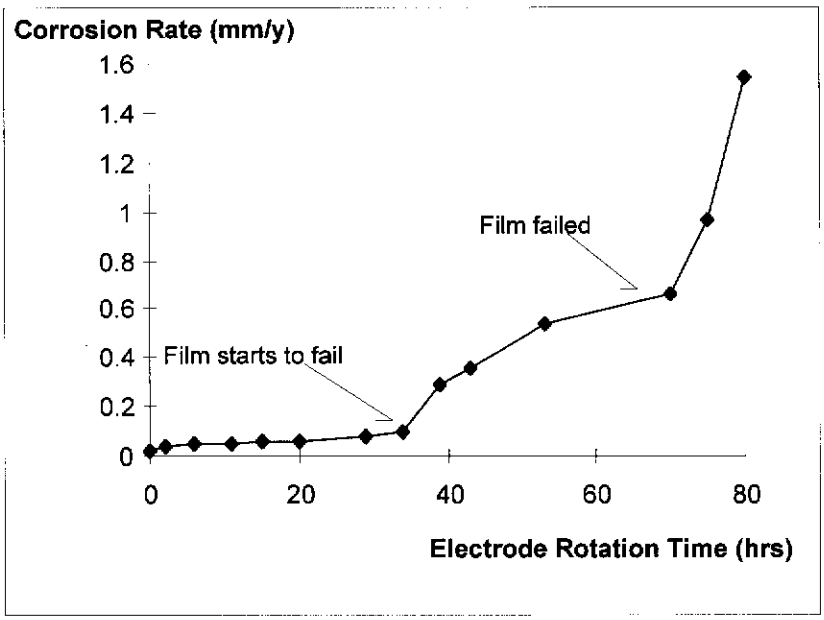


**Figure 4.15.** Inhibitor film failure after rotating the filmed electrode at 1000 rpm in inhibitor-free brine.

## 4.3.2 Other Inhibitor films

A commercial formulated $CO_2$ corrosion inhibitor (C-798) and two commercial inhibitor bases, a quaternised amine and a polymerised vegetable fatty acid, were also studied using EIS.

### 4.3.2.1. Quaternised amine

Figures 4.16 show EIS plots recorded on electrodes exposed to brines containing 50 ppm of quaternised amine inhibitor.

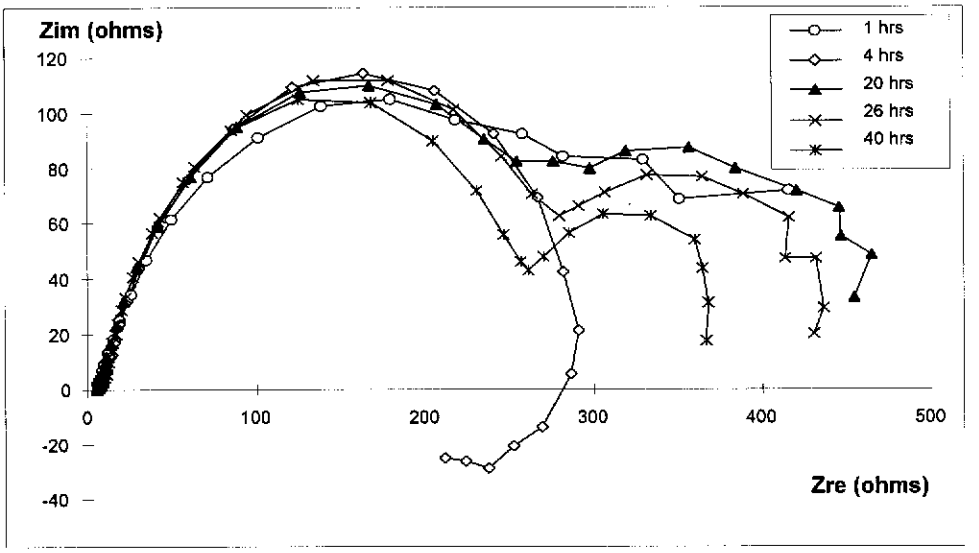


Figure 4.16 (a). EIS Nyquist plots

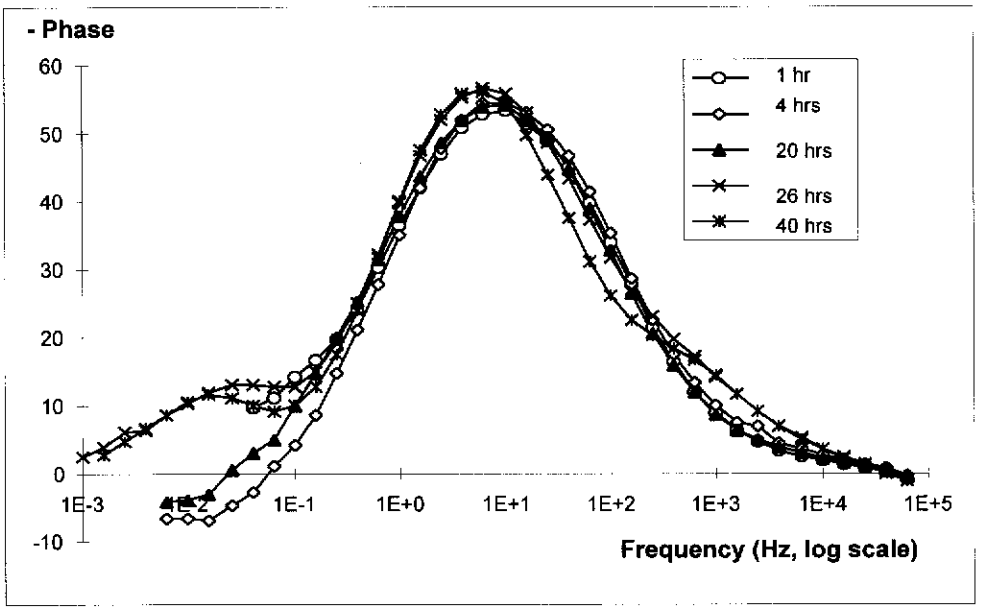


Figure 4.16 (b). EIS Bode phase plots

**Figure 4.16.** EIS plots recorded on a mild steel electrode after filming with quaternised amine inhibitor (50 ppm) for different periods. Testing base solution was 3% NaCl brine with continuous $CO_2$ sparging at 30 °C. The electrode was kept stationary.

Significant differences can be found by comparison of the EIS plots in Figures 4.16 with the plots in Figure 4.3. The diameters of Nyquist plots in Figures 4.16 (a) are

much smaller than those in Figure 4.3 (a), which suggests that the corrosion preventive ability of the quaternised amine was not as good as imidazoline. Unlike the imidazoline film, the formation of quaternised amine film was shown to be a rapid process because the electrode impedance, indicated by the diameters of Nyquist plots in Figures 4.16 (a), did not change much during the 40 hours filming period.

The Bode phase plots in Figure 4.16 (b) do not show a high frequency peak as was found in Figure 4.3 (b), which suggests that no three-dimensionally intact surface film was formed during the inhibitor filming process. The inhibitor film formed in brine containing the quaternised amine is likely a physically or electrostatically adsorptive molecular layer which forms rapidly and inhibits corrosion by affecting the electrochemical double layer on the electrode surface. A surface model is suggested in Figure 4.17. The characteristics of the quaternised amine matches the characterisation of interface inhibition (Mansfeld *et al.* 1985). Interface inhibition presumes a strong interaction between the corroding substrate and the inhibitor forming a two-dimensional adsorbate layer. Interphase inhibition presumes a three-dimensional layer between the corroding substrate and electrolyte.

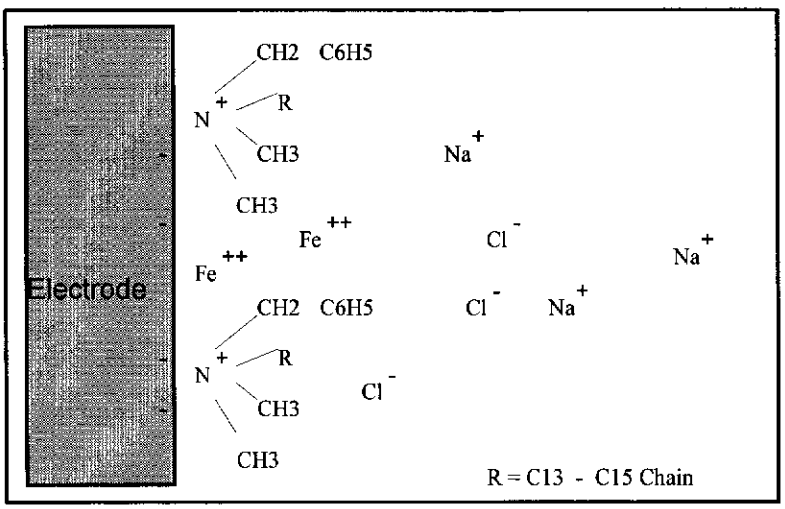


**Figure 4.17.** A surface model of an electrode filmed with quaternised amine inhibitor.

The adsorption of quaternised amine molecules on the electrode surface is much stronger than that of imidazoline molecules. As shown in Figure 4.18, imidazoline loses efficiency when quaternised amine is present. This is because the rapid (prior) adsorption of quaternised amine molecules on the electrode surface kept imidazoline molecules away from the surface, preventing them from chemically reacting with electrode surface. Indeed, the electrode impedance values in Figure 4.18 are very close to those in Figure 4.16, where only quaternised amine is present.

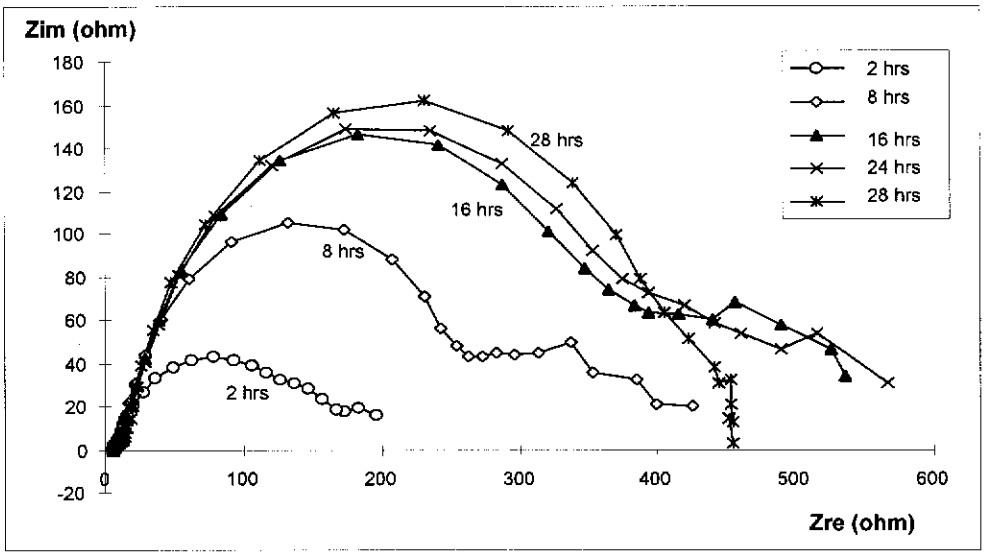


**Figure 4.18.** EIS plots recorded on a mild steel electrode after exposure to a brine containing mixed inhibitors (quaternised amine 50 ppm + imidazoline 50 ppm) for different periods. Base solution was 3% NaCl brine with continuous $CO_2$ sparging at 30 °C. The electrode was kept stationary.

The extra phase angle peak in Figure 4.16 (b) at very low frequency ($10^{-1}$ to $10^{-3}$ Hz), which corresponds to the low frequency arc of the Nyquist plots in Figure 4.16 (a), is likely a depressed diffusion tail, arising from the $CO_2$ molecular diffusion through the layer of corrosion products. A similar analysis was made by Bonnel *et al.* (1983) and Dabosi *et al.* (1983).

When the concentration of quaternised amine inhibitor is diluted to 5 ppm, as shown in Figure 4.19, the electrode impedance shows a rapid and continuous decrease. This behaviour suggests again that this inhibitor film is just an adsorptive molecular layer which desorbs easily and quickly.

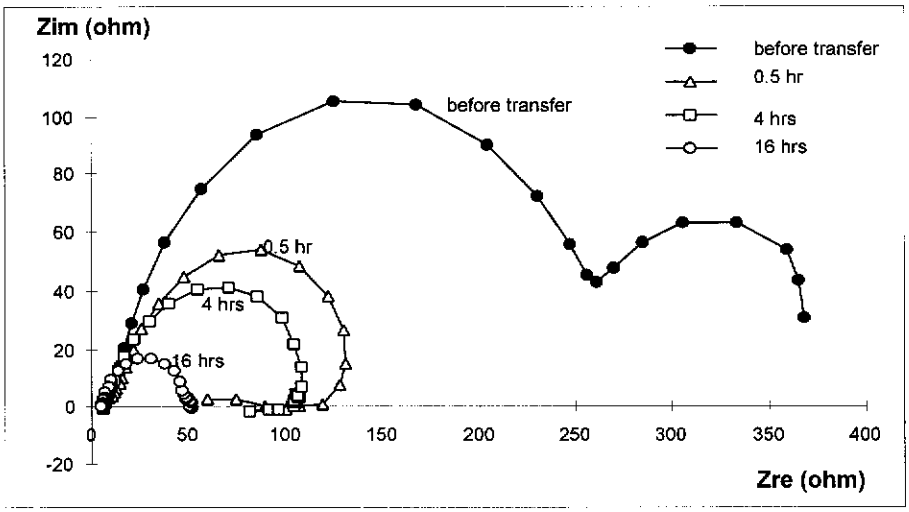


**Figure 4.19.** EIS Nyquist plots after the concentration of quaternised amine inhibitor in brine is diluted to 5 ppm. Base solution was 3% NaCl brine with continuous $CO_2$ sparging at 30 °C. The electrode was kept stationary.

### 4.3.2.2. Polymerised vegetable fatty acid

Figure 4.20 shows EIS plots recorded on electrodes exposed to brines containing 50 ppm of polymerised vegetable fatty acid.

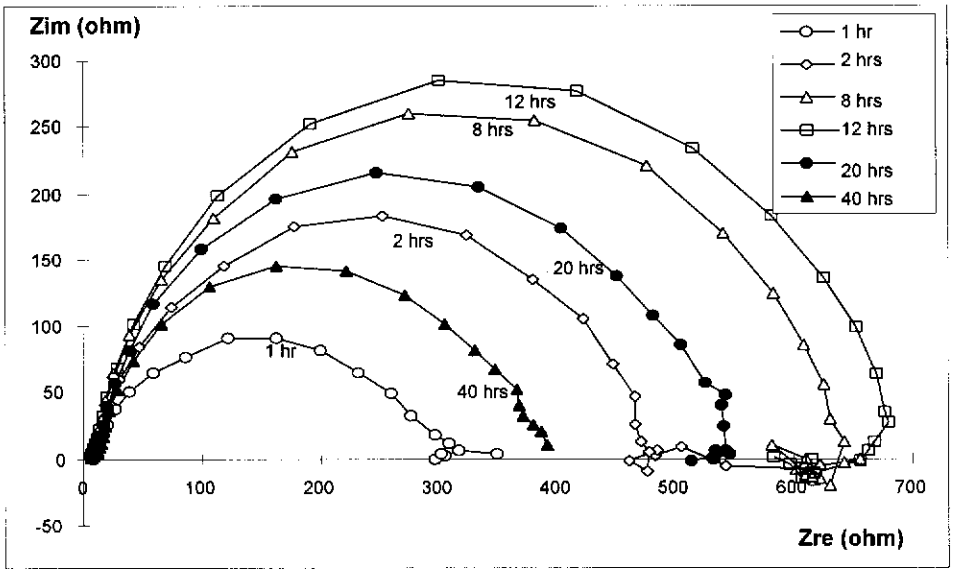


Figure 4.20 (a). EIS Nyquist plots

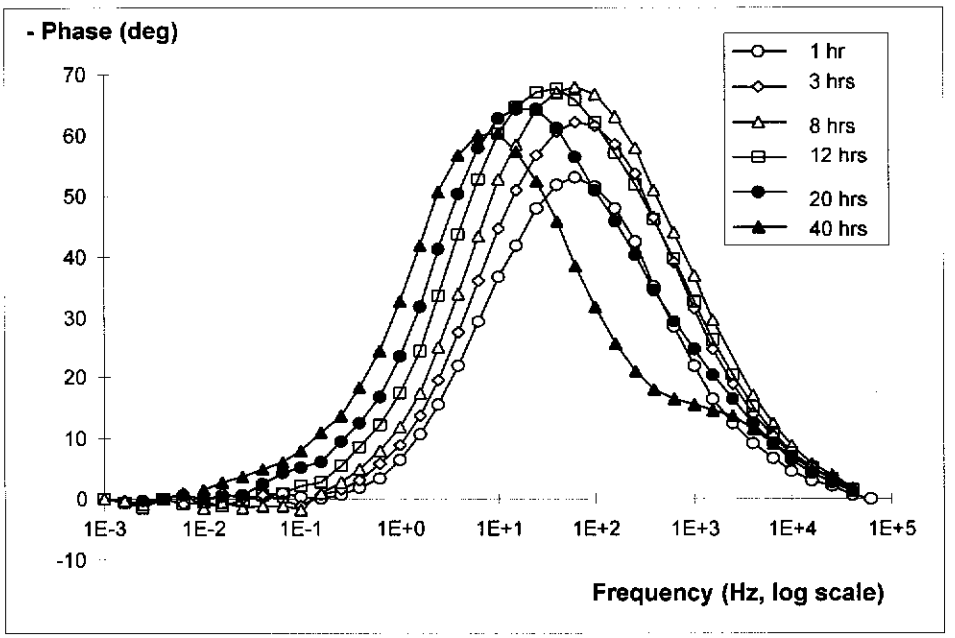


Figure 4.20 (b). EIS Bode phase plots

**Figure 4.20.** EIS plots recorded on a mild steel electrode after being exposed to a brine containing 50 ppm polymerised vegetable fatty acid for different periods. Base solution was 3% NaCl brine with continuous $CO_2$ sparging at 30 °C. The electrode was kept stationary.

Although the electrode impedance increased with time in the first 12 hours, as indicated by the diameter of the Nyquist plots in Figure 4.20 (a), the electrode impedance decreased afterwards. This is a surprising result and its mechanism is not known. The Bode phase plots in Figure 4.20 (b) do not show a high frequency peak and so no three-dimensionally intact surface film was formed during the inhibitor filming process.

However after adding a surfactant to the filming fluid, the inhibitor film was improved and stabilised and a high frequency peak emerged, as shown in Figure 4.21 (a ,b). The surfactant, nonyl phenol ethoxylate, is normally used to enhance the adsorption of inhibitor at the metal surface and itself has no inhibition to corrosion, which was proven by EIS measurements.

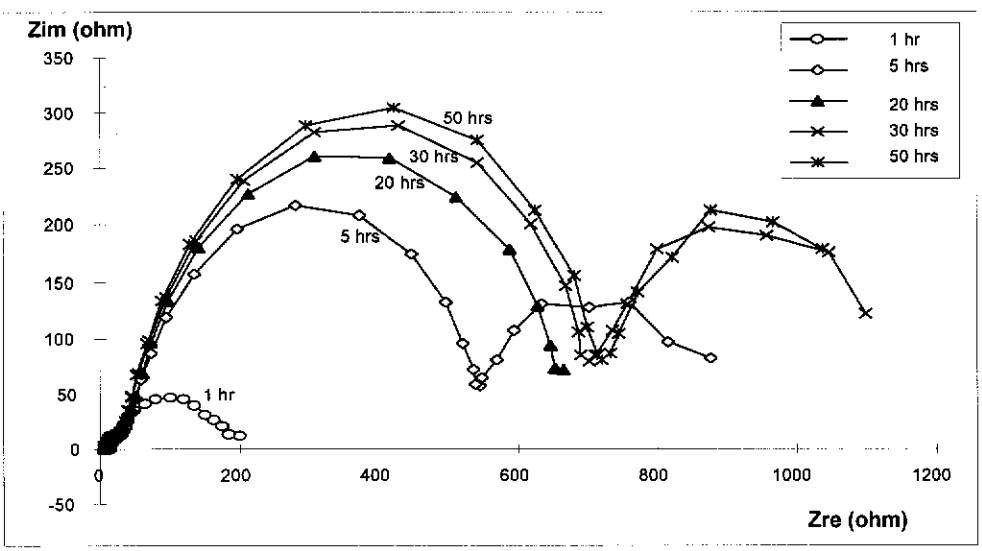


Figure 4.21 (a). EIS Nyquist plots

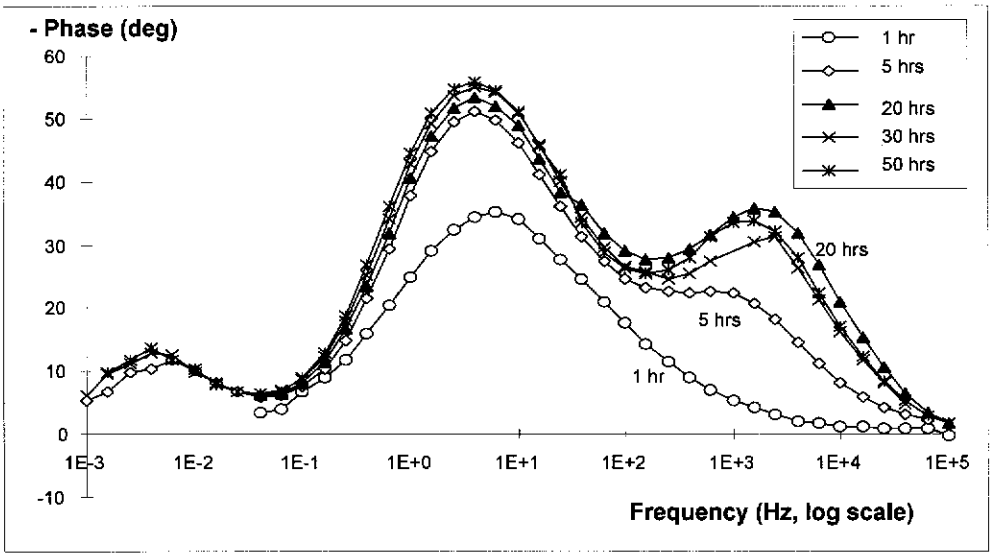


Figure 4.21 (b). EIS Bode plots

**Figure 4.21.** EIS plots recorded on a mild steel electrode after being exposed to a brine containing 50 ppm of polymerised vegetable fatty acid and 50 ppm of nonyl phenol ethoxylate, for different periods. Base solution was 3% NaCl brine with continuous $CO_2$ sparging at 30 °C. The electrode was kept stationary.

As shown in Figure 4.21 (a), the electrode impedance shows a continuous increase and does not drop with extended exposure time, as it does in Figure 4.20 (a). A well resolved high frequency phase peak emerges in Figure 4.21 (b) which suggests the formation of a non-conductive surface inhibitor film. Polymerised vegetable fatty acid inhibitor and nonyl phenol ethoxylate surfactant therefore show synergistic effects in the formation of a protective inhibitor film. Polymerised vegetable fatty acid seems to have characteristics between interphase and interface inhibition.

### 4.3.2.3. Formulated inhibitor

Figure 4.22 shows EIS plots recorded from an electrode exposing to a brine containing 50 ppm of commercial formulated $CO_2$ corrosion inhibitor, C-798 (Applied Chemicals, Australia).

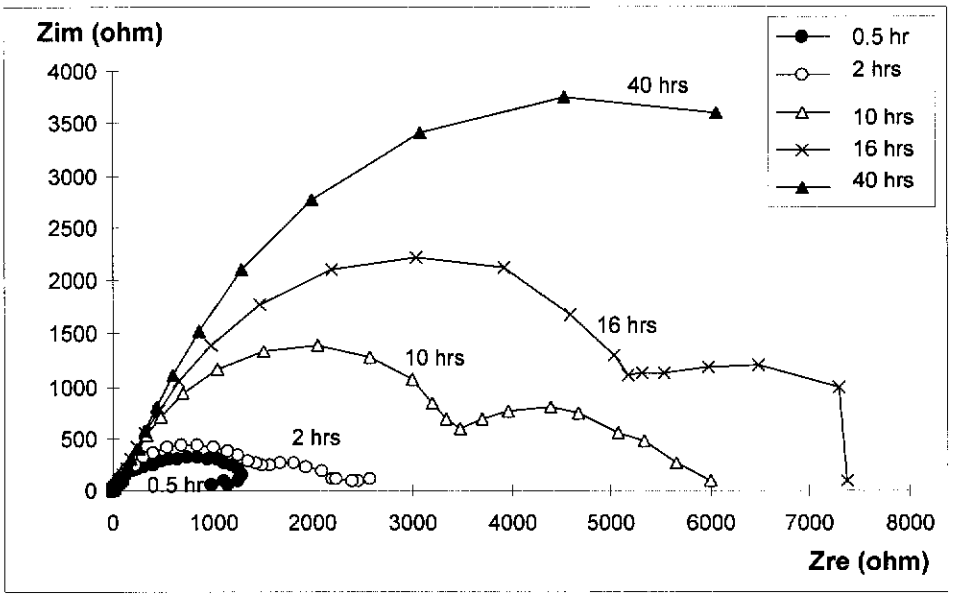


Figure 4.22 (a). EIS Nyquist plots

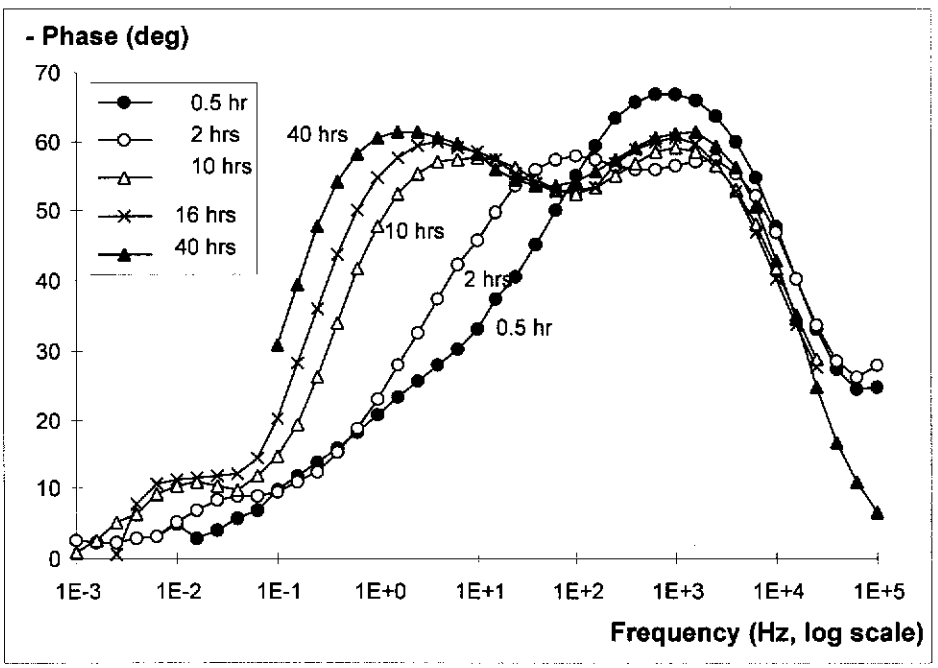


Figure 4.22 (b). EIS Bode plots

**Figure 4.22.** EIS plots recorded on a mild steel electrode after being exposed to a brine containing 50 ppm of commercial formulated $CO_2$ corrosion inhibitor, C-798 (Applied Chemicals, Australia) for different periods. Base solution was 3% NaCl brine with continuous $CO_2$ sparging at 30 °C. The electrode was kept stationary.

The formation of the C-798 inhibitor film was shown to be a very fast process, indicated by the very fast formation of the high frequency phase peak in Figure 4.22 (b). Similarities can be found by comparing Figure 4.22 with Figure 4.3 which shows the EIS plots of an electrode filming with imidazoline inhibitor. Thus C-798 inhibitor may work in a similar way to imidazoline. Indeed, inhibitor C-798 showed a similar self-repairing ability to imidazoline, as shown in Figure 4.23. Figure 4.23 shows similar EIS characteristics to Figures 4.12 and 4.13 which were also obtained by transferring the filmed electrodes into an inhibitor-free brine solution.

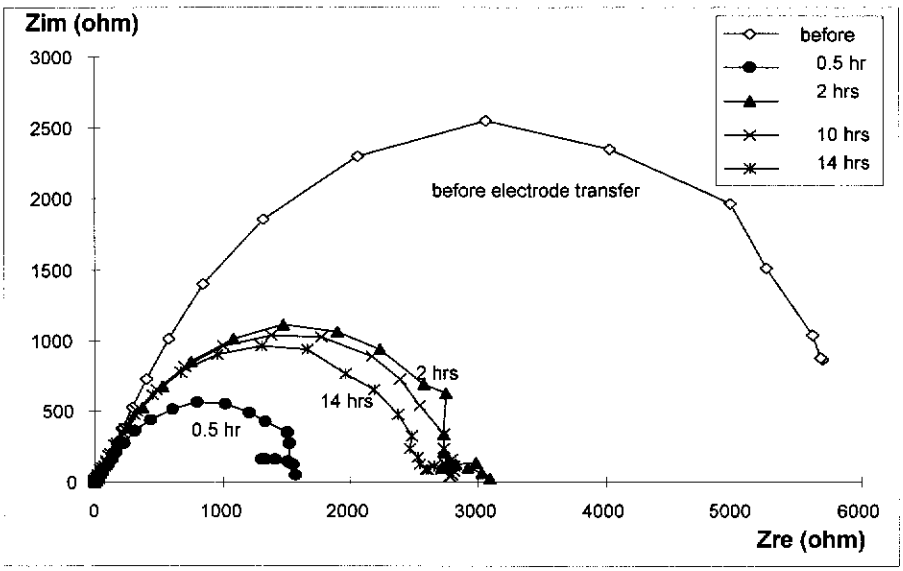


**Figure 4.23.** EIS Nyquist plots after transferring the inhibitor filmed electrode from 5 ppm inhibitor brine into an inhibitor-free 3% NaCl brine.

## 4.4 Results and discussion II: The monitoring of inhibitor film performance and persistency using ENA

Although electrochemical impedance spectroscopy (EIS) was shown to be a powerful technique for studying the mechanism of inhibitors and for estimating corrosion rate, as with many electrochemical techniques, EIS has limitations. Each EIS measurement takes quite a long time (often more than two hours) and so it is difficult to monitor inhibitor film performance continuously. EIS cannot reliably be used in a corrosion system where parameters such as potential are changing rapidly, as discussed in section 2.2.1, thus EIS can not be used to study rapid corrosion electrochemical process, e.g. immediately after inhibitor addition. In addition, the instruments for carrying out EIS measurement are generally expensive and complicated.

In this work, electrochemical noise analysis (ENA) was used to continuously monitor inhibitor performance and corrosion electrochemical processes, especially the rapid inhibitor film formation and breakdown processes. The objectives of this work are to develop ENA as a combined technique with EIS and to develop ENA as an *in-situ* technique. The new developments in the electrochemical noise analysis technique and theory, described in section 2.4, were also tested experimentally.

### 4.4.1 The monitoring of inhibitor film formation

A dual mild steel electrode was placed in a brine solution containing 25 ppm of imidazoline inhibitor for filming, as shown in Figure 4.2. Electrochemical noise recording was carried out continuously to monitor the inhibitor film formation processes. EIS and linear polarisation (LP) measurements, as reference techniques, were carried out alternately with electrochemical noise recording using the same

electrode in the same electrochemical cell. In this way, ENA, EIS and LP were compared directly.

After exposure to the inhibited brine, as shown in Figure 4.24, the corrosion potential of the dual electrode quickly became positive (the potential shifted about 40 mV in the first 1000 seconds). Although the potential shift *vs.* time in Figure 4.24 (a) can provide some information about the corrosion mechanism, corrosion potential shift does not necessarily have any correlation with corrosion rate. The corresponding current *vs.* time record is shown in Figure 4.24 (b).

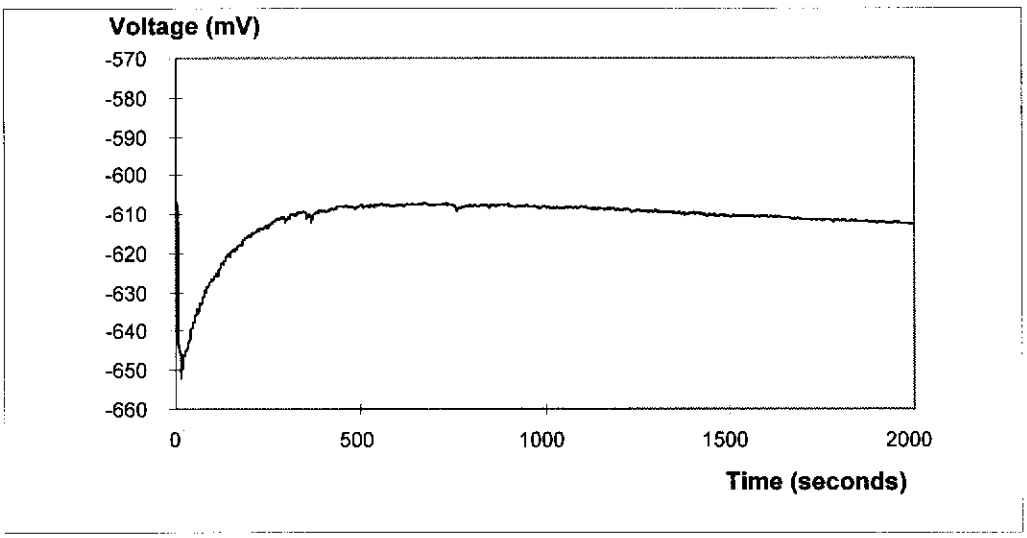


Figure 4.24 (a), raw potential noise record

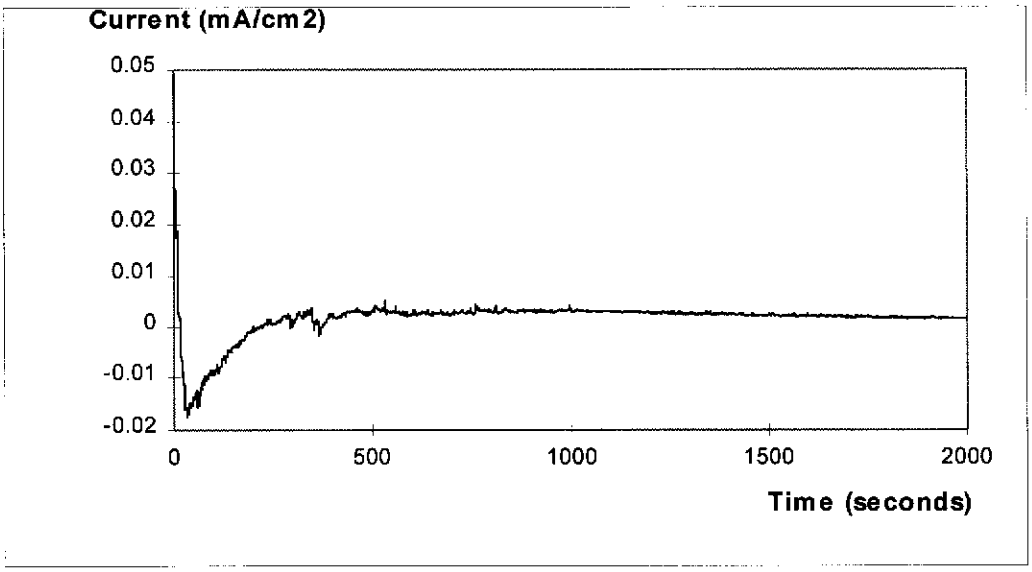


Figure 4.24 (b), raw current noise record

**Figure 4.24.** Original voltage (a) and current (b) noise records on a mild steel electrode immediately after being exposed to a brine containing 25 ppm of imidazoline inhibitor. Base solution was 3% NaCl brine with continuous $CO_2$ sparging at 30 °C. The electrode was kept stationary.

Using the moving average removal treatment, as described in section 2.4.1, the real voltage noise was extracted from the potential vs. time curve in Figure 4.24 (a) and is shown in Figure 4.25 (a), the real current noise was extracted from the current vs. time curve in Figure 4.24 (b) and is shown in Figure 4.25 (b).

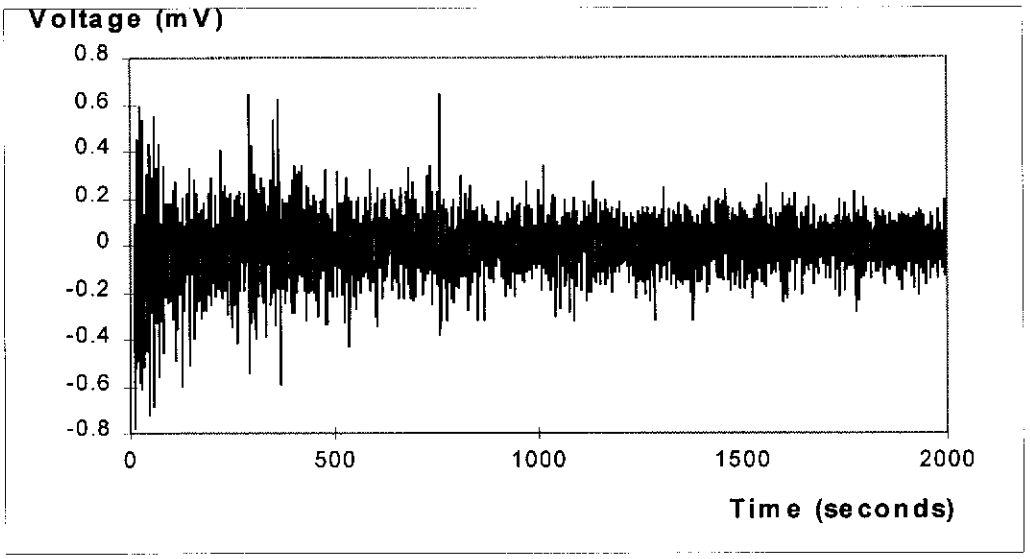


Figure 4.25 (a), Voltage noise in the first 2000 seconds

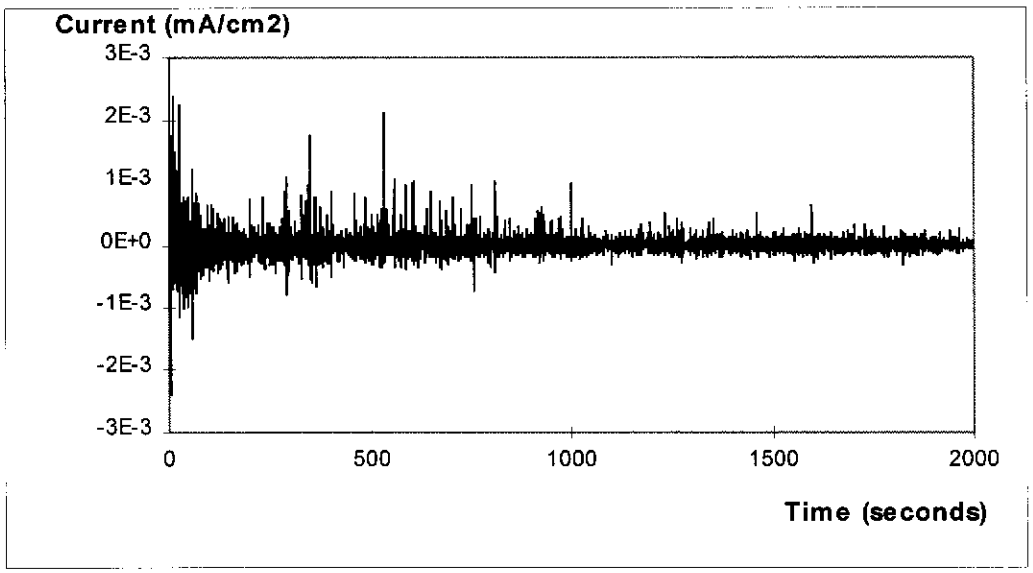


Figure 4.25 (b), current noise in the first 2000 seconds

**Figure 4.25.** Voltage noise (a) and current noise (b), after moving average removal treatment, during the first 2000 seconds of the inhibitor filming process.

The voltage noise amplitude decreased slightly during the first 2000 seconds immediately after the electrode was placed into the inhibited brine, as shown in Figure 4. 25 (a). Afterwards, the voltage noise amplitude did not continuously decrease with filming time, which can be seen by comparison of Figure 4.25 (a) with Figure 4.26 (a)

which shows voltage noise after the electrode has been exposed to inhibited brine for 2 hours. So the voltage noise amplitude did not appear to show any obvious correlation with the inhibitor filming process, or the corrosion rate. To this extent, the results of this work do not agree with the direct relationships between voltage noise and corrosion rate suggested by some researchers (Searson and Dawson 1988; Gusmano *et al.* 1993), although it should be noted that those works were dealing with the corrosion of steel by oxygen.

The current noise amplitude, however, showed a stronger correlation with the inhibitor filming process. In Figure 4.25 (b), the current noise amplitude is continuously decreasing with time. After about 2 hours, as shown in Figure 4.26 (b), the current noise amplitude has already significantly decreased. After about 45 hours the current noise shown in Figure 4.27 became negligible compared to the current noise in Figure 4.25 (b). This continuous decrease in current noise may correspond with the formation of the inhibitor film.

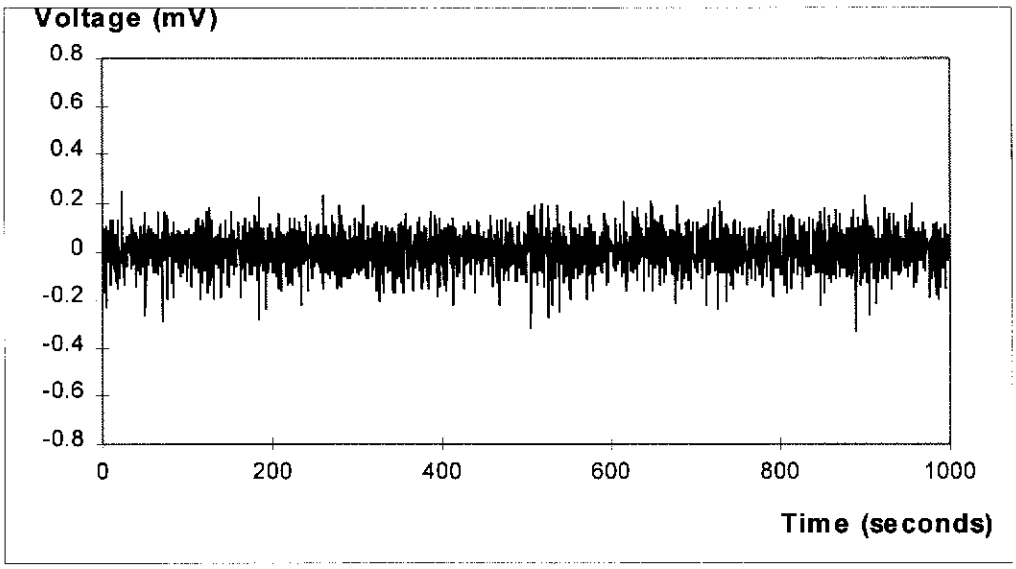


Figure 4.26 (a), Voltage noise after 2 hours

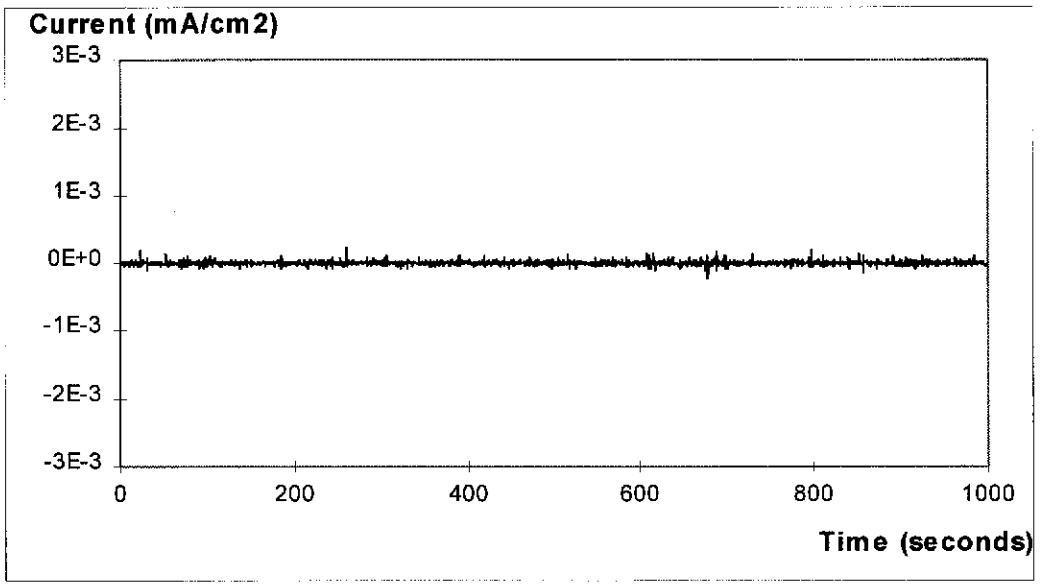


Figure 4.26 (b), current noise after 2 hours

**Figure 4.26.** Voltage and current noise (after moving average removal treatment) after the electrode has been exposed to inhibited brine for 2 hours.

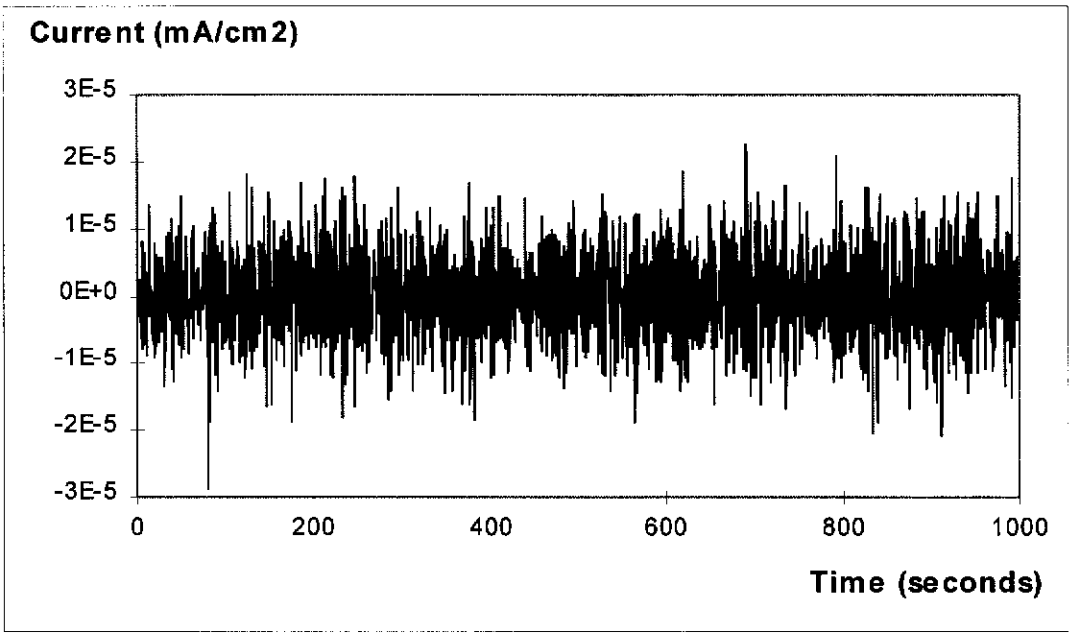


**Figure 4.27.** Current noise after inhibitor filming for about 45 hours (after moving average removal treatment).

The decrease in noise amplitude with time cannot be associated with the moving average removal procedure, as this procedure only involves a few adjacent data

points. Actually, the same effect can be seen in the raw noise data before average removal procedure, but obviously not so clearly.

The reference electrode can not affect current noise because the reference electrode (Ag/AgCl) is not in the current noise recording electric circuit. The influence of reference electrode on voltage noise can also be discounted because the voltage noise of reference electrode, as shown in Figure 4.28, is about 10 times smaller in amplitude than the normal voltage noise of a corroding electrode.

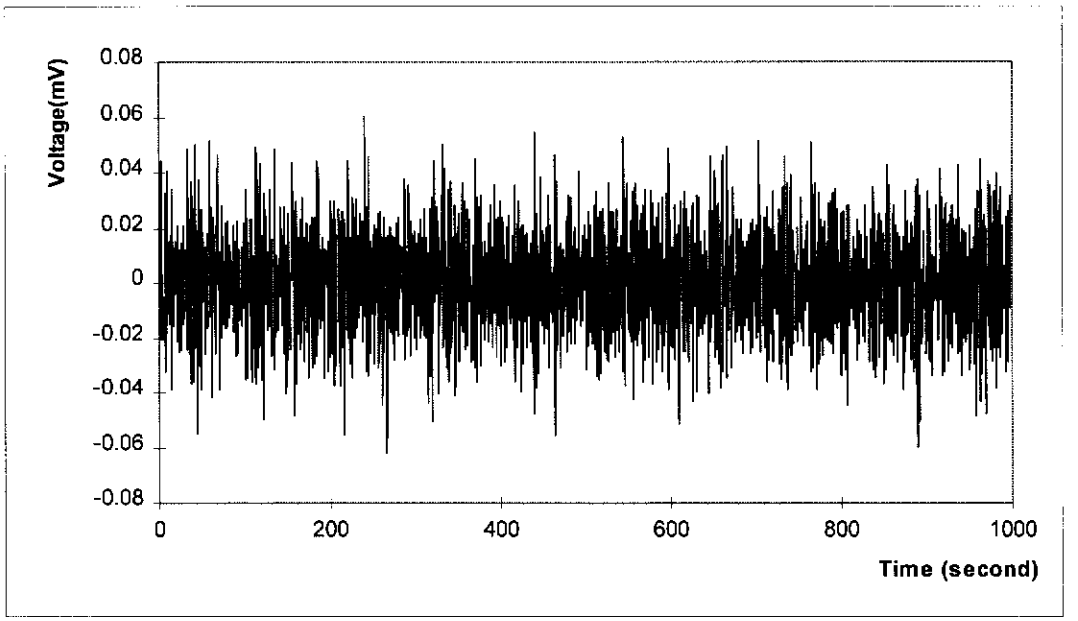


**Figure 4.28.** Voltage noise (after moving average removal treatment) of a reference electrode system (Ag/AgCl electrode vs. $Hg/Hg_2Cl_2$ electrode). The noise level of the $Hg/Hg_2Cl_2$ electrode was reported to be very low (Uruchurtu and Dawson 1987).

Although the current noise obviously correlates with the inhibitor filming process, the exact relationship between current noise and the corrosion process has not yet been found. However, as discussed in section 2.3.1.1, the ratio of the standard deviation of voltage noise and the standard deviation of current noise, denoted noise resistance ($R_n$), was found to be comparable to the charge transfer resistance or polarisation

resistance and can be used to calculate corrosion rate. Figure 4.29 shows the change of noise resistances (time intervals $\Delta t$ = 9.5 seconds), which are calculated from the voltage noise in Figure 4.25 (a) and current noise in Figure 4.25 (b) using the new method proposed in section 2.4.2.

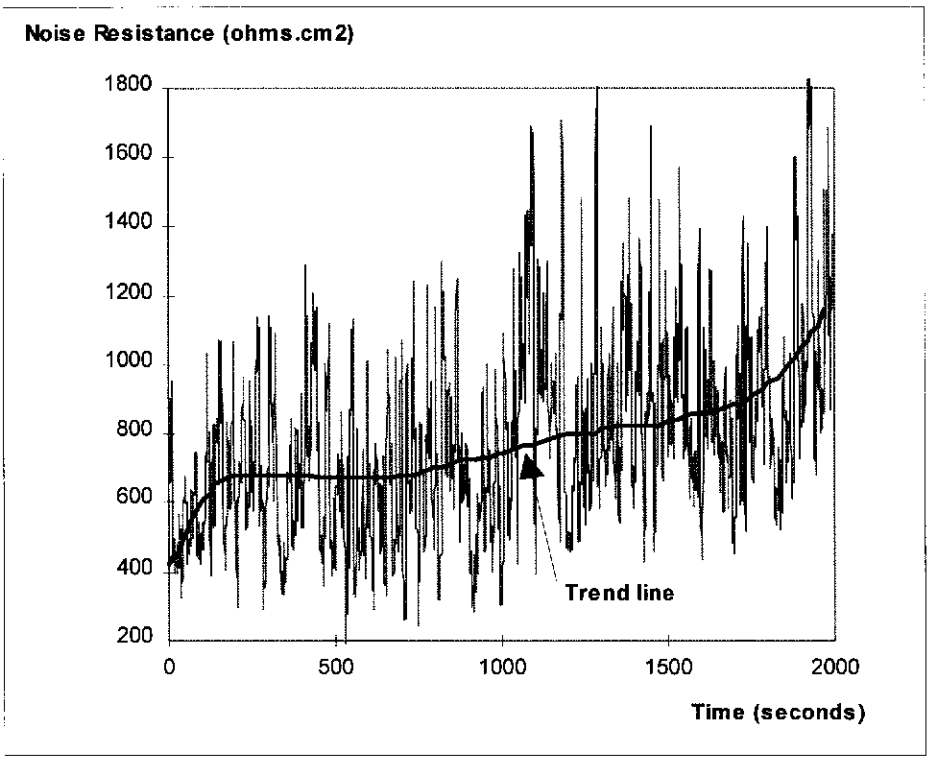


**Figure 4.29.** The change of electrochemical noise resistance ($R_n$) during the first 2000 seconds of the inhibitor filming process. $R_n$ values are calculated from DC trend removed voltage and current noise data using formula: $R_n = \sigma_V(\Delta t)/\sigma_I(\Delta t)$, where $\Delta t$ is 9.5 seconds.

Although $R_n$ in Figure 4.29 shows large fluctuations, the trend line appears to follow the formation of the inhibitor film. If $R_n$ is really comparable to polarisation resistance in this system, then Figure 4.29 in fact shows the continuous change of polarisation resistance, and so ENA would be the first technique capable of continuously monitoring the corrosion rate.

To test the suggested equivalence of $R_n$ and $R_p$, LP and EIS measurements were also carried out alternately using the same electrochemical cell and electrode. Table 4.5 shows resistance values from these techniques for comparison.

In Table 4.5, $R_n$ was calculated from DC trend removed voltage and current noise data ($R_n = \sigma_V(\Delta t)/\sigma_i(\Delta t)$, where $\Delta t$ is 1000 seconds). $R_t + R_{film}$ were calculated by semicircle fitting of EIS Nyquist plots. $R_p$ was deduced by linear fitting of linear polarisation data.

**Table 4.5.** A comparison of resistance values calculated from ENA, LP and EIS data during the formation and destruction processes of inhibitor film. All three techniques were applied on the same electrode alternately. All measurements were carried out at 30 °C and with $CO_2$ sparging.

| **Filming Time** | $R_n$ (ohms.cm2) | $R_p$ (top) (ohms.cm2) | $R_p$ (bottom) (ohms.cm2) | $R_{film} + R_t$ (ohms.cm2) |
|---|---|---|---|---|
| Film Formation | | | | |
| 0.5 | 847 | 1796 | 1552 | 1920 |
| 2 | 2236 | 3327 | 3126 | 3600 |
| 5 | 3575 | 3702 | 3846 | |
| 18 | 5640 | 5977 | 6060 | 6000 |
| 20 | 4835 | 5536 | 5548 | 6400 |
| 24 | 4757 | 5728 | 6387 | |
| 30 | 4513 | 5961 | 6560 | 6700 |
| 42 | 5273 | 8057 | 6835 | 6900 |
| Film Destruction | | | | |
| 46 | 1754 | 1789 | 2216 | |
| 48 | 1469 | 1408 | 1432 | 1400 |
| 51 | 743 | 696 | 704 | |
| 60 | 527 | 483 | 500 | |

Over the 60 hours test period, as shown in Table 4.5, it can be seen that $R_n$ values are quite comparable to $R_p$ or $R_t+R_{film}$ values although they are not completely equivalent. $R_n$ showed a very similar trend with $R_p$ or $R_t+R_{film}$ throughout the test period. This result confirms the similarity of noise resistance and polarisation resistance and strongly suggests a correlation of electrochemical noise with the corrosion rate. Although the theoretical background, data analysis method and their

limitations are still worth further investigation, the relationship between $R_n$ and $R_p$ or $R_t$+$R_{film}$ is obviously of some significance. It suggests that ENA can be used to continuously monitor corrosion processes such as the inhibitor film formation process and also may be used to continuously measure corrosion rate by using the Stern-Geary equation.

It is also found that DC trend removal is important in the calculation of noise resistance. Figure 4.30 shows a comparison of noise resistances, with and without DC trend removal, with $R_p$ and $R_t$+$R_{film}$ during the inhibitor film formation process. Without DC trend removal, electrochemical noise resistance, as shown in Figure 4.30, showed poor correlation with $R_p$ and $R_t$+$R_{film}$ and also showed large fluctuations. After DC trend removal, however, noise resistance showed good correlation with the reference resistances. This result also suggests that the 'moving average removal' method can be used to remove DC trend in voltage and current records.

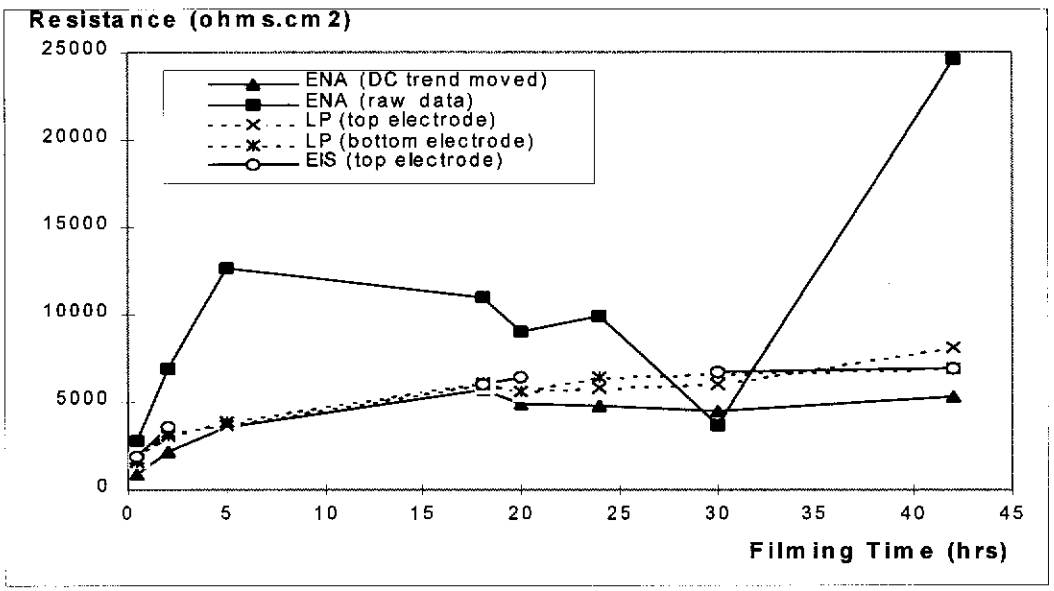


**Figure 4.30.** The changes of electrochemical noise resistance ($R_n$, with and without DC trend removal), $R_{film}$ + $R_t$ (EIS) and $R_p$ (LP) resistances during inhibitor filming process. In EIS and LP measurements, the bottom and top electrodes of the dual cylinder electrodes were tested individually.

### 4.4.2 The monitoring of inhibitor film destruction

After about 45 hours inhibitor film formation, the dual electrode was quickly transferred into an inhibitor-free 3% NaCl brine (pre-sparged with $CO_2$) with 1000 rpm stirring. Electrochemical noise recording and EIS, LP measurements were carried out alternately to monitor the inhibitor film formation process.

Figure 4.31 shows the raw current noise recorded before and after electrode transference. After the electrode transfer, the current noise amplitude obviously increased and this can be observed in the raw noise record (Figure 4.31) and is clearly shown in Figure 4.32, where DC trend was removed from the raw noise data.

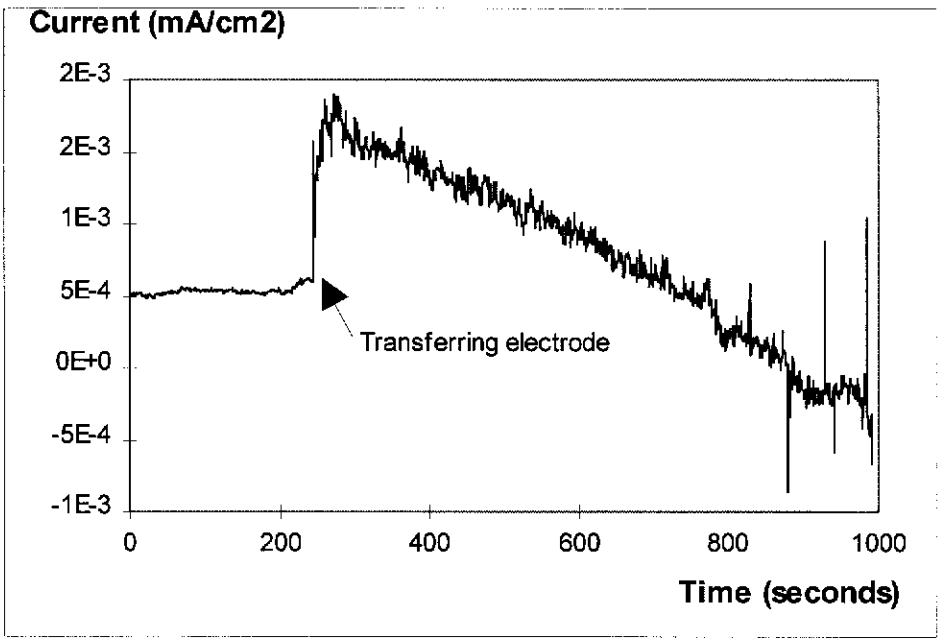


**Figure 4.31.** Original current noise records after transferring the inhibitor filmed electrode into an inhibitor-free brine (with 1000 rpm stirring).

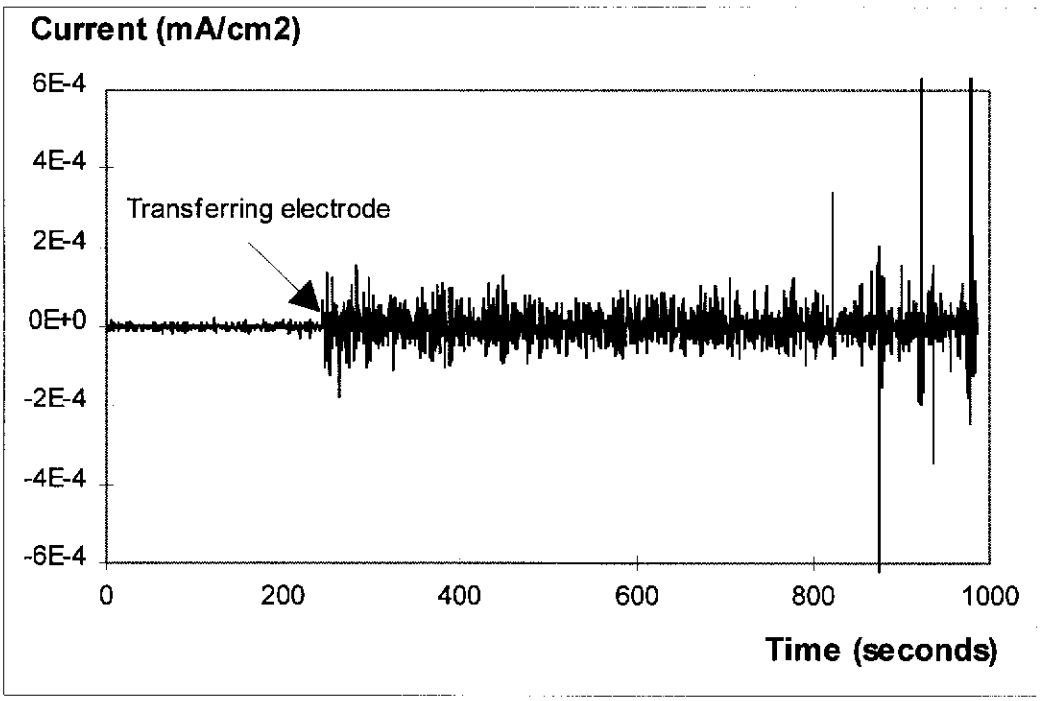


**Figure 4.32.** Current noise (after moving average removal treatment) after transferring the inhibitor filmed electrode into an inhibitor-free brine (with 1000 rpm stirring).

Noise resistance showed a rapid decrease after electrode transfer, as shown in Figure 4.33 which shows the change of noise resistances (time intervals $\Delta t$ = 9.5 seconds) before and after the electrode transference.

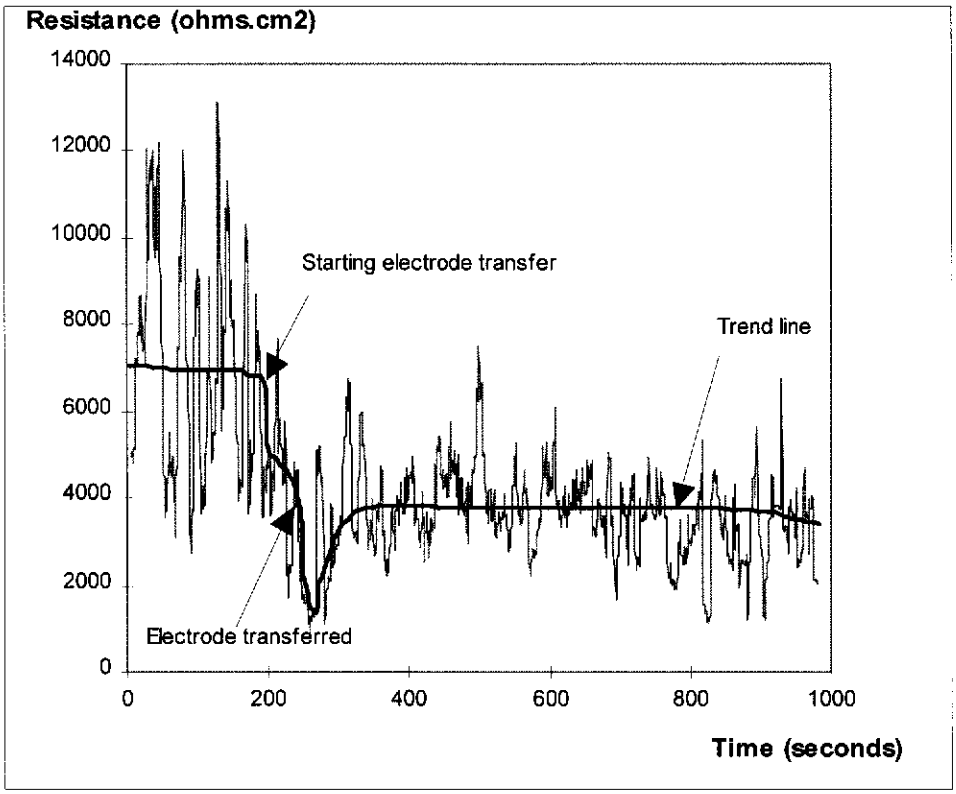


**Figure 4.33.** The change of electrochemical noise resistance ($R_n$) after transferring inhibitor filmed electrode into an inhibitor-free 3% NaCl brine (with 1000 rpm stirring).

Although $R_n$ in Figure 4.33 shows large fluctuations, the trend line appears to follow the breakdown process of the inhibitor film. This result suggests that electrochemical resistance could be a convenient method to monitor inhibitor film breakdown and so to evaluate inhibitor film persistency.

As shown in Figure 4.32, after about 800 seconds, some very large current noise can be observed which may be due to the localised breakdown of the inhibitor film because these large noise excursions have similar characteristics to those Hladky and Dawson (1981) observed in pitting corrosion.

Figure 4.34 shows the inhibitor failure process. Generally ENA and LP showed very similar trends during the inhibitor film failure process. Compared to LP and EIS,

ENA has advantages in the continuous monitoring of inhibitor film performance and in the convenient experimental arrangement. So ENA is a convenient method for evaluating inhibitor film persistency. In fact, it appears that inhibitor film persistency may be readily assessed by simply monitoring the current noise amplitude although more work is needed to establish the theoretical background of such a procedure.

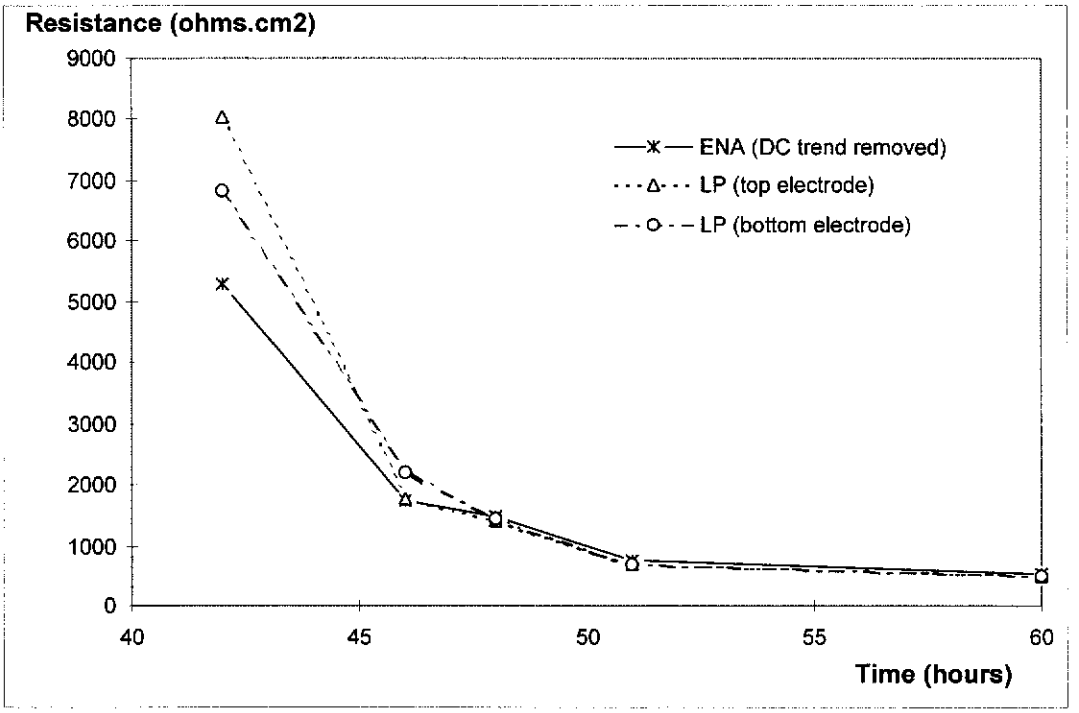


**Figure 4.34.** Inhibitor film failure after exposing the filmed electrode to an inhibitor-free brine and rotating at 1000 rpm.

## 4.5 Conclusions

(i). EIS has been shown to be a valuable technique for studying the mechanism of inhibitor film formation and destruction, and for evaluating the film persistency of $CO_2$ corrosion inhibitors. EIS can be used to measure corrosion related electrochemical parameters such as the resistances and capacitances of inhibitor layers, charge transfer resistance and double layer capacitance. These parameters can be used to analyse the inhibitor mechanism and to calculate the corrosion rate.

(ii). Imidazoline was shown to be a very effective $CO_2$ corrosion inhibitor. It forms a chemically bonded film on the metal surface. The inhibitor film seems to be a combination of an inner-layer which is likely to be an inhibitor-metal complex and several outer-layers which are likely to be inhibitor layers with possible inhibitor molecular cross-linking. The inhibitor film showed a strong self-repairing ability, but surface water shear stress can gradually remove the inhibitor film and cause inhibitor film failure. Quaternised amine inhibitor film formed on the electrode surface is probably a physically or electrostatically adsorptive molecular layer which forms rapidly and desorbs easily. Polymerised vegetable fatty acid seems to have characteristics between interphase and interface inhibition.

(iii). Experimental results showed that the trend of electrochemical noise effectively followed the inhibitor film formation and destruction processes. Electrochemical data analysis strongly suggests that ENA is a practical technique in the continuous monitoring of inhibitor film performance and in the evaluation of inhibitor film persistency.

(iv). Electrochemical noise resistance ($R_n$) is confirmed to be strongly correlated to linear polarisation resistance ($R_p$) or the sum of charge transfer resistance and

inhibitor film resistance ($R_t$+$R_{film}$) in the corrosion-inhibition system studied here. Experimental results also showed that the moving average removal procedure can be successfully used to remove DC trend in raw noise recording.

# Chapter V

# STUDIES OF BATCH TREATMENT INHIBITOR FILMS USING ELECTROCHEMICAL IMPEDANCE SPECTROSCOPY AND ELECTROCHEMICAL NOISE ANALYSIS

## 5.1 Introduction

Although continuous treatment inhibition, studied in the previous Chapter, is the simplest technique of inhibitor application in the oil and gas production industry, in deep wells and in three phase gas pipelines, batch-treatment techniques are often used because of the difficulty of injecting an inhibitor continuously downhole and because of the need for the inhibitor to reach the top wall of the gas flowlines.

With batch-treatment of flowlines, a concentrated solution of inhibitors is drawn through the tubing between two "*pigs*". During downhole application the well is shut-in, and the inhibitor is allowed to drop through the column of gas or oil and water. Alternatively, in gas wells the inhibitor may be applied by a brush. These processes allow the inhibitor to form a protective coating or film on the steel surface. The process needs to be repeated periodically because the inhibitor film is gradually removed by dissolution in the produced fluids flowing through the tubing.

Here a problem arises as to how often the batch-treatment should be repeated. This question is frequently asked in oil and gas fields because the determination of a

suitable treatment period is not only a requirement for optimising the batch-treatment technique but also a requirement for the safe application of batch-treatment inhibitors. In practice, an inhibitor film that works in one oil or gas well may not work in another if the corrosion environment is different. The optimum period of batch-treatment may also be different if an inhibitor is applied in different corrosion environments. So the determination of the preferred treatment interval is a key concern when using batch treatment techniques.

The key to determine the treatment interval of a batch-treatment inhibitor is to assess the inhibitor film persistency. However, as mentioned in the section 1.4.1, there is not a good technique available which can quickly evaluate and monitor inhibitor efficiency and inhibitor film persistency. The current technology for assessing inhibitor film persistency is the subject of much discussion and, in many cases, disagreement (NACE Task Group T-1D-8 1982).

The previous Chapter describes how electrochemical impedance spectroscopy (EIS) and electrochemical noise analysis (ENA) were successfully used to monitor the performance of, and to evaluate the persistency of, continuous treatment inhibitors. However, batch treatment inhibitors are quite different from continuous treatment inhibitors. Batch treatment inhibitors, unlike continuous treatment inhibitors, are normally water insoluble fluids and in most cases are varnish-like. Applied on the metal surface, the batch treatment inhibitor film often looks like a wet organic coating or a grease layer, which normally has a high film resistance. Most commercial batch treatment inhibitors have much better persistency than continuous treatment inhibitors because the key requirement of batch treatment inhibitors is to form highly persistent films for lasting protection. Hence, the suitability of EIS and ENA to monitor batch-treatment inhibitor film performance and to determine inhibitor film persistency have to be examined.

In this Chapter, EIS and ENA have been used to study the formation and deterioration processes of batch treatment inhibitor films. The possibilities of using EIS as a method for evaluating batch treatment inhibitor film persistency have been explored. Experiments were also carried out to test the reliability of the noise resistance method for inhibitor performance monitoring. The possibility of using ENA to continuously monitor the film formation and destruction processes of batch treatment inhibitor films was also examined.

## 5.2 Experimental

### 5.2.1 Materials and fluids

(i). Electrodes

The cylinder working electrode, dual cylinder working electrode, reference electrode and counter electrode used in this work are the same as those described in section 4.2.1. The weight-loss rings are also described in section 4.2.1.

(ii). Fluids and inhibitors

The base testing solution was a 3% NaCl solution, which was prepared in a same way as the testing solution described in section 3.2.1.

The diesel and kerosene, used as the hydrocarbon phase in the simulated oil well fluid, were additive-free pure diesel and kerosene. All testing fluids were pre-sparged with carbon dioxide before use.

The inhibitors studied in this work are typical commercial batch treatment inhibitors. Although it is ideal to study batch treatment inhibitors with simple chemical composition, that is not possible because all batch treatment inhibitors are formulated and have a complicated chemical composition. In this work three typical formulated batch treatment inhibitors, which are from major chemical companies and are currently used in oil and gas fields, were selected and studied:

(a). Inhibitor 'A': A non-volatile, high viscosity, dense fluid which has imidazoline and polymerised vegetable fatty acids as the main components.

(b). Inhibitor 'B': A binary corrosion inhibitor which has epoxy resin and amine as the main components.

(c). Inhibitor 'C': A volatile brown fluid which was taken from an oil-field where it was under use. It is a commercially available inhibitor but its composition was unknown.

### 5.2.2. Electrochemical measurements

EIS and LP measurements used the same electrochemical cell, the same instruments and the same measurement method as described in section 3.2.3. ENA measurements used the same electrochemical cell, the same experimental set-up and the same measurement method as described in section 4.2.2. However, the testing fluids and procedures are different from the previous studies and will be described in the following sections.

### 5.2.3. Inhibitor film formation Process

Inhibitors 'A', 'B' and 'C' were filmed on the electrode surface using different methods corresponding to different batch treatment methods.

(i). Filming inhibitor 'A'

Inhibitor 'A' was filmed by placing the electrode in a filming fluid (an emulsion of brine, diesel and inhibitor). The filming fluid was made by mixing 16 mL of inhibitor 'A', 640 mL of 3% NaCl brine and 160 mL of diesel. During inhibitor filming periods, magnetic stirring was applied to form the multi-phase filming fluid into an emulsion. After a certain period of time, magnetic stirring was stopped to allow separation of the brine and hydrocarbon/inhibitor phases. Electrochemical measurements were carried out in the brine phase of the stagnant filming fluid for monitoring inhibitor film formation. This procedure was repeated several times for studying inhibitor film formation after different filming times. The electrochemical

cell for EIS and ENA measurements of inhibitor film formation is shown in Figure 5.1.

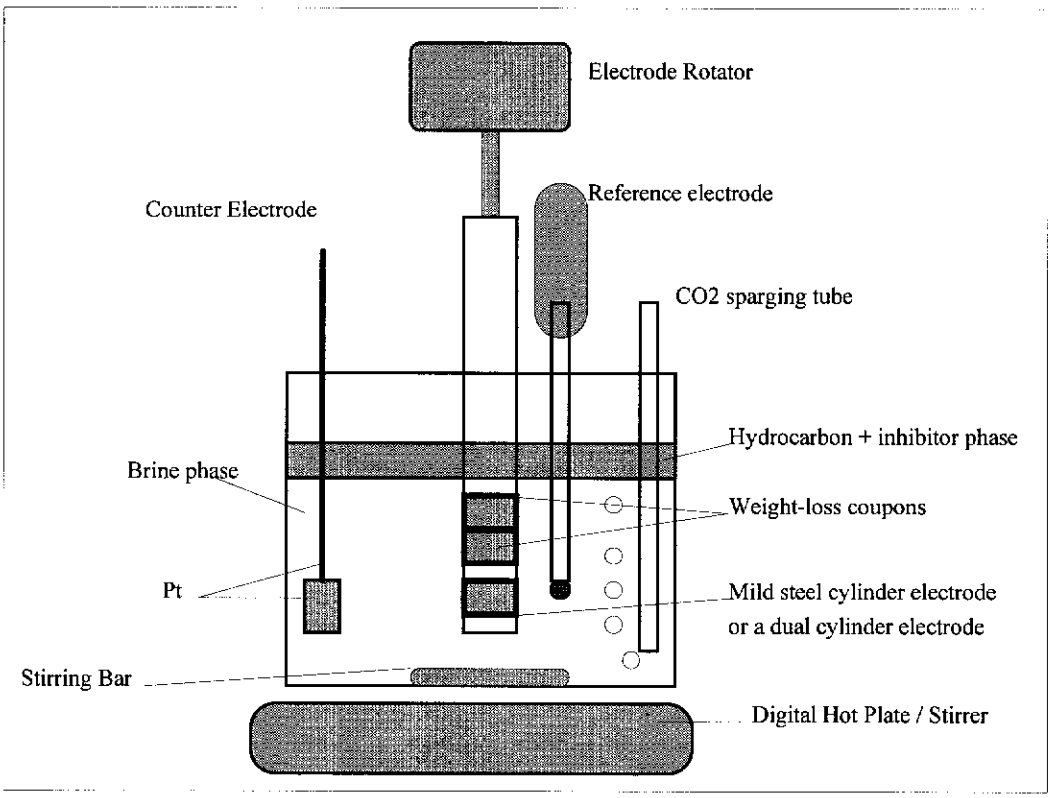


**Figure 5.1.** A schematic diagram of the electrochemical cell set-up (stagnant status)

(ii). Filming inhibitors 'B' and 'C'

Inhibitors 'B' and 'C' are varnish-like fluids. With reference to the instructions from the manufacturers, test electrodes were filmed by dipping the electrodes in inhibitor fluids which were pre-sparged with $CO_2$. The filming fluid for inhibitor 'B' was made by mixing the two inhibitor components (4 parts : 1 part by volume). The filming fluid for inhibitor 'C' was simply the original inhibitor fluid provided by manufacturer. After being filmed, the electrodes were transferred into a rinsing fluid where the inhibitor films were tested using electrochemical techniques.

(iii). Rinsing

After inhibitor film formation, the electrodes/coupons were quickly transferred into a rinsing fluid for rinsing off loose inhibitor clinging to the electrode. The rinsing fluid used in this work was an emulsion of 3% NaCl brine (640 mL) and hydrocarbon (160 mL). For testing inhibitors 'B' and 'C' films formed on electrodes, electrochemical measurements were also carried out in the rinsing fluid (when the rinsing fluid was stagnant).

### 5.2.4. Inhibitor film deterioration

After being rinsed, the electrodes were transferred into a corrosive fluid (called washing fluid) where the inhibitor film may deteriorate. Two washing fluids were used in this work: (a). a 3% NaCl brine (800 mL); (b). An emulsion made by mixing 3% NaCl brine (640 mL) with hydrocarbon (160 mL). Various washing conditions were applied (with different temperatures, shear speeds etc.) for investigating the influence of washing conditions on inhibitor performance and persistency.

EIS measurements were carried out in the brine phase of the stagnant washing fluid for studying the inhibitor film deterioration processes and for testing inhibitor film persistency. Weight-loss coupons were incorporated on the electrode assembly, as shown in Figure 5.1, for weight-loss measurements.

For all the tests, $CO_2$ sparging was continued to maintain a oxygen-free corrosion condition.

## 5.3 Results and discussion I: EIS studies of batch treatment inhibitor films and their persistency

### 5.3.1 The formation of Inhibitor films

Mild steel electrodes and weight-loss coupons were placed in inhibitor filming fluids and kept in the filming fluids with stirring for a period of time for inhibitor film formation. Then the filmed electrodes were rapidly transferred into a rinsing fluid. EIS measurements were carried out in the brine phase of the stagnant rinsing fluid in order to investigate the process of formation of the inhibitor films. For inhibitor 'A', EIS measurements were carried out in the brine phase of the filming fluid.

Figures 5.2 (a) and (b) show EIS Bode plots recorded on an electrode after filming with inhibitor 'A' for 10, 20 and 30 minutes. The EIS plots recorded on a diesel filmed electrode, and a bare electrode, which represent the spectral data before inhibitor film formation, are also shown in Figure 5.2 for comparison. Bode modulus plots are used in this Chapter instead of Nyquist plots because the former have advantages in presenting EIS data which have large differences in impedance values.

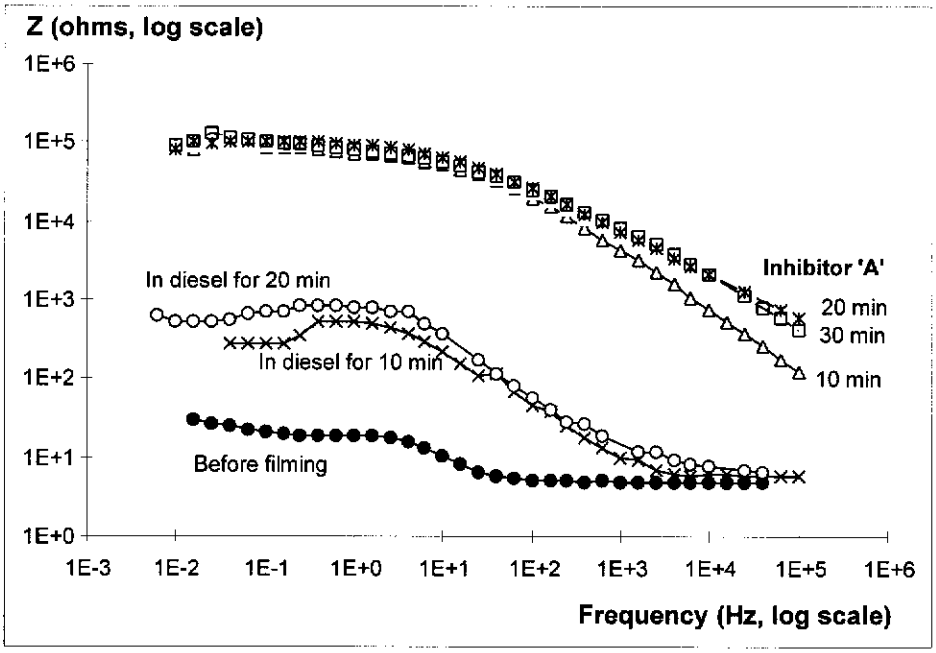


Figure 5.2 (a): Bode modulus plots

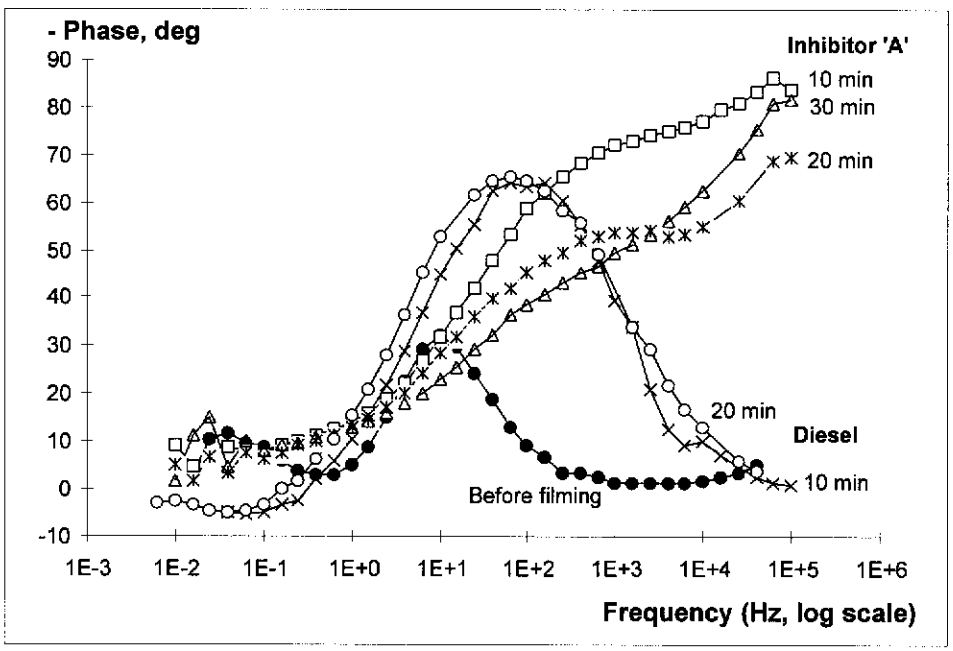


Figure 5.2 (b): Bode phase angle plots

**Figure 5.2.** EIS Bode plots before and after forming inhibitor 'A' film at 30 °C, with $CO_2$ sparging. (a) modulus plots; (b) phase angle plots.

The formation of the inhibitor 'A' film was a very fast process, as shown by the similarity of spectra in Figure 5.2 after filming inhibitor 'A' for different periods (10, 20 and 30 minutes).

After filming with inhibitor 'A', as shown in the modulus plot in Figure 5.2, the electrode impedance greatly increased compared with the spectra recorded on bare and diesel filmed electrodes. The electrode impedance values at low frequency for the inhibitor-filmed electrodes were near $10^5$ ohms which is much larger than the impedance recorded on the diesel filmed electrodes (of the order of $10^2$ ohms) and bare electrodes (of the order of 10 ohms).

The Bode phase angle *vs.* frequency (in log scale) plots of inhibitor 'A' filmed electrodes, which are shown in Figure 5.2 (b) and which correspond to the same experimental data shown in Figure 5.2 (a), show a capacitive behaviour in the high frequency range and a gradual transition from capacitive (-90°) to resistive (0°) behaviour with the decrease in frequency. Bare electrodes and diesel filmed electrodes, however, showed obviously different characteristics in Bode phase plots which only show a phase angle shift in the intermediate frequency range.

Similar spectral characteristics can also be observed in the EIS Bode plots which were recorded before and after the formation of inhibitors 'B' + kerosene and 'C' + kerosene films. As shown in Figures 5.3 and 5.4, electrode impedance was greatly increased and a capacitive behaviour can be observed in the high frequency range after being filmed with inhibitor 'B' + kerosene and inhibitor 'C' + kerosene. However, when electrodes were only filmed with inhibitor 'B' or 'C', without the presence of kerosene, lower electrode impedance and different Bode phase plots were recorded.

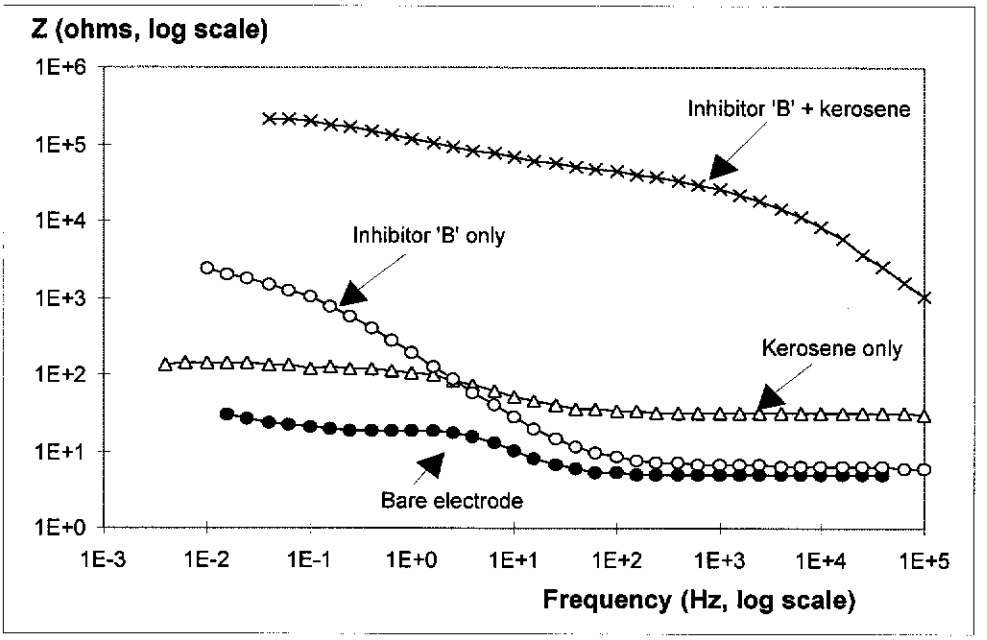


Figure 5.3 (a): Bode modulus plots

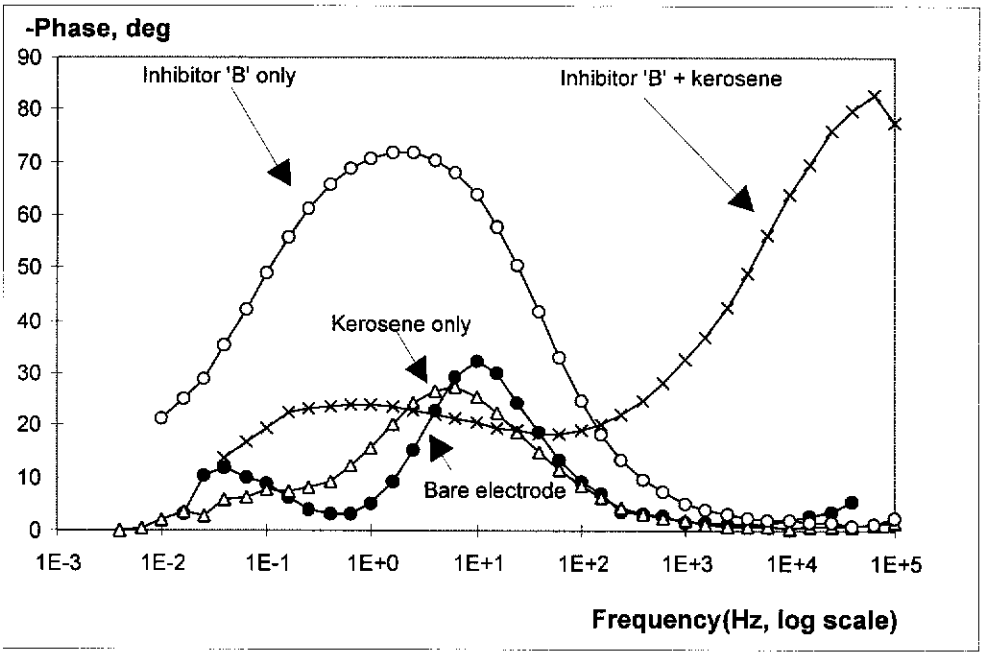


Figure 5.3 (b): Bode phase angle plots

**Figure 5.3.** EIS Bode plots before and after forming inhibitor 'B' film at 70 °C. (a) modulus plots; (b) phase angle plots.

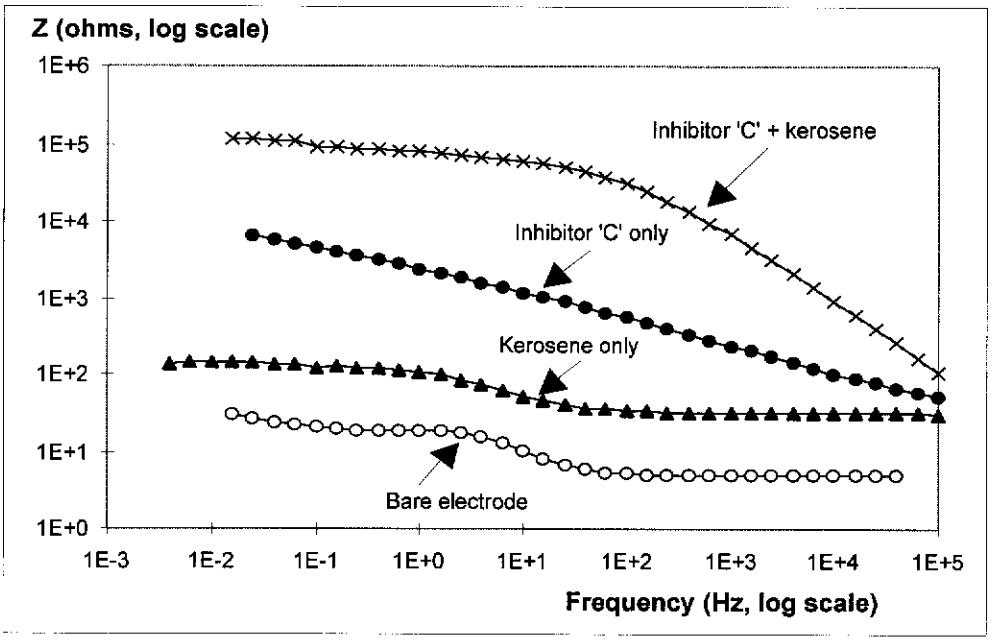


Figure 5.4 (a): Bode phase angle plots

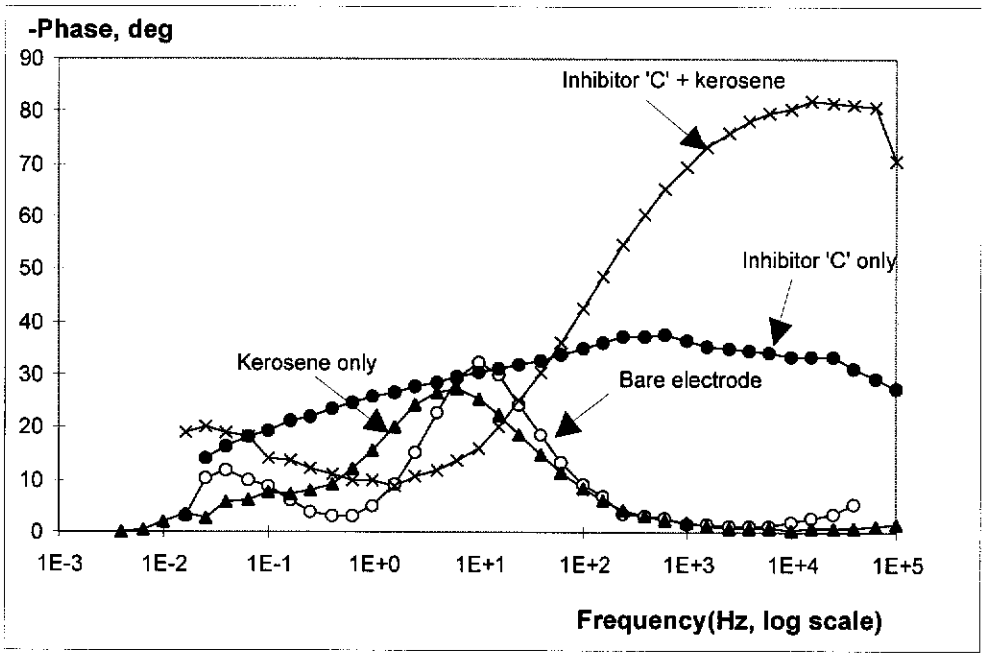


Figure 5.4(b): Bode modulus plots

**Figure 5.4.** EIS Bode plots before and after forming inhibitor 'C' film at 70 °C. (a) modulus plots; (b) phase angle plots.

The high frequency peaks in the Bode phase *vs.* frequency plots of electrodes filmed with inhibitors 'A', 'B' + kerosene and 'C' + kerosene, as shown in Figures 5.2 (b), 5.3 (b) and 5.4 (b), can be attributed to the inhibitor film because a surface dielectric film normally has a faster (i.e. smaller) time constant (Feliu *et al.* 1990; Mansfeld and Lorenz 1991; Tsai and Mansfeld 1993; Thompson and Campbell 1994). By comparison with weight-loss measurements, the author and co-workers (Tan *et al.* 1995) confirmed that the high frequency phase angle shift is not due to the electrochemical corrosion reaction but is most likely due to the impedance of inhibitor film, or due to the combination of inhibitor film impedance and corrosion reaction impedance because in some cases inhibitor film impedance and electrochemical reaction impedance may not be clearly separated when the criteria suggested by Walter (1986) are not completely met.

The phase angle peaks at intermediate frequencies in the spectra of diesel (Figure 5.2) and kerosene (Figures 5.3 and 5.4) filmed electrodes can be attributed to the electrochemical corrosion process. An experiment was run to confirm this conclusion where the weight-loss calculated from EIS data (0.7 $mg/cm^2$) is close to the actual weight-loss of coupons (1.0 $mg/cm^2$) after about 24 hours of a parallel exposure test. The reason that the diesel/kerosene film impedance did not appear in the spectra may be that the time constant for the diesel/kerosene film was too small (too fast) and so did not respond in the frequency range applied.

The phase angle peak for bare electrodes was confirmed by the authors to be due to the electrochemical charge transfer process because an excellent agreement was reached between the weight-loss measurements and EIS data (Tan *et al.* 1995).

The spectral characteristics of inhibitor-filmed electrodes in Figures 5.2, 5.3 and 5.4 are very similar to those of electrodes covered by organic coatings with micro-pores present. So the impedance characterisation of electrodes filmed with batch-treatment

inhibitors could also be simulated by the equivalent electrical circuit suggested for an electrode with an organic coating (Beaunier *et al.* 1976; Mansfeld and Tsai 1991), as shown in Figure 5.5. A similar equivalent circuit model has been used to simulate electrodes with corrosion product scale (section 3.3.1.1.1) and electrodes with continuous treatment inhibitor film (section 4.3.1.1) in the previous Chapters.

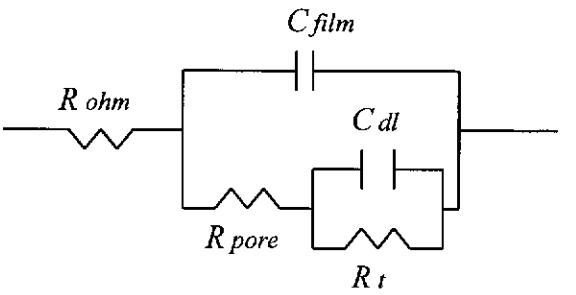


**Figure 5.5.** Equivalent circuit for an electrode filmed with a batch treatment inhibitor film. $R_{ohm}$ is the solution resistance. $R_{pore}$ is the resistance of pore areas in a batch treatment inhibitor film. $C_{film}$ is the capacitance of the inhibitor film. $R_t$ is the charge transfer resistance. $C_{dl}$ is the double layer capacitance.

Compared with the spectral analysis made in the previous Chapters, in the case of electrodes covered with a batch treatment inhibitor film the spectral analysis is more difficult. Electrochemical parameters in Figure 5.5 are not always deducible because sometimes the electrochemical charge transfer resistance can be masked by a large inhibitor film resistance and so the corrosion rate can not be accurately calculated. In these cases, empirical relationships may be used as follows.

A very interesting observation can be made by comparison of the spectra of inhibitors 'B' + kerosene and 'C' + kerosene with those of inhibitors 'B' and 'C' only in Figures 5.3 and 5.4. This shows that the presence of kerosene greatly contributed to the formation of protective inhibitor films. These results support the theory that hydrocarbon can interact with the inhibitors' alkyl chain through van der Waals forces

and form a hydrocarbon layer on the top of the inhibitor molecular layer enhancing protection (Kinsella *et al.* 1995).

### 5.3.2 The destruction of Inhibitor films

After being rinsed, the inhibitor-filmed electrodes were quickly transferred into a corrosive fluid (called washing fluid) where the inhibitor film may deteriorate. EIS measurements were carried out regularly in the brine phase of the washing fluid for monitoring the deterioration process of the inhibitor film. Before each measurement, the washing fluid was kept stagnant for about 0.5 hour.

Figure 6 shows the EIS Bode plots recorded after exposing an inhibitor 'A' filmed electrode to 3% NaCl brine (a simple washing fluid).

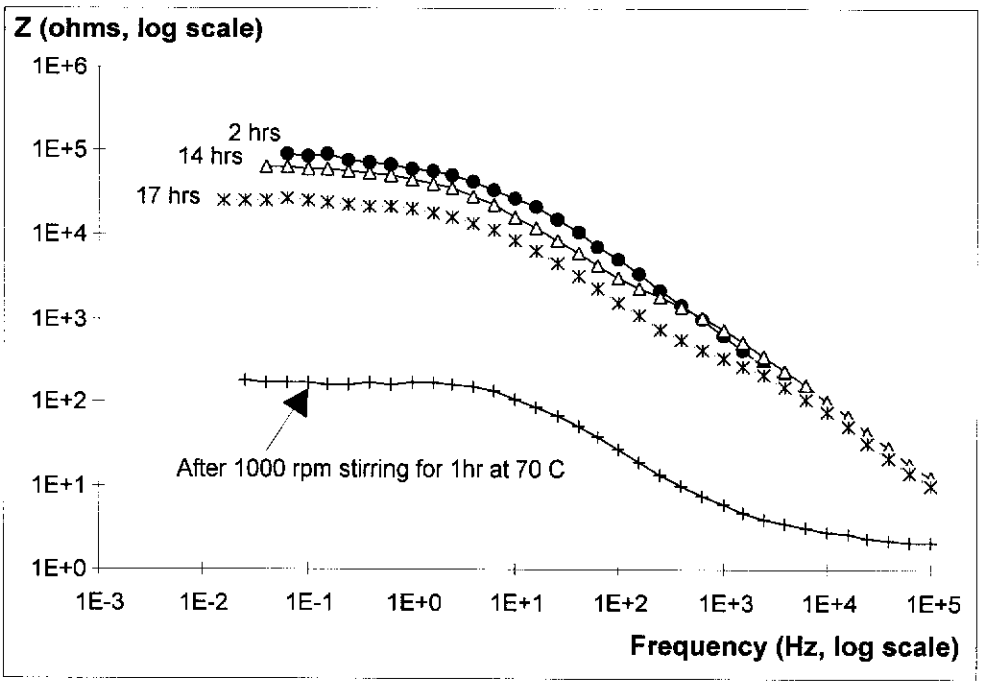


Figure 5. 6 (a): Bode modulus plots

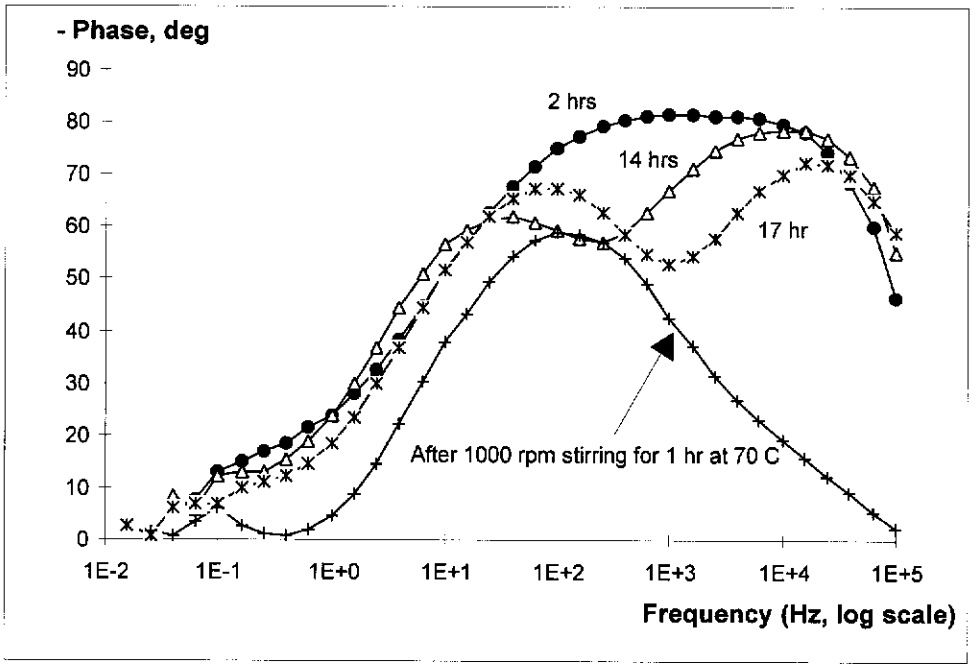


Figure 5.6 (b): Bode phase angle plots

**Figure 5.6.** EIS Bode plots after exposing an inhibitor 'A' filmed electrode to 3% NaCl brine under various washing conditions. (a) modulus plot; (b) phase angle plot.

After exposing the electrode to a stagnant washing fluid for 14 and 17 hours at 30 °C, as shown in Figure 5.6 (b), EIS Bode phase plots showed characteristic changes. The large peak in the 2 hours curve was overtaken by two new peaks in the 14 and 17 hours curves, one in the high frequency range and the other one in the intermediate frequency range. During that period, the electrode impedance gradually decreased, changing from the 2 hours curve to the 14 and 17 hours curves in Figure 5.6 (a), indicating the slow deterioration of the inhibitor film.

In order to accelerate the inhibitor film deterioration, the washing fluid was stirred using a magnetic stirrer (1000 rpm) while the temperature of the washing fluid was increased from 30 to 70 °C. After 1 hour, the electrode impedance had undergone a large decrease, as shown in Figure 5.6 (a), indicating the occurrence of a fast inhibitor film destruction. In the Bode phase plot, the phase angle shift in the high frequency

range disappeared which suggests the break-down of the inhibitor film. These results suggest that inhibitor 'A' film can be easily washed away by brine at 70 °C under mechanical shear stress and that inhibitor 'A' film exhibited poor persistency under this experimental condition.

Similar characteristics were also observed in the spectra of inhibitors 'B' and 'C' filmed electrodes after being exposed in washing fluids (an emulsion of 640 mL of brine and 160 mL of kerosene, 70 °C with 1000 rpm stirring), as shown in Figures 5.7 and 5.8, although these inhibitor films deteriorated much slower than inhibitor 'A'. In Figure 5.7 (b), the large high frequency phase peak in the 4 hours curve was replaced by two peaks in the 3 and 5 days curves. Similarly, in Figure 5.8 (b), the large high frequency peak in the 1 and 6 days curves was replaced by two peaks in the 9 days curves. The new peak appeared at intermediate frequencies, and is presumably due to the electrochemical charge transfer process (Silverman and Carrico 1988; Silverman 1990). As a general trend, as shown in Figures 5.7 (a) and 5.8 (a), electrode impedance slowly decreased with exposure time, indicating the deterioration of the inhibitor film.

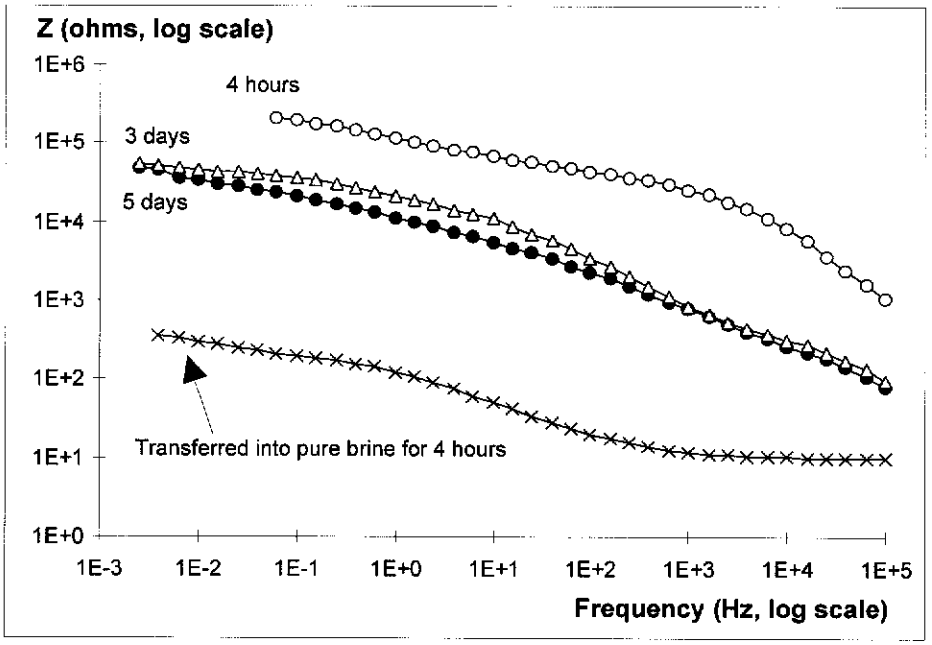


Figure 5.7 (a)

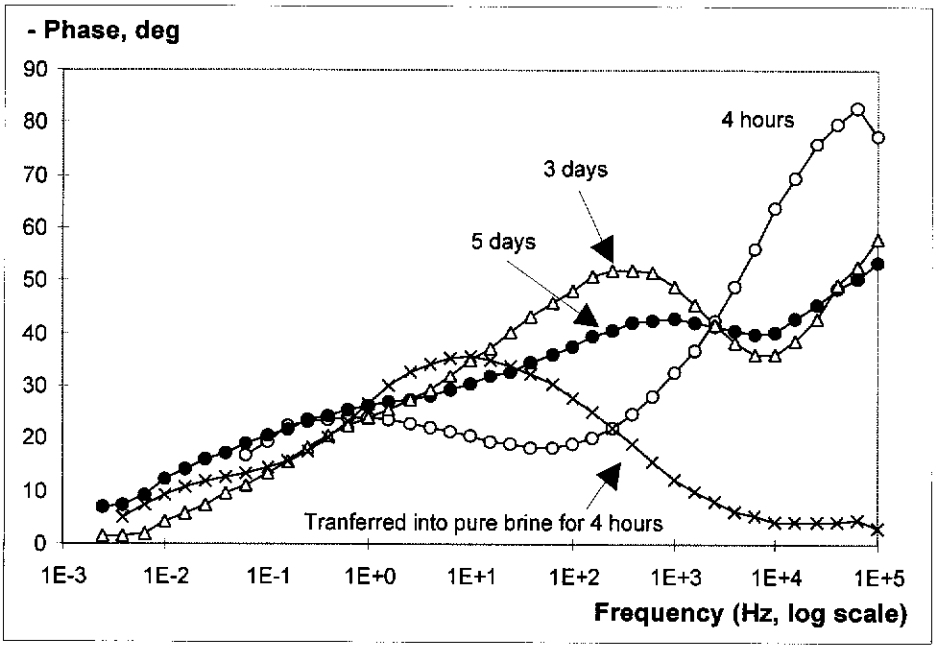


Figure 5.7 (b)

**Figure 5.7.** EIS Bode plots after exposing an inhibitor 'B' filmed electrode to a mixture of brine and kerosene and then a 3% NaCl brine. (a) modulus plot; (b) phase angle plot.

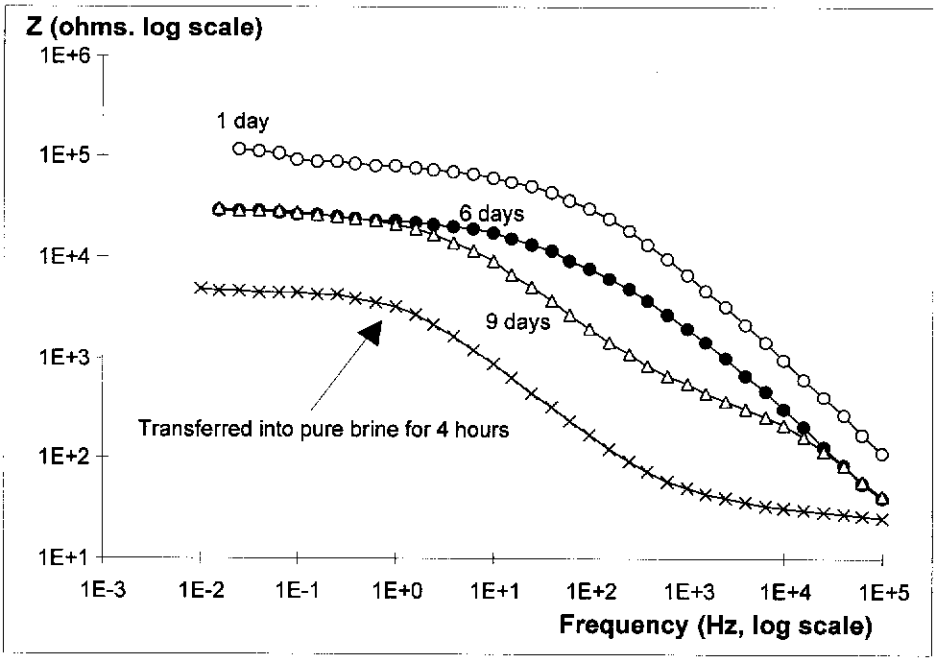


Figure 5.8 (a)

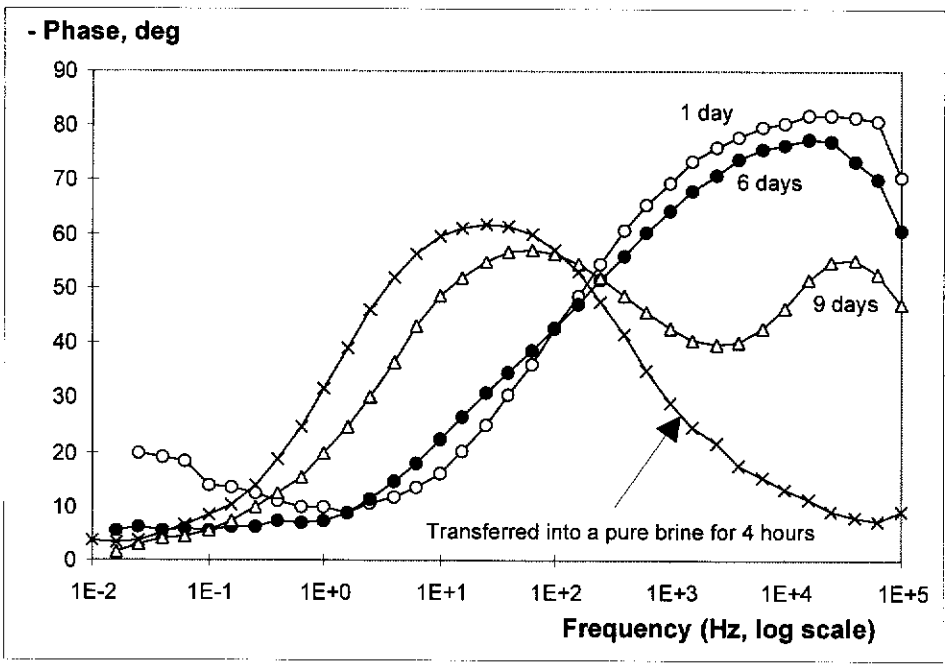


Figure 5.8(b)

**Figure 5.8.** EIS Bode plots after exposing an inhibitor 'C' filmed electrode to a mixture of brine and kerosene and then a 3% NaCl brine. (a) modulus plot; (b) phase angle plot.

Although the deterioration of inhibitors 'B' and 'C' films was very slow in the washing fluid containing brine and kerosene, the deterioration was immediately accelerated after transferring the electrodes into a brine-only washing fluid. The fast decrease in electrode impedance and the disappearance of the high frequency phase peak, as shown in Figures 5.7 and 5.8, suggest inhibitor film destruction. The significant influence of kerosene on the inhibitor film deterioration process, again suggests that the presence of hydrocarbon greatly contributes to the inhibitor films.

Empirically, the inhibitor film deterioration process can be classified into three stages using the Bode plots as an indicator. In the first stage, the inhibitor film retains the characteristics of an intact non-conductive film (with micro-pores present), which typically shows a large phase angle peak at high frequency range and has high electrode impedance, such as shown in the 2 hours curves in Figures 5.6, the 4 hours curve in Figure 5.7 and the 1 day curve in Figure 5.8. At this stage, the decrease in electrode impedance only happens very slowly. The second stage is characterised by two separate phase angle peaks at high and intermediate frequency ranges, such as the 14 hours curve in Figure 5.6, the 3 days curve in Figure 5.7 and the 9 days curve in Figure 5.8. The decrease in inhibitor film pore resistance due to inhibitor film deterioration may be responsible for the appearance of the phase angle peak in the intermediate frequency range, which is due to electrochemical double layer impedance. In the third stage, the high frequency range phase angle peak has disappeared. A typical EIS spectrum at this stage shows a phase angle peak in the intermediate frequency range, as shown in the low impedance curves in Figures 5.6, 5.7 and 5.8. The disappearance of the phase angle peak in the high frequency range is due to a major inhibitor film breakdown, resulting in a smaller pore resistance or larger disbonding area and so a very small inhibitor film time constant results, which does not respond in the frequency range applied.

### 5.3.3 Corrosion rate estimation using EIS data

The determination of inhibitor performance and inhibitor film persistency is normally based on the measurements of instantaneous corrosion rate because the failure and breakdown of inhibitor film is always accompanied by a large increase in corrosion rate. However, in the case of electrodes filmed with batch treatment inhibitors the correlation between corrosion rate and EIS data is more complicated than in other cases. A clear understanding of the relationships between impedance spectra and corrosion is important for the industrial application of EIS.

#### 5.3.3.1 The first stage of inhibitor film deterioration

During the first stage of inhibitor film deterioration, as discussed in the previous section, the corrosion rate is not determinable using EIS data. In this stage, the measured impedance, such as the impedance of inhibitor 'A' filmed electrodes (in Figures 5.2), is not due to the electrochemical double layer impedance and so is not directly correlated with the corrosion rate. In these cases, the electrochemical double layer impedance is masked by the large inhibitor film impedance, or is merged with inhibitor film impedance, and so the corrosion rate is not accessible.

However, an empirical relationship can be found by comparison of EIS data with weight-loss measurements. As shown in Table 5.1, very small corrosion rates in weight-loss measurements were recorded when electrode impedance spectra show a large inhibitor film pore resistance ($R_{pore}$) and a capacitive behaviour in the high frequency range. These experimental results suggest an empirical relationship that at the first stage of inhibitor film deterioration, the inhibitor film on the electrode is undamaged and a very low corrosion rate is expected, although the exact corrosion rate is not determinable by EIS.

**Table 5.1.** A comparison of weight-loss measurements and EIS data from batch-treatment inhibitor-filmed coupons/electrodes.

| Test | Experimental Details and Conditions | EIS | Weight-loss (Visual Observation and Corrosion Rate) |
|---|---|---|---|
| 1 | Electrode and coupons were filmed with inhibitor 'A', and exposed to a pure 3% NaCl brine for 5.5 days at 50 °C with $CO_2$ sparging. | * | Corr. Rate: ~ 0.02 mm/y. A few isolated dark-brown corrosion dots found. |
| 2 | Electrode/coupons were filmed with inhibitor 'B', and then exposed to an emulsion of 80% brine + 20% kerosene for 14 days at 70 °C, 1000 rpm rotation and with $CO_2$ sparging. | * | Corr. Rate: < 0.01 mm/y. No obvious change found on electrode surface. |
| 3 | Electrode/coupons were filmed with inhibitor 'C', and then exposed to an emulsion of 80% brine + 20% kerosene for 14 days at 70 °C, 1000 rpm rotation and with $CO_2$ sparging. | * | Corr. Rate: < 0.01 mm/y No obvious change found on electrode surface. |

* During the measurement period, the impedance spectra of electrodes showed a large inhibitor film pore resistance (values of $R_{pore}$ were in the order of $10^4$ ohms) and a capacitive behaviour in the high frequency range.

This empirical relationship is not surprising since, in fact, the inhibitor film pore resistance ($R_{pore}$) is a reflection of the penetration of inhibitor film by electrolyte (Mansfeld and Tsai 1991). A larger $R_{pore}$ may suggest a better inhibitor molecular coverage of the metal surface and a higher resistance to ion permeability, resulting in greater resistance to corrosion. In the study of the deterioration of organic coatings, it was also suggested that coating pore resistance ($R_{pore}$) is related to the delamination (deterioration) of organic coating films (Tsai and Mansfeld 1993).

### 5.3.3.2 The second and third stages of inhibitor film deterioration

When inhibitor-filmed electrodes were in the second and the third stages of deterioration, however, obvious corrosion could be found after a short time of exposure, as shown in Table 5.2, suggesting the occurrence of rapid corrosion at the second and the third stages.

**Table 5.2.** A comparison of EIS spectra with observations of corresponding batch-treatment inhibitor-filmed weight-loss coupons.

| inhibitor | Experimental Details and Conditions | EIS | Surface Visual Observation |
|---|---|---|---|
| 'A' | Exposed to a pure brine for 2 days at 70 °C, 1000 rpm rotation and with $CO_2$ sparging. | * | Electrode covered with black corrosion product. |
| 'B' | Exposed to a pure brine for 2 days at 70 °C, 1000 rpm rotation and with $CO_2$ sparging. | * | Electrode surface showed serious localised corrosion |
| 'C' | Exposed to a pure brine for 6 days at 70 °C, 1000 rpm rotation and with $CO_2$ sparging. | * | Deep corrosion pits found on electrode surface. |

* During the measurement period, the impedance spectra of electrodes showed that inhibitor films were in the second and third stages of deterioration.

During the second and the third stages of inhibitor film deterioration, the corrosion rate is accessible because the electrochemical charge transfer resistance is determinable. The electrochemical charge transfer resistance ($R_t$) could be calculated by fitting a semicircle to the Nyquist plot, corresponding to the phase angle peak at intermediate frequency, which is due to the electrochemical corrosion process. Corrosion rates can then be estimated using $R_t$ data and the Stern-Geary equation:

$$I_{corr} = \frac{b_a b_c}{2.303(b_a + b_c)} \times \frac{1}{R_p} \approx \frac{b_a b_c}{2.303(b_a + b_c)} \times \frac{1}{R_t} \qquad (5.1)$$

### 5.3.4 The evaluation of Inhibitor film persistency

Based on the discussion above, a method can be suggested here for the determination of inhibitor film persistency:

(1). Determine the stage of inhibitor film deterioration using the Bode phase plots as an indicator. If the inhibitor film is at the first stage of deterioration, i.e. electrode impedance spectra show a large inhibitor film pore resistance ($R_{pore}$) and a capacitive

behaviour at high frequency range, a low corrosion rate is expected and the inhibitor film is largely undamaged, or at least still highly protective.

(2). Determine corrosion rate using $R_p$ or $R_t$. When inhibitor film deterioration reaches the second and the third stages, corrosion rate is accessible using equation (5.1). The period just before the corrosion rate begins to increase rapidly gives the inhibitor persistency.

An example of inhibitor film persistency evaluation is given in Figure 5.9. Inhibitor 'A' was filmed both on a pre-corroded and a fresh bare electrode at 70 °C and then washed in brine for 1 hour at 1000 rpm before monitoring inhibitor film persistency. The increase in corrosion rate clearly shows the failure process of the inhibitor films. Inhibitor 'A' film showed much better persistency on a pre-corroded electrode than on a bare electrode. The pre-corroded electrode was prepared by placing a bare electrode in brine for 24 hours at 70 °C under continuous $CO_2$ sparging. The corrosion of the pre-corroded electrode surface is generally uniform.

Compared with the linear polarisation method, EIS has obvious advantages. EIS can measure corrosion rate, at the second and the third stages of inhibitor film deterioration, more accurately by separating inhibitor film resistance and solution resistance. In this way the risk of possible incorrect evaluation of inhibitor film persistency can be avoided. EIS can also provide a lot of mechanistic information about inhibitor film deterioration by determining the increase in electrode capacitance and the decrease in inhibitor film pore resistance and charge transfer resistance. For example, the increase in electrode capacitance may be related to the increase of inhibitor film broken area and may be used to estimate the area of inhibitor film which has delaminated.

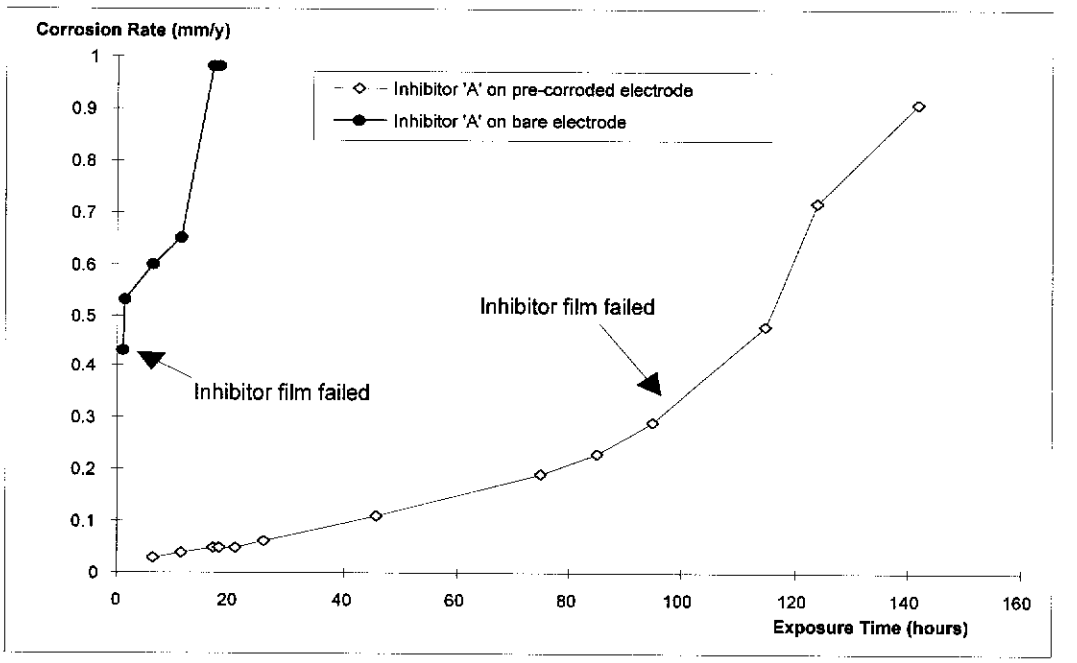


**Figure 5.9.** The evaluation of film persistency of inhibitor 'A'. No corrosion rate was detected for the pre-corroded electrode during the first 1.5 hours of exposure because the inhibitor film was at the first stage of deterioration and the corrosion rate was not measurable.

## 5.4 Results and discussion II: Monitoring the performance and persistency of batch treatment inhibitor films using ENA

EIS has similar limitations in the study and evaluation of batch treatment inhibitor films as it does in the study and evaluation of continuous treatment inhibitors, which was discussed in section 4.4. In this work, electrochemical noise analysis (ENA) was used to continuously monitor inhibitor film performance and persistency. The objectives of this work are to develop ENA as a combined technique with EIS and to develop ENA as an *in-situ* technique for monitoring batch treatment inhibitor film performance. The new developments in the electrochemical noise analysis technique and theory, discussed in section 2.4, were also tested in the batch treatment inhibitor system.

### 5.4.1 Monitoring the formation of batch treatment inhibitor film

A dual mild steel electrode was placed in the brine phase of a base fluid of 640 mL of brine and 160 mL of diesel, as shown in Figure 5.1. The recording of the corrosion potential and coupling current between the dual electrodes in the base fluid was commenced immediately. Then 16 mL of batch-treatment inhibitor 'A' was added into the base fluid and an emulsion of inhibitor filming fluid was formed by magnetic stirring for 60 seconds (1000 rpm). The inhibitor film was formed in the emulsion.

Figures 5.10 (a) and (b) show the voltage and current records before and after adding inhibitor 'A'. After adding inhibitor and starting stirring of the filming fluid, as shown in Figure 5.10 (a), the coupling current between the dual electrodes quickly decreased approaching zero current. The corrosion potential of the dual electrode quickly

shifted in the positive direction with large potential fluctuations which may be due to interference from the magnetic stirring.

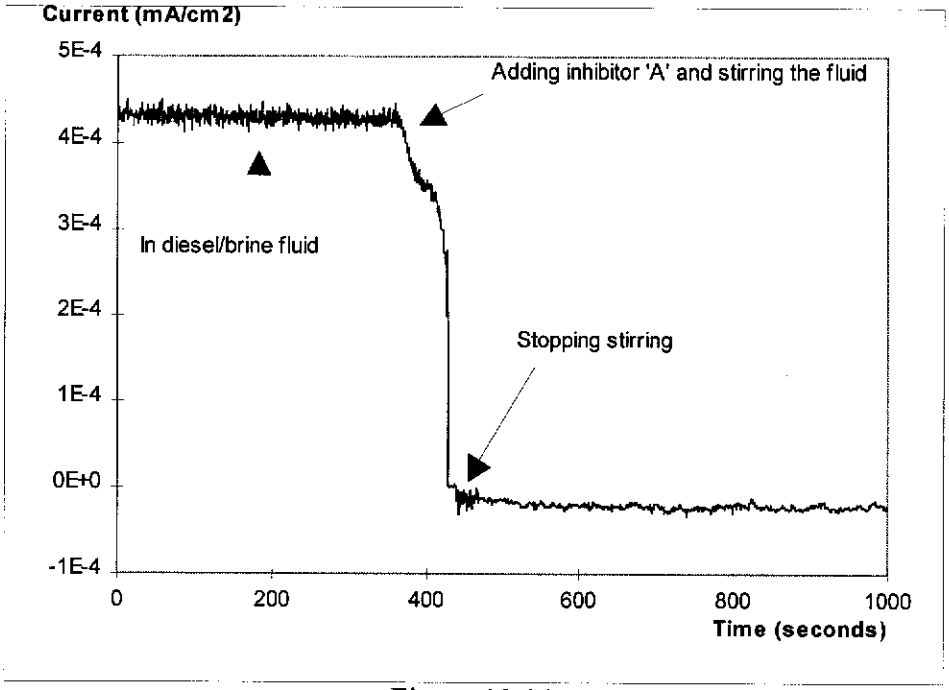


Figure 10 (a)

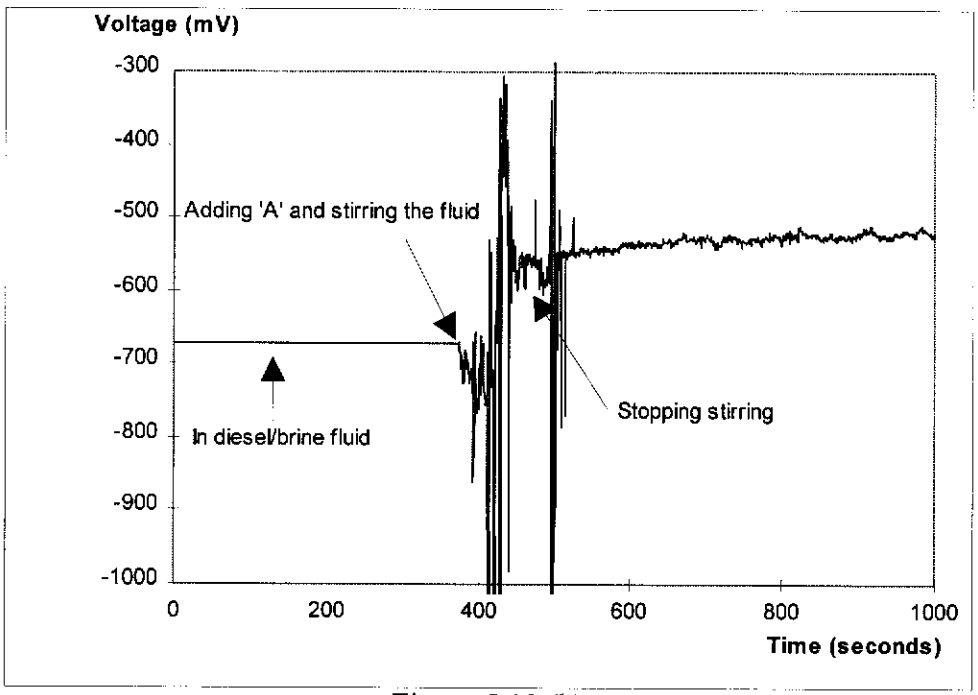


Figure 5.10 (b)

**Figure 5.10.** (a) current and (b) voltage vs. time records before and after filming with inhibitor 'A'.

After removing the large DC shift in the current and potential records using the moving average removal method, as described in section 2.4.1, it can be seen that the underlying current noise amplitude continuously decreased, while the underlying voltage noise amplitude increased with the formation of inhibitor film, as shown in Figures 5.11 (a) and (b).

The continuous decrease in the amplitude of current noise was expected and is similar to the experimental findings in continuous treatment inhibitor systems (section 4.4.1), which suggests a direct correlation between current noise and the formation of inhibitor film.

However, the increase in potential noise amplitude was not expected and was not in accordance with the direct relationships between voltage noise and corrosion rate suggested (see section 2.3.1.1) by some researchers (Searson and Dawson 1988; Gusmano *et al.* 1993). The large noise amplitude may be related to the instability of the newly formed inhibitor film.

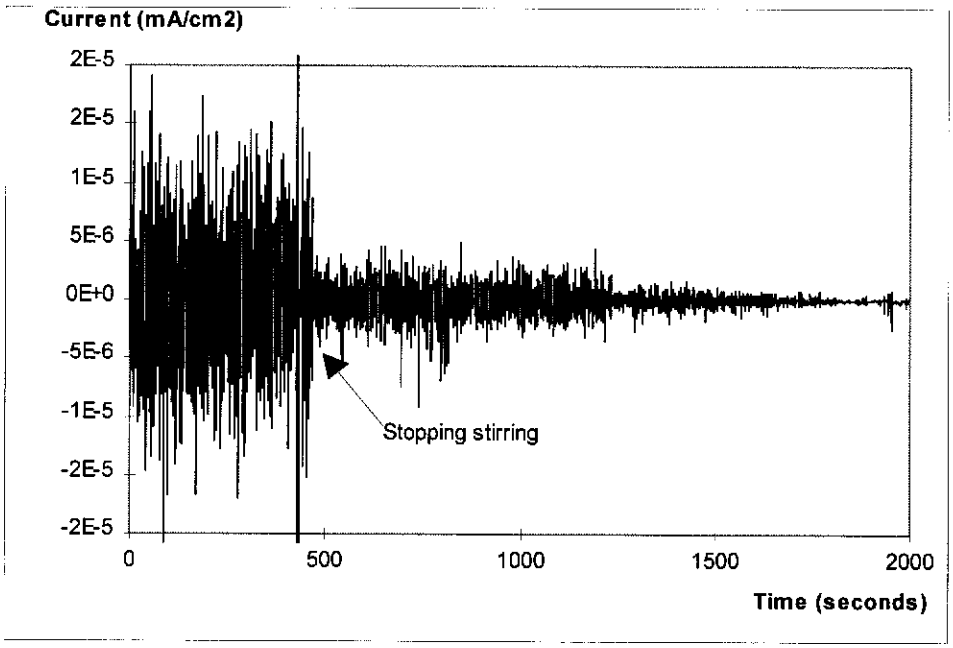


Figure 11 (a)

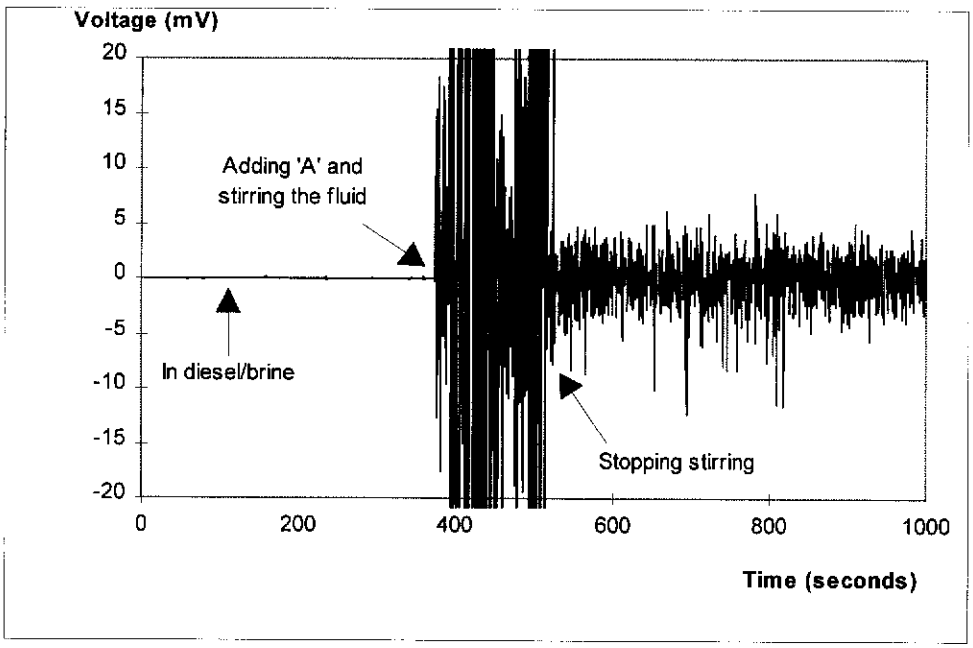


Figure 5.11 (b)

**Figure 5.11.** (a) current noise and (b) voltage noise, after removing DC trends, before and after filming with inhibitor 'A'.

Using the method described in section 2.4.2, instantaneous noise resistance can be calculated from voltage and current noise data in Figures 5.11 (a) and (b), yielding the results shown in Figure 5.12.

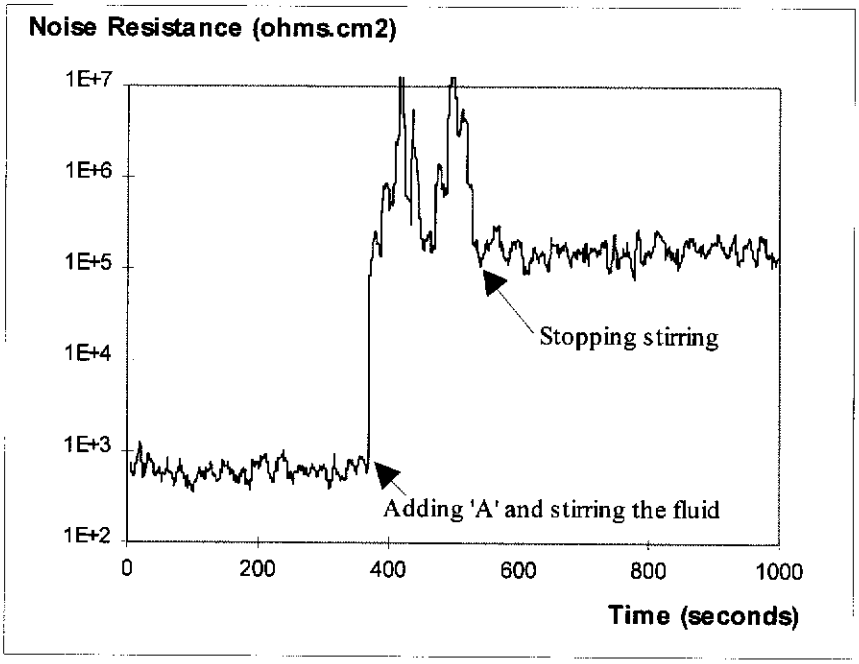


**Figure 5.12.** The changes of instantaneous electrochemical noise resistance ($R_n$) during the rapid inhibitor 'A' film formation process.

Although the noise resistance in Figure 5.12 shows fluctuations, it clearly indicates the rapid formation process of a protective inhibitor film. A rapid and large increase in noise resistance after adding inhibitor suggests that the formation of the inhibitor film is a very rapid process.

With statistical treatment of voltage and current noise data, the noise resistance can be deduced. Figure 5.13 shows noise resistance , $R_t+R_{pore}$ (EIS) and $R_p$ (LP) before and after inhibitor addition, which were from parallel ENA and EIS /LP experiments in two separate electrochemical cells.

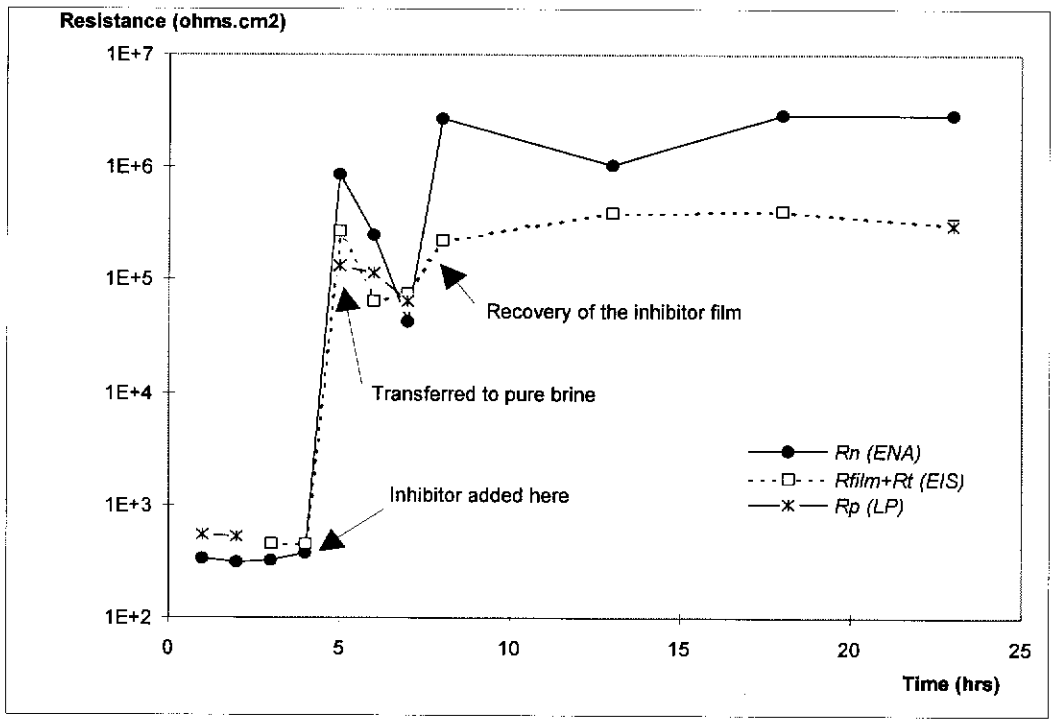


**Figure 5.13.** Noise resistance ($R_n$), polarisation resistance ($R_p$) and EIS resistance ($R_t$+$R_{pore}$) before and after filming inhibitor 'A' (parallel tests).

After adding inhibitor into the brine/diesel base fluid, as shown in Figure 5.13, noise resistance, $R_t$+$R_{pore}$ (EIS) and $R_p$ (LP) greatly increased indicating the formation of an inhibitor film. When filmed electrodes were transferred into an inhibitor-free pure 3% NaCl brine, electrode resistances decreased to a minimum and then increased again (recovered). The recovery of the inhibitor film may be due to the self-repairing ability, which was reported in section 4.3.1.2, of the inhibitor component imidazoline.

The noise resistance, $R_t$+$R_{pore}$ (EIS) and $R_p$ (LP) in Figure 5.13 all showed similar trends. Noise resistance clearly indicated the formation of an inhibitor film and the inhibitor film recovery processes.

### 5.4.2 Monitoring the destruction of batch treatment inhibitor film

After being filmed with inhibitor 'A', electrodes were transferred into a washing fluid (inhibitor-free pure 3% NaCl brine) for investigating the inhibitor film destruction process. Initially, the test temperature was 30 °C and the washing fluid was stagnant. After a period of time, the washing fluid was heated to 70 °C and was stirred at 1000 rpm to accelerate the inhibitor film breakdown. Electrochemical noise was recorded throughout the whole testing period. Some EIS and LP measurements were also carried out using the same electrode as that used for noise recording.

Figures 5.14 (a) and 5.14 (b) show the current noise and potential noise changes vs. time during the fast destruction of inhibitor film which was due to the increase in fluid temperature and fluid shear stress.

With the breakdown of inhibitor film, as shown in Figure 5.14 (a), current noise amplitude increased rapidly. However, no significant change was observed for the voltage noise, which again suggests that no direct relationship exists between voltage noise and the corrosion process.

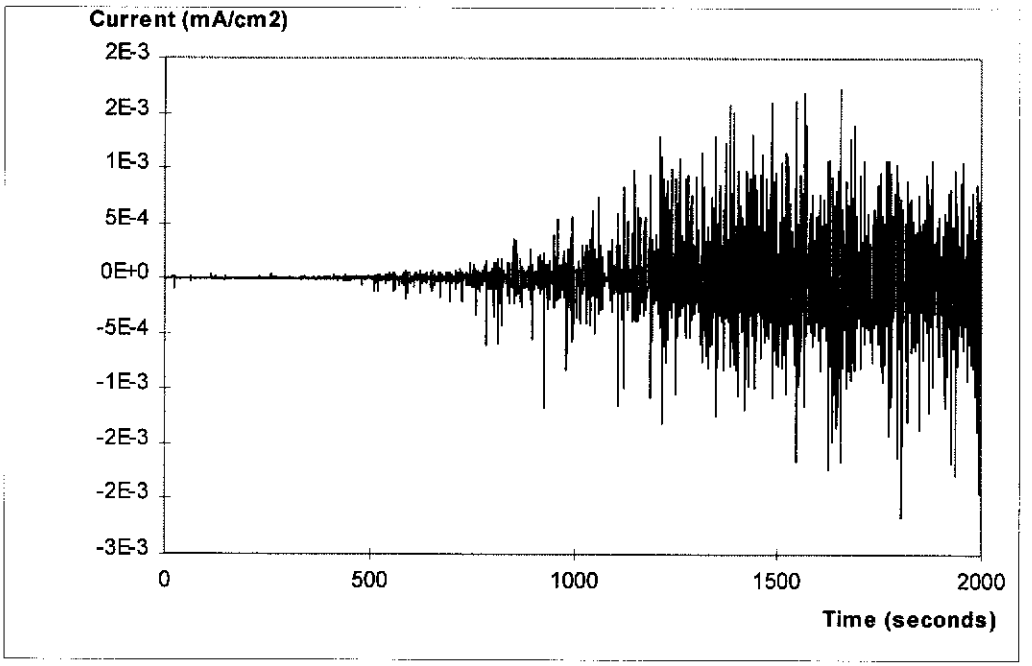


Figure 5.14 (a)

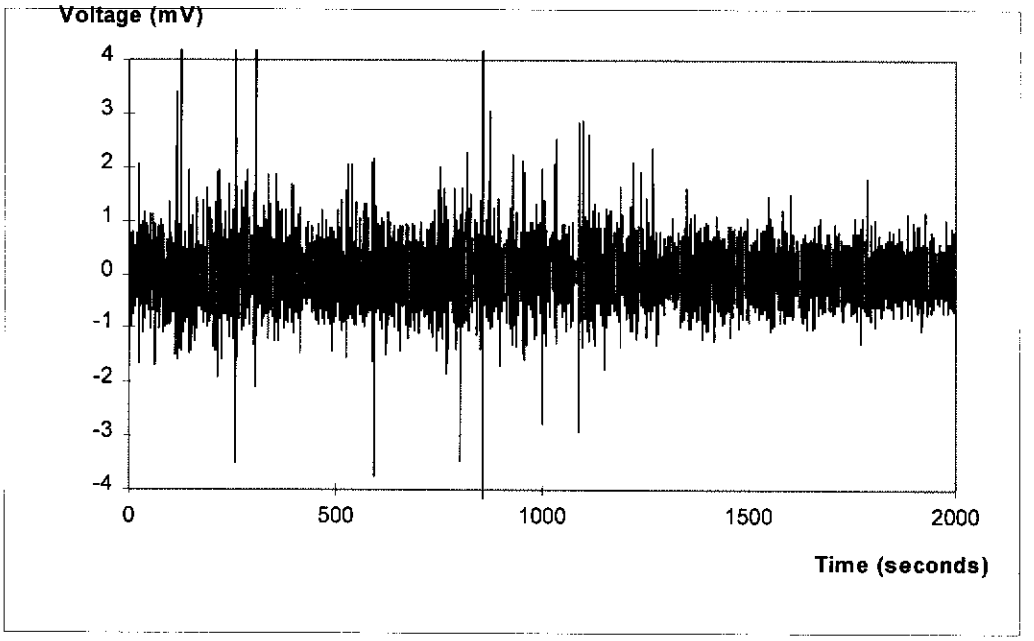


Figure 5.14 (b)

**Figure 5.14.** Noise patterns, after removing DC trend, recorded during the fast destruction process of the inhibitor 'A' film. (a) Current noise, (b) Voltage noise.

Using statistical treatment of voltage and current noise data (after removing the DC shift), the noise resistance can be deduced. Figure 5.15 shows the change of noise resistances, $R_t$+$R_{pore}$ (EIS) and $R_p$ (LP) during the inhibitor film deterioration process.

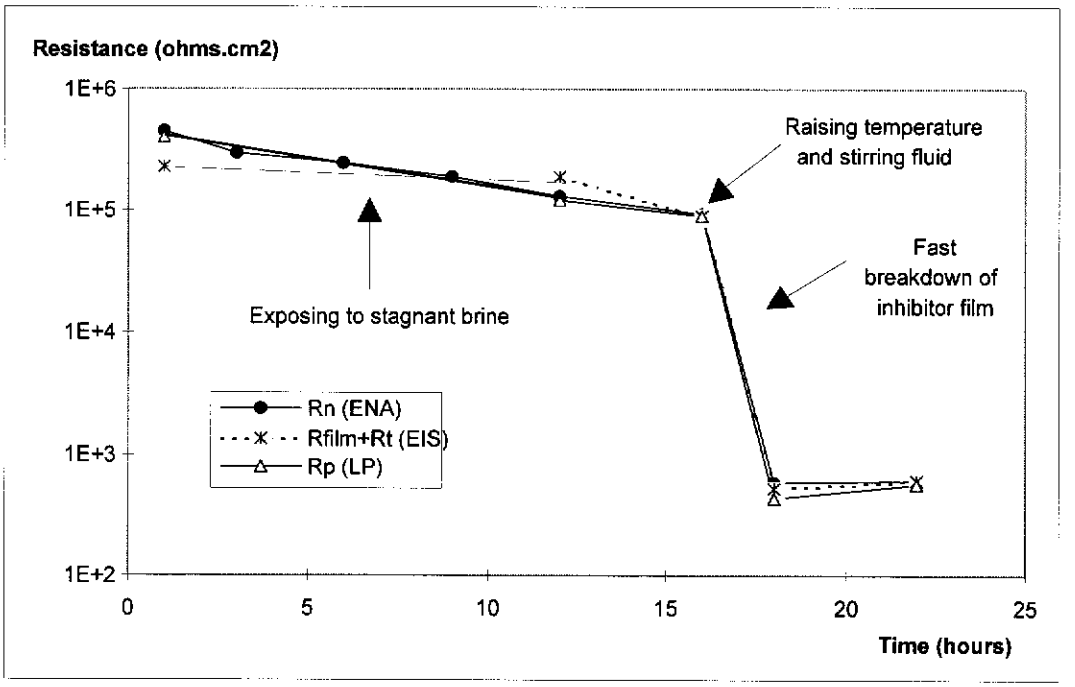


**Figure 5.15.** The change of electrochemical noise resistance ($R_n$), $R_t$+$R_{pore}$ (EIS) and $R_p$ (LP) during the inhibitor film deterioration process.

The noise resistance, $R_t$+$R_{pore}$ (EIS) and $R_p$ (LP) in Figure 5.15 again show very similar trends. Noise resistance clearly indicates the deterioration process of the inhibitor film.

In Figure 5.15, it is shown that a rapid inhibitor film breakdown occurred from 16 to 18 hours, which was due to the effects of increasing the fluid temperature and the fluid shear stress. Using the method described in section 2.4.2, the instantaneous noise resistance of the rapid film breakdown process can be calculated from the corresponding voltage and current noise data (shown in Figures 5.14 (a) and (b)).

Although fluctuations occur, as shown in Figure 5.16, the trend clearly follows the breakdown process of the inhibitor film. Significant evidence comes from the EIS $R_t$+$R_{pore}$ values, measured just before and just after the 2000 second noise recording. These values, shown in Figure 5.16, show excellent correlation with $R_n$. Thus the instantaneous noise resistance data provides a detailed information about the rapid inhibitor film breakdown process.

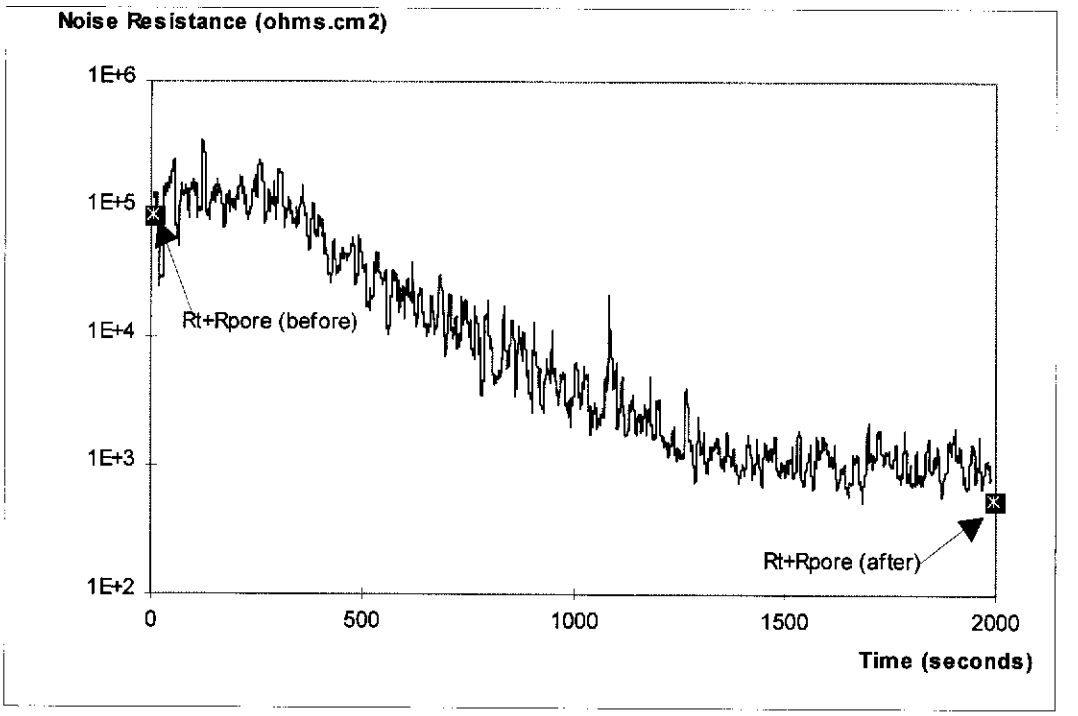


**Figure 5.16.** The change of electrochemical noise resistance ($R_n$) during the 2000 seconds inhibitor film breakdown process. The time interval $\Delta t$ used for noise resistance calculation was 9.5 seconds.

Compared with the inhibitor film formation process as shown in Figure 5.12, the inhibitor film breakdown is a relatively slow process.

This analysis procedure again shows that ENA has the potential to study corrosion processes which are under rapid change. Here ENA has again been demonstrated to be a technique which can monitor corrosion process instantaneously and continuously.

### 5.4.3 The limitations of the noise resistance method

The similarity between noise resistance, $R_t+R_{pore}$ (EIS) and $R_p$ (LP), as shown in Figures 5.13, 5.15 and 5.16 and also in Figures 4.30, 4.34 of the previous Chapter strongly suggest a direct correlation between noise resistance and the electrochemical corrosion process. These experimental results can be explained by a theoretical analysis which was carried out in section 2.4.3, based on a concept called statistical linear polarisation.

The basic idea of statistical linear polarisation is that the difference in voltage noise signal, which is produced randomly by each of the two 'identical' electrodes, actually works as an internal polarisation voltage signal, producing current noise. The polarisation is linear because the dual electrodes are identical, and are thus supposed to have very similar (identical) corrosion potentials, and so polarisation is in the vicinity of the corrosion potential and in the linear polarisation zone. The noise resistance, which is deduced from statistical analysis of voltage and current noise signals, is reasonably equivalent to linear polarisation resistance which is measured using an externally applied voltage signal.

In the theoretical analysis of the noise resistance (see section 2.4.3), several prerequisite conditions were suggested and used:

(i). All electrochemical properties of the two identical electrodes are the same.
(ii). Potential noise consists of random signals, and is very small in magnitude, although its origin is not clearly known.
(iii). Corrosion reactions are totally activation-controlled and corrosion is uniform.
(iv). DC components and shifts in voltage and current records are removed.

These prerequisite conditions explained why the removal of DC components and shifts in voltage and current records is important in the calculation of noise resistance.

The prerequisite conditions also suggest limitations of the ENA technique. Obviously ENA has similar limitations to polarisation resistance measurement techniques.

### 5.4.4 The advantages of the noise resistance method

In the study and evaluation of batch treatment inhibitors, obviously, ENA has limitations in providing accurate values of corrosion rate because the noise resistance contains inhibitor film resistance, charge transfer resistance etc.. However, ENA has many advantages over the traditional linear polarisation technique. As shown in Figures 5.13, 5.15 and 5.16, noise resistance can give a very clear estimation of inhibitor film persistency. ENA is the only technique which can monitor corrosion processes instantaneously and continuously, as suggested in section 2.4.2 and shown in Figure 5.16, thus it may be very useful for studying fast corrosion processes, e.g. inhibition and passivation processes. Electrochemical noise measurement supposes to be working in a free corrosion condition and there is no need to apply a perturbation on the test system by an externally imposed polarisation. Furthermore, electrochemical noise recording requires only simple instruments, and is experimentally simple, thus offering greater convenience for on-site application.

## 5.5 Conclusions

(i). EIS was shown to be a very suitable tool for studying batch-treatment inhibitors. Useful information can be obtained on the inhibitor film formation and deterioration processes, and batch-treatment inhibitor film persistency can be evaluated.

(ii). It was found that the formation of batch-treatment inhibitor films was accompanied by characteristic spectral changes and a rapid increase in electrode impedance. The presence of a hydrocarbon phase made a significant contribution to the formation of a protective inhibitor film.

(iii). It was also found empirically that the inhibitor film deterioration process has three stages. Each stage showed characteristic Bode phase-angle plots and a decrease in electrode impedance.

(iv). A method for determining inhibitor film persistency was suggested from comparison of EIS results with weight-loss measurements, based on the determination of the stage of inhibitor film deterioration using the Bode phase-angle plots as an indicator, and the continuous measurement of instantaneous corrosion rate, which is accessible at the second and the third stages of inhibitor film deterioration.

(v). ENA was shown to be able to continuously follow the deterioration processes of batch-treatment inhibitor films. With the deterioration of the inhibitor film, current noise amplitude was found to increase rapidly and the noise resistance, which is deducible from voltage and current noise records, was found to decrease sharply.

(vi). The noise resistance was confirmed to be similar to linear polarisation resistance ($R_p$) in the corrosion-inhibition system studied. This empirical similarity was

explained based on a concept named statistical linear polarisation which suggests that ENA is actually a special form of linear polarisation technique in which the polarisation voltage is produced by the system itself. ENA has advantages over the normal linear polarisation technique.

# Chapter VI

# CONCLUDING REMARKS AND SUGGESTIONS FOR FURTHER WORK

## 6.1 Concluding remarks

This thesis has mainly explored the application of electrochemical impedance spectroscopy (EIS) and electrochemical noise analysis (ENA) in the study of $CO_2$ corrosion and its inhibitors. Focus is on the use of EIS and ENA to monitor inhibitor film performance and to evaluate inhibitor film persistency.

EIS was shown to be a very valuable technique in studying $CO_2$ corrosion product scale, and in evaluating inhibitor films. The formation and deterioration of a protective corrosion product scale, a continuous or batch treatment inhibitor film are always accompanied by characteristic spectral changes and a rapid change in electrode impedance. EIS data can be used to calculate corrosion related electrochemical parameters such as the resistances and capacitances of inhibitor layers, charge transfer resistance and double layer capacitance. These parameters can be used to analyse the inhibitor mechanism, to calculate the corrosion rate and thus to evaluate inhibitor film persistency.

ENA was shown to be able to effectively and continuously follow the formation and deterioration processes of continuous and batch treatment inhibitor films, thus ENA is a very convenient tool in monitoring inhibitor film performance and persistency. Several technical and theoretical developments were made in this thesis including the

introduction of a new method to remove DC trends in noise recording (moving average removal); a method of instantaneous corrosion rate measurement; and a new theoretical concept to explain the meaning of noise resistance (statistical linear polarisation). Experimentally, the noise resistance was confirmed to be similar to linear polarisation resistance in the corrosion-inhibition systems studied. The advantages and disadvantages of the ENA technique were also discussed.

EIS and weight-loss results confirmed that corrosion scales formed at higher temperature and high pressure have better protective ability. It was also confirmed that the protectiveness of $CO_2$ corrosion product scales is a function of exposure time. The volume of brine is the main factor determining how fast scale initiates. Under certain conditions, it was found that corrosion scale can form at 30 °C which questions the validity limits of the de Waard-Milliams equation. The correlation between weight-loss measurement results and the calculations using the de Waard-Milliams equation was poor. The surface morphology showed obvious correlation to the protective ability of scales. Two kinds of corrosion product crystals were found under SEM on the surface of corroded coupons. The fine crystals contribute to the corrosion protection. The chemical compositions were found to be quite similar for all scales formed under different conditions and did not show correlation to its corrosion protective ability. $FeCO_3$, $Fe_3C$, and iron oxides were found to be the main corrosion products. No $FeHCO_3$ was found in any sample tested in this study.

Imidazoline was shown by EIS to be a very effective $CO_2$ corrosion inhibitor. It forms a chemically bonded film on the metal surface. The inhibitor film seems to be a combination of an inner-layer which is likely to be an inhibitor-metal complex and several outer-layers which are likely to be inhibitor layers with possible inhibitor molecular cross-linking. The inhibitor film showed a strong self-repairing ability, but surface water shear stress can gradually remove the inhibitor film and cause inhibitor film failure. Quaternised amine inhibitor films formed on electrode surfaces are most

likely physically or electrostatically adsorptive molecular layers which form rapidly and desorb easily. Films formed from polymerised vegetable fatty acid seem to have characteristics between interphase and interface inhibition.

It was found that the deterioration of batch treatment inhibitor film proceeds through three stages. Each stage showed characteristic Bode phase-angle plots and a decrease in electrode impedance. A method for determining inhibitor film persistency was suggested from comparison of EIS results with weight-loss measurements. The method is based on the determination of the stage of inhibitor film deterioration using the Bode phase-angle plots as an indicator, and the continuous measurement of instantaneous corrosion rate, which is accessible at the second and the third stages of inhibitor film deterioration. The presence of a hydrocarbon phase made a significant contribution to the formation of a protective inhibitor film. A synergistic effect between inhibitor film and corrosion product scale was also found in this work.

## 6.2 Suggestions for Further Work

This research raises some possibilities for further work and also some new questions. For example, the findings about the synergistic effect of inhibitor film and corrosion product scale, about the significant contribution of hydrocarbon to the protectiveness of inhibitor films, and about the influence of scaling duration on corrosion scale properties may prove useful in developing new inhibitor formulations. However, these findings also questioned some of the current laboratory tests which are carried out over short time periods.

An obvious limitation of this work is that all EIS and ENA measurements were carried out under 1 atm pressure conditions using pre-scaled or pre-filmed electrodes. Better work may be done if all these measurements are carried out directly in high pressure and high temperature electrochemical systems, where oil and gas well corrosion conditions may be better simulated. If EIS measurements are carried out in a high temperature and high pressure electrochemical system, the effects of most of the factors on $CO_2$ corrosion, such as pH, water chemistry, gas and oil composition, fluid flow speed and flow regime, solid particles content, metal surface condition, and the microstructure of steel etc., may be quantitatively explained based on their effects on $CO_2$ corrosion product scale using EIS analysis. In this way, a better modification of the de Waard-Milliams equation may become possible.

The protection offered by $CO_2$ corrosion product scale may be greatly improved by optimising the scaling conditions and $CO_2$ corrosion product scale may become the simplest and cheapest method of $CO_2$ corrosion control. For example, the protectiveness of $CO_2$ corrosion product scale may be greatly improved by adding small amounts of passivating chemicals. A better understanding of the synergistic

effects between $CO_2$ corrosion product scale and inorganic and organic inhibitors may be helpful to develop a better inhibition technique.

ENA may be used to detect the localised destruction of inhibitor films and corrosion product scales and to investigate their possible links to localised corrosion. This is normally done by computing noise spectra which was described in section 2.3.1.2. However, this technique has currently only been studied in very simple corrosion systems. This method may have problems when it is applied in the complicated oil and gas well corrosion system where many factors can interfere with the noise power spectral pattern.

Another method may be suggested to detect localised corrosion by combining the ENA technique with the wire beam electrode technique. The wire beam electrode (WBE) technique which has been developed by the author and co-workers in 1991 (Tan; Tan and Yu 1991) was used to monitor crevice corrosion (Tan 1994) and localised coating defects (Wu *et al.* 1995). In these works, the WBE technique has been shown to be capable of monitoring the occurrence of localised corrosion. The wire beam electrode, as shown in Figure 6.1, has many mini-electrode pairs for ENA measurements. ENA measurements may be carried out by connecting two of the wires in the wire beam electrode. The corrosion rates at different locations of the wire beam electrode could be mapped by connecting to different wires at corresponding locations. If localised inhibitor film breakdown occurs, the corrosion rate at different locations of the electrode surface will be different. In this way, uniform and localised corrosion can be monitored.

Figure 6.1 (a)

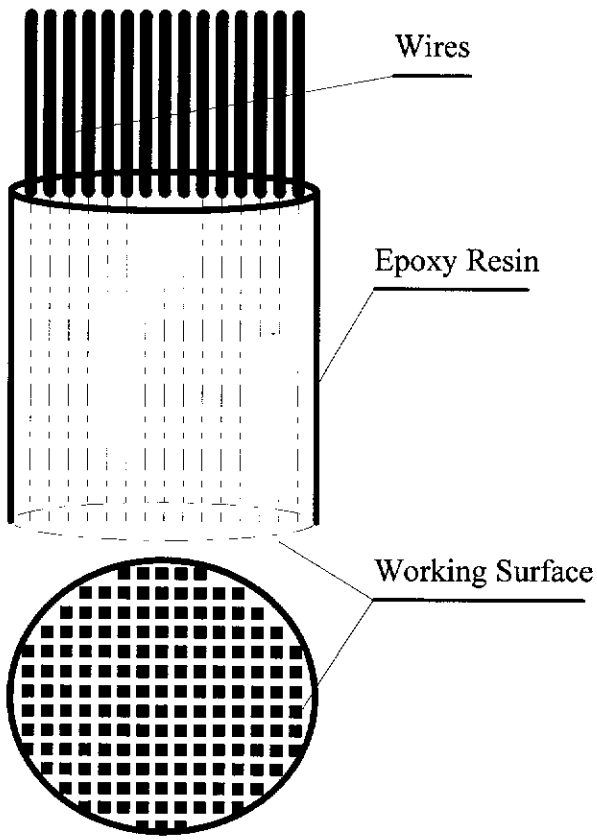


Figure 6.1 (b)

**Figure 6.1.** A schematic diagram of the wire beam electrode. The electrode consists of a metal wire beam prepared by binding a large number of metal wires together and embedding in epoxy resin. Each wire is insulated from its neighbours and constitutes a mini-sensor.

Figure 6.2 shows a possible experimental design using the WBE for carbon dioxide corrosion inhibitor film persistency evaluation and localised carbon dioxide corrosion monitoring.

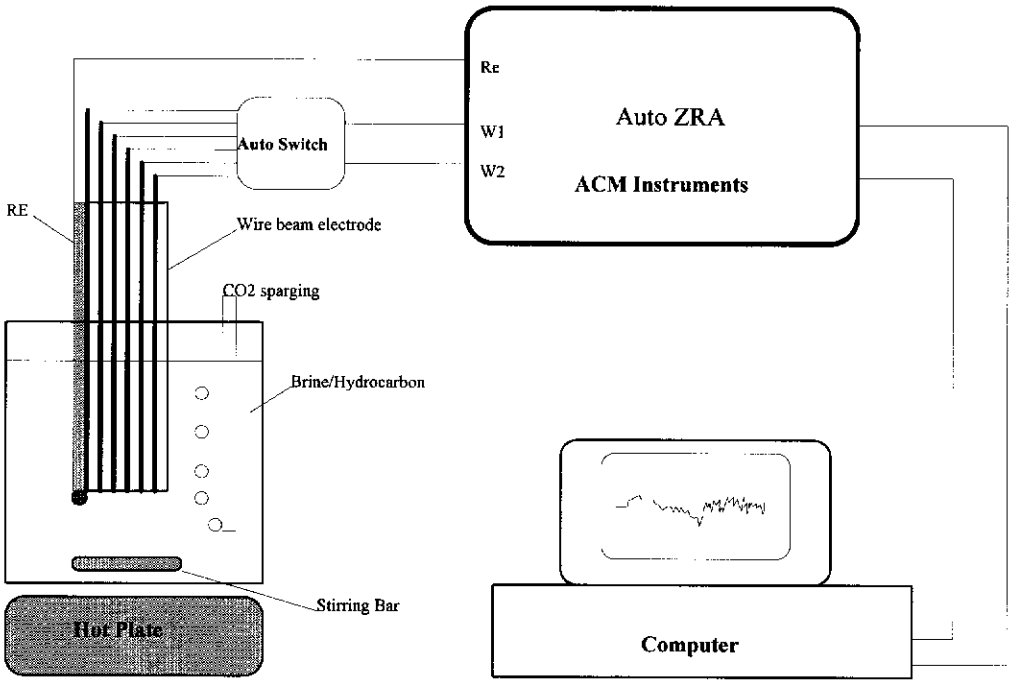


**Figure 6.2.** The experimental arrangement for electrochemical noise recording using a wire beam electrode. The corrosion system shown in this experiment is the evaluation of carbon dioxide corrosion inhibitor.

# REFERENCES

Agarwal, P. Moghissi, O. C. Orazem and M. E. Garcia-Rubio, L. H. 1993, 'Application of measurement models for analysis of impedance spectra', *Corrosion*, vol. 49, no. 4, p278

Alkire, J. D. Lunden, K. C. Kochanczyk, R. W. and Abdulla, A. 1993, 'Inhibitor protection of high velocity gas condensate wells in Sharjah', Corrosion 93, Paper 103, NACE (Houston)

Azim, S. S. Muralidharan, S. and Iyer S. V. 1995, 'Studies on the influence of iodide ions on the synergistic inhibition of the corrosion of mild steel in an acidic solution', *Journal of applied electrochemistry*, vol. 25, p495

Bandy, R. and Jones, D. A. 1976, 'Analysis of errors in measuring corrosion rates by linear polarisation', *Corrosion*, vol. 32, no. 4, p127

Barker, G. C. 1969, 'Noise connected with electrode processes', *Journal of Electroanalytical Chemistry,* vol. 21, no. 1, p127

Barnartt, S. 1970, 'Two-point and three-point methods for the investigation of electrode reaction mechanisms', *Electrochimica Acta*, vol. 15, no. 8, p1313

Beaunier, L. Epelboin, I. Lestrade J. C. and Takenouti, H. 1976, 'Electrochemical study with a scanning electron microscope of paint coated iron', *Surface Technology,* vol. 4, no. 3, p237

Beavers, J.A. Thompson N. G. and Silverman, D. C. 1993, 'Corrosion engineering applications of electrochemical techniques: laboratory testing', Corrosion 93, paper 348, NACE (Houston)

Bendat, J. S. and Piersol, A. G. 1986, 'Random data: analysis and measurement procedures', Second Edition, John Wiley & Sons Publication, New York

Bertocci, U. 1980, 'Applications of a low noise potentiostat in electrochemical measurements', *Journal of the Electrochemical Society*, vol. 127, p1931

Bertocci, U. 1981, 'Separation between deterministic response and random fluctuations by means of the cross-power spectrum in the study of electrochemical noise', *Journal of the Electrochemical Society*, vol. 128, p520

Bertocci, U and Kruger J. 1980, 'Studies of passive film breakdown by detection and analysis of electrochemical noise', *Surface Science*, vol. 101, no. 1-3, p608

Bertocci, U. Mullen, J.L. and Ye, Y. X. 1983, in 'Passivity of Metals and Semiconductors', Froment, M. (ed.), Elsevier, Amsterdam, p229

Bewick, A. Kalaji, M. and Larramona, G. 1991, '*In-situ* infrared spectroscopic study of the anodic oxide film on iron in alkaline solutions', *Journal of Electroanalytical Chemistry*, vol. 318, p207

Blair, C. M. and Gross, W. F. 1949, U.S. Patents 2,466,517; 2,466,530; 2,468,163

Bodu, J. J. Brunin, M. Keddam, M. and Takenouti, H. 1977, 'Application of an impedance method to control the anodic oxidation of light alloys', *Metaux: Corrosion -Industrie*, vol. 52, p165

Bonnel, A. Dabosi, F. Deslouis, C. Duprat, M. Keddam, M. and Tribollet, B. 1983, 'Corrosion study of a carbon steel in neutral chloride solutions by impedance techniques', *Journal of the Electrochemical Society*, vol. 130, no. 4, p753

Boukamp, B. A. 1989, 'Equivalent Circuit (EQUIVCRT.PAS)', Version 3.96, Second edition

Bretherton, N. Turgoose S. and Thompson G. E. 1993, 'Electrochemical studies of phosphate conversion coating growth and performance', Corrosion 93, Paper 444, NACE (Houston)

Butler, J. A. V. 1924, 'Studies in heterogeneous equilibria. I. Conditions at the boundary surface of crystalline solids and liquids, and the application of statistical mechanics', *Transactions of the Faraday Society*, vol. 19, p729

Butler, J. A. V. 1924, 'Studies in heterogeneous equilibria. II. The kinetic interpretation of the Nernst theory of electromotive force', *Transactions of the Faraday Society*, vol. 19, p734

Bradburn, J. D. 1977, 'Water production - an index to corrosion', presented at South Central NACE meeting

Burke, P. 1984, 'Synopsis: recent progress in the understanding of $CO_2$ corrosion', *Advances in $CO_2$ Corrosion,* Hausler, R. H. and Godard, H. P. (ed.), NACE, Houston, Texas, p3

Byars H. G. and Galbraith, J. M. 1984, 'An integrated corrosion control and monitoring program for Prudhoe Bay oil field', *Advances in $CO_2$ Corrosion,* Hausler, R, and Godard, H, (ed.), NACE, Houston, Texas, p103

Cameron, G. R. and Coker, L. G. 1986, 'Oil production corrosion inhibitor optimisation by laboratory and field application of electrochemical techniques', ASTM Special Technical Publications, 908 (Corrosion Monitoring in Industrial Plants Using Nondestructive Testing and Electrochemical Methods), p251

Chamberlain, T. E. 1985, 'Practical application of potentiodynamic polarisation curves in oil well corrosion', Corrosion 85, paper 28, NACE (Houston)

Chen, H. J. 1994, 'Evaluation of oilfield corrosion inhibitors by EIS', Corrosion 94, paper 92, NACE (Houston)

Chen, J. F. and Bogaerts, W. F. 1995, 'The physical meaning of the noise resistance', *Corrosion Science*, vol. 37, no. 11, p1839

Chesnut, G. and Choi, H. J. 1994, 'Laboratory testing and selection of corrosion inhibitors for continuous application in multiphase pipelines', Corrosion 94, paper no. 35, NACE (Houston)

Choi, H. J. and Cepulis, R. L. 1987, 'Inhibitor film persistence measurement by electrochemical techniques', *SPE Production Engineering*, November 1987, p325

Choi, H. J. and Cepulis, R. L. 1989, 'Inhibitor film persistence measurements in carbon dioxide environments', *Materials Performance*, vol. 28, no. 3, NACE (Houston)

Cizek, A. 1992, ' A review of corrosion inhibitors used in acidizing', Corrosion 93, Paper 92, NACE (Houston)

Cole, E. L. 1979, 'Evaluation of corrosion monitoring methods in oilfield systems', *Materials Performance*, vol. 18, no. 1, NACE (Houston)

Cole, K. S. and Cole, R. H. 1941, 'Dispersion and adsorption in dielectrics. I. Alternating-current characteristics', *Journal of Chemical Physics,* vol. 9, p341

Cossar, J. and Carlile, J. 1993, 'A new method for oilfield corrosion inhibitor measurement', Corrosion 93, paper 98, NACE (Houston)

Crolet J.L and Samaran J. P. 1993, 'The use of the anti-hydrate treatment for the prevention of $CO_2$ corrosion in long crude gas pipelines', Corrosion 93, Paper 102, NACE (Houston)

Crolet J.L. Olsen S. and Wilhelmsen W. 1994, 'Influence of a layer of undissolved Cementite on the rat of $CO_2$ corrosion of carbon steel', Corrosion 94, Paper 4, NACE (Houston)

Crolet J.L. Thevenot N. and Nesic S. 1996, 'Role of conductive corrosion products on the protectiveness of corrosion layers', Corrosion 96, Paper 96004, NACE (Houston)

Dabosi, F. Deslouis, C. Duprat, M. and Keddam, M. 1983, 'Corrosion inhibition study of a carbon steel in neutral chloride solutions by impedance techniques', *Journal of the Electrochemical Society*, vol. 130, no. 4, p761

Dawson, J. L., Rothwell, A. N., Walsh, T. G., Lawson, K. and Palmer, J. W., 1993, 'Electrochemical measurements for inhibitor assessments', Corrosion 93, Paper 108, NACE (Houston)

Dawson, J. L. Shih, C. C. Miller, R. G. and Palmer, J. W. 1990, 'Inhibitor evaluations under controlled hydrodynamic shear', Corrosion 90, paper 14, NACE (Houston)

de Waard, C. and Lotz, U. 1993, 'Prediction of $CO_2$ corrosion of carbon steel', Corrosion 93, paper 69, NACE, Houston

de Waard, C. Lotz, U. and Milliams D. E. 1991, 'Predictive model for $CO_2$ corrosion engineering in wet natural gas pipelines', *Corrosion*, vol. 47, no. 12, p976

de Waard C. and Milliams D. E. 1975a, 'Carbonic acid corrosion of steel', *Corrosion*, vol. 31, no. 5, p177

de Waard C. and Milliams D. E. 1975b, 'Prediction of carbonic acid corrosion in natural gas pipelines', First international conference on the internal and external protection of pipes', Paper F1, University of Durham, UK

Dunlop, A. K. Hassell, H. L. and Rhodes, P. R. 1984, 'Fundamental considerations in sweet gas well corrosion', in *Advances in $CO_2$ Corrosion*, Hausler, R. H. and Godard, H. P. (ed.), NACE, Houston, Texas, p52

Duprat, M. Lafont, M. C. Dabosi, F. and Moran, F. 1985, 'Study of the corrosion and inhibition processes of a carbon steel in a low conductivity medium by electrochemical methods', *Electrochimca Acta*, vol. 30, p353

Eden, D. A. Hladky, K. John, D. G. and Dawson, J. L. 1986, 'Electrochemical noise resistance', Corrosion 86, Paper 274, NACE, Houston

Eden, D. A. and Rothwell, A. N. 1992, 'Electrochemical noise data: analysis, interpretation and presentation, Corrosion 92, paper 292, NACE, Houston

EG&G Princeton Applied Research, Electrochemical Instruments Division, 'Evaluation of organic coatings by EIS', Application Note AC-2, EG&G Instruments Corporation, USA

EG&G Princeton Applied Research, 1993 'Model 352/252 SoftCorr$^{TM}$ II corrosion measurement & analysis software: user's guide', EG&G Instruments Corporation, USA

Epelboin, I. Gabrielli, C. and Keddam, M. 1984, 'Non-steady state techniques', In *Comprehensive Treatise of Electrochemistry* (Yeager, E. Bockris, J. O'M. Conway, B. E. and Sarangapani, S. eds.), vol. 9, p.62. Plenum, New York

Epelboin, I. Gabrielli, C. Keddam, M. and Raillon L. 1979, 'Measurement of the power spectral density of electrochemical noise: direct two-channel method', *Journal of Electroanalytical Chemistry,* vol. 105, p389

Epelboin, I. and Keddam, M. 1970, 'Faradaic impedances: diffusion impedance and reaction impdance', *Journal of the Electrochemical Society*, vol. 117, p1052

Epelboin, I. Keddam, M. and Takenouti, H. 1972, 'Use of impedance measurements for the determination of the instant rate of metal corrosion', *Journal of applied electrochemistry*, vol. 1, no. 2, p71

Eriksrud, E. and Sontvedt T. 1984, 'Effect of flow on $CO_2$ corrosion rates in real and synthetic formation waters', in *Advances in $CO_2$ Corrosion*, Hausler, R. H. and Godard, H. P. (ed.), NACE, Houston, Texas, p20

Esteban, J. M. Hickey, G. S. and Orazem, M. E. 1990, 'The impinging jet electrode: measurement of the hydrodynamic constant and its use for evaluating film persistency', *Corrosion*, vol. 46, no. 11, Houston, p896

Evans, U. R., 1981, 'An introduction to metallic corrosion', 3rd edition, Edward Arnold press, p174

Feliu, S. Galvan, J. C. and Morcillo, M. 'The charge transfer reaction in Nyquist diagrams of painted steel', *Corrosion Science*, vol. 30, no. 10, p989

Fisher, L. E. 1993, 'Corrosion inhibitor and neutralisers past, present and future', Corrosion 93, paper 537, NACE (Houston)

Gabrielli, C. 1980, 'Identification of electrochemical processes by frequency response analysis', Solartron Instrument Group, Solartron Schlumberger, Farnborough, Hants, U.K.

Gabrielli, C. Huet, F. and Keddam, M. 1991, 'Investigation of metallic corrosion by electrochemical noise techniques', NATO ASI Series, Series E: Applied Science, vol. 203 (Electrochemical and optical techniques for the study and monitoring of metallic corrosion), p135

Gabrielli, C. and Keddam, M. 1992, 'Review of applications of impedance and noise analysis to uniform and localised corrosion', *Corrosion*, vol. 48, no. 10, p794

Gabrielli, C. Ksouri, C. and Wiart R. 1978, 'Electrocrystallization noise: a phenomenological model', *Journal of Electroanalytical Chemistry*, vol. 86, p233

Garber, J. D. Braun, R. D. Reinhardt, J. R. Walters, F. H. Lin, J. H. and Perkins, R. S. 1994, 'Comparison of various test methods in the evaluation of $CO_2$ corrosion inhibitors for downhole and pipeline use', Corrosion 94, paper 42, NACE (Houston)

Gatzke, L. K. and Hausler, R. H. 1983 'The COPRA correlation - a quantitative assessment of deep, hot gas well corrosion and its control', Corrosion 83, paper 48, NACE (Houston)

Gatzke, L. K. and Hausler, R. H. 1984, 'A novel correlation of tubing corrosion rates in deep, hot gas wells with water and gas production rates', in *Advances in $CO_2$ Corrosion*, Hausler, R. H. and Godard, H. P. (ed.), NACE, Houston, Texas, p87

Goodson, A.R and Jackson, G.E. 1986, 'A comparison of corrosion inhibitor performance tests for application in oil production systems', Proc. U.K. Corrosion'86, Birmingham, UK

Gross, W.F. and Andrews, H. W. 1948, 'Prevention of corrosion in sour wells with organic inhibitors,' *The Oil and Gas Journal,* October, 1948

Gusmano, G. Montesperelli, G. and Traversa, E. 1993, "Comparison between A.C. impedance spectroscopy and potential noise measurements in the evaluation of mild steel passivation in cooling waters", Corrosion 93, paper no. 355, NACE (Houston)

Harris, R. W. and Ledwidge, T. J. 1974, 'Introduction to noise analysis', Pion Limited, London

Hausler, R. H. 1984, 'The mechanism of $CO_2$ corrosion of steel in hot, deep gas wells', in *Advances in $CO_2$ Corrosion*, Hausler, R. H. and Godard, H. P. (ed.), NACE, Houston, Texas, p72

Heusler, K. E. 1989, 'The influence of electrolyte composition on the formation and dissolution of passivating films', *Corrosion Science,* vol. 29, no. 2-3, p131

Hilliard, H. 1978, 'Use of inhibitors for downhole corrosion control in gas wells', in *$CO_2$ corrosion in oil and gas production - selected paper, abstracts and references*, ed. NACE Task Group T-1-3, NACE, Houston, Texas, p357

Hladky, K. and Dawson, J. L. 1981, 'The measurement of localised corrosion using electrochemical noise', *Corrosion Science*, vol. 21, p317

Hladky, K. and Dawson, J. L. 1982, 'The measurement of corrosion using electrochemical $1/f$ noise', *Corrosion Science*, vol. 22, p231

Hoar, T. P. and Wood, G. C. 1962, 'Sealing of porous anodic oxide films on Aluminium', *Electrochimica Acta*, vol. 7, p333

Iverson, W. P. 1968, 'Transient voltage changes produced in corroding metals and alloys', *Journal of the Electrochemical Society*, vol. 115, p617

Ikeda, A. Ueda, M. and Mukai S. 1984, '$CO_2$ behaviour of carbon and Cr steels', in *Advances in $CO_2$ Corrosion*, Hausler, R. H. and Godard, H. P. (ed.), NACE, Houston, Texas, p39

Jasinski, R. 1987, 'Corrosion of N80-type steel by $CO_2$/water mixtures', *Corrosion,* vol. 43, no. 4, p214

Kalman, E. Varhegyi, B. Bako, I. Felhosi, I. Karman, F. H. and Shaban, A. 1994, 'Corrosion inhibition by 1-hydroxy-ethane-1,1-diphosphonic acid: an electrochemical impedance spectroscopy study', *Journal of the Electrochemical Society*, vol. 141, no. 12, p3357

Kendig, M. Mansfeld, F. and Tsai, S. 1983, 'Determination of the long term corrosion behaviour of coated steel with A.C. impedance measurements', *Corrosion Science,* vol. 23, no. 4, p317

Kinsella, B. Bailey, S. Parentich, A. and Tan, Y. J. 1994, 'Corrosion Inhibitor Film Persistency', Proc. ACA Conference Corrosion & Prevention 94, Adelaide, Australia

Kinsella, B. Tan, Y. J. and S. Bailey, 1995, 'The application of electrochemical techniques and cylinder electrodes in the study of inhibitor film persistency', Proc. ACA Conference Corrosion & Prevention 95, Perth, Australia

Kirkley, C. 1982, 'Corrosion control - oil and gas production', Petroleum Extension Service, University of Texas at Austin

Kolts, J. 1993, 'Effect of selected organic corrosion inhibitors on performance of corrosion resistant alloys', Corrosion 93, Paper 121, NACE (Houston)

Legat, A. and Zevnik, C. 1993, "The electrochemical noise of mild and stainless steel in various water solutions", *Corrosion Science*, vol. 35, p1661

Linda Garverick Essential Research 1994, 'Corrosion in the petrochemical industry', ASM International, The Materials Information Society, USA

Lorenz, W. J. and Mansfeld, F. 1981, 'Determination of corrosion rates by electrochemical DC and AC methods', *Corrosion Science,* vol. 21, no. 9, p647

Lotz, U. Bodegom, L. V. and Ouwehand, C. 1990, 'The effect of type of oil or gas condensate on carbonic acid corrosion', Corrosion 90, paper 41, NACE (Houston)

Lumsden, J. B. Kendig, M. W. and Jeanjaquet, S. 1992, 'Electrochemical noise for carbon steel in sodium chloride solution-effect of chloride and oxygen activity', Corrosion 92, Paper 224, NACE (Houston)

Lynch, P. F. Brown, C. W. and Heidersbach R. 1983, 'The use of infrared and Raman spectroscopy to study corrosion inhibitors on metal surfaces', *Corrosion,* vol. 39, no. 9, p357

Macdonald, D. D. 1990, 'Some advantages and pitfalls of electrochemical impedance spectroscopy', *Corrosion,* vol. 46, no. 3, p229

Macdonald, D. D. 1991, 'Application of electrochemical impedance spectroscopy in electrochemistry and corrosion science', in *Techniques for characterisation of electrodes and electrochemical processes,* Ravi Varma and J. R. Selman (ed.), John Wiley & Sons, Inc.

Macdonald, J. R. 1987, 'Impedance spectroscopy and it use in analysing the steady-state AC response of solid and liquid electrolytes', *Journal of Electroanalytical Chemistry,* vol. 223, p25

Mansfeld, F. 1976a, 'The polarisation resistance technique for measuring corrosion currents', in *Advances in Corrosion Science and Technology* (ed. by Fontana, M. G. and Staehle R. W.), vol. 6, Plenum Press, New York, p163

Mansfeld, F. 1976b, 'The effect of uncompensated IR-drop on polarisation resistance measurements', *Corrosion,* vol. 32, no. 4, p143

Mansfeld, F. 1981, 'Recording and analysis of AC impedance data for corrosion studies', *Corrosion,* vol. 36, no. 5, p301

Mansfeld, F. 1988, 'Don't be afraid of electrochemical techniques - but use them with care!', *Corrosion,* vol. 44, no. 12, p856

Mansfeld, F. and Kendig, M. W. 1985, 'Impedance spectroscopy as quality control and corrosion test for anodised Al alloys', *Corrosion,* vol. 41, no. 8, p490

Mansfeld, F. Kendig, M. W. and Lorenz, W. J. 1985, 'Corrosion inhibition in neutral, aerated media', *Journal of the Electrochemical Society*, vol. 132, no. 2, p290

Mansfeld, F. Kendig, M. W. and Tsai S. 1982a, 'Evaluation of corrosion behaviour of coated metals with AC impedance measurements', *Corrosion,* vol. 38, no. 9, p478

Mansfeld, F. Kendig, M. and Tsai S. 1982b, 'Corrosion kinetics in low conductivity media - I. iron in natural waters', *Corrosion Science*, vol. 22, no. 5, p455

Mansfeld, F. and Lorenz, W. J. 1991, 'Electrochemical impedance spectroscopy: application in corrosion science and technology', in *Techniques for characterisation of electrodes and electrochemical processes*, Ravi Varma and J. R. Selman (ed.), John Wiley & Sons, Inc.

Mansfeld, F. and Tsai, C. H. 1991, 'Determination of coating deterioration with EIS, 1. basic relations' *Corrosion*, vol. 47, no. 12, p958

Mansfeld, F. and Xiao, H. 1993, 'Electrochemical noise analysis of iron exposed to NaCl solutions of different corrosivity', *Journal of the Electrochemical Society*, vol. 140, p2205

Martin, R. L. 1993, 'Corrosion consequences and inhibition couples in petroleum production equipment', Corrosion 93, paper 113, NACE (Houston)

Mills, D. 1994, 'Electrochemical noise for corrosion applications', *British Corrosion Journal,* vol. 29, no. 3, p179

Mishra, B. 1993, 'Prediction of microstructural effect on corrosion of pipeline steels in $CO_2$-brine solution', Corrosion 93, paper 90, NACE (Houston)

Monticelli, C. Brunoro, G. Frignani, A. and Trabanelli, G. 1992, 'Evaluation of corrosion inhibitors by electrochemical noise analysis', *Journal of the Electrochemical Society*, vol. 139, no. 3, p706

Murata, T. Sato, E. Matsuhashi, R. 1984, 'Factors controlling corrosion of steels in $CO_2$-saturated environments', in *Advances in $CO_2$ Corrosion*, Hausler, R. H. and Godard, H. P. (ed.), NACE, Houston, Texas, p64

Murphy T. 1991, 'Electrochemical noise: the technique for the '90s?', *British Corrosion Journal,* vol. 26, no. 4, p238

NACE, 1979, 'Corrosion control in petroleum production', TPC publication 5, NACE, Houston, Texas, p60

NACE Task Group T-1D-8, 1982, 'Wheel Test Procedure Used for Evaluating Film Persistent Inhibitors for Oilfield applications', NACE Publication 1D182, item no. 54238

NACE Task Group T-1-3 1984, 'Introduction', in *$CO_2$ corrosion in oil and gas production - selected papers, abstracts and references*, ed. NACE Task Group T-1-3, NACE, Houston, Texas, p3

NACE T-D-2 Task Group Report, 1966, 'Cooperative evaluation of inhibitor film persistency test', *Materials Protection*, vol. 5, no. 10, NACE, p69

Nakamoto, K. 1986, 'Infrared Spectra of Inorganic and Coordination Compounds', Fourth Edition, Wiley-Interscience Publication (New York).

Nesic, S. 1993, '$CO_2$ corrosion of carbon steel in two-phase flow', Corrosion 93, paper 640, NACE (Houston)

Nestle, A. 1973, 'Corrosion inhibitors in petroleum production primary recovery', Corrosion Inhibitors, C. C. Nathan (ed.), NACE (Houston)

Noegroho, H. 1990, 'Carbon dioxide corrosion in oil and gas production wells and its prevention', *Lembaran Publikasi Lemigas,* vol. 24, no. 1, p29 (Indonesian)

Orazem, M. E. Agarwal, P. Garcia-Rubio, L. H. 1994, 'Critical issues associated with interpretation of impedance spectra', *Journal of Electroanalytical Chemistry*, vol. 378, p51

Palacios, C. and Shadley, J. 1991, 'Characteristics of corrosion scales on steel in a $CO_2$-saturated NaCl brine', *Corrosion,* vol. 47, no. 2, p124

Palacios, C. A. and Shadley, J.R., 1993, '$CO_2$ corrosion of N-80 steel at 70 °C in a two-phase flow system', *Corrosion,* vol. 49, p686

Park, J. R. and Macdonald, D. D. 1983, 'Impedance studies of the growth of porous magnetite films on carbon steel in high temperature aqueous systems', *Corrosion Science*, vol. 23, no. 4, p295

Pourbaix, M. 1973, 'Lectures on electrochemical corrosion', Plenum Press, New York, p252

Rice, P. W. 1993, 'History of metallurgy in the oil field', Corrosion 93, paper 151, NACE (Houston)

Roberge, P. R. Halliop, E. Sastri, V. S. 1992, 'Corrosion of mild steel using electrochemical impedance spectroscopy data analysis', *Corrosion*, vol. 48, no. 6, p447

Rothwell, A. N. Eden, D. A. 1992, 'Electrochemical noise techniques for determining corrosion rates and mechanism', , Corrosion 92, paper 223, NACE (Houston)

Schmitt, G, 1984a, '$CO_2$ Corrosion of steels - an attempt to range parameters and their effects', in *Advances in $CO_2$ Corrosion*, Hausler, R. H. and Godard, H. P. (ed.), NACE, Houston, Texas, p1

Schmitt, G. 1984b, 'Fundamental aspects of $CO_2$ corrosion', in *Advances in $CO_2$ Corrosion*, Hausler, R. H. and Godard, H. P. (ed.), NACE, Houston, Texas, p10

Schmitt G. and Rothmann B. 1977, 'Studies on the corrosion mechanism of unalloyed steel in oxygen-free carbon dioxide solutions, part I. kinetics of the liberation of

hydrogen', in *$CO_2$ corrosion in oil and gas production - selected papers, abstracts and references*, ed. NACE Task Group T-1-3, NACE, Houston, Texas, (1984), p154

Schmitt G. and Rothmann B. 1978a, 'Studies on the corrosion mechanism of unalloyed steel in oxygen-free carbon dioxide solutions, part II. kinetics of iron dissolution', in *$CO_2$ corrosion in oil and gas production - selected papers, abstracts and references*, ed. NACE Task Group T-1-3, NACE, Houston, Texas, (1984), p163

Schmitt G. and Rothmann B. 1978b, 'Corrosion of unalloyed and low alloyed steels in carbonic acid solutions', in *$CO_2$ corrosion in oil and gas production - selected papers, abstracts and references*, ed. NACE Task Group T-1-3, NACE, Houston, Texas, (1984), p167

Schmitt, G. Simon, T. and Hausler, R. H. 1993, '$CO_2$ erosion corrosion and its inhibition under extreme shear stress II. performance of inhibitors', Corrosion 93, paper 86, NACE (Houston)

Schofield, M. J. and Kane, R. D. 'Corrosion resistant alloy for oilfield application selection criteria methodology and options', Corrosion 93, paper 165, NACE (Houston)

Scully, J. R. 1989, 'Electrochemical impedance of organic-coated steel: correlation of impedance parameters with long-term coating deterioration', *Journal of the Electrochemical Society*, vol. 136, no. 4, p979

Searson P. C. and Dawson, J. L. 1988, "Analysis of electrochemical noise generated by corroding electrodes under open-circuit conditions", *Journal of the Electrochemical Society*, vol. 135, no. 8, p1908

Shah, S. 1993, 'Characterisation of interphases in corrosion by *ex-situ* FTIR spectroscopy', Corrosion 93, paper 361, NACE (Houston)

Silverman, D. C. 1989, 'Corrosion rate estimation from pseudo-inductive electrochemical impedance response', *Corrosion*, Vol. 45, no. 10, p824

Silverman, D. C. 1990, 'Rapid corrosion screening in poorly defined systems by electrochemical impedance technique', *Corrosion*, vol. 46, no. 7, p589

Silverman, D. C. 1991, 'On ambiguities in modelling electrochemical impedance spectra using circuit analogues', *Corrosion*, Vol. 47, p87

Silverman, D. C. and Carrico, J. E. 1988, 'Electrochemical impedance technique - a practical tool for corrosion prediction', *Corrosion,* vol. 44, no. 5, p280

Simoes, A. M. P. and Ferreira, M. G. S. 1987, 'Crevice corrosion studies on stainless steel using electrochemical noise measurements', *British Corrosion Journal,* vol. 22, no. 1, p21

Stern, M. and Geary, A. L., 1957, 'Electrochemical polarisation. I. A theoretical analysis of the shape of polarisation curves', *Journal of the Electrochemical Society,* vol. 104, p56.

Tafel, Z. 1905, *Physik. Chem.*, vol. 50, p641

Tan Y. J. 1991, 'The effect of inhomogeneity in organic coatings on electrochemical measurements using a wire beam electrode, part 1', *Progress in Organic Coatings*, vol. 19, p89

Tan, Y. J. 1994, 'A new method for crevice corrosion studies and its use in the investigation of oil-stain', *Corrosion*, vol. 50, no. 4, p266

Tan, Y. J. Bailey, S. and Kinsella, B. 1996a, "The evaluation of corrosion inhibitor film persistency using electrochemical impedance spectroscopy and electrochemical noise analysis', Corrosion 96, paper 352, NACE (Houston), Denver

Tan, Y. J. Bailey, S. and Kinsella, B. 1996b, 'Electrochemical investigations on the formation and destruction of corrosion inhibitor films using electrochemical noise analysis', *Corrosion Science*, in press

Tan, Y. J. Bailey S. and Kinsella B. 1996c, 'Monitoring batch treatment inhibitor performance continuously using electrochemical noise analysis', *British Corrosion Journal*, submitted

Tan, Y. J. Bailey S. and Kinsella B. 1996d, 'Investigations on the formation and destruction processes of corrosion inhibitor films using electrochemical impedance spectroscopy', *Corrosion Science,* in press

Tan, Y. J. Kinsella B. and Bailey S. 1995 'An experimental comparison of corrosion rate measurement techniques: weight-loss measurement, linear polarisation, electrochemical impedance spectroscopy and electrochemical noise analysis', Corrosion & Prevention 95, Australasian Corrosion Association, Perth, 1995

Tan, Y. J. and Yu S. T. 1991, 'The effect of inhomogeneity in organic coatings on electrochemical measurements using a wire beam electrode, part 2', *Progress in Organic Coatings*, vol. 19, p257

Thomas, E. C. 1985, 'Practical application of potentiodynamic polarisation curves in oil well corrosion', Corrosion 85 paper 28, NACE (Houston)

Thompson, I. and Campbell, D. 1994, 'Interpreting Nyquist Responses from Defective Coatings on Steel Substrates', *Corrosion Science*, vol. 36, no. 1, p187

Tsai, C. H. and Mansfeld, F. 1993, 'Determination of Coating Deterioration with EIS: Part II. Development of a Method for Field Testing of Protective Coatings', *Corrosion*, vol. 49, no. 9, p727

Townsend, P. E. Colegate, G. T. and van Waart, T. L., 1972 'Carbon dioxide corrosion at low partial pressures in major submarine pipelines', in *$CO_2$ corrosion in oil and gas production - selected papers, abstracts and references*, ed. NACE Task Group T-1-3, NACE, Houston, Texas, (1984), p501

Treseder, R. S. 1980, 'NACE corrosion engineer's reference book', ed. Treseder, R. S. NACE, Houston, Texas

Uruchurtu, J. C. and Dawson, J. L. 1987, 'Noise analysis of pure aluminium under different pitting conditions', *Corrosion*, vol. 43, no. 1, p19

van Hunnik E. and Hendriksen E. L. J. A. 1996, 'The formation of protective $FeCO_3$ corrosion product layers in $CO_2$ corrosion', Corrosion 96, Paper 96004, NACE (Houston)

Vera, J. Viloria, A. Castillo, M. Ikeda, A. and Ueda, M. 1994, 'Flow velocity effect on carbon steel $CO_2$ corrosion using a dynamic field tester', Paper for 1st Pan-American Congress on Corrosion and Protection

Videm, K. and Dugstad, A. 1987, 'Effect of flow rate, pH, $Fe^{2+}$ concentration and steel quality on the $CO_2$ corrosion of carbon steels', Corrosion 87, paper 42, NACE (Houston)

Volmer, M. and Erdey-Gruz, T. 1930, 'The theory of hydrogen overvoltage', *Zeitschrift fuer Physikalische Chemie*, vol. 150A, p203

Videm, K. 'The influence of pH and concentration of bicarbonate and ferrous ions on the $CO_2$ corrosion of carbon steels', Corrosion 93, paper 83, NACE (Houston)

Walter, G. W. 1986, 'A review of impedance plot methods used for corrosion performance analysis of painted metals', *Corrosion Science*, vol. 26, no. 9, p681

Webster, S. Harrop, D. Mcmahon, A. J. and Partridge, G. J. 1993, 'Corrosion inhibitor selection for oilfield pipelines', Corrosion 93, Paper 109, NACE (Houston)

Whitman, G. W. Russel, R. P. and Altieri, V. J. 1924, 'Effect of hydrogen-ion concentration on the submerged corrosion of steel', *Industrial and Engineering Chemistry*, vol. 16, no. 7, p665

Williams, E. and Leckie, H. P. 1968, 'Corrosion and its prevention in a Monoethanolamine gas treating plant', in *$CO_2$ corrosion in oil and gas production - selected papers, abstracts and references*, ed. NACE Task Group T-1-3, NACE, Houston, Texas, (1984), p321, reprinted from *Material Protection*, vol. 7, no. 7

Williams D. E. and Asher J. 1984, 'Measurement of low corrosion rates: comparison of A.C. impedance and thin layer activation methods', *Corrosion Science,* vol. 24, no. 3, p185

Wu, C. L. Zhou, X. J. and Tan, Y. J. 1995, 'A study on the electrochemical inhomogeneity of organic coatings', *Progress in Organic Coatings*, vol. 25, p379

Wu, Y. 1994, 'Corrosion inhibitor screening tests and selection for field applications', Corrosion 94, paper no. 43, NACE (Houston)

Xia, Z. Chou, K. C. and Szklarska-Smialowska, Z. 1989, 'Pitting corrosion of carbon steel in $CO_2$-containing NaCl brine', *Corrosion,* vol. 45, p636